

**“STUDIES ON THE SORPTION AND DESORPTION BEHAVIOUR
OF SOME TRIVALENT COMPLEX CATIONS ON AND FROM
CLAY MINERALS, RESINS AND MOLECULAR SIEVES”**

**Thesis Submitted for the Degree of Doctor
Of Philosophy (Science) of the
University of North Bengal.
1980**

**By
GAURENDRA NATH SARKAR, M. Tech.**

631-117
S 245b

77471

*Dedicated to the
Sacred Memory of
my Beloved Father*

P R E F A C E

The work embodied in the thesis deals with an investigation on the sorption and desorption behaviour of two Co(III) complex cations viz., tris 1,2 propane diamine Co(III) chloride, $[\text{Co}(\text{pn})_3\text{Cl}_3]$, and tris 1,3 propane diamine Co(III) chloride or tris-trimethylene diamine Co(III) chloride, $[\text{Co}(\text{tn})_3\text{Cl}_3]$, by ion-exchangers. It is well known that $\text{Co}(\text{pn})_3\text{Cl}_3$ is a five membered ring complex whereas $\text{Co}(\text{tn})_3\text{Cl}_3$ is a six membered one and the sizes of the two compounds are also somewhat different. In the present work two natural exchangers, viz., Bentonite and Vermiculite and three synthetic exchangers, viz., Laponite (a hectorite), Amberlite IRC-50 and Linde Molecular Sieve 13X have been selected as adsorbents. In order to understand the physico-chemical aspects of exchange equilibrium considerable attention has been devoted to studies on the desorption of $\text{Co}(\text{pn})_3^{3+}$ and $\text{Co}(\text{tn})_3^{3+}$ ions from the respective exchangers. Monovalent and divalent inorganic cations as well as alkyl quaternary ammonium ions of varying sizes have been used as desorbing ions. A systematic attempt has been made to interpret the data of both sorption and desorption in the light of prevalent approaches and models and also to express the data in qualitative and quantitative terms.

The present thesis embodies the results of research carried out by the candidate at the Department of Chemistry, University of North Bengal.

A O K N O W L E D G E M E N T

The candidate takes this opportunity to offer his sincere thanks to Dr. J.L.Daskanungo, Reader in Chemistry, University of North Bengal for his valuable guidance and continued interest during the progress of the work.

The candidate is highly indebted to Dr. S.K. Chakravarti, Professor of Chemistry, University of North Bengal, for his keen interest, valuable suggestions and encouragement.

The candidate expresses his thanks to the University Grants Commission, New Delhi, for the award of a Teacher Fellowship and Balurghat College, Balurghat, West Dinajpur, West Bengal for granting leave. The candidate is also thankful to the Head of the Department of Chemistry and the authorities of the University of North Bengal for laboratory facilities.

Thanks are also due to the Research Fellows, Teacher Fellows, teaching and non-teaching staff of the Department for their kind co-operation.

The candidate also expresses his thanks to his wife, son and daughter for their constant inspiration and encouragement during the progress of the work.

Finally, the candidate expresses his thanks to his brothers and sisters and his regards to his mother and other members of his family for their inspiration and encouragement during the progress of the work.

C O N T E N T S

	<u>Page</u>
<u>CHAPTER I</u>	
Section A : Introduction and Review of Previous Work.	1-14
Section B : Ion Exchange Formulations.	15-21
Section C : Exchange studies and selectivities of clay minerals, resins and molecular sieves.	22-29
<u>CHAPTER II</u>	
Scope and object of the work.	30-35
<u>CHAPTER III</u>	
Experimental	36-44
<u>CHAPTER IV</u>	
Sorption and Desorption of $\text{Co}(\text{pn})_3^{3+}$ and $\text{Co}(\text{tn})_3^{3+}$ on Bentonite system.	45-77
Section A: Sorption of $\text{Co}(\text{pn})_3^{3+}$ and $\text{Co}(\text{tn})_3^{3+}$ on bentonite.	46-62
Section B: Desorption of $\text{Co}(\text{pn})_3^{3+}$ and $\text{Co}(\text{tn})_3^{3+}$ from bentonite complexes.	63-77
<u>CHAPTER V</u>	
Sorption and Desorption of $\text{Co}(\text{pn})_3^{3+}$ and $\text{Co}(\text{tn})_3^{3+}$ on vermiculite system.	78-94

- Section A : Sorption of $\text{Co}(\text{pn})_3^{3+}$ and $\text{Co}(\text{tn})_3^{3+}$ on vermiculite. 80-86
- Section B : Desorption of $\text{Co}(\text{pn})_3^{3+}$ and $\text{Co}(\text{tn})_3^{3+}$ from vermiculite complexes. 87-94

CHAPTER VI

- Sorption and Desorption of $\text{Co}(\text{pn})_3^{3+}$ and $\text{Co}(\text{tn})_3^{3+}$ on Na-Laponite system. 95-101
- Section A: Sorption of $\text{Co}(\text{pn})_3^{3+}$ and $\text{Co}(\text{tn})_3^{3+}$ on Na-Laponite. 97
- Section B : Desorption of $\text{Co}(\text{pn})_3^{3+}$ and $\text{Co}(\text{tn})_3^{3+}$ from Laponite complexes. 98-101

CHAPTER VII

- Sorption and Desorption of $\text{Co}(\text{pn})_3^{3+}$ and $\text{Co}(\text{tn})_3^{3+}$ on Na-IRC-50 system. 102-111
- Section A: Sorption of $\text{Co}(\text{pn})_3^{3+}$ and $\text{Co}(\text{tn})_3^{3+}$ on Na-IRC-50. 104
- Section B : Desorption of $\text{Co}(\text{pn})_3^{3+}$ and $\text{Co}(\text{tn})_3^{3+}$ from Na-IRC-50-complexes. 105-111

CHAPTER VIII

Sorption and Desorption of
 $[\text{Co}(\text{NH}_3)_6]^{3+}$, $[\text{Coen}_3]^{3+}$,
 $[\text{Copn}_3]^{3+}$ and $[\text{Cotn}_3]^{3+}$ on
 Molecular Sieve 13X.

112-120

Section A : Sorption of $[\text{Co}(\text{NH}_3)_6]^{3+}$,
 $[\text{Coen}_3]^{3+}$, $[\text{Co}(\text{tn})_3]^{3+}$ and
 $[\text{Copn}_3]^{3+}$ on Molecular
 Sieve 13X.

116-117

Section B : Desorption of $\text{Co}(\text{pn})_3^{3+}$ and
 $\text{Co}(\text{tn})_3^{3+}$ from Molecular Sieve
 13X complexes.

118-120

CHAPTER IX

Summary and Conclusion

121-132

Bibliography

..

..

I-X V

CHAPTER I

SECTION A

Introduction and Review of Previous Work

Plant roots take up ions as nutrients from the soil by a process of ion exchange. In this process, the clay fraction of the soil plays a significant and vital role. Hence, a study of the exchange characteristics of clay fraction reveals, generally, the exchange behaviour of the soil as a whole. The colloidal properties of clay minerals have been used for hundreds of years, especially in the manufacture of pottery and in foundry. A systematic attempt has, however, been made only in this century to understand the origin of their behaviour. But even then the surface and colloid chemistry of clays have not been adequately investigated. Considerable success has been achieved in the past fifty years in regard to the search for high purity clays and for evidences of their crystallinity. The atomic structures of the common clay minerals have been to a great extent determined, and applied to explain the properties of the individual members by numerous investigators.

The structures of some of the clay minerals used in the present investigation are briefly discussed, indicating their differences from each other and their peculiarities, which are responsible for the special colloidal behaviour of

the minerals. Clay minerals viz. kaolinite, montmorillonite, illite, chlorite and vermiculite and mixed layer-lattice type minerals have been identified in the vast majority of natural soils.

The correlation between the structure and exchange properties of these minerals has been established from a crystallo-chemical point of view on the basis of the important contributions of Pauling (1), Bragg (2), Gruner (3), Brindley (4), Hofmann (5), Marshall (6), Hendricks (7) and others (8), (9), (10), (11), (12), (13), (14). From these studies clay minerals are recognised to consist essentially of two structural units. One is composed of two sheets of closely packed oxygens or hydroxyls in which aluminium or magnesium atoms are arranged in octahedral coordination, so that they are equidistant from six oxygens or hydroxyls. With aluminium in the octahedral position, only two-thirds of the possible positions are filled to balance the structure. It is the gibbsite structure having the formula $Al_2(OH)_6$. When magnesium is present, all the possible positions are filled to balance the structure giving the brucite structure which has the formula $Mg_3(OH)_6$.

The second unit is the tetrahedrally co-ordinated silica. A silicon atom being placed at the centre of a tetrahedron is equidistant from four oxygens or hydroxyls. The silica

tetrahedra are joined together in the a,b-directions, through oxygen, to form a hexagonal network which is repeated indefinitely to form a sheet of composition $\text{Si}_4\text{O}_6(\text{OH})_4$. The tips of all the tetrahedra are in the same direction.

Kaolinite: The kaolinite is composed of a single silica tetrahedral sheet and a single alumina octahedral sheet combined in a unit so that the tips of the silica tetrahedra and one of the layers of the octahedral sheet form a common layer. All the tips of the silica tetrahedra point in the same direction and toward the centre of the unit made of the silica and octahedral sheets. These sheets which are continuous in the a,b-directions are stacked one above the other in the c-direction. During stacking the oxygens of the tetrahedral layer are placed very close to the hydroxyls of the octahedral layer, so that the sheets are held tightly by hydrogen bonding as a result of which very little expansion in the c-direction is possible.

Montmorillonite: According to the currently accepted concept, montmorillonite is composed of units made up of two silica tetrahedral sheets with a central alumina octahedral sheet. All the tips of the tetrahedrons point in the same direction and toward the centre of the unit. The tetrahedral and octahedral

sheets are combined so that the tips of the tetrahedra of each silica sheet and one of the hydroxyl layers of the octahedral sheet form a common layer. The atoms common to the tetrahedral and octahedral layers become O instead of OH.

The minerals of this group are also developed by stacking of these unit sheets one above the other in the c-direction. During stacking the O layers of one unit are close to the O layers of the other unit, so that there is an excellent cleavage between the sheets. Polar molecules can enter the space between the sheets causing expansion of the axis in the c-direction. Isomorphous substitution of other metal ions for silicon and aluminium in both the tetrahedral and octahedral layers is known to occur. Complete replacement of aluminium by iron and magnesium is found in the minerals nontronite and saponite respectively. Substitution in the tetrahedral layer in montmorillonite does take place but to a limited extent.

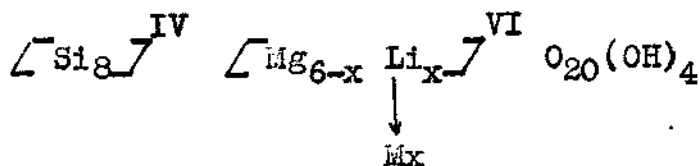
Vermiculite: It consists of alternate stacking of mica and water layers. Isomorphous replacement of Al for Si always takes place in the tetrahedral layer and replacement of Fe or Mg for Al in the octahedral layer is limited. In natural vermiculites the net resulting charge deficiency is balanced primarily by Mg^{2+} and to some extent by Ca^{2+} . These ions are held as exchangeable ions in between the mica layers. It has also been

suggested that these exchangeable ions are responsible for the orientation of water molecules. The Mg^{2+} are present in octahedral grouping with six water molecules causing the existence of two layers of water molecules, but with K^+ in place of Mg^{2+} the thickness of water layer is monomolecular. The c-axis expansion is limited to the thickness of two water molecules.

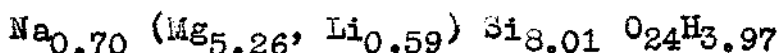
Laponite: One of the better known natural swelling clays is the mineral hectorite. This substance occurs heavily contaminated with other minerals such as dolomite and quartz which are not easily removed. In addition, the deposits of hectorite are limited.

Laponite, being a manufactured product, provides, for the first time, a reliable consistent supply of high purity swelling clay. In addition, the material has a number of other important properties not found in its natural equivalent.

Laponites are magnesium silicates with a layered structure, and are obtained as granular, free-flowing white powders. When the powders are dispersed in water they form thixotropic gels. The layered structure of these products is identical to that of natural hectorite. Hectorite is the trioctahedral equivalent of montmorillonite and owes its charge to octahedral replacements of Mg by Li. Its structural formula is



The charge x is of the order of 0.6 to 0.7 valences per unit cell. The structural formula of Na-Laponite GP is :



In certain of the Laponite products, there are no fluorine atoms in the structure, these being replaced by hydroxyl ions. The layers (platelets) are about a Nanometer (10\AA) thick and extend in two dimensions. If the only cations present were silicon and magnesium, a single layer would be electrically neutral. However, since some magnesium is substituted by lithium and some structural positions normally occupied by these cations may be unoccupied, these layers have a negative charge which is balanced by exchangeable cations — normally sodium ions — situated outside the structure, between the multiple layers.

An important phenomenon exhibited by clay minerals is their property of sorbing cations and retaining these in an exchangeable state. This can be explained by considering the existence of a net negative charge of clay particles at all pH

values above two or three which is compensated by the presence of positive counterions. They form negatively charged micelles in contact with water and either adsorb cations from the dispersion medium or dissociate ions which are adsorbed in its structure, thus exhibiting ion exchange reactions (15,16). Ion exchange sorption of inorganic as well as organic ions is known to occur on clay minerals. Hence the origins of this charge on the clay lattice are believed to be due to isomorphic substitution, lattice imperfections, broken bonds at the edges of the particles and exposed structural hydroxyls.

The **neg**ative charge on the clay minerals is compensated by adsorption of cations. The counterions are held on the external surfaces of the aggregates and between the unit layers in clays which swell in aqueous suspension, whereas the sorption of counterions takes place onto the external surfaces only in non swelling clays. In aqueous suspension, some of these cations remain in a closely held stern layer; others diffuse away from the surface and form a diffuse double layer. Provided that they are not fixed by engaging in strong, specific bonding with the clay or by being trapped between unit layers that have collapsed together irreversibly (lattice collapse), the counterions can undergo ion exchange with other cations present in the system. The magnitude of the cation exchange capacity of a clay depends largely on the type of clay and to a lesser extent on the source of a particular sample.

The experimentally measured specific surface area of a clay mineral depends on the type of clay and the method of measurement employed; among clays of the same type the values vary from sample to sample, and in any one mineral sample the nature of the counterions present may influence the measured surface area. The theoretical surface areas were calculated from the weights of the unit cells, and their dimensions as indicated by x-ray diffraction.

Systematic studies of cation exchange in pure clay minerals were carried out by Page and Baver (17), Bar and Lenderloo (18), Hendricks and Alexander (19), Schachtschabel (20), Mukherjee (21) and others. Most of these investigations were based upon exchange equilibria, selectivity etc. with simple inorganic ions (22,23). Exchange reactions involving clay minerals with organic compounds have also been established by different scientists (24,25,26,27), but study on the adsorption and desorption of inorganic trivalent complex cations (28, 29) is rather meagre. The physico chemical aspects of many of these reactions, being still unknown in their fundamental details, constitute one of the objectives of the present investigation. The relevant literature has been reviewed below.

Amongst earlier workers, Renold (30) (1936) was perhaps the first to study systematically the exchange behaviour of Cu, Pb, Ni, Ag, Zn, Hg and Cd-permutites and observed an increase

in the exchangeability of these cations in the order shown. Zn was found by him to be as effective as Ba in its exchanging power. Jeny and Engabaly (31) (1943) showed, on the basis of the exchange characteristics of zinc-montmorillonite that Zn ion is partially rendered non-exchangeable by being co-ordinated to the clay mineral. Basu and Mukherjee (32,33) have studied in detail the interaction of montmorillonite clay and trace element cations. They observed the release of the metal ions in the order : $Zn^{2+} > Mn^{2+} > Ni^{2+} = Co^{2+} > Cu^{2+}$ from the clay surface by H^+ . Moreover, quantitative measurements revealed that the amount released was much less than that adsorbed, so that a part of the adsorbed cations was considered to be 'fixed'. Martin and Claesar (34) studied the adsorption of $Co(NH_3)_6Cl_3$ on montmorillonite under various pH conditions. They found that it also permits the estimation of the internal and external exchange capacities. Connel and Maatman (35) from a study of the interactions of the complexes of Co(III) in the pores of silica gel could measure the pore volume of a high surface area silica gel. A continuous extraction of recoil products from the Szilard-Chalmers reaction on hexammine cobaltic ion and tris ethylene diamine cobaltic ion adsorbed on an ion exchange resin has been proposed for obtaining a high yield and specific activity (36). The Szilard-Chalmers reaction is usually studied

batchwise, i.e., some suitable compounds are irradiated with neutrons and then the new species produced by recoil are separated from the parent by some chemical procedure. For the best results in this process the stability of the complex ion towards the eluant should be high and both the resin and the complex ion should be resistant to radiolysis and the radiolytic products from the eluant. A cation exchange resin loaded with hexammine cobalt (III) ion or tris ethylene diamine cobalt (III) ion is suitable for this method, because these complex ions give rise to the bivalent cobaltous ion upon neutron irradiation (37-40). The retention of hexammine cobalt ion is, however, found to be lower than the corresponding value for the tris ethylene diamine cobalt ion using the **dynamic** method (36). Chakravarti and Laitinen (41) studied sorption and desorption of Coen_3Cl_3 on Pyrex glass. The exchange capacity determined from the exchange of $\left[\text{Coen}_3\right]^{3+}$ agreed well with those obtained from the sorption and desorption studies of Cr_{51}^{3+} and Cs_{137}^{+} . Das Kanungo, Chakravarti and Mukherjee (42,43,44) studied adsorption and desorption of hexammine cobalt (III) chloride and tris ethylene diamine cobalt (III) chloride on bentonite and vermiculite and observed that adsorption is according to Langmuir's equation and the desorbing cations arrange themselves according to the lyotrope series. Recently V.J.Thielmann and J.L. McAtee, Jr. (45) investigated the gas chromatographic behaviour of metal-tris (ethylene diamine) complex cation-

exchanged montmorillonites for the separation of oxides of nitrogen and light hydrocarbons and showed that N_2O is involved in an adsorption process on the oxygens of the basal surface of the clay, whereas the light hydrocarbons were most probably involved in a sieving separation. The cation exchange process between tris (ethylene diamine) cobalt (III) and Na^+ on montmorillonite has been studied by M.I. Knudson, Jr. and J.L. McAtee, Jr. (46) and concluded that the exchange of $Co(en)_3^{3+}$ for Na^+ was found to be extremely favourable, with a tendency toward segregation of the two kinds of cations in the mixed clays studied. The studies on exchange characteristics of Zeolites, either synthetic or natural by Barrer (47) and others have received a great deal of attention in recent years. R.M. Barrer and R.P. Townsend (48) studied the exchange of cuprammine and zincammine ions in ammonium forms of clinoptilolite, mordenite and phillipsite in ammoniacal solution, $pH > 10$, and similar investigations are reported on the $[Co(NH_3)_6]^{3+}$ ion at pH values of ~ 5 and ~ 10 in mordenite. Isotherms were too rectangular to calculate values of the standard free energy of exchange, and selectivities were very much higher than for the corresponding aquo ions in mordenite at low pH. Barrer et al concluded that the increase in selectivities observed with mordenite when the cobalt, copper and zinc ions were complexed with ammonia might be rationalised in terms of dielectric theory.

From the study of the reactions between organic compounds and different types of clays made by a large number of workers, the specific nature of clay mineral-organic ion reactions has now been fairly well established. Thus, Smith (49), Giesecking (50) and his Colleagues (51,52) definitely showed from their work with different organic bases and their salts, and with gelatin and albumin solutions, that organic ions enter into cation exchange reactions with clay minerals, particularly montmorillonite. The adsorption of primary n-alcohols (C₂-C₉) from dilute aqueous solutions by calcium and sodium montmorillonite has been studied by German and Harding (53) and they reported that the lower members of the series were adsorbed to an appreciable extent. This behaviour seems to be at variance with the earlier observations of Hoffmann and Brindley (54) who reported that polar compounds with chain lengths less than six units were not measurably adsorbed by calcium montmorillonite. Mac Ewan (55) was the first to study the formation and properties of complexes between ammonium montmorillonite and an homologous series of primary n-alcohols. He observed that except for methanol and ethanol, both of which gave a double layer complex, primary aliphatic alcohols formed single-layer complexes with the alkyl chain lying parallel to the silicate layer. Subsequently, Barshad (56) also reported similar observation for calcium montmorillonite. Brindley and Ray (57) studied

complexes of calcium-montmorillonite with even numbered straight chain alcohols with 2 to 18 carbon atoms and observed four series of basal spacing. They conclude that mono - and bilayers are formed between the unit layers of the clay with the chain of the alcohol parallel to the surface of the clay and suggest that hydrogen bonds are formed between alcoholic hydroxyls and siloxane oxygens. Glaeser (58) and Mac Ewan (55) were among the first to prepare complexes of montmorillonite with ketones. By treating the clay with a large excess of acetone and nitrobenzene, with or without boiling, Mac Ewan was able to form two layer complexes with calcium and ammonium montmorillonite, respectively. Montmorillonite with alkyl ammonium or pyridine-type counterions has only one or two layers of water between the unit layers in aqueous suspension, compared to four and greater than 30, for the analogous calcium and sodium substituted clays, respectively (59-61). It was also observed by Slabaugh and Carter that the hydrophobicity of an organo-clay increases with increasing size of the organic counterion (62). A pyridinium montmorillonite was found to adsorb five times as much benzene vapour as the sodium clay from which it was made (63). Alkyl ammonium montmorillonites swell in most organic solvents (64). The adsorption of amino acids and peptides on H-montmorillonite shows a Langmuir type isotherm; such adsorption occurs primarily through ion exchange of the protonated molecules, although a small amount of the organic molecule

is adsorbed beyond the cation exchange capacity (65). Thermodynamic data show that the negative free energy of exchange of n-alkyl ammonium ions on sodium montmorillonite increases with increasing chain length (66). This indicates not only the clay-cation interaction, but also interactions between the alkyl chains of these cations.

R.K.Schofield (67) observed that the adsorption of quaternary ammonium cations on kaolinite is sufficiently strong to reverse the charge on the particles from negative to positive.

Thorough investigations by other workers (68-70) have also been made specially on the interaction between organic molecules and clays. Our knowledge of the desorption of inorganic cations from the clay surface by organic ions is still meagre. It is in this context that an attempt has been made in the present investigation to study the sorption and desorption characteristics of some trivalent inorganic complex ions by a number of inorganic and organic cations of varying sizes and shapes.

SECTION B

Ion-Exchange Formulations.

A number of approaches (71), both qualitative and quantitative, have been made to understand the equilibria between an ion-exchanger and ions in solution. Experiments were performed in which concentrations of ions were varied, the result suggested an exponential relationship between the ions adsorbed (or desorbed) and concentration of the exchanging ions. Limitations have been tacitly accepted in most mathematical treatments of exchange reactions. Thus (i) the simultaneous presence of both cation and anion exchange reactions in a given system has been **considered** rarely, (ii) the exchange capacity of the cation or anion exchanger has been assumed to be constant, though cases are known where the exchange capacity varies markedly with the pH and the nature of the exchanging ion, (iii) simple stoichiometric equivalence between ions taken up and released is generally assumed to be present; deviations are usually explained in terms of simultaneous adsorption of molecules or formation of complex ions, (iv) finally, perfect reversibility exists in an exchange process under consideration.

On this basis, the Freundlich and Langmuir adsorption equations were proposed. The original form of the Freundlich

equation is

$$\frac{x}{m} = kC^{\frac{1}{p}}$$

where x is the amount adsorbed, m the weight of the material taken and C the equilibrium concentration of the electrolyte; K and 1/p are constants. Wiegner (72) used this equation in 1912. This equation has two weaknesses: (a) it does not flatten out at higher values of C, as a system with a fixed exchange capacity should, (b) it shows that the exchange varies with the variation of the total volume, whereas Wiegner showed that the position of equilibrium was independent of volume. Jenny however, in 1926 overcame the second objection by suggesting the equation:

$$\frac{x}{m} = k \frac{C^{\frac{1}{p}}}{a - C}$$

With the variable character of two constants incorporated in this equation, a good agreement is often obtained with experimental data over a limited range. However, Marshall (73) has shown that it was superior as regards K, but 1/p varied erratically. A similar type of equation to the Langmuir's, with only one constant was proposed by Vageler (74), but it could not account for the variability of equilibrium with volume.

The first use of the law of mass action in formulating ionic exchange as a completely reversible reaction was made by

Ganssen (75), Kerr (76) investigated specific mass action equations for uni-univalent and uni-bivalent exchangers. They were of the forms:

$$\frac{(\bar{X}) \cdot (Y^+)}{(\bar{Y}) \cdot (X^+)} = K_1 ; \quad \frac{(\bar{X})^2 \cdot (Y^{+2})}{(\bar{Y}) \cdot (X^{+2})} = K_2$$

the bar indicates the ion in the exchanger phase.

The constants K_1 and K_2 are termed as selectivity coefficients. The ionic terms represent concentrations in equilibrium solutions. But owing to the lack of knowledge about the activities of the ionic species in the exchanger phase the equilibrium constant could only be evaluated qualitatively or empirically. Bauman (77) and Gregor (78) pointed out the difficulties in terms of swelling and volume change particularly of the resins. The model introduced by Gregor, although thermodynamically less well defined brings out clearly the physical action of the swelling pressure. A more rigorous application of the law of mass action has been made by Boyd and his co-workers (79) in which the "solid solution" idea of Vanselow (80) has been the basis on the assumption that the ion exchange is a "solid solution" process.

In the above formulations all the exchange sites were tacitly assumed to be of equal value. Doubts regarding this were first clearly expressed by Wiegner (81) and his co-workers.

In order to explain some of their experimental results they postulated the existence of loosely and firmly bound ions on the surface of the same exchange substance. Without the necessary information regarding the surface characteristics of the silicates which Wiegner used for his work he had to invoke the idea of the existence of micro pores, edges and cleavages.

Jenny (82) envisaged a kinetic condition on the surface and derived a mass action equation representing the exchange process of univalent ions. This idea was later developed by Davis (83) to multiply charged ions. Krishnamoorthy and Overstreet (84) applied the statistical method as has been used by Fowler (85) and Guggenheim (86) in the case of gas adsorption on solid surface. The attempts to understand ion exchange reactions on the basis of the electrical double layer, as postulated by Mukherjee (87) yields no doubt qualitative results but the concept in many respects, conforms better with observations. He assumed two categories of exchangeable ions, the osmotically active ions which constitute the mobile part of the double layer and the osmotically inactive ones constituting the immobile part of the double layer. The interpretation of the electrochemical properties of clays in terms of these two categories of ions has been in many ways very fruitful. The relationship of crystalline structure of clays, their electrochemical properties and ion-exchange characteristics have been studied with fundamental details by Mukherjee and Mitra (88),

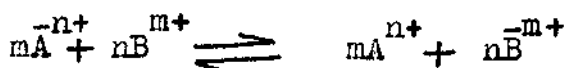
Mitra and Bagchi (39), Ganguly and Mukherjee (90) and Chakravarti (91).

In the present thesis the exchange data obtained with bentonite, vermiculite, laponite, resin and molecular sieve and some inorganic and organic cations have been attempted to fit in the models like (i) Kielland's (92) and (ii) Pauley's (93).

Kielland's Model:

The first attempt to describe the ion-exchange equilibria by a theoretical equation which deviates from the regular pattern was made by Kielland. He introduced the use of solid phase activity coefficients and followed Vanselow (94) in treating the heteroionic form of ion exchanger as a solid solution of the components \bar{A} and \bar{B} , the bars referring to the exchanger phase.

For the exchange of ions of any valency according to the reaction



Kielland's equation takes the general form as

$$\log K = \log K_a - C \left[n - 2n\bar{x}_B + (n-m) \bar{x}_B^2 \right]$$

where K = selectivity coefficient

K_a = thermodynamic equilibrium constant

\bar{x}_B = equivalent ionic fractions of B in the exchanger phase

C = a constant.

Recently this equation has been given a sounder theoretical foundation by Barrer and Falconer (222). They derived the Hielland equation (92) by using statistical mechanical arguments for the special case when both the cations of the exchanging pair are univalent.

Pauley's model:

Pauley has interpreted selectivities in ion exchange equilibria in the language of a very simple model. Its essential feature is the electrostatic attraction between the counterions and the fixed ionic groups. It is assumed that all the counter ions in the ion-exchanger are found at their distance of closest approach to the fixed ionic groups. Writing AR and BR for the pairs of fixed ionic groups and counterions at the distance of closest approach, one can split the exchange of A for B into the two processes;



Coulomb's law (without any correction) leads to the following results for the above processes:

$$\Delta G_1^{\circ} = \int_{a_A^{\circ}}^{\infty} \frac{e^2}{r^2 \epsilon} dr = \frac{e^2}{a_A^{\circ} \epsilon} \dots \dots \dots (3)$$

and
$$\Delta G_2^{\circ} = \int_{\infty}^{a_B^{\circ}} \frac{e^2}{r^2 \epsilon} dr = - \frac{e^2}{a_B^{\circ} \epsilon} \quad \dots (4)$$

where ΔG_1° and ΔG_2° are the free energy changes for the processes (1) and (2); e = electronic charge; ϵ = dielectric constant; r = distance from center of fixed charge; a_i° = distance of closest approach between counter ion i and fixed ionic group. Hence the overall free energy change is

$$\Delta G^{\circ} = \Delta G_1^{\circ} + \Delta G_2^{\circ} = \frac{e^2}{\epsilon} \left(\frac{1}{a_A^{\circ}} - \frac{1}{a_B^{\circ}} \right) \quad \dots (5)$$

and the thermodynamic equilibrium constant K_A^B is

$$\ln K_A^B = - \frac{\Delta G^{\circ}}{kT} = \frac{e^2}{kT\epsilon} \left(\frac{1}{a_B^{\circ}} - \frac{1}{a_A^{\circ}} \right) \quad \dots (6)$$

In the exchanges of various univalent counter ions i for an arbitrary univalent reference ion A , a linear relationship should exist between $\ln K_A^i$ and $1/a_i^{\circ}$. For multivalent ions, the calculation is not quite as simple because assumptions must be made as to how the (univalent) fixed ionic groups and the polyvalent counter ions are paired. The model leads qualitatively to preference of the ion exchanger for counter ion with smaller a° value and higher valency.

SECTION C

Exchange studies and Selectivities of Clay minerals, Resins and Molecular Sieves.

The exchange properties of clay minerals have been thoroughly investigated by a number of workers and their characteristics have been well established. The following generalisations may be made regarding the tendency of a cation to exchange onto a negative surface. There is an increase in exchangeability (a) with decreasing hydrated radius and increasing polarizability, (b) with decreasing ease of cation hydration and (c) with increasing counterion charge. The above criteria however, do not hold good in cases where some specific interactions take place. In accordance with the above observations, the order of increasing preference of alkali metal ions for ion exchange onto montmorillonite (33, 95-115), vermiculite (116) and kaolinite (117, 118) is $Li^+ < Na^+ < K^+ < Rb^+ < Cs^+$. The exchange of ammonium ion is complicated by physical adsorption of ammonia (119) and fixation of ammonium ion (120). It was observed that ammonium ion is held more strongly than sodium ion (121) or even rubidium ion (122).

Similarly, the exchange of hydrogen ion is also complicated due to its attack onto the clay lattice, freeing aluminium

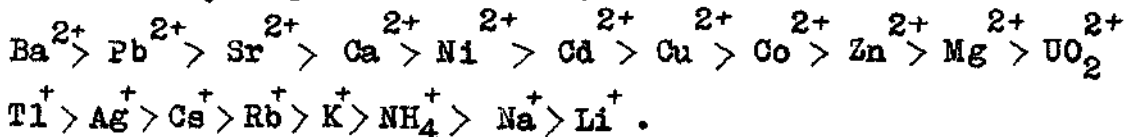
and magnesium ions which may be taken up by the exchange sites (123-130). It was reported that hydrogen ion is apparently preferred over some divalent cations in ion exchange on montmorillonite and clay soils (102, 131, 132), and over caesium on vermiculite (116). Several other investigations deal with the exchangeability of hydrogen ion on clay; the reported relative orders of exchange on montmorillonite are $H^+ < Cs^+$ (108), $K^+ < H^+ < Ca^{2+}$ (133), and $K^+ < NH_4^+ < H^+ < Mg^{2+}$ (33). Under conditions which minimise dissolution of clay by acid attack, the corresponding orders were $H^+ < Na^+ < K^+$ (99), and $Na^+ < H^+ < NH_4^+$ (121). The order of exchange of alkaline earth ions on clays has generally been reported as $Mg^{2+} < Mn^{2+} < Ca^{2+} < Sr^{2+} < Ba^{2+}$ (99, 102, 121, 134-144). The reverse order is sometimes found in vermiculite (141, 145, 146). The orders of exchange of divalent transition metal cations on clays reported are $Mn^{2+} \approx Ni^{2+} \approx Fe^{2+} < Co^{2+} < Zn^{2+} < Cu^{2+}$ (147), $Ca^{2+} < Co(II)^{2+}$ (148) and $Ni^{2+} < Ba^{2+}$ (143). A generalisation may be made from studies comparing the exchange of mono, di and trivalent cations on clays that there is a preference for cations of higher charge (33, 98, 100, 102, 106, 107, 131, 133, 136, 140-142, 148-153), although there is exception to this trend.

The exchange of various alkyl ammonium cations from aqueous solution by sodium laponite has been studied by Vansant and Peeters (154). They observed that the affinity of the clay

for these organic cations was linearly related to the molecular weight, molecular size or chain length of the alkyl ammonium ions. The affinity for the clay increases regularly with increasing chain length of the primary amines. Vansant and Yariv (155) have studied adsorption and oxidation of dimethyl aniline by laponite and the colour reaction mechanism was investigated.

In the usual general-purpose cation exchangers the

selectivity sequence of the most common cations is (156-159):



The sequences of the univalent and bivalent cations overlap in resins of high capacity and moderate and high degree of cross linking. For strong acid resins, H^+ usually falls between Na^+ and Li^+ . For weak-acid resins, the position of H^+ depends on the acid strength of the fixed anionic groups.

The selective uptake of Li^+ , Na^+ , and K^+ by a series of methacrylic acid cation-exchange resins of various divinyl benzene contents was measured by Gregor *et al* (160). The general order of preference was $\text{Li}^+ > \text{Na}^+ > \text{K}^+$. This preference became more marked as the degree of neutralisation of any given resin increased. This resin behaviour was compared by the authors with the association evidenced by the alkali metal acetates.

The ion-exchange properties of the synthetic zeolites X and Y have been investigated by a number of workers. Sherry (161) has determined exchange isotherms for a range of monovalent

inorganic cations in Na-X and Na-Y. His results have led to the conclusion that there is more extensive ion binding in Zeolite X as compared with the type Y which has a higher silica content and a lower exchange capacity. The effect of different silica- to - alumina ratios on cation selectivity has also been observed by Ames (162, 163) for a number of naturally occurring and synthetic zeolites. The crystal structure of zeolites X and Y encloses three different kinds of inter-connecting cavities in which the exchangeable cations are located on different crystallographic sites (164-166). Sherry (161) has interpreted his exchange isotherms in terms of the distribution of Na⁺ ions over different crystallographic sites as revealed by the early x-ray studies of Broussard and Shoemaker (164) and summarised by Breck (166). Since the cavities are entered by windows of definite dimensions, steric and ion sieve effects have been observed in exchanges involving large cations (161,167). The intra crystalline space may be filled by these large cations before complete replacement of the ions initially present, is achieved. Hence, the extent of exchange may also be limited by the space requirement of the cations (167). Barrer et al (167), Theng (168) and Vansant et al (169) studied the exchange adsorption of ammonium and some of its alkyl derivatives in different natural and synthetic zeolites. They observed that for steric reasons, none of the alkyl ammonium ions could effect a complete replacement of the Na⁺ ions initially present in the

zeolite so that the exchange reaction was confined to the large cavities in the crystal. The maximum extent of exchange decreased with an increase in molecular weight and polarizability of the cations but was always below the limit imposed by the space requirement of the respective ions. This decrease was also greater for the di- and tri alkyl derivatives than for the mono alkyl ammonium ions of comparable molecular weight and was more pronounced in X than in Y. The importance of affinity of the cations in determining the upper limit to exchange was further shown by the observation that for a given alkyl ammonium ion this limit decreased with an increase in the affinity of the inorganic ion which it replaced from the zeolite, the order being $\text{Li} > \text{Na} > \text{K} > \text{Ag} > \text{Tl}$ (1). Vansant and Vanhoof (170) recently studied the exchange of alkane diammonium ions in the zeolites X and Y. They concluded that for steric reasons, none of the organic cations could effect a complete replacement of Na ions initially present in the zeolite. For any given alkane diammonium ion the maximum exchange capacity decreases with an increase in the affinity of the cations initially present in the zeolite, the order being $\text{Li}^+ > \text{Na}^+ > \text{K}^+$. Barrer (171), Sherry (161) and Cremers (172) described the exchange equilibria and selectivities of alkali, alkaline earth and rare earth ions for different zeolite ion exchangers. These results have led to the conclusion that there is more extensive ion binding in the X zeolite as compared with the Y type, which has a higher

silica content and a lower total exchange capacity. Barrer & Rees et al (173) have studied the thermo chemistry and thermodynamics of ion exchange with the Na ions in Linde Sieve X. They observed that from the determination of the standard free energy of exchange, ΔG^0 , the following affinity sequence was established : $Li^+ < Na^+ < Ca^{2+}$, $K^+ < Sr^{2+}$, $Cs^+ < Ba^{2+} < Rb^+$.

The ion exchange behaviour of some transition metal ions in synthetic zeolite X and Y was studied by A. Maes et al (174) and they observed that the overall selectivity of both X and Y zeolite for bivalent transition metal ions increases in the order $Ni < Co < Zn < Cu$. In addition to the ion hydration characteristics and ionic radius the exchange is governed by the coordination ability of the transition metal ion.

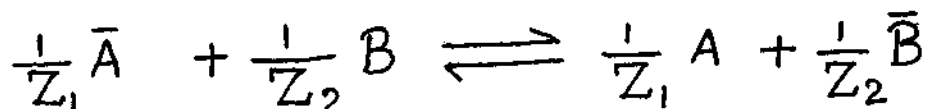
Hence the more important characteristics of exchange studies are:

(i) the observation of the lyotropic series though exceptions are often observed.

(ii) obedience to the Langmuir equation of the data on exchange sorption of large organic molecules especially the dye molecules.

A simple equivalent fraction exchange equation has been proposed to fit in with the exchange data of Na^+ , K^+ and Ca^{2+} for Al^{3+} on bentonite (175) at 0.50 and 1.0(M) external salt concentration.

(iii) Formulation of selectivity coefficient. Exchange measurements can be written in a general way as follows:



(where the bar denotes the species in the clay phase and Z_1 , Z_2 , the valencies of A and B respectively), from which selectivity coefficient is expressed by the equation,

$$K_A^B = \frac{[A]^{\frac{1}{Z_1}} [\bar{B}]^{\frac{1}{Z_2}}}{[\bar{A}]^{\frac{1}{Z_1}} [B]^{\frac{1}{Z_2}}}$$

The selectivity coefficient measurements and obedience to the Langmuir equation are not, however, exclusive of one another.

All these studies are confined to the replacement of one inorganic cation for another. There is very little work on exchange reactions involving two organic cations.

Barrer (176) in a series of papers studied the exchange of one inorganic ion for organic ions. The sorption properties of montmorillonite was seen to change with the adsorption of quaternary ammonium ions $(CH_3)_4N$ and $(C_2H_5)_4N$. The tetramethyl ammonium or tetraethyl ammonium derivative of montmorillonite adsorbs an increased amount of oxygen at 78° and 90°K. Due to the adsorption of the quaternary ammonium ions the lamella of

the clay minerals are opened up and oxygen in increased amounts is adsorbed in the interlamellar space. McAtee (177) treated sodium bentonite with dimethyl benzyl lauryl ammonium (DMBL) ion. It was seen that almost 1:1 replacement of sodium took place upto 90 m.e/100 gm. of dry clay. The clay was thus converted into the DMBL form. This organic - clay derivative was taken in a suspension of a mixture of isopropyl alcohol and isooctane (20% isopropyl alcohol) and different amounts of dimethyl diocta decyl ammonium ion (DMDO) were added. The amounts of DMBL released was then measured using ultraviolet spectroscopy. It was seen that 16% of the DMBL cation was exchanged.

CHAPTER II

SCOPE AND OBJECT OF THE WORK

The process of ion-exchange is one of the mechanisms considered to be operative in the uptake of ions by plant roots from clay minerals possessing ion-exchange properties. The plant tissues contain acid groups, capable of binding and exchanging cations and basic groups with a similar role towards anions. In the process of exchange between the plant and the soil, the clay fraction of the latter plays the most important part. Hence a study of the exchange behaviour of the clay fraction reveals, generally, the exchange characteristics of the soil as a whole.

Although literature records a large amount of work on the adsorption of trace element cations on different clay minerals, such studies with inorganic trivalent complex cations are rather meagre. Sorption and desorption studies with trivalent inorganic ions have been carried out by earlier workers. Not always could satisfactory results be obtained as the experiments were generally carried out either at low pH or at high pH.

At low pH of the medium, the interference of the H^+ in the exchange process can not be ignored, whereas high pH favours the existence of metal hydroxy ions rather than the simple metal ions. So, in most of the studies a proper knowledge

of the interaction of the adsorbate with the adsorbent was lacking. Unless this is known in reasonable details, an appreciation of the adsorption and desorption measurements may be difficult. It was therefore thought that for a systematic study adsorbents with well-defined surface characteristics and adsorbates which are stable over a wide range of pH would be most convenient. The inorganic ion-exchangers used in the present investigation consist of the clay minerals, bentonite, vermiculite and laponite (a synthetic hectorite), molecular sieve 13 X (powder form), and the organic exchanger is the resin Amberlite IRC-50. These provide more or less known features. The adsorbates

(a) Tris (1,2 propane diamine)cobalt(III) chloride
($\text{Co}(\text{pn})_3\text{Cl}_3$),

(b) Tris (1,3 propane diamine) cobalt (III) chloride
($\text{Co}(\text{tn})_3\text{Cl}_3$),

(c) Tris (ethylene diamine) cobalt (III) chloride
($\text{Co}(\text{en})_3\text{Cl}_3$)

and (d) Hexamine Cobalt (III) chloride $\left[\text{Co}(\text{NH}_3)_6\text{Cl}_3 \right]$
are trivalent complex compounds of known structure. From structural considerations, the stability of these complex compounds is also well known.

The interaction of the above exchangers and the trivalent complex cations was therefore investigated under

different conditions and from different angles in order to understand the mechanism of interaction and specificity of the ions. So the main objective of the present investigation is to study in fundamental details the physico-chemical aspects of ion-exchange equilibrium of the trivalent complex cations onto the exchangers mentioned above. For this purpose, adsorption isotherms of different trivalent complex cations on the above adsorbents were studied and the sorption data was analysed in the light of Langmuir equation. For a better understanding of the mechanism of sorption, the cation exchange process between tris (1, 2 propane diamine) cobalt (III) and Na^+ on bentonite was studied by x-ray diffraction, differential thermal analysis, and nitrogen sorption. In order to compare the results of exchange, natural and synthetic clays having different charge densities have also been chosen. The complex ions are suitable from another point of view. Very low concentrations of the ions are measurable spectrophotometrically. This is helpful to study desorption, in particular as well as sorption occurring at very low concentrations. To get a better insight into the nature of adsorbent - adsorbate interaction, relative binding strength, cation specificities etc., the desorption of the trivalent complex cations was studied with different monovalent, bivalent inorganic ions and also alkyl quaternary ammonium ions of varying sizes. Such studies also reveal the extent of extractibility of these ions from the

adsorbent surface from which we can have an idea of the affinity of the ions for the minerals, zeolites and resin surface as well as the relative desorbing abilities of the ions.

It may be mentioned in this connection that although the occurrence of the trivalent cobalt complex in soil is not reported in literature, the presence of cobalt²⁺ is well known and its function as soil nutrient is well established. Cobalt as Co^{3+} forms complex organic compounds. A considerable part of cobalt is dispersed through the soil in the crystal lattices of the aluminosilicates or fixed by the humus of the soil; another part is more loosely bound to the silicates as a result of base exchange. However, the main interest of the present work is restricted particularly to the study of the ion-exchange characteristics of the component of the soil using these complexes.

The studies of the adsorption and desorption onto clay minerals, resins and molecular sieves are useful from other points of view also. As for example, due to their characteristic structures and high exchange capacity, bentonite and vermiculite have recently been used for the decontamination of waste waters from nuclear pile plants. Another important application of these minerals is in the mining practice. The adsorption of gold and other precious metals on these clays especially for exploring the "lost or locked in" gold in barren land

sediments may be recalled. The properties of the synthetic hectorite, laponite XLG inorganic colloids make it suitable for use in a wide range of products viz. cosmetics, deodorants, food, shampoos, soap, suspensions, tablets, toothpaste, veterinary/pharmaceuticals etc., Dispersions of laponite, because of the large surface area and surface activity of the platelets, exhibit higher adsorptive powers. Laponite XLG, which is a synthetic hectorite, was also chosen because it forms stable colloid suspensions suitable for ion-exchange studies.

The study of the use of molecular sieves in adsorption and catalysis has deservedly received a great deal of interest in recent years. So with a view to obtaining insight into factors controlling the exchange, synthetic molecular sieve 13 X has been studied with regard to its cation exchange behaviour with the trivalent complex cations mentioned earlier. Also in view of the recent wide spread use of the clay, resin and molecular sieve complexes with these trivalent complex cations in gas chromatography as column packing material for the separation of light hydrocarbons and oxides of nitrogen and in Szilard Chalmers reaction for obtaining high yield and specific activity, a detailed investigation of the sorption and desorption behaviour of the amine, ethylene diamine and propylene diamine (1,2 and 1,3) complexes of Co(III) on bentonite, vermiculite, laponite and also on well defined ion exchangers

like a weak cation exchange resin, Amberlite IRC-50 and molecular sieve 13 X has been undertaken. Apart from various practical applications, the experimental data may also be used for testing and developing different existing theoretical models and equations for describing ion-exchange equilibria.

CHAPTER III

EXPERIMENTAL

Silicate minerals, used as adsorbents in the investigation are described below in Table 1.

Table 1

Sample	Description	Total Exchange capacity (m.e./100 gm) *	Source
1. Bentonite	Light grey powder	95	Evans Medical Ltd, Liverpool, England.
2. Vermiculite	Grey-green powder (Allentype)	112	Supplied kindly by "Zonolite", South Carolina, U.S.A., as gift.
3. Laponite XLG	White powder	**	Supplied kindly by Laporte Industries Limited, England, as gift.

The clay fractions of minerals 1,2 having particle size $< 2.0\mu$ were isolated by the usual method of grinding, dispersion and fractionation by sedimentation. The fractions so

* Determined by $\text{BaCl}_2 - \text{Ba}(\text{OH})_2$ method.

** Not determined by $\text{BaCl}_2 - \text{Ba}(\text{OH})_2$ method.

collected were then treated several times with dilute HCl and after removal of acid warmed with 6% H_2O_2 in an attempt to remove any organic matter present. The excess of H_2O_2 was decomposed by heating the samples over a water bath. The clay suspension was then converted into H-form by passing through a H^+ saturated resin (Dowex 50W x 8) and subsequently an OH^- saturated resin column (Dowex 2 x 8). The process was repeated till the conversion was complete. The resulting exchangers in the H-forms were then used for adsorption and desorption studies. The total exchange capacity values of the samples were found to be in order.

Na-clays were prepared by passing an approximately 2 percent suspension of the clay through an ion exchange column containing Dowex 50W x 8 in the sodium form. In order to assure complete ion exchange to the Na-form, the clay slurry was passed through the column twice. Na-clays ($pH \approx 7$) so formed were used for adsorption and desorption studies.

Preparation of Na-Laponite : The synthetic hectorite clay used in this investigation was Na-Laponite XLG. To ensure complete saturation with sodium, the Na-Laponite was brought into dialysis bags and washed several times with 1 N NaCl solutions, before dialysing against distilled water until free of chloride.

Adsorption Studies

10 ml. portions of the suspensions, of known clay-content, were pipetted into separate stoppered pyrex bottles and $\text{Co}(\text{pn}_3\text{Cl}_3)^*$ and $\text{Co}(\text{tn}_3\text{Cl}_3)^{**}$ solutions, of ~~known~~ concentration, were added in increasing amounts. The total volumes were brought to 15 ml. by quantitatively adding the necessary amount of distilled water. The bottles, with their contents, were shaken for one hour and allowed to stand a minimum of 18 hours to attain exchange equilibrium. Experiments at several days equilibration produced the same results indicating 18 hours were sufficient for equilibrium. The resulting exchange clay was then centrifuged (10,000 r.p.m.) for 10 minutes or so and the supernatant liquids were analysed colorimetrically using Beckman DU-2 Spectrophotometer. From the difference between the initial concentration and that of the equilibrium concentration, measured above, the amount adsorbed was determined. All operations were carried out in a constant temperature room.

Exploratory experiments revealed that the adsorption of $\text{Co}(\text{pn}_3\text{Cl}_3)$ and $\text{Co}(\text{tn}_3\text{Cl}_3)$ on clays varies with pH.

The clay contents of the suspensions were determined by evaporating a known volume to dryness at 105-110°C in an air oven.

* Abbreviations for Tris (1,2 propane diamine) Cobalt (III) Chloride.

** Abbreviations for Tris (1,3 propane diamine) Cobalt (III) Chloride or Tris trimethylene diamine Cobaltic Chloride.

The contents expressed in gms/100 ml vary slightly with the systems used and are given in Table 2.

Table 2

Sample	For $\text{Co}(\text{NO}_3)_3$ sorption	For $\text{Co}(\text{NO}_3)_3$ sorption
H-bentonite	1.00	1.00
Na-bentonite	1.0734	1.0734
H-vermiculite	0.819	0.819
Na-vermiculite	1.82	1.82
Na-laponite	1.30	1.30

In order to study the dependence of adsorption on pH, the following procedure was adopted. To mixtures of H-bentonite and $\text{Co}(\text{NO}_3)_3$ or $\text{Co}(\text{NO}_3)_3$ containing known amounts of each were added varying amounts of NaOH in order to bring them to different pH values. The amounts of $\text{Co}(\text{NO}_3)_3$ or $\text{Co}(\text{NO}_3)_3$ adsorbed after equilibrium were then determined by absorbance measurements as above.

Desorption Studies.

For studying desorption the mineral suspensions were mixed with $\text{Co}(\text{NO}_3)_3$ or $\text{Co}(\text{NO}_3)_3$ solution in concentrations approximately three times the cec, shaken for two hours and

allowed to equilibrate overnight in thermostat. After 24 hr the excess salt was washed out with distilled water by repeated centrifugation of the clay-complex till the leachate gave zero optical density. The resulting clay was then resuspended in distilled water and used for desorption studies. The percentage colloid content of the suspension was determined by drying a known amount of it at 105-110°C to constant weights, and are given in Table 3.

Table 3

Sample	H-Copn ₃ -Clay	Na-Copn ₃ -Clay	H-Co ₂ n ₃ -Clay	Na-Co ₂ n ₃ -Clay
Bentonite	1.493	1.334 & 1.59	1.638	2.119 & 1.80
Vermiculite	-	1.771	-	2.047
Laponite	-	1.506	-	2.182

For the purpose of desorption studies 10 ml. portions of the suspension were taken in a number of pyrex bottles and varying amounts of different electrolytes were added. The total volumes were adjusted to 15 ml by quantitatively adding requisite amounts of distilled water. The bottles, with their contents, were shaken for 2 hours and kept overnight to equilibrate.

Preliminary studies showed that this period was sufficient for the purpose. The mixtures were centrifuged (10,000 r.p.m.) for 15 minutes or so and the $\text{Co}(\text{pn}_3\text{Cl}_3)$ or $\text{Co}(\text{tn}_3\text{Cl}_3)$ content of the clear centrifugates was estimated colorimetrically as described earlier.

Tris (ethylene diamine) cobalt(III) chloride ($\text{Co}(\text{en}_3\text{Cl}_3)$) was prepared by the method of Jorgenson (178) from ethylene diamine and cobalt chloride by aerial oxidation and crystallised three times from alcohol-water medium.

Similarly, hexamine cobalt (III) chloride $\text{Co}(\text{NH}_3)_6\text{Cl}_3$ was prepared by the method of Fernelius (179) by vigorous aerial oxidation from ammonium chloride, ammonia and cobalt chloride in the presence of activated carbon. It was also crystallised 2-3 times from water before use.

Tris (1,2 propane diamine) Cobalt (III) Chloride ($\text{Co}(\text{pn}_3\text{Cl}_3)$) was prepared by the method of Jenkins and Monk (180) from pure propylene diamine (1,2 propane diamine) (K.L., England) partly neutralised with HCl and cobalt chloride by bubbling oxygen. It was crystallised from alcohol-water medium.

Tris (1,3 propane diamine) cobalt (III) chloride ($\text{Co}(\text{tn}_3\text{Cl}_3)$) was prepared following the method of Bailar, Jr. and work (181) by vigorous aerial oxidation from trimethylene diamine (1,3 propane diamine) (Fluka), amine hydrochloride and cobalt chloride. It was then crystallised from alcohol-water medium.

NaCl, KCl, NH₄Cl, RbCl, CsCl were of E.Merck quality, cetyl pyridinium chloride (CPCL), cetyl trimethyl ammonium bromide (CTABr) were of BDH-AR quality. Decyl trimethyl ammonium bromide (DTABr), do-decyl trimethyl ammonium bromide (DDTABr) were obtained through the courtesy of Prof. Masaru Mitsuishi*. Ethane diammonium hydrochloride (EDA) was obtained from "Chempure", India, and 1,3 propane diammonium hydrochloride (PrDA) was prepared in the laboratory. Standard solutions of these electrolytes were prepared by direct weighing of vacuum dried salts. LiCl was of BDH-AR quality and (CH₃)₄NCl, (C₂H₅)₄NBr, (C₃H₇)₄NI, (C₄H₉)₄NBr were "Fluka" products. These were standardised by titration with AgNO₃ of E.Merck quality using potassium chromate as indicator. MgCl₂ and CaCl₂ solutions, prepared with reagent quality samples, were standardised by EDTA titration, using Eriochrome Black T as indicator. The concentrations of SrCl₂ and BaCl₂ prepared with A.R. quality samples were determined by precipitating as sulphates. A.R. grade HCl solution was standardised by NaOH and oxalic acid of the same quality.

* Faculty of Textile Science and Technology, Shinshu University, Tokida, Japan.

Preparation of $\text{Co}(\text{pn})_3^{3+}$ exchanged clay and $\text{Co}(\text{tn})_3^{3+}$ exchanged clay samples for x-ray diffraction, differential thermal analysis and nitrogen sorption at 78°K .

For preparing clay-Co(III) complex at different percentages of saturation, appropriate amounts of standard $\text{Co}(\text{pn})_3\text{Cl}_3$ or $\text{Co}(\text{tn})_3\text{Cl}_3$ solutions were added to the H-clay or Wa-clay suspension, and after equilibration, centrifuged several times to wash off the excess salts. Few drops of each clay dispersion were taken prior to the last centrifugation and placed onto microscope slides. The samples were then allowed to air dry on the slides and placed in a desiccator over saturated $\text{Ca}(\text{NO}_3)_2$ (51% r.h.), until needed for x-ray diffraction. Two samples were also placed in a desiccator over saturated $\text{CuSO}_4 \cdot 5\text{H}_2\text{O}$ (98% r.h.) for x-ray diffraction. After the final washing, the clay samples were dried overnight in an air oven at 50°C , then lightly ground with a mortar and pestle and stored in a 51 percent r.h. atmosphere. But the samples for D.T.A analysis were stored over concentrated sulphuric acid for at least 20 hours prior to analysis. The 80+ mesh ^{powder} was used for D.T.A. and N_2 sorption studies.

The x-ray diffraction of oriented films of clay on glass slides were carried out at the Department of Metallurgy, Indian

Institute of Technology, Madras. The samples were run at the rate of $\frac{1^\circ}{4}$ per minute. The radiation used is CuK_α at 30 Kv/20 MA, with the Philips X-ray generator PW 1140. The charts were recorded using a proportional counter and a pulse height analyser. The chart speed employed is 20 mm/min. However, a few samples in the form of powder (80+ mesh) were also used for x-ray studies. X-ray diffraction patterns of the powder samples were taken by Guinier Camera at the Fertilizer (Planning and Development) India Ltd., Sindri. The radiation used was CuK_α and the tube voltage and current were maintained at 40 Kv and 22 mA respectively. All the samples were exposed for 4 hours and after developing, only the basal reflection were scanned at the rate of $\frac{1}{4}$ degree per minute. Diffraction pattern of two samples (100% $\text{Co}(\text{OH})_2$ -bentonite and 100% $\text{Co}(\text{OH})_2$ -bentonite) were also taken by high temperature Guinier Camera at 250°C.

The DTA apparatus used to record the DTA spectra was "Derivatograph", manufacturer: MOM Budapest. Type: Erdey, Paulik. The differential thermal analysis was done at Regional Research Laboratory, Jorhat, Assam, India.

B.E.T. experiments were done at the Fertilizer (P & D) India Limited, Sindri, by nitrogen adsorption at liquid nitrogen temperature in all glass BET sorption apparatus. The degassing temperature and time maintained were 50°C and 16 hours respectively.

CHAPTER IV

Sorption and Desorption of $[\text{Co}(\text{pn}_3)]^{3+}$ and $[\text{Co}(\text{tn}_3)]^{3+}$ on Bentonite - System.

A bentonite clay has been found expedient for the investigations on sorption and desorption of complex ions viz. $[\text{Co}(\text{pn}_3)]^{3+}$ and $[\text{Co}(\text{tn}_3)]^{3+}$ due to its high cation exchange capacity and other interesting surface properties it exhibits.

The sorption and desorption characteristics of $[\text{Co}(\text{pn}_3)]^{3+}$ and $[\text{Co}(\text{tn}_3)]^{3+}$ on H-bentonite and Na-bentonite are discussed below on the basis of experimental results obtained by Beckman DU-2 Spectrophotometer, X-ray diffraction, differential thermal analysis and nitrogen sorption at 78°K. The characteristics of sorption are presented in Sec. A and those of desorption in Sec. B.

SECTION A

Studies on Sorption

Sorption of $[\text{Co}(\text{pnc}_3)]^{3+}$ on H-bentonite.

The adsorption isotherm of $\text{Co}(\text{pnc}_3)\text{Cl}_3$ on H-bentonite is shown in Fig. 1(a). The adsorption data are seen to fit into the Langmuir adsorption equation. Accordingly, the plot of C/X Vs. C , where C is the equilibrium concentration of $\text{Co}(\text{pnc}_3)\text{Cl}_3$ and X is the amount adsorbed per 100 gm. of adsorbent, yields a good straight line [Fig. 1(a)]. From the slope of the line, the value of V_m (the amount required to form a complete monolayer) is found to be 83.3 m.e./100 gm as against the c.e.c of bentonite (95 me/100 gm) and the maximum of the sorption isotherm (83 me/100 gm) indicating here a monomolecular adsorption. It may be noted that the pH of the clay suspension before and after adsorption was 3.6 and 2.6 respectively. The sorption at low pH probably corresponds to exchange due to isomorphous lattice replacement. This behaviour can also find an explanation in the fact that during the interaction of $\text{Co}(\text{III})$ complex with H-bentonite, only the negatively charged flat surface electrical diffuse layer is available for the adsorption of $\text{Co}(\text{III})$ complex cations and the positive diffuse double layer on the edges of the clay (182) at low pH values remains ineffective for exchange.

Sorption of $[\text{Co}(\text{NH}_3)_6]^{3+}$ on bentonite at different pH.

Adsorption of $\text{Co}(\text{NH}_3)_6\text{Cl}_3$ at different pH [Fig. 1(b)] shows that within the range of pH 2.6 to 10.4 two distinct stages of adsorption can be recognised : 33 to 106 me (difference 23 me) and again from 106 to 120 me (difference 14 me). The value of 33 me probably corresponds to change due to isomorphous lattice replacement or what has been termed 'internal acidity' as distinct from 'peripheric acidity' which refers to the last two stages mentioned above.

According to one point of view (183) the stages correspond respectively to the adsorption at edges (23 m.e) primarily caused by Si-O sites, and at the lateral surface (14 m.e.) constituted of Al-O adsorption sites. The other point of view has been expressed by Martin and Glaeser (34) who observed similar stages of adsorption with hexamine cobaltic chloride. According to them at high pH the adsorbate ions are no longer $\text{Co}(\text{NH}_3)_6^{3+}$ but may be $[\text{Co}(\text{NH}_3)_6(\text{OH})]^{2+}$ or $[\text{Co}(\text{NH}_3)_6(\text{OH})_2]^+$ or both, depending on the pH. A similar postulation of $[\text{Co}(\text{NH}_3)_6(\text{OH})]^{2+}$ or $[\text{Co}(\text{NH}_3)_6(\text{OH})_2]^+$ may be made about the adsorbate ions at higher pH in the present case.

This behaviour may also be explained by assuming that during the interaction of Co(III) complex ion with H-bentonite, only the negatively charged flat surface electrical diffuse layer is available for the adsorption of Co(III) complex cations and the positive diffuse double layer on the edges of the clay

at low pH values remains ineffective for exchange. But as the pH of the clay suspension is increased, the sign of the diffuse double layer at the edge is reversed and the adsorption of Co(III) complex cations at the edges of the clay can take place.

X-ray diffraction studies:

X-ray diffraction data were obtained for each of the partially exchanged $\left[\text{Co}(\text{NO}_3)_3 \right]^{3+}$ clays. The results are given in Fig. 2. Each sample, prepared as described earlier, was allowed to equilibrate in a desiccator over saturated $\text{Ca}(\text{NO}_3)_2$ (51% r.h.) for at least 20 hours prior to analysis. The X-ray data (Fig. 2) shows that as $\left[\text{Co}(\text{NO}_3)_3 \right]^{3+}$ ion is added, even in small amounts, the d_{001} -spacing begins to increase indicating some degree of interlamellar exchange. It appears, that instead of complete randomness of interlayers of cations, there is a strong tendency toward segregation of $\left[\text{Co}(\text{NO}_3)_3 \right]^{3+}$ and H^+ in bentonite into the separate interlayers in the mixed clays. The d_{001} of the H-bentonite was found to be 12.72 Å and those of the 20 percent, 60 percent and 100 percent saturated $\left[\text{Co}(\text{NO}_3)_3 \right]^{3+}$ clay, are 13.32 Å, 14.41 Å and 14.85 Å respectively.

Differential thermal analysis (D.T.A) studies:

The 20 and 100 percent $\left[\text{Co}(\text{NO}_3)_3 \right]^{3+}$ exchanged clay samples prepared as described earlier were stored over concentrated sulphuric acid for 20 hours prior to analysis. The results

are shown in Fig. 3. The D.T.A studies were carried out in an attempt to determine the type of interaction between $\left[\text{Copn}_3 \right]^{3+}$ complex ion and the clay surface or clay edges. Figure 3 shows the D.T.A. results for the $\text{Copn}_3^{3+} - \text{H}^+$ bentonite complexes run under conditions of air flow and all heating rates were 10°C per minute. The strong endothermic peak at approximately 150°C was related to the adsorbed water on the clay complex. Following the water loss peak there appeared an exothermic peak at approximately 240°C which corresponds to the melting point of the $\left[\text{Copn}_3 \right]^{3+}$. This was then followed by a larger and broader exothermic peak at about 525°C which was probably due to the pyrolysis or decomposition of the organic portion of the $\left[\text{Copn}_3 \right]^{3+}$ with a large tailing upto the maximum temperature of about 660°C . But the decreasing 240°C and 525°C exothermic peaks are larger for 100 percent $\left[\text{Copn}_3 \right]^{3+}$ exchanged bentonite than those for the 20 percent $\left[\text{Copn}_3 \right]^{3+}$ exchanged H-bentonite. It might be noted that the bentonite used in this work has a very strong dehydroxylation endothermic peak at approximately 665°C . The dehydroxylation endothermic peak was also observed at about 660°C in the 20 percent (weak peak) and 100 percent (strong peak) exchange capacity curves.

So the DTA curve for the 20 percent exchanged sample was significantly different from that of 100 percent exchanged sample. This observation may also relate to the change in the

environment of a $\left[\text{Co}(\text{OH})_3 \right]^{3+}$ cation as the occupancy of the clay exchange sites by $\left[\text{Co}(\text{OH})_3 \right]^{3+}$ increases.

Nitrogen sorption at 78°K:

As shown by Barrer et al (223), gas sorption can be, under the proper conditions, a valuable method for studying partial cation exchange in montmorillonites. Knudson and Mc Atee (1973) (184) have also observed that interlamellar nitrogen penetration readily occurs for a tris (ethylene diamine) cobalt (III) -montmorillonite. Therefore, the partially exchanged $\text{Co}(\text{OH})_3^{3+}$ clays were studied by the sorption technique. The sorption isotherms obtained in the relative pressure range $P/P_0 = 0.05-0.25$ were found to describe either B.E.T., Type II isotherm or the B.E.T., Type I (Langmuir) isotherm. The B.E.T. equation for type II adsorption assumes adsorption in multilayers. It has been shown that this model is a good approximation when applied at low relative pressure (approximately $P/P_0 = 0.05 - 0.30$) and when adsorption is occurring on predominantly open surfaces where multilayer formation can occur freely.

The B.E.T. equation for the Type I isotherm differs from Type II in that it assumes that only one layer of sorbate is present. Typical plots for the mixed $\text{Co}(\text{OH})_3^{3+} - \text{H}^+$ bentonites are shown in the Figs. 5-9.

The relative pressure range used in this investigation ($0.05 \leq P/P_0 \leq 0.25$) gave a clear distinction between B.E.T., Type II and B.E.T., Type I adsorption. This distinction became quite clear when the adsorption data were plotted in the linear forms of the Types II and I equations. With both plots on the same graph, a direct comparison of the fit of the data to the two equations could be made. The surface areas were calculated from the equation which gave the more linear plot (B.E.T., Type II, for the H-bentonite, 12.5% and 25% $\left[\text{Co}(\text{pn})_3 \right]^{3+}$ bentonite clays and the Langmuir equation for the others). Figure 4 is a plot of monolayer volume (STP) of sorbed nitrogen versus percent $\left[\text{Co}(\text{pn})_3 \right]^{3+}$ exchange, for mixed H- $\text{Co}(\text{pn})_3^{3+}$ -bentonite. Several isotherms were drawn for the 0%, 12.5%, 25%, 50% and 100% (Figs. 5,6,7,8 and 9) exchanged $\text{Co}(\text{pn})_3^{3+}$ clays to ensure reproducibility. Interestingly it is observed that at first there is a gradual decrease in nitrogen sorption with increase in $\left[\text{Co}(\text{pn})_3 \right]^{3+}$ content, reaching a minimum value at about 17% of the $\left[\text{Co}(\text{pn})_3 \right]^{3+}$ saturation of the H-clay and then nitrogen sorption increases almost linearly with $\text{Co}(\text{pn})_3^{3+}$ content in the clay. Thus there seems to have been at least two different processes involved in the interaction of $\text{Co}(\text{pn})_3^{3+}$ with the clay which influence the nitrogen sorption in this way. The increase in surface area would be expected if, as also implied by the X-ray diffraction data (the d_{001} basal spacing of the H-bentonite

was found to be 12.72 Å while that of the saturated $\text{Co}(\text{pn})_3^{3+}$ -clay was 14.85 Å), there is a strong tendency toward segregation of $\text{Co}(\text{pn})_3^{3+}$ and H^+ cations into separate interlayers in the mixed clays. As more $\text{Co}(\text{pn})_3^{3+}$ is added to the clay, more interlayers would be opened up for nitrogen penetration and the nitrogen sorption capacity of the H-clay should increase accordingly. This mechanism, however, does not explain the initial decrease in nitrogen sorption in Fig. 4. The results may be explained by assuming two kinds of exchange sites on the clay that $\text{Co}(\text{pn})_3^{3+}$ can occupy and the exchange occurs on the clay edges first and then on the flat surfaces. The decrease in surface area could be caused due to the covering of the edge area by edge to edge ^{and/or face to face} binding of the clay platelets by the multivalent $\text{Co}(\text{pn})_3^{3+}$ and the net result of larger, denser aggregates would, however, be a decrease in measured surface area. From this figure it also appears that a large amount of micropore was present, but relatively little multilayer sorption was occurring. This conclusion is supported by the linear Langmuir plots obtained for 50 percent exchanged $\text{Co}(\text{pn})_3^{3+}$ clay and higher.

Figure 5 shows the comparative plots of the nitrogen sorption data obtained for the hydrogen bentonite used in this work. B.E.T., Type II equation gave the linear plot and was therefore assumed to define the adsorption process. So the predominant process for nitrogen sorption on H-bentonite was

thus concluded to be external or multilayer sorption (i.e. not on the interlamellar surfaces). This conclusion is supported by complete N₂ isotherm studies by several workers [Barrer and MacLeod, (224); Brooks, (225); Aylmore and Quirk, (226)].

Figure 6 shows the comparative plots of the nitrogen sorption data obtained for the 12.5 percent exchanged Co(pn)₃³⁺ clay. In this case also B.E.T., Type II plot is linear and hence the predominance of external or multilayer sorption for the 12.5 percent exchanged Co(pn)₃³⁺ clay.

Figure 7 illustrates the comparative plots for nitrogen sorption on 25 percent exchanged Co(pn)₃³⁺ clay. The plot is neither linear B.E.T., Type II, nor linear Langmuir. This isotherm could have arisen from nitrogen sorption that was neither predominately multilayer nor predominantly microporous.

Figure 8 compares Type I and Type II plots for nitrogen adsorption on 50 percent Co(pn)₃³⁺ exchanged H-bentonite. As in the case of the fully exchanged Co(pn)₃³⁺ clay (Fig. 9), Type I plot (i.e. Langmuir plot) is linear, while the Type II plot turns upward. It is concluded, therefore, that predominantly interlamellar sorption occurs for the Co(pn)₃³⁺ - clay.

Adsorption isotherm of $\left[\text{COPn}_3 \right]^{3+}$ on Na-bentonite at pH 7.

The adsorption isotherm of Copn₃Cl₃ on bentonite at pH 7 and the corresponding reciprocal graph are shown in Fig. 18. They are characteristic of the Langmuir type of isotherm.

The value of V_m calculated from the slope of the linear graph is equal to 95.23 m.e. and compares well with the maximum of the ~~isotherm~~ which is 96 m.e.

X-ray diffraction studies on $\text{Co}(\text{pn})_3^{3+}$ exchanged Na-bentonite.

X-ray diffraction data were obtained for each of the partially exchanged $\text{Co}(\text{pn})_3^{3+}$ clays. The results are given in Figs. 19(a) and 19(b). The samples were prepared as described earlier (P 43). The X-ray data [Figs. 19(a) and 19(b)] shows that as $\text{Co}(\text{pn})_3^{3+}$ ion is added in increasing amounts, the d_{001} - spacing begins to increase thereby indicating some degree of interlamellar exchange. There is a strong tendency toward segregation of $\text{Co}(\text{pn})_3^{3+}$ and Na^+ ions into the separate interlayers in the mixed clays. The d_{001} of the Na-bentonite was found to be 12.2 \AA and the d_{001} values of 20 percent, 55 percent, 75 percent, 85 percent and 100 percent exchanged $\text{Co}(\text{pn})_3^{3+}$ clays are 13 \AA , 14 \AA , 14.7 \AA , 14.9 \AA and 15 \AA respectively.

In order to investigate the effect of humidity on d_{001} - spacing of 100% $\text{Co}(\text{pn})_3^{3+}$ exchanged Na-bentonite, the clay film on glass slides were kept in a desiccator over saturated $\text{CuSO}_4 \cdot 5\text{H}_2\text{O}$ (98% r.h.) to equilibrate and the X-ray diffraction pattern was recorded. The d_{001} basal spacing was found to be 15 \AA and the same as in the case of 100% $\text{Co}(\text{pn})_3^{3+}$

exchanged clay kept over saturated $\text{Ca}(\text{NO}_3)_2$ (51% r.h.). This clearly demonstrates that the adsorption of $\text{Co}(\text{pn})_3^{3+}$ in bentonite suppresses the effect of swelling or expansion in moisture i.e. a water-proof character is developed. A similar observation was reported by Martin and Glaesser (34) with $\text{Co}(\text{NH}_3)_6$ - montmorillonite.

X-ray diffraction analysis of 100% $\text{Co}(\text{pn})_3^{3+}$ -bentonite were also taken by high temperature Guinier Camera at 250°C and its d_{001} - spacing was found to be 14.5 \AA [Fig. 19(b)]. So there is a decrease of 0.5 \AA in the d_{001} -spacing. This decrease is probably due to melting point of $\text{Co}(\text{pn})_3^{3+}$.

Differential thermal analysis studies on $\text{Co}(\text{pn})_3^{3+}$ exchanged Na-bentonite.

The 0%, 20%, 55% and 100% $\text{Co}(\text{pn})_3^{3+}$ exchanged clay samples were prepared and stored over concentrated sulphuric acid as described earlier (P 43). The results are shown in Fig. 20. D.T.A. curves were obtained under flowing - air condition for these bentonite complexes and all heating rates were 10°C per minute.

It will be noted that a strong endothermic peak at approximately 120°C was obtained which was probably due to adsorbed water. This was followed by a weaker exothermic peak at approximately 250°C except in the 20% $\text{Co}(\text{pn})_3^{3+}$ exchanged sample

which was then followed by a broad exothermic peak starting at about 500°C and ending at approximately 650°C. The first exothermic peak at about 250°C may be related to the melting point of the $\text{Co}(\text{pn})_3^{3+}$. The second exothermic peak was probably due to the decomposition of the organic portion of the $\text{Co}(\text{pn})_3^{3+}$. Hence in the D.T.A. curves there exists very little difference between 55% and 100% $\text{Co}(\text{pn})_3^{3+}$ exchanged Na-bentonite but the D.T.A. curve for 20% exchanged sample was significantly different from the former curves. As stated before with H-bentonite (P49) this observation may also relate to the change in the environment of a $\text{Co}(\text{pn})_3^{3+}$ cation as the occupancy of the clay exchange sites by $\text{Co}(\text{pn})_3^{3+}$ increases. However, the differences in the D.T.A. curves could also be due to higher local concentrations of decomposition gases for the higher percent $\text{Co}(\text{pn})_3^{3+}$ samples.

B.E.T. surface area studies on $\text{Co}(\text{pn})_3^{3+}$ exchanged Na-bentonite.

The sorption isotherms obtained in the relative pressure range used in this investigation ($0.05 \leq P/P_0 \leq 0.25$) were found to describe either B.E.T., Type II isotherm or the B.E.T., Type I (Langmuir) isotherm. Figures 21, 22, 23 and 24 show the comparative plots of the nitrogen sorption data obtained for the sodium bentonite systems used in this investigation. The Type II equation gave the linear plot and it was concluded that there was predominance of external or multilayer sorption

for the sodium bentonite (Fig. 21). The ideal surface area of montmorillonite, both external and interlamellar, is roughly $750 \text{ m}^2/\text{gm}$ (Van Olphen, 227) while in this investigation only $57.58 \text{ m}^2/\text{gm}$ could be measured by nitrogen sorption. Such low value of surface area of Na-bentonite measured by nitrogen sorption has also been observed by Knudson and Mc Atee, Jr. (1974) (185). The surface areas were calculated from the equation which gave the more linear plot (B.S.T., Type II, for the Na-bentonite, 12% and 20% $\text{Co}(\text{pn})_3^{3+}$ -bentonite and the Langmuir equation for greater exchange).

The comparative nitrogen sorption plots for the 12% exchanged $\text{Co}(\text{pn})_3^{3+}$ -clays are shown in Fig. 22. The linearity of the Type II plot and the low surface area ($43.34 \text{ m}^2/\text{gm}$) provide evidence of no significant interlamellar sorption.

Comparative plots of the nitrogen sorption data for 20% exchanged $\text{Co}(\text{pn})_3^{3+}$ -clay are given in Fig. 23. The plot is neither linear B.S.T., Type II, nor linear Langmuir. So it was concluded that nitrogen sorption in this case was neither predominantly multilayer nor predominantly interlamellar.

Fig. 24 illustrates the comparative plots for 45% $\text{Co}(\text{pn})_3^{3+}$ exchanged Na-bentonite. Interlamellar sorption is implied by the linear Type I plot (i.e. Langmuir plot). Similar are the plots for 60% and 100% exchanged clays.

Fig. 25 is a plot of monolayer volume (STP) of sorbed nitrogen versus percent $\text{Co}(\text{pn})_3^{3+}$ exchange, for mixed Na- $\text{Co}(\text{pn})_3^{3+}$ -bentonite. As in the case of H-bentonite, it is also observed that the B.E.T. nitrogen surface area gradually decreases first, appears to reach a minimum at about 15% exchange, then the surface area increases almost linearly with $\text{Co}(\text{pn})_3^{3+}$ content in the clay. The increase in surface area would be expected if, as implied by the X-ray diffraction data, there is a strong tendency toward segregation of $\text{Co}(\text{pn})_3^{3+}$ and Na^+ cations into separate interlayers in the mixed clays. As explained in the case of similar studies with H-bentonite (P 52), the decrease in surface area may be explained by assuming two kinds of exchange sites on the clay that $\text{Co}(\text{pn})_3^{3+}$ can occupy and the exchange occurs on the clay edges first and then on the flat surfaces. The decrease in surface area could be caused due to the covering of the edge area by edge to edge ^{and/or face to face} binding of the clay platelets by the multivalent $\text{Co}(\text{pn})_3^{3+}$ and the resulting larger, denser aggregates would, have a corresponding lower external surface area.

Sorption of $\text{Co}(\text{pn})_3^{3+}$ on H-bentonite.

The adsorption isotherm of $\text{Co}(\text{pn})_3\text{Cl}_3$ on H-bentonite is shown in Fig. 38(a). The isotherm is similar to that observed earlier and conforms to the Langmuir type. Both V_m (= 94 m.e.)

and the amount corresponding to maximum adsorption (= 92.5 m.e.) are slightly less than the exchange capacity of the clay mineral, namely 95 m.e. The pH of the solution before and after adsorption varied between 3.3 and 3.4.

Adsorption of $\left[\text{Co}(\text{tn})_3 \right]^{3+}$ on H-bentonite at different pH.

It is apparent from Fig. 38(b) that as the pH decreases below 2.3 the adsorption of $\left[\text{Co}(\text{tn})_3 \right]^{3+}$ also decreases, but above pH 3.4, the adsorption increases upto pH 10.2. It may be noted that within the range of pH 3 to 10.2 two stages of adsorption can be recognised (Fig. 38) : 93 to 123 m.e. (difference = 25 m.e.) and again from 123 to 132 m.e. (difference = 9 m.e.). The results are similar to those as observed earlier with $\text{Co}(\text{pn})_3^{3+}$ (P 47) and may be explained in the same manner.

X-ray diffraction studies.

The partially exchanged H- $\text{Co}(\text{tn})_3$ -bentonite samples were prepared as described earlier (P 43). The X-ray data (Fig. 39) reveal that the d_{001} spacing begins to increase on gradual addition of $\text{Co}(\text{tn})_3^{3+}$ ion indicating some degree of interlamellar exchange. It appears that there is also a strong tendency toward segregation of $\left[\text{Co}(\text{tn})_3 \right]^{3+}$ and H^+ in bentonite into the separate interlayers in the mixed clays as is observed in the H- $\text{Co}(\text{pn})_3$ -bentonite system. The d_{001} of the H-bentonite was found to be 12.72\AA and that of the fully exchanged $\text{Co}(\text{tn})_3^{3+}$ clay is 13.65\AA .

Sorption of $[\text{Co}(\text{tn})_3]^{3+}$ on Na-bentonite at pH 7.

The adsorption isotherm of $\text{Co}(\text{tn})_3\text{Cl}_3$ on bentonite at pH 7 and the corresponding reciprocal graph are shown in Fig. 48. They are characteristic of the Langmuir type of isotherm. The value of V_m calculated from the slope of the linear graph is equal to 111 m.e. and compares well with the maximum of the isotherm which is about 112 m.e.

X-ray diffraction studies.

X-ray diffraction data are reported in Fig. 49 and 19(b) which reveals that as $\text{Co}(\text{tn})_3^{3+}$ is added in increasing amounts, the d_{001} spacing begins to increase thereby indicating some degree of interlamellar exchange.

It appears that segregation of cations occurs into the separate interlayers in the mixed clays. The d_{001} basal spacing of the fully exchanged $\text{Co}(\text{tn})_3^{3+}$ clay was 13.5\AA .

X-ray diffraction analysis of 100% exchanged $\text{Co}(\text{tn})_3^{3+}$ clay were also taken by high temperature Guinier Camera at 250°C and d_{001} spacing for 100% $\text{Co}(\text{tn})_3^{3+}$ -bentonite was found to be 13\AA [Fig. 19(b)]. So there is a decrease of 0.5\AA in the d_{001} - spacing. This decrease is probably due to melting point of $\text{Co}(\text{tn})_3^{3+}$.

X-ray diffraction patterns of air-dried clay film deposited on glass slides and stored in a desiccator over saturated $\text{CuSO}_4 \cdot 5\text{H}_2\text{O}$ solution (r.h. 98%) were also taken. It

was observed that the characteristic spacing of 100% $\text{Co}(\text{tn})_3^{3+}$ -bentonite (13.5 \AA) does not vary with humidity showing the non-swelling character of the clay-Co(III) complex.

Differential thermal analysis studies on $\text{Co}(\text{tn})_3^{3+}$ exchanged Na-bentonite.

The 20%, 60% and 100% $\text{Co}(\text{tn})_3^{3+}$ exchanged clay samples were prepared and stored over concentrated sulphuric acid for 20 hours prior to analysis. The results are shown in Fig. 50. D.T.A. curves were obtained under conditions of air flow and all heating rates were 10 $^{\circ}\text{C}$ per minute. The endothermic peak at approximately 120 $^{\circ}\text{C}$ on the three curves was related to the adsorbed water on the clay complex. This was followed by a broad exothermic peak at approximately 480 $^{\circ}\text{C}$ for 20% exchanged sample, but for 100% exchanged sample a medium exothermic peak at approximately 540 $^{\circ}\text{C}$ which was then followed by a weaker exothermic peak at 660 $^{\circ}\text{C}$ was seen. D.T.A. studies of 60% exchanged sample also showed a weaker exothermic peak at about 360 $^{\circ}\text{C}$ which was then followed by a pair of exothermic peaks at about 450 $^{\circ}\text{C}$ (medium) and 580 $^{\circ}\text{C}$ (broad). The broad exothermic peak was probably due to breakdown and pyrolysis of the organic portion of the $\text{Co}(\text{tn})_3^{3+}$. So little difference was seen between the 60% and 100% exchanged samples, but the D.T.A. curve for the 20% exchanged sample was significantly different. As stated earlier (P 56) this observation may also relate to the change

in the environment of a $\text{Co}(\text{tn})_3^{3+}$ cation as the occupancy of clay exchange sites by $\text{Co}(\text{tn})_3^{3+}$ increases.

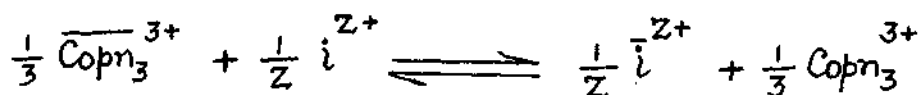
SECTION B

Desorption Studies

Desorption of $[\overline{\text{Copn}_3}]^{3+}$ from H-Copn₃-bentonite.

The results of desorption of $[\overline{\text{Copn}_3}]^{3+}$ from H-Copn₃-bentonite by inorganic and organic ions are given in Figs. 10, 11, 12, 13 and 14.

For the problem under consideration an exchange



equilibrium may be assumed, where the bar denotes the species in the clay phase and Z is the valency of the desorbing ion. The selectivity coefficient is given by

$$K_{\text{Copn}_3}^i = \frac{[\overline{i}^{Z+}]^{\frac{1}{Z}} [\text{Copn}_3^{3+}]^{\frac{1}{3}}}{[\overline{\text{Copn}_3}^{3+}]^{\frac{1}{3}} [i^{Z+}]^{\frac{1}{Z}}}$$

where the bracket means the concentration of the corresponding substances.

The concentrations used to calculate $K_{\text{Copn}_3}^i$ are expressed in moles/1000 gm for the solid phase and moles/1000 ml for the liquid phase.

Since the values of the activity coefficients of $\text{Co}(\text{pn})_3^{3+}$ and $\text{Co}(\text{tn})_3^{3+}$ ions are not available in literature, the concentrations of the ions have been used in the present work to calculate the selectivity coefficients.

The distribution coefficients have been calculated according to the equation

$$\lambda_1 = \frac{\bar{m}_1}{m_1}$$

where again \bar{m}_1 and m_1 are the molal concentrations of the species in the solid and liquid phases respectively.

The values of the selectivity coefficients and distribution coefficients calculated from the above relations are given in Table-4.

The selectivity coefficient $K_{\text{Copn}_3}^i$ is a measure of the preference of the desorbing species i with respect to $[\text{Copn}_3]^{3+}$ for the mineral surface. If the value is less than 1.0, the species i has got a smaller affinity for the clay surface than $[\text{Copn}_3]^{3+}$. Conversely if it is greater than 1.0, then the species i is preferred to $[\text{Copn}_3]^{3+}$; while a value of 1.0, which is very rarely observed, indicates that both the species are equally preferred by the exchanger. The selectivity coefficient, however, is not a constant quantity but varies with the concentration of the species.

Table 4 records the values of the selectivity coefficients of the inorganic ions. It is evident that the trivalent $[\text{Copn}_3]^{3+}$ ions are much more preferred by bentonite to the monovalent and bivalent inorganic ions. However, the case is reversed with the organic quaternary ammonium ions. The selectivity coefficients increase in the order: $\text{Li} < \text{Na} < \text{H} < \text{K} < \text{NH}_4 < \text{Rb} < \text{Cs}$ for the monovalent and $\text{Mg} < \text{Ca} < \text{Sr} < \text{Ba}$ for the bivalent

Table 4

Desorption characteristics of $\left[\text{Co}(\text{NO}_3)_3 \right]^{3+}$ with respect to different ions from H-Co $\text{p}(\text{NO}_3)_3$ -bentonite.

Electrolyte used	Concentration of electrolyte	Distribution Coefficient	Selectivity Coefficient
<u>1:1 Electrolyte</u>			
LiCl	$0.50 \times 10^{-1} \text{ (M)}$	0.70	0.0537
	1.0 "	0.7518	0.075
	1.50 "	0.701	0.079
	2.0 "	0.70	0.0888
	2.50 "	0.68	0.0933
NaCl	$0.50 \times 10^{-1} \text{ (M)}$	0.9027	0.075
	1.0 "	0.8523	0.0887
	1.50 "	0.836	0.1014
	2.0 "	0.8272	0.112
	2.5 "	0.822	0.122
	3.0 "	0.785	0.124
KCl	$0.50 \times 10^{-1} \text{ (M)}$	1.104	0.0996
	1.0 "	1.053	0.119
	1.50 "	1.07	0.1427
	2.0 "	1.053	0.158
	2.50 "	1.023	0.168
	3.0 "	0.9698	0.1694

(Contd..)

Table 4 (Contd..)

Electrolyte used.	Concentration of electrolyte.	Distribution Coefficient	Selectivity Coefficient
NH ₄ Cl	0.50 x 10 ⁻¹ (M)	1.305	0.124
	1.0 "	1.255	0.152
	1.50 "	1.241	0.176
	2.0 "	1.204	0.192
	2.50 "	1.164	0.203
RbCl	0.25 x 10 ⁻¹ (M)	2.217	0.200
	0.50 "	2.114	0.239
	0.75 "	2.081	0.275
	1.0 "	2.013	0.2948
	1.50 "	1.979	0.349
	2.0 "	1.886	0.381
	2.50 "	1.81	0.4126
CsCl	0.25 x 10 ⁻¹ (M)	5.714	0.7225
	0.50 "	5.188	0.852
	0.75 "	4.87	0.898
	1.0 "	4.26	0.925
	1.50 "	3.54	0.9142
	2.0 "	3.03	0.897

(Contd..)

Table 4 (Contd..)

Electrolyte used	Concentration of electrolyte	Distribution Coefficient	Selectivity Coefficient
HCl	0.50 x 10 ⁻¹ (M)	1.003	0.087
	1.0 "	0.902	0.096
	1.50 "	0.819	0.0989
	2.0 "	0.802	0.1069
	2.50 "	0.762	0.109
	3.0 "	0.719	0.109
<u>2:1 Electrolyte</u>			
MgCl ₂	0.50 x 10 ⁻¹ (M)	2.152	0.252
	1.0 "	2.11	0.323
	1.50 "	2.02	0.362
	2.0 "	1.90	0.375
	2.5 "	1.79	0.377
	3.0 "	1.69	0.373
CaCl ₂	0.50 x 10 ⁻¹ (M)	2.66	0.368
	1.0 "	2.36	0.402
	1.50 "	2.17	0.420
	2.0 "	2.0	0.421
	2.5 "	1.87	0.416

(Contd..)

Table 4 (Contd..)

Electrolyte used.	Concentration of electrolyte	Distribution Coefficient	Selectivity Coefficient
SrCl ₂	1.0 x 10 ⁻¹ (M)	2.42	0.4228
	1.50 "	2.235	0.447
	2.0 "	2.057	0.4468
	2.50 "	1.926	0.4458
BaCl ₂	0.50 x 10 ⁻¹ (M)	2.848	0.417
	1.0 "	2.52	0.461
	1.50 "	2.28	0.467
	2.0 "	2.117	0.478
	2.50 "	1.978	0.476
<u>Quaternary ammonium salt</u>			
(CH ₃) ₄ NCl	0.50 x 10 ⁻² (M)	19.14	2.04
	1.0 "	16.89	2.25
	2.0 "	15.789	2.814
	4.0 "	14.40	3.876
	6.0 "	10.61	3.239

(Contd..)

Table 4 (Contd..)

Electrolyte used	Concentration of electrolyte	Distribution Coefficient	Selectivity Coefficient
$(C_2H_5)_4NBr$	$0.50 \times 10^{-2}(M)$	38.37	5.26
	1.0 "	41.1	7.85
	2.0 "	28.461	7.274
	4.0 "	17.177	5.671
	6.0 "	11.507	3.94
	8.0 "	8.687	3.054
	12.0 "	5.6	1.90
$(C_3H_7)_4NI$	$0.50 \times 10^{-2}(M)$	54.37	8.52
	1.0 "	42.18	8.44
	2.0 "	27.59	6.88
	4.0 "	14.68	4.028
	6.0 "	10.00	2.848
$(C_4H_9)_4NBr$	$0.50 \times 10^{-2}(M)$	54.24	8.46
	1.0 "	31.1	5.36
	2.0 "	18.08	3.44
	4.0 "	10.62	2.266
	6.0 "	7.167	1.556

(Contd..)

Table 4 (Contd..)

Electrolyte used	Concentration of electrolyte	Distribution Coefficient	Selectivity Coefficient
DTABr	5.0 x 10 ⁻³ (M)	50.936	7.79
	7.0 "	38.858	5.75
	10.0 "	30.87	5.304
CTABr	5.0 x 10 ⁻³ (M)	70.37	12.21
	7.0 "	54.898	10.21
	10.0 "	39.59	7.662
	13.0 "	29.56	5.72
GPCl	5.0 x 10 ⁻³ (M)	76.44	13.71
	7.0 "	60.99	11.92
	10.0 "	43.47	8.84
	13.0 "	32.85	6.74
EDA	4.0 x 10 ⁻² (M)	3.73	0.630
	6.0 "	3.45	0.667
	8.0 "	3.23	0.689
	10.0 "	3.01	0.687

(Contd..)

Table 4 (Contd..)

Electrolyte used	Concentration of electrolyte	Distribution Coefficient	Selectivity Coefficient
PrDA	2.0×10^{-2} (M)	5.21	0.865
	4.0 "	4.54	0.954
	6.0 "	4.02	0.945
	8.0 "	3.65	0.934
	10.0 "	3.41	0.952

cations. For the monovalent organic ions used the selectivity coefficients are in the sequence : $(\text{CH}_3)_4\text{N}^+ < (\text{C}_2\text{H}_5)_4\text{N}^+ < (\text{C}_3\text{H}_7)_4\text{N}^+ < (\text{C}_4\text{H}_9)_4\text{N}^+ < \text{decyl trimethyl ammonium (DTA)} < \text{cetyl trimethyl ammonium (CTA)} < \text{cetyl pyridinium (CP)}$ in the low concentration range. The order is reversed at high concentrations in the case of tetra alkyl ammonium ions. However, for the divalent organic salts the order is ethane diammonium hydrochloride (EDA) $< 1,3$ propane diammonium hydrochloride (PrDA) (Fig. 14). It can be seen from the figure 12 that the exchange of $\text{Co}(\text{pn})_3^{3+}$ from bentonite by $(\text{C}_4\text{H}_9)_4\text{N}^+$ or $(\text{C}_3\text{H}_7)_4\text{N}^+$ is initially very effective but complete displacement of $\text{Co}(\text{pn})_3^{3+}$ by these large ions is apparently very difficult. This observation is believed due to the contraction of the silicate layers in suspension once a critical level of surface coverage by $(\text{C}_4\text{H}_9)_4\text{N}^+$ or $(\text{C}_3\text{H}_7)_4\text{N}^+$ has been reached [Theng et al (1958) and McBride & Mortland (1964)]. This contraction entraps $\text{Co}(\text{pn})_3^{3+}$ ions still present in the interlayers and may prevent further diffusion of the large $(\text{C}_4\text{H}_9)_4\text{N}^+$ or $(\text{C}_3\text{H}_7)_4\text{N}^+$ ions into the interlamellar regions. As a result, further exchange of $\text{Co}(\text{pn})_3^{3+}$ may be inhibited by the large size of the $(\text{C}_4\text{H}_9)_4\text{N}^+$ or $(\text{C}_3\text{H}_7)_4\text{N}^+$ ions, which fill the interlayer volume to a large extent, preventing diffusion of interlayer $\text{Co}(\text{pn})_3^{3+}$ to edges. Thus, a quasi-equilibrium state may be reached, with $\text{Co}(\text{pn})_3^{3+}$ unavailable for exchange on the clay surface, and not at true equilibrium with

the solution phase. The above collapse of layers occurs for $\text{Co}(\text{pn})_3^{3+}$ - $(\text{CH}_3)_4\text{N}^+$ - bentonite systems as well, but the quasi-equilibrium state would not be so prominent because large inter-lamellar volumes are left vacant by the smaller $(\text{CH}_3)_4\text{N}^+$ as a result of which more complete exchange of $\text{Co}(\text{pn})_3^{3+}$ by tetra methyl ammonium ions is achieved. Similar observations have been reported by McBride and Mortland (186) in the exchange of Cu^{2+} from Cu-montmorillonite by various tetra alkyl ammonium ions and have been explained as above from X-ray and B.E.T. surface area determinations. A detailed X-ray analysis of the swelling properties of the mixed Na- $\text{Co}(\text{pn})_3$ -tetra alkyl ammonium-bentonites has been done and is recorded later in p.71-72.

Especially interesting is the desorption by the cationic long chain organic ions viz. DTA, CTA and CP. The peculiar behaviour of these reagents may be due to their strong adsorbability (187), geometrical relationship to the mineral surface, surface active properties (27) and their strong affinity for the altered clay surface (27). It is noted from figs. 12 and 13 that the smaller quaternary ammonium ions desorb more $\text{Co}(\text{pn})_3^{3+}$ than the larger CTA or CP while the concentration is high. This may, however, be explained on the basis of the covering-up effect of the larger ions (188); a fraction of the $\text{Co}(\text{pn})_3^{3+}$ is inaccessible for the exchange process. Further the order of desorption efficiency $\text{CP} > \text{CTA} > \text{DTA}$ may be explained on the basis of their increasing critical micelle concentration (cmc)

values; the c.m.c values of OP, CTA and DTA are $8.0 \times 10^{-4} \text{ M}$, $1.0 \times 10^{-3} \text{ M}$ and $7.0 \times 10^{-2} \text{ M}$ respectively.

An attempt has also been made to correlate the selectivity coefficient which gives a measure of the selectivities of ions for the clay surface with some other properties of the ions, viz., hydrated ionic radius (189) and the parameter a^0 (190) of the Debye-Hückel equation $-\log \gamma_{\pm} = A\sqrt{\mu}/(1 + Ba^0\sqrt{\mu})$, where the symbols have their usual significance. It appears from the graphs in Fig. 15 that Rb^+ and Cs^+ are more strongly attached than what is expected from the hydrated ionic radii. NH_4^+ and K^+ which, as expected, stay close together and occupy an intermediate position between the two pairs $\text{Rb}^+ - \text{Cs}^+$ and $\text{Na}^+ - \text{Li}^+$. On the other hand, if $\frac{1}{a^0}$ is plotted against \log (selectivity coefficient) (Fig. 15), a straight line is obtained. The latter strongly suggests that in the process of desorption of $\text{Co}(\text{pn})_3^{3+}$ from the clay surface by smaller inorganic cations the Debye-Hückel parameter a^0 rather than the hydrated ionic radius shows a better correlation. Similar findings have been reviewed by Kressman and Kitchener (191) who reported similar results with phenol sulphonate resin exchangers. The plot of \log (selectivity coefficient) vs. $\frac{1}{a^0}$ is however on the basis of the simple model of Pauley (192), which suggests that electrostatic attraction between the counter ions and the fixed ionic groups is the significant factor.

It has been noted earlier (PP 19-20) that Kielland postulated a model with the help of which thermodynamic equilibrium constant and the free energy change in an exchange reaction may be computed. Utilising the equation of Kielland, the above quantities have been evaluated from the studies of desorption of $\text{Co}(\text{pn})_3^{3+}$ from H-Copn₃-bentonite. However, it is to be noted that since the selectivity coefficients have been calculated without considering the activity of the ions, the computed thermodynamic constants from the above model are somewhat approximate. The results are given in Figs. 16 and 17 and in Table 5. The values of the thermodynamic equilibrium constants are in order : $\text{Li} < \text{H} < \text{Na} < \text{K} < \text{NH}_4 < \text{Rb} < \text{Cs}$ for the monovalent, $\text{Mg} < \text{Ca} < \text{Sr} < \text{Ba}$ for the bivalent inorganic ions.

As the study of free energy change usually provides a satisfactory approach to the problem of exchange equilibrium, it has been computed and recorded in Table 5. The values give an idea about the affinities of the respective ions for the montmorillonite surface. It is observed that Li^+ has the minimum affinity for the montmorillonite surface while the affinity of Cs^+ is maximum. The behaviour of Li^+ may be expected from its large hydrated ionic size. The values, $K_{\text{Copn}_3}^{\text{Cs}}$ and ΔG° are seen to deviate considerably from those of the other alkali cations. Compared to Li^+ , Na^+ , K^+ etc., Cs^+ has a distinct fixation tendency for montmorillonite. The ionic volume of the Cs^+ , which is just appropriate for the cavity between two adjacent particle surfaces with $[\text{Si}_2\text{O}_5]_{\text{c}}$ tetrahedral layers in contact with each other, plays a significant role in the

Table 5

Evaluation of thermodynamic quantities from
Kielland's equation at 25°C.

Exchange system	Thermodynamic equilibrium constant	ΔG° Cal/mole
$K_{\text{Copn}_3}^{\text{Li}}$	0.153	1111.38
$K_{\text{Copn}_3}^{\text{Na}}$	0.2384	848.87
$K_{\text{Copn}_3}^{\text{K}}$	0.2756	763.06
$K_{\text{Copn}_3}^{\text{NH}_4}$	0.315	683.16
$K_{\text{Copn}_3}^{\text{Rb}}$	0.476	438.99
$K_{\text{Copn}_3}^{\text{Cs}}$	0.933	40.90
$K_{\text{Copn}_3}^{\text{H}}$	0.1578	1093.02
$K_{\text{Copn}_3}^{\text{Mg}}$	0.409	528.368
$K_{\text{Copn}_3}^{\text{Ca}}$	0.4327	495.92

(Contd..)

Table 5 (Contd..)

Exchange system	Thermodynamic equilibrium constant	ΔG° Cal/mole
$K_{\text{CoPn}_3}^{\text{Sr}}$	0.455	465.88
$K_{\text{CoPn}_3}^{\text{Ba}}$	0.479	435.26
$K_{\text{CoPn}_3}^{(\text{CH}_3)_4\text{N}}$	3.09	-668.19
$K_{\text{CoPn}_3}^{(\text{C}_4\text{H}_9)_4\text{N}}$	1.258	-136.36
$K_{\text{CoPn}_3}^{\text{DTA}}$	3.31	-707.38
$K_{\text{CoPn}_3}^{\text{OTA}}$	4.46	-886.47
$K_{\text{CoPn}_3}^{\text{OP}}$	4.67	-913.65
$K_{\text{CoPn}_3}^{\text{EDA}}$	0.691	218.18
$K_{\text{CoPn}_3}^{\text{PrDA}}$	0.944	34.09

Table 6

Desorption characteristics of Co^{3+} with respect to different ions from Na- Co^{3+} -bentonite.

Electrolyte used	Concentration of electrolyte	Distribution Coefficient	Selectivity Coefficient
<u>1:1 Electrolyte</u>			
LiCl	$1.0 \times 10^{-1} \text{ (M)}$	0.9527	0.0949
	1.50 "	0.9359	0.108
	2.0 "	0.8772	0.110
	2.50 "	0.822	0.1104
	3.0 "	0.769	0.1085
NaCl	$0.50 \times 10^{-1} \text{ (M)}$	1.40	0.124
	1.0 "	1.40	0.161
	1.50 "	1.10	0.135
	2.0 "	1.055	0.142
	2.50 "	1.00	0.146
	3.0 "	0.936	0.145
KCl	$0.50 \times 10^{-1} \text{ (M)}$	1.71	0.163
	1.0 "	1.60	0.194
	1.50 "	1.49	0.206
	2.0 "	1.45	0.227
	2.50 "	1.40	0.241
	3.0 "	1.388	0.2578

(Contd..)

Table 6 (Contd..)

Electrolyte used	Concentration of electrolyte	Distribution Coefficient	Selectivity Coefficient
NH ₄ Cl	0.50 x 10 ⁻¹ (M)	2.187	0.229
	1.0 "	1.96	0.2577
	1.50 "	1.80	0.272
	2.0 "	1.708	0.2898
	2.50 "	1.613	0.2998
RbCl	0.50 x 10 ⁻¹ (M)	3.332	0.408
	0.75 "	3.162	0.4507
	1.0 "	2.95	0.4629
	1.50 "	2.688	0.4977
	2.0 "	2.442	0.510
CsCl	0.125 x 10 ⁻¹ (M)	8.196	0.832
	0.25 "	7.985	1.05
	0.50 "	6.94	1.177
	0.75 "	5.97	1.17
	1.0 "	5.38	1.195
	1.5 "	4.321	1.1287

(Contd..)

Table 6 (Contd..)

Electrolyte used	Concentration of electrolyte	Distribution Coefficient	Selectivity Coefficient
HCl	0.50 x 10 ⁻¹ (M)	3.03	0.384
	1.0 "	1.81	0.246
	1.50 "	1.339	0.190
	2.0 "	1.206	0.185
<u>2:1 Electrolyte</u>			
MgCl ₂	0.25 x 10 ⁻¹ (M)	2.70	0.263
	0.50 "	2.54	0.309
	1.0 "	2.25	0.330
	1.50 "	2.05	0.335
	2.0 "	1.91	0.336
CaCl ₂	0.25 x 10 ⁻¹ (M)	3.27	0.366
	0.50 "	2.84	0.378
	1.0 "	2.44	0.386
	1.50 "	2.20	0.384
	2.0 "	2.03	0.382
SrCl ₂	0.25 x 10 ⁻¹ (M)	3.45	0.402
	0.50 "	2.91	0.393
	1.0 "	2.50	0.405
	1.50 "	2.25	0.402
	2.0 "	2.05	0.391

(Contd..)

Table 6 (Contd..)

Electrolyte used	Concentration of electrolyte	Distribution Coefficient	Selectivity Coefficient
BaCl ₂	0.25 x 10 ⁻¹ (M)	3.69	0.452
	0.50 "	3.13	0.449
	1.0 "	2.58	0.431
	1.50 "	2.30	0.423
	2.0 "	2.10	0.411
<u>Quaternary</u>			
<u>ammonium salt</u>			
(CH ₃) ₄ NCl	1.0 x 10 ⁻² (M)	22.38	3.02
	2.0 "	22.97	4.445
	4.0 "	17.63	4.832
(C ₂ H ₅) ₄ NBr	1.0 x 10 ⁻² (M)	35.35	5.81
	2.0 "	32.32	7.825
	4.0 "	19.29	5.88
	8.0 "	10.10	3.453

(Contd..)

Table 6 (Contd..)

Electrolyte used	Concentration of electrolyte	Distribution Coefficient	Selectivity Coefficient
$(C_3H_7)_4NI$	$1.0 \times 10^{-2}(M)$	45.24	8.76
	2.0 "	35.45	9.666
	4.0 "	17.30	4.879
	6.0 "	11.30	3.187
$(C_4H_9)_4NBr$	$1.0 \times 10^{-2}(M)$	50.70	10.40
	2.0 "	26.22	5.77
	4.0 "	12.53	2.75
DTABr	$5.0 \times 10^{-3}(M)$	111.73	21.97
	7.0 "	83.179	17.52
	10.0 "	53.50	11.27
	14.0 "	36.26	7.639
DDTABr	$5.0 \times 10^{-3}(M)$	119.3	24.07
	7.0 "	85.50	18.25
	10.0 "	57.69	12.63

(Contd..)

Table 6 (Contd..)

Electrolyte used	Concentration of electrolyte	Distribution Coefficient	Selectivity Coefficient
CTABr	5.0 x 10 ⁻³ (M)	123.563	25.322
	7.0 "	92.979	20.708
	10.0 "	62.195	14.239
CPCL	5.0 x 10 ⁻³ (M)	126.373	25.445
	7.0 "	97.605	21.676
	10.0 "	64.285	14.48
	14.0 "	43.548	9.8
EDA	4.0 x 10 ⁻² (M)	3.66	0.684
	6.0 "	3.45	0.637
	8.0 "	3.23	0.651
	10.0 "	3.04	0.653
PrDA	4.0 x 10 ⁻² (M)	4.43	0.850
	6.0 "	4.02	0.881
	8.0 "	3.72	0.899
	10.0 "	3.47	0.901

has also a strong affinity for the clay until about 60 percent of the $\left[\text{Copr}_3 \right]^{3+}$ ions have been exchanged. Then the preference of clay exchange sites for tetrapropyl ammonium ion over $\left[\text{Copr}_3 \right]^{3+}$ at about 61-62 percent exchange is reversed at the concentrations used. In contrast, tetra methyl ammonium ion and tetra ethyl ammonium ion became more effective than tetrapropyl ammonium ion and tetra butyl ammonium ion above 60% exchange of $\left[\text{Copr}_3 \right]^{3+}$; hence more complete exchange of $\left[\text{Copr}_3 \right]^{3+}$ by tetra methyl ammonium ion and tetra ethyl ammonium ion are achieved because of large interlamellar volumes left vacant by the smaller tetramethyl ammonium ion and tetraethyl ammonium ion, whereas incomplete exchange of $\left[\text{Copr}_3 \right]^{3+}$ ion by tetra propyl ammonium ion and tetra butyl ammonium ion are observed due to larger sizes of these ions which fill interlayer volume to a large extent and $\left[\text{Copr}_3 \right]^{3+}$ ion is not available for exchange on the clay surface at the concentrations used. The results may be explained as pointed out earlier (P 65) in H-Copr₃ - bentonite system, by assuming contraction of the silicate layers in suspension once a critical level of surface coverage by the large tetra alkyl ions has been reached as shown by Mc Bride and Mortland⁽¹⁸⁶⁾ and Theng et al(168).

It is observed that the swelling properties of the air dry (51% r.h.) mixed Co(pn)₃ - tetra alkyl ammonium bentonites, determined by X-ray diffraction (Figs. 31, 32, 33 and 34) depend

strongly on the proportion of the ions. For example, the $\text{Co}(\text{pn})_3 - (\text{CH}_3)_4\text{N}^-$ bentonite system (Fig. 31) shows a progressive increase in d_{001} spacing from 0% $(\text{CH}_3)_4\text{N}^-$ to about 65% tetra methyl ammonium saturation (14.4\AA) and further exchange by $(\text{CH}_3)_4\text{N}^+$ does not change this spacing. These diffraction peaks indicate random interstratification (Mc Bride & Mortland) of $\text{Co}(\text{pn})_3^{3+}$ and $(\text{CH}_3)_4\text{N}^-$ -rich layers from 0 to 65% exchange and beyond 65%, there is apparent ion-homogeneity. The $\text{Co}(\text{pn})_3^{3+}$ - tetra propyl ammonium mixed systems (Fig. 33) show a pattern similar to the $\text{Co}(\text{pn})_3^{3+}$ tetra methyl ammonium system. Fig. 32 illustrates X-ray diffraction study of tetraethyl ammonium $\text{Co}(\text{pn})_3^{3+}$ bentonite system. The X-ray diffraction data for the above systems can thus be explained by segregation of $\text{Co}(\text{pn})_3^{3+}$ and organic cations from 0% to about 65% exchange, and ion-homogeneity when rich in tetra alkyl ammonium ions Fig. 34 represents the X-ray diffraction data for tetra butyl ammonium - $\text{Co}(\text{pn})_3^{3+}$ -bentonite system. However, tetra butyl ammonium ion is most effective in exchanging $\text{Co}(\text{pn})_3^{3+}$ at low concentration and these are randomly interstratified from 0% to about 55% exchange and apparent ion homogeneity above 55% exchange.

From a linear plot of Kielland's equation (Figs. 35 and 36), the values of thermodynamic equilibrium constant, and Gibbs free energy change at 25°C , which is a measure of the relative affinities of the ions for the mineral, have been evaluated and are presented in Table 7. The results are similar to those obtained earlier (Table 5).

Table 7

Evaluation of thermodynamic quantities
from Kielland's equation at 25°C.

Exchange system	Thermodynamic equilibrium constant	ΔG° Cal/mole
$K_{\text{Copn}_3}^{\text{Li}}$	0.194	970.34
$K_{\text{Copn}_3}^{\text{Na}}$	0.239	845.46
$K_{\text{Copn}_3}^{\text{K}}$	0.32	673.49
$K_{\text{Copn}_3}^{\text{NH}_4}$	0.3518	618.51
$K_{\text{Copn}_3}^{\text{Rb}}$	0.554	349.32
$K_{\text{Copn}_3}^{\text{Cs}}$	1.222	-118.9
$K_{\text{Copn}_3}^{\text{Mg}}$	0.396	548.23
$K_{\text{Copn}_3}^{\text{Ca}}$	0.407	531.82

(Contd..)

Table 7 (Contd..)

Exchange system	Thermodynamic equilibrium constant	ΔG° Cal/mole
$K_{\text{Copn}_3}^{\text{Sr}}$	0.416	518.19
$K_{\text{Copn}_3}^{\text{Ba}}$	0.431	497.73
$K_{\text{Copn}_3}^{(\text{CH}_3)_4\text{N}}$	4.57	-900.01
$K_{\text{Copn}_3}^{\text{DDTA}}$	4.168	-845.46
$K_{\text{Copn}_3}^{\text{CTA}}$	7.76	-1213.65
$K_{\text{Copn}_3}^{\text{EDA}}$	0.676	231.82
$K_{\text{Copn}_3}^{\text{PrDA}}$	0.912	54.54

As in the desorption of $\text{Co}(\text{pn})_3^{3+}$ from its H-bentonite complex, the plot of log (selectivity coefficient) vs. hydrated ionic radius is a curved one but when the former is plotted against Debye Huckel parameter $\frac{1}{a^0}$, a linear curve is obtained (Fig. 37).

It should be pointed out that the values of the selectivity coefficients and thermodynamic equilibrium constants (Tables 6 and 7) are greater in the case of Na-Copn₃ -bentonite than H-Copn₃ -bentonite which suggest that $\text{Co}(\text{pn})_3^{3+}$ ion is more strongly attached to the H-bentonite system. Therefore the order of preference of $\text{Co}(\text{pn})_3^{3+}$ for the bentonite surface is : H-bentonite > Na - bentonite.

Desorption of $\text{Co}(\text{pn})_3^{3+}$ from H-Cotn₃ - bentonite.

The results of desorption of $\text{Co}(\text{pn})_3^{3+}$ from H-Cotn₃ - bentonite complex are shown in Figs. 40,41,42,43 and 44. The curves obtained are very similar to those for $\text{Co}(\text{pn})_3^{3+}$ desorption from its bentonite complex as discussed above. The selectivity coefficients (Table 8) are less than 1.0 for Li^+ , Na^+ , K^+ , NH_4^+ , Rb^+ , Cs^+ , Mg^{2+} , Ca^{2+} , Sr^{2+} , Ba^{2+} , indicating a lower binding energy of the ions with respect to $\text{Co}(\text{pn})_3^{3+}$ for the mineral surface.

The observed order of preference is $\text{Li} < \text{Na} < \text{H} < \text{K} < \text{NH}_4 < \text{Rb} < \text{Cs}$ for the monovalent ions and $\text{Mg} < \text{Ca} < \text{Sr} < \text{Ba}$ for the divalent ions, $(\text{CH}_3)_4\text{N} < (\text{C}_2\text{H}_5)_4\text{N} < (\text{C}_3\text{H}_7)_4\text{N} < (\text{C}_4\text{H}_9)_4\text{N} < \text{DTA} <$

Table 8

Desorption characteristics of $[Co^{3+}]$ with respect to different ions from H- Co^{3+} -bentonite.

Electrolyte used	Concentration of electrolyte	Distribution Coefficient	Selectivity Coefficient
<u>1:1 Electrolyte</u>			
LiCl	$1.75 \times 10^{-1}(M)$	0.1429	0.0097
	2.0 "	0.1751	0.0133
	2.50 "	0.200	0.0173
	3.0 "	0.2168	0.0204
NaCl	$1.50 \times 10^{-1}(M)$	0.200	0.0143
	2.0 "	0.275	0.0243
	2.50 "	0.300	0.0295
	3.0 "	0.317	0.0342
	3.50 "	0.3146	0.0358
KCl	$0.75 \times 10^{-1}(M)$	0.4344	0.033
	1.0 "	0.4759	0.0412
	1.50 "	0.501	0.0499
	2.0 "	0.5259	0.0586
	2.50 "	0.521	0.063
	3.0 "	0.517	0.0675

(Contd..)

Table 8 (Contd..)

Electrolyte used	Concentration of electrolyte	Distribution Coefficient	Selectivity Coefficient
NH ₄ Cl	0.50 x 10 ⁻¹ (M)	0.651	0.0474
	1.0 "	0.350	0.0266
	1.50 "	0.584	0.0618
	2.0 "	0.576	0.0667
	2.50 "	0.601	0.0773
	3.0 "	0.651	0.0931
RbCl	0.25 x 10 ⁻¹ (M)	1.812	0.151
	0.75 "	1.744	0.211
	1.0 "	1.71	0.231
	1.50 "	1.677	0.267
	2.0 "	1.634	0.295
	2.50 "	1.569	0.3133
CsCl	0.25 x 10 ⁻¹ (M)	5.299	0.641
	0.50 "	4.78	0.739
	0.75 "	4.40	0.795
	1.0 "	4.059	0.823
	1.25 "	3.77	0.839
	1.50 "	3.581	0.875

(Contd..)

Table 8 (Contd..)

Electrolyte used	Concentration of electrolyte	Distribution Coefficient	Selectivity Coefficient
HCl	0.50 x 10 ⁻¹ (M)	0.400	0.0246
	1.0 "	0.526	0.046
	1.50 "	0.383	0.0349
	2.0 "	0.363	0.035
	2.50 "	0.340	0.035
	3.0 "	0.317	0.034
<u>2:1 Electrolyte</u>			
MgCl ₂	0.50 x 10 ⁻¹ (M)	1.05	0.074
	1.0 "	1.026	0.0898
	1.50 "	1.034	0.105
	2.0 "	1.028	0.1147
	2.50 "	1.011	0.1223
	3.0 "	0.976	0.122
CaCl ₂	0.50 x 10 ⁻¹ (M)	1.184	0.0899
	1.0 "	1.163	0.112
	1.50 "	1.128	0.122
	2.0 "	1.108	0.130
	2.50 "	1.076	0.136

(Contd..)

Table 8 (Contd..)

Electrolyte used	Concentration of electrolyte	Distribution Coefficient	Selectivity Coefficient
SrCl ₂	0.50 x 10 ⁻¹ (M)	1.267	0.101
	1.0 "	1.224	0.1219
	1.50 "	1.2	0.1363
	2.0 "	1.155	0.139
BaCl ₂	0.50 x 10 ⁻¹ (M)	1.34	0.110
	1.0 "	1.322	0.139
	1.50 "	1.267	0.149
	2.0 "	1.206	0.1529
	2.5 "	1.133	0.149
<u>Quaternary ammonium salt</u>			
(CH ₃) ₄ NCl	1.0 x 10 ⁻² (M)	16.98	2.23
	2.0 "	15.31	2.619
	4.0 "	12.274	2.752
	6.0 "	10.378	2.827
	8.0 "	8.639	2.648

(Contd..)

Table 8 (Contd..)

Electrolyte used	Concentration of electrolyte	Distribution Coefficient	Selectivity Coefficient
$(C_2H_5)_4NBr$	$1.0 \times 10^{-2}(M)$	32.40	5.53
	2.0 "	26.30	5.987
	4.0 "	15.86	4.318
	6.0 "	10.557	2.919
	8.0 "	7.975	2.242
$(C_3H_7)_4NI$	$1.0 \times 10^{-2}(M)$	37.5	6.83
	2.0 "	25.697	5.76
	4.0 "	12.68	2.9
	6.0 "	8.41	1.94
$(C_4H_9)_4NBr$	$1.0 \times 10^{-2}(M)$	42.77	8.29
	2.0 "	21.856	4.459
	4.0 "	10.64	2.186
	6.0 "	7.09	1.469
DTABr	$5.0 \times 10^{-3}(M)$	64.19	10.43
	7.0 "	54.88	9.86
	10.0 "	41.42	7.91
	14.0 "	29.25	5.67

Contd..)

Table 8 (Contd..)

Electrolyte used	Concentration of electrolyte	Distribution Coefficient	Selectivity Coefficient
DDTAbR	5.0 x 10 ⁻³ (M)	101.36	19.66
	7.0 "	85.04	18.64
	10.0 "	62.57	14.86
CTAbR	5.0 x 10 ⁻³ (M)	108.9	21.759
	7.0 "	92.55	21.22
	10.0 "	70.35	18.00
	14.0 "	49.78	13.34
CP.OI	5.0 x 10 ⁻³ (M)	127.19	27.11
	7.0 "	104.53	25.58
	10.0 "	79.25	22.09
	14.0 "	53.84	15.399
EDA	4.0 x 10 ⁻² (M)	2.36	0.268
	6.0 "	2.28	0.297
	8.0 "	2.18	0.307
	10.0 "	2.10	0.315

(Contd..)

Table 8 (Contd..)

Electrolyte used	Concentration of electrolyte	Distribution Coefficient	Selectivity Coefficient
PrDA	4.0 x 10 ⁻² (M)	2.85	0.376
	6.0 "	2.92	0.465
	8.0 "	2.87	0.520
	10.0 "	2.81	0.561

Table 9Evaluation of thermodynamic quantities
from Kielland's equation at 25°C

Exchange system	Thermodynamic equilibrium constant	ΔG° Cal/mole
$K_{\text{Co}(\text{NO}_3)_3}^{\text{Na}}$	0.288	736.37
$K_{\text{Co}(\text{NO}_3)_3}^{\text{K}}$	0.4528	469.06
$K_{\text{Co}(\text{NO}_3)_3}^{\text{NH}_4}$	0.398	545.46
$K_{\text{Co}(\text{NO}_3)_3}^{\text{Rb}}$	0.452	469.74
$K_{\text{Co}(\text{NO}_3)_3}^{\text{Cs}}$	0.9120	54.54
$K_{\text{Co}(\text{NO}_3)_3}^{\text{H}}$	0.1295	1210.28
$K_{\text{Co}(\text{NO}_3)_3}^{\text{Mg}}$	0.288	736.37
$K_{\text{Co}(\text{NO}_3)_3}^{\text{Ca}}$	0.331	654.55

(Contd..)

DDTA < CTA < CP for the monovalent organic ions and EDA < PrDA for the divalent organic ions. As in the case of $[\text{Co}(\text{NH}_3)_6]^{3+}$ desorption from its bentonite complex, here also there is reversal of selectivity coefficients with tetra alkyl ammonium ions at higher concentrations used. This behaviour may be explained in a similar manner as stated earlier (P 65).

The curves showing the desorption by DTA, DDTA, CTA and CP (Fig. 43) are almost similar to those for $[\text{Co}(\text{NH}_3)_6]^{3+}$ desorption from its bentonite complex. Here also the order of desorption of the above surface active ions from the clay complex has been observed to be DTA < DDTA < CTA < CP which is in reverse order of their c.m.c. values.

From a linear plot of Kielland's equation (Figs. 45 and 46) thermodynamic equilibrium constants and standard Gibbs free energy change of some of the exchange reactions have been evaluated and are shown in Table 9.

As in the desorption of $[\text{Co}(\text{NH}_3)_6]^{3+}$ from its H-bentonite complex, here also (Fig. 47) the plot of log (selectivity coefficient) vs. hydrated ionic radius is a curved one but when the former is plotted against Debye-Huckel parameter $\frac{1}{a_0}$ a linear curve is obtained.

Table 9 (Contd..)

Exchange system	Thermodynamic equilibrium constant	ΔG° Cal/mole
$K_{\text{Co}^{2+}}^{\text{Sr}}$	0.354	613.64
$K_{\text{Co}^{2+}}^{\text{Ba}}$	0.371	586.37
$K_{\text{Co}^{2+}}^{\text{EDA}}$	0.416	518.19
$K_{\text{Co}^{2+}}^{\text{PrDA}}$	0.630	272.73

Description of $\left[\text{Co}(\text{tn}_3) \right]^{3+}$ from Na-Co tn_3 - bentonite.

The results of desorption of $\left[\text{Co}(\text{tn}_3) \right]^{3+}$ from Na-Co tn_3 -bentonite are shown in Figs. 51, 52, 53, 54 and 55. The curves are almost alike to those obtained earlier (Figs. 26, 27, 28, 29 and 30).

The desorption curves (Fig. 54) of the DTA, DDTA, OTA and OP are S shaped with the initial slope gradually changing from a lower to a higher value. But after that as the amount to be desorbed gets less and less, the rate of desorption attains nearly a constant value, so that the isotherm is almost flat. Usually the S-curve indicates "co-operative adsorption", with solute molecules tending to be adsorbed packed in rows or clusters (194). The converse, however, does not necessarily apply. Recent theoretical treatment for the classification of the solute adsorption isotherms by Giles, Smith and Huitson (195) shows that S-curve occurs when the activation energy for the desorption of the solute is concentration-dependent, and/or is markedly reduced by large negative contributions of the solvent or a second solute. This may explain the S-group of curves observed in the desorption of $\left[\text{Co}(\text{tn}_3) \right]^{3+}$ from the clay matrix by the large organic ions.

As in other cases, the desorbing efficiency of quaternary ammonium ions has been observed to be $(\text{CH}_3)_4\text{N} < (\text{C}_2\text{H}_5)_4\text{N} < (\text{C}_3\text{H}_7)_4\text{N} < (\text{C}_4\text{H}_9)_4\text{N}$ at low concentrations, but there is a reversal

of the preference at higher concentrations of the alkyl quaternary salts and may be explained as stated earlier (P 71).

Figs. 56, 57 and 58 represent the d_{001} basal spacings of the air dry (51% r.h.) mixed Na-Cotn₃-tetra alkyl ammonium bentonites, which show that the swelling properties depend strongly on the proportion of the ions. It can be seen from the Fig. 58 that the Cotn₃-(C₄H₉)₄N⁺-bentonite system shows a gradual increase in d_{001} spacing as the % of (C₄H₉)₄N⁺ in the clay phase is increased and reaches a constant value of 14.36 Å at about 50% (C₄H₉)₄N⁺ saturation. According to McBride and Mortland⁽¹²⁶⁾ this would indicate that the systems consist of randomly interstratified Co(tn)₃³⁺ and (C₄H₉)₄N⁺ layers from 0 to 50% exchange, while beyond 50%, there is no interstratification and the spacings are determined by (C₄H₉)₄N⁺. The Cotn₃-(CH₃)₄N⁺ - bentonite system (Fig. 56) and Cotn₃-(C₂H₅)₄N⁺-bentonite system (Fig. 57) exhibit a pattern similar to Cotn₃-(C₄H₉)₄N⁺ -bentonite system and can thus be explained by assuming segregation of Co(tn)₃³⁺ and organic cations from 0% to about 55% exchange, and apparant ion homogeneity above 55% exchange.

The order of increasing preference of alkali ions is $Li^+ < Na^+ < K^+ < Rb^+ < Cs^+$. The order of exchange of alkaline earth ions is $Mg^{2+} < Ca^{2+} < Sr^{2+} < Ba^{2+}$ (Table 10).

The selectivity coefficients (Table 10) of the following organic ions are in the order : EDA < PrDA < DTA < DDTA < CTA < CP .

Here also, the plot of log(selectivity coefficient) vs. hydrated ionic radius is a curved one but when the former is

Table 10

Desorption characteristics of $[Co^{3+}]$ with respect to different ions from Na-Co₃-bentonite.

Electrolyte used	Concentration of electrolyte	Distribution Coefficient	Selectivity Coefficient
<u>1:1 Electrolyte</u>			
LiCl	1.0 x 10 ⁻¹ (M)	0.5514	0.0497
	1.50 "	0.568	0.0596
	2.0 "	0.601	0.0718
NaCl	0.75 x 10 ⁻¹ (M)	0.6016	0.0503
	1.0 "	0.7023	0.0688
	1.50 "	0.702	0.0799
	2.0 "	0.678	0.083
	2.50 "	0.622	0.0817
NH ₄ Cl	0.50 x 10 ⁻¹ (M)	1.41	0.1389
	1.0 "	1.3	0.160
	1.50 "	1.206	0.168
	2.0 "	1.08	0.1622
	2.50 "	0.944	0.1468

(Contd..)

Table 10 (Contd..)

Electrolyte used	Concentration of electrolyte	Distribution Coefficient	Selectivity Coefficient
KCl	0.50 x 10 ⁻¹ (M)	1.205	0.1059
	1.0 "	1.256	0.144
	1.50 "	1.071	0.1356
	2.0 "	0.978	0.1338
	2.50 "	0.883	0.127
RbCl	0.25 x 10 ⁻¹ (M)	3.658	0.371
	0.50 "	3.06	0.378
	0.75 "	2.56	0.3466
	1.0 "	2.27	0.329
	1.50 "	1.848	0.292
CsCl	0.125 x 10 ⁻¹ (M)	8.75	0.996
	0.25 "	7.08	0.968
	0.50 "	5.44	0.892
	0.75 "	4.564	0.831
	1.0 "	4.08	0.812
	1.50 "	3.49	0.800

(Contd..)

Table 10 (Contd..)

Electrolyte used	Concentration of electrolyte	Distribution Coefficient	Selectivity Coefficient
HCl	0.50 x 10 ⁻¹ (M)	2.429	0.290
	1.0 "	1.363	0.1676
	1.50 "	0.9395	0.118
	2.0 "	0.778	0.1023
	2.50 "	0.722	0.1007
<u>2:1 Electrolyte</u>			
MgCl ₂	0.50 x 10 ⁻¹ (M)	1.85	0.184
	1.0 "	1.677	0.202
	1.50 "	1.542	0.2028
	2.0 "	1.417	0.196
CaCl ₂	0.50 x 10 ⁻¹ (M)	2.07	0.2225
	1.0 "	1.78	0.225
	1.25 "	1.678	0.220
SrCl ₂	0.50 x 10 ⁻¹ (M)	2.199	0.250
	1.0 "	1.828	0.234
	1.50 "	1.61	0.220
	2.0 "	1.45	0.204

(Contd..)

Table 10 (Contd..)

Electrolyte used	Concentration of electrolyte	Distribution Coefficient	Selectivity Coefficient
BaCl ₂	0.50 x 10 ⁻¹ (M)	2.229	0.2545
	1.0 "	1.89	0.249
	1.50 "	1.655	0.230
	2.0 "	1.49	0.215
<u>Quaternary</u>			
<u>ammonium salt</u>			
(CH ₃) ₄ Cl	1.0 x 10 ⁻² (M)	12.72	1.52
	2.0 "	12.447	1.941
	4.0 "	11.327	2.3446
	6.0 "	10.139	2.51
	8.0 "	8.652	2.38
(C ₂ H ₅) ₄ NBr	1.0 x 10 ⁻² (M)	25.81	3.98
	2.0 "	26.43	5.746
	4.0 "	17.34	4.63
	6.0 "	11.62	3.174
	8.0 "	8.789	2.45

(Contd..)

Table 10 (Contd..)

Electrolyte used	Concentration of electrolyte	Distribution Coefficient	Selectivity Coefficient
$(C_3H_7)_4NI$	$1.0 \times 10^{-2}(M)$	34.96	6.05
	2.0 "	29.64	6.84
	4.0 "	16.48	4.28
	6.0 "	11.247	2.997
	8.0 "	8.59	2.34
$(C_4H_9)_4NBr$	$1.0 \times 10^{-2}(M)$	40.47	7.41
	2.0 "	26.745	5.84
	4.0 "	14.42	3.41
	6.0 "	9.947	2.44
DTABr	$5.0 \times 10^{-3}(M)$	65.44	10.43
	7.0 "	95.23	20.41
	10.0 "	65.44	14.75
	13.0 "	46.99	10.59
DDTABr	$5.0 \times 10^{-3}(M)$	76.29	12.82
	7.0 "	107.75	24.29
	10.0 "	72.48	17.13
OTABr	$5.0 \times 10^{-3}(M)$	100.29	18.41
	7.0 "	121.34	28.68
	10.0 "	78.08	19.13
	13.0 "	55.33	13.57

(Contd..)

Table 10 (Contd..)

Electrolyte used	Concentration of electrolyte	Distribution Coefficient	Selectivity Coefficient
CPCl	5.0 x 10 ⁻³ (M)	118.75	23.05
	7.0 "	132.55	32.51
	10.0 "	83.79	21.29
	14.0 "	59.05	15.00
EDA	2.0 x 10 ⁻² (M)	2.66	0.26
	4.0 "	2.36	0.272
	6.0 "	2.32	0.308
	8.0 "	2.19	0.318
	10.0 "	2.13	0.325
PrDA	2.0 x 10 ⁻² (M)	3.198	0.356
	4.0 "	3.12	0.445
	6.0 "	3.03	0.501
	8.0 "	3.00	0.558
	10.0 "	2.93	0.597

plotted against Debye Huckel parameter $\frac{1}{a_0}$, a linear graph is obtained (Fig. 59).

From a linear plot of Kielland's equation (Fig. 60), thermodynamic equilibrium constants and standard Gibbs free energy change of some of the exchange reactions have been calculated and are shown in Table 11. It should be noted that the values of the selectivity coefficients and thermodynamic equilibrium constants (Table 11) are greater in the present case than those obtained from H-Co₃-bentonite. So it may be said that $\left[\text{Co}(\text{OH})_3 \right]^{3+}$ is attached to the Na-bentonite surface with a weaker force. The order of preference of $\left[\text{Co}(\text{OH})_3 \right]^{3+}$ ions for the bentonite surface is, therefore, H-bentonite > Na-bentonite, which has also been observed with $\left[\text{Co}(\text{OH})_3 \right]^{3+}$ and bentonite.

Table 11

Evaluation of thermodynamic quantities
from Kielland's equation at 25°C

Exchange system	Thermodynamic equilibrium constant	ΔG° Cal/mole
$K_{\text{Co}^{\text{Na}}\text{Co}^{\text{Na}}\text{Co}^{\text{Na}}}$	0.1698	1050
$K_{\text{Co}^{\text{K}}\text{Co}^{\text{K}}\text{Co}^{\text{K}}}$	0.188	988.65
$K_{\text{Co}^{\text{NH}_4}\text{Co}^{\text{NH}_4}\text{Co}^{\text{NH}_4}}$	0.199	955.92
$K_{\text{Co}^{\text{Rb}}\text{Co}^{\text{Rb}}\text{Co}^{\text{Rb}}}$	0.2137	913.65
$K_{\text{Co}^{\text{Cs}}\text{Co}^{\text{Cs}}\text{Co}^{\text{Cs}}}$	0.7217	193.10
$K_{\text{Co}^{\text{Ca}}\text{Co}^{\text{Ca}}\text{Co}^{\text{Ca}}}$	0.263	790.92
$K_{\text{Co}^{\text{Mg}}\text{Co}^{\text{Mg}}\text{Co}^{\text{Mg}}}$	0.251	818.19
$K_{\text{Co}^{\text{EDA}}\text{Co}^{\text{EDA}}\text{Co}^{\text{EDA}}}$	0.630	272.73
$K_{\text{Co}^{\text{PrDA}}\text{Co}^{\text{PrDA}}\text{Co}^{\text{PrDA}}}$	0.794	136.36

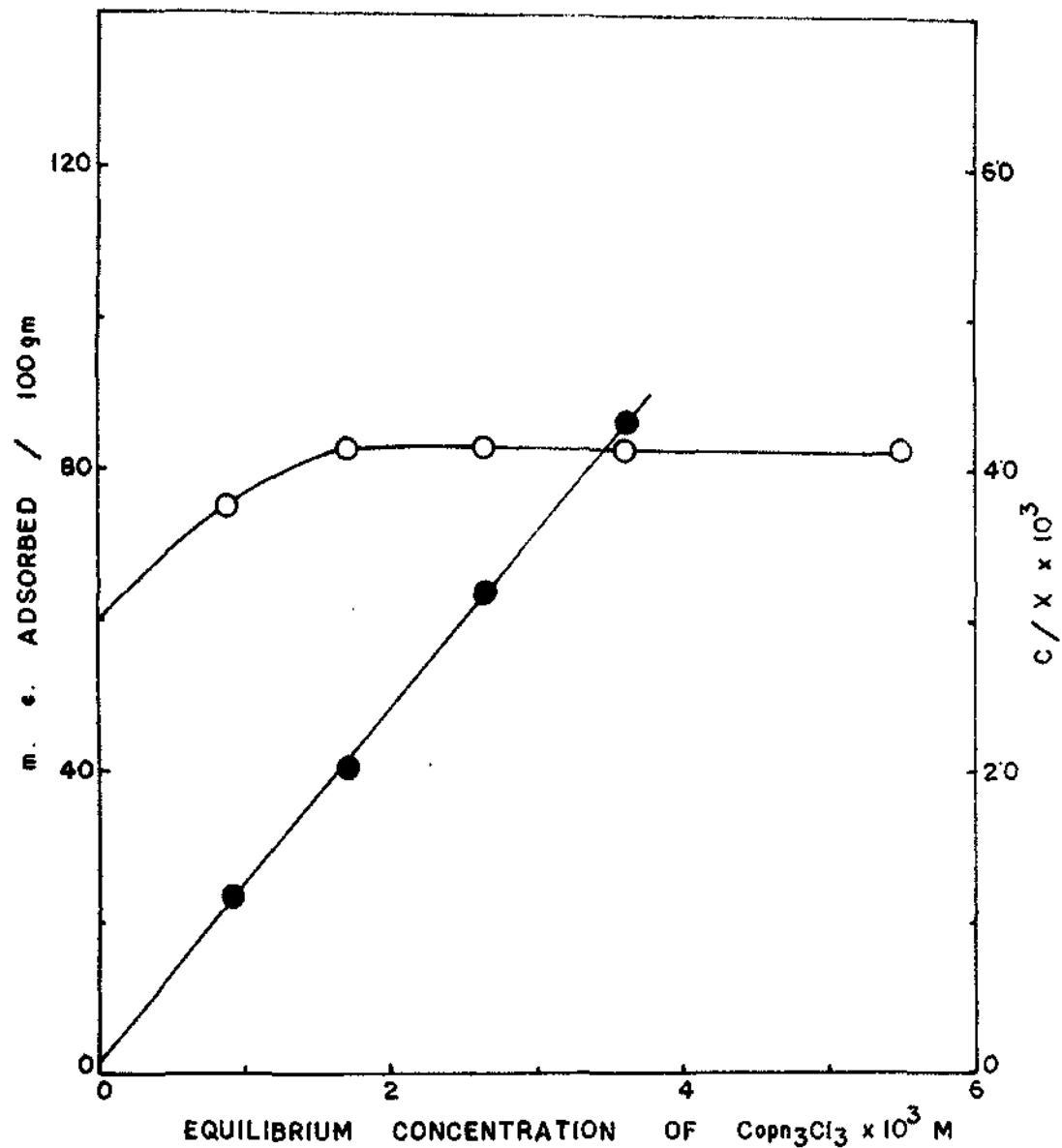


FIG. 1a. ADSORPTION ISOTHERM OF Copn_3Cl_3 ON H-BENTONITE.

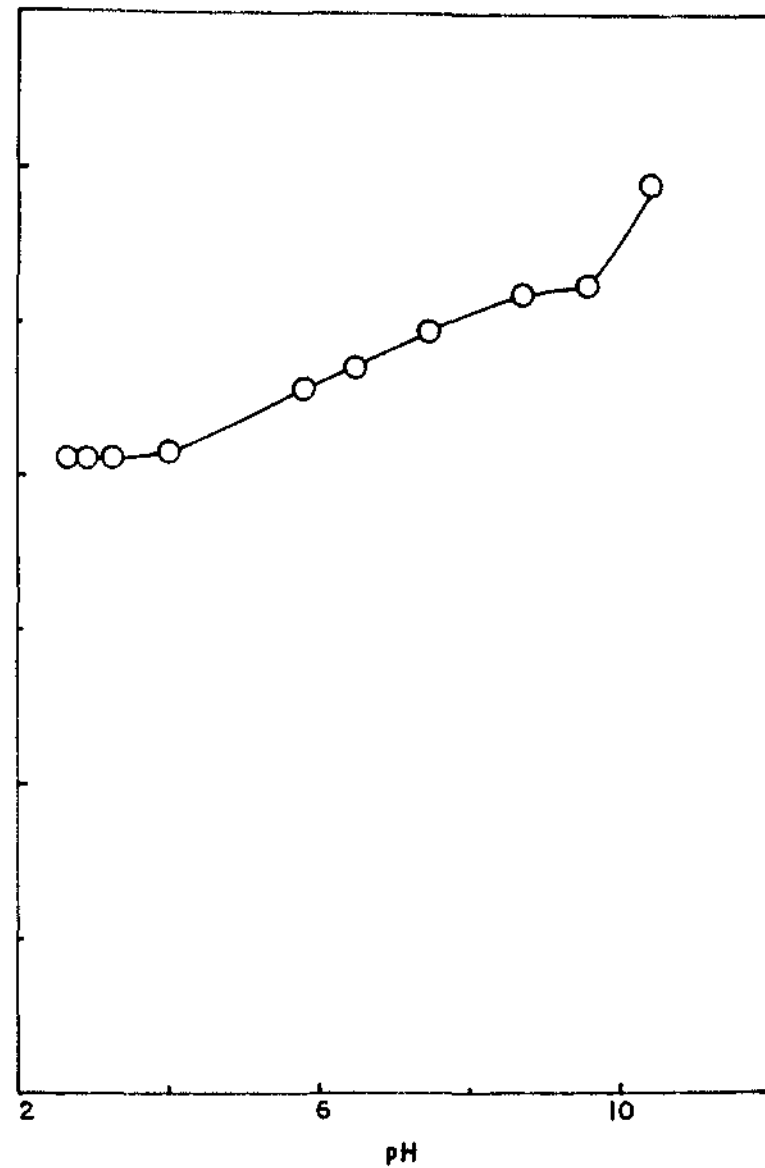


FIG. 1b. ADSORPTION OF Copn_3Cl_3 ON BENTONITE AT DIFFERENT pH.

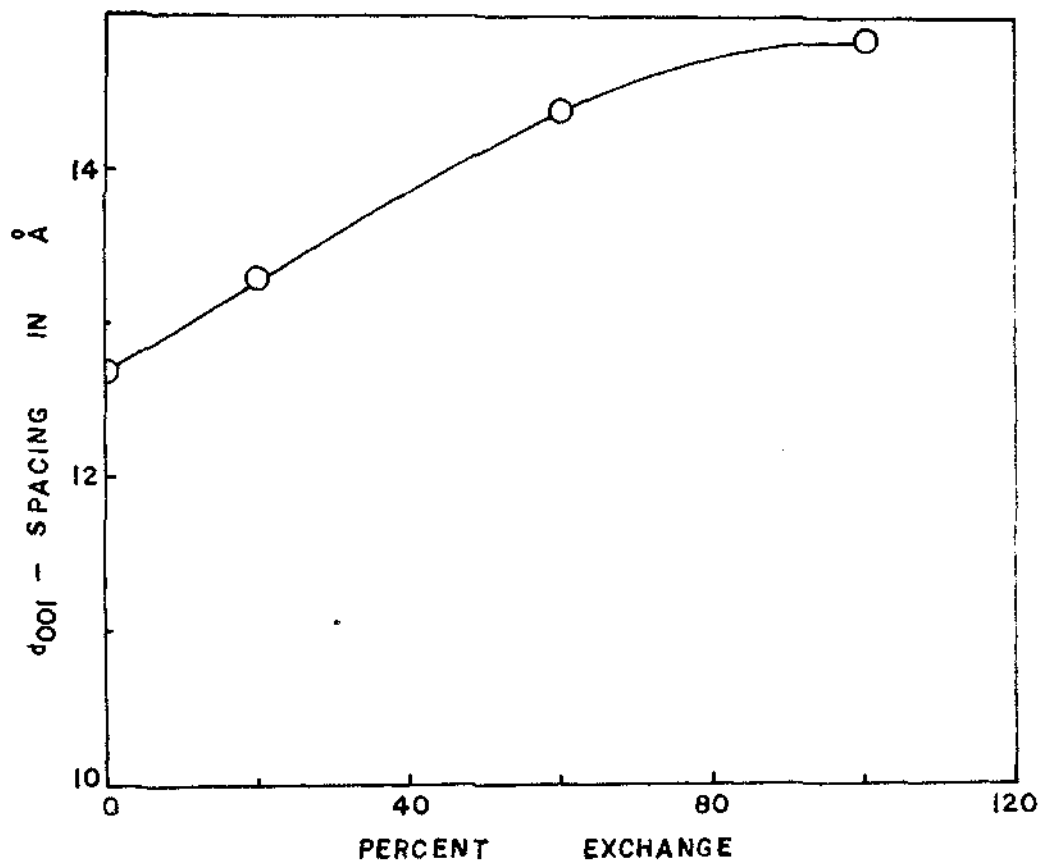


FIG. 2. d_{001} - SPACING VS. PERCENT EXCHANGE
FOR $H - Co(pH)_3^+$ - BENTONITE.

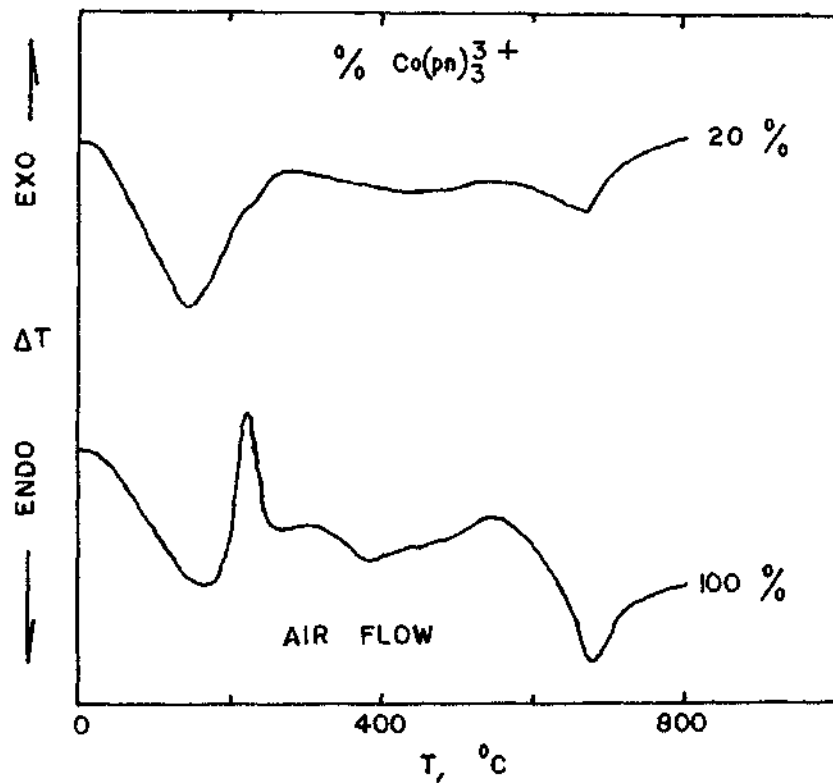


FIG. 3. D. T. A. CURVES FOR MIXED $\text{Co}(\text{pn})_3^+$ H^+ - BENTONITES (PRETREATED OVER CONC. H_2SO_4) USING AIR FLOW, HEATING RATE $10^\circ \text{C}/\text{min}$.

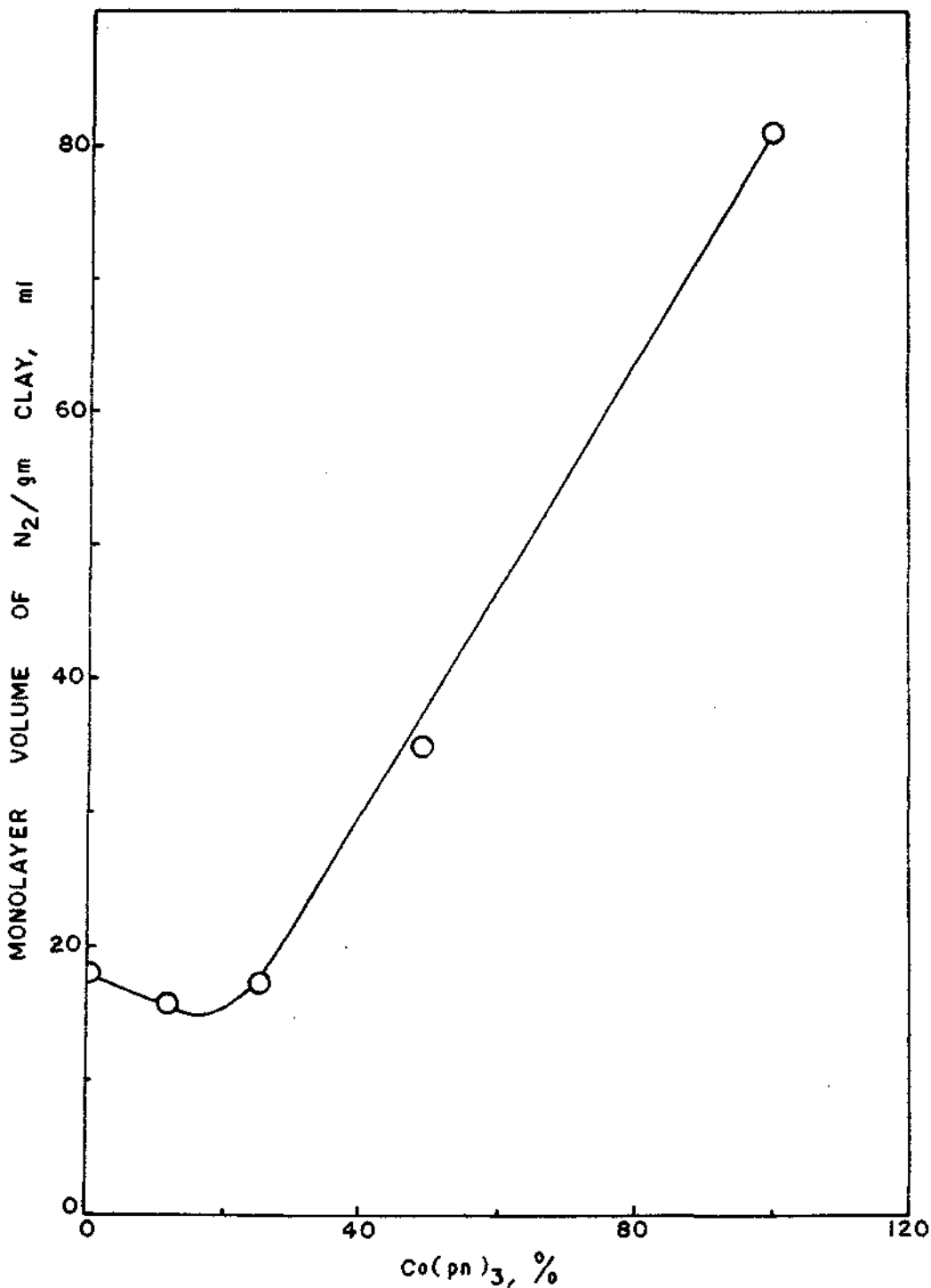


FIG. 4. NITROGEN MONOLAYER VOLUME (STP) AS A FUNCTION OF PERCENT $\text{Co}(\text{pn})_3^{3+}$ EXCHANGE, FOR MIXED $\text{Co}(\text{pn})_3^{3+}-\text{H}^+$ BENTONITE.

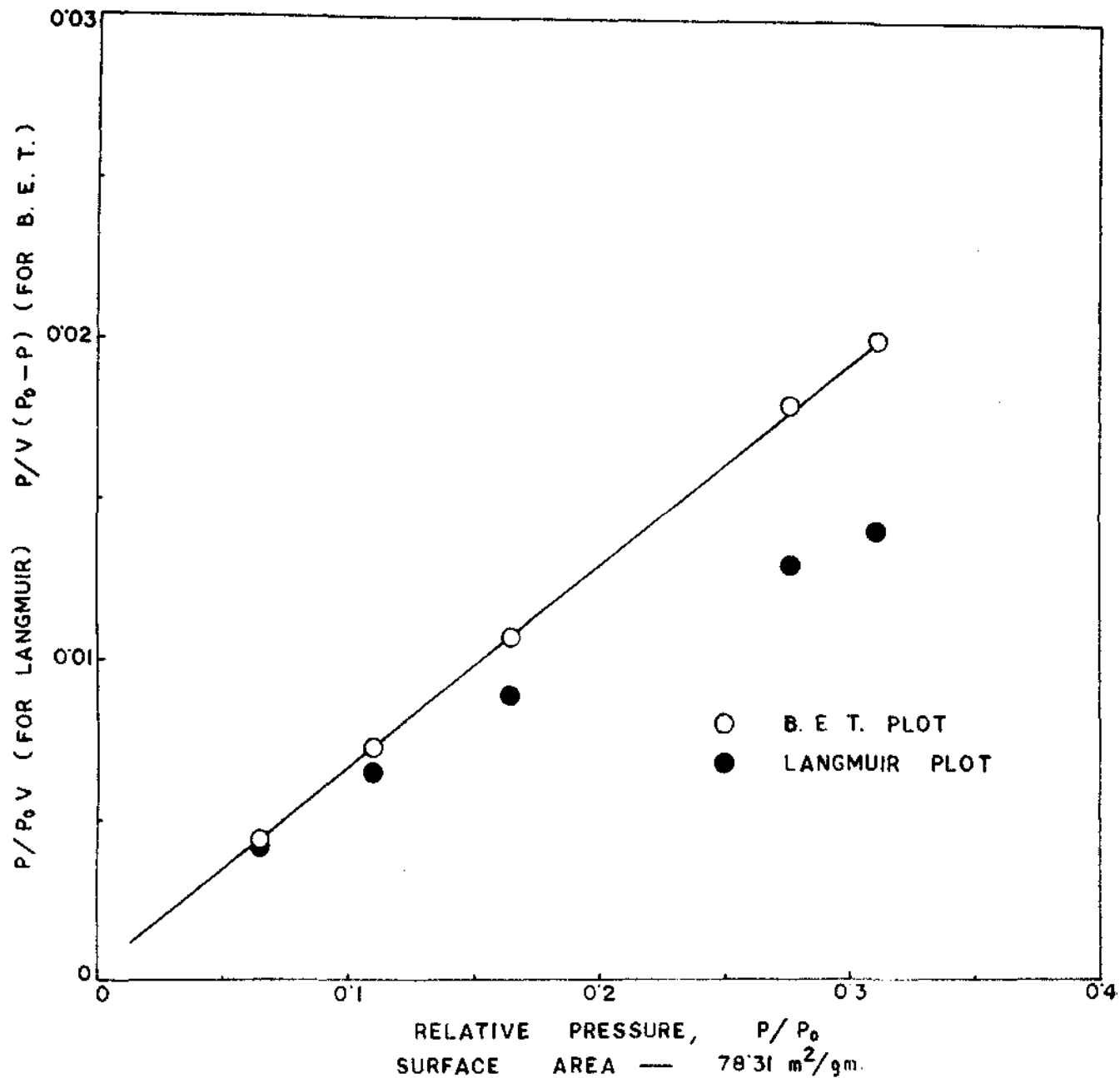


FIG. 5. NITROGEN SORPTION DATA FOR H^+ BENTONITE.

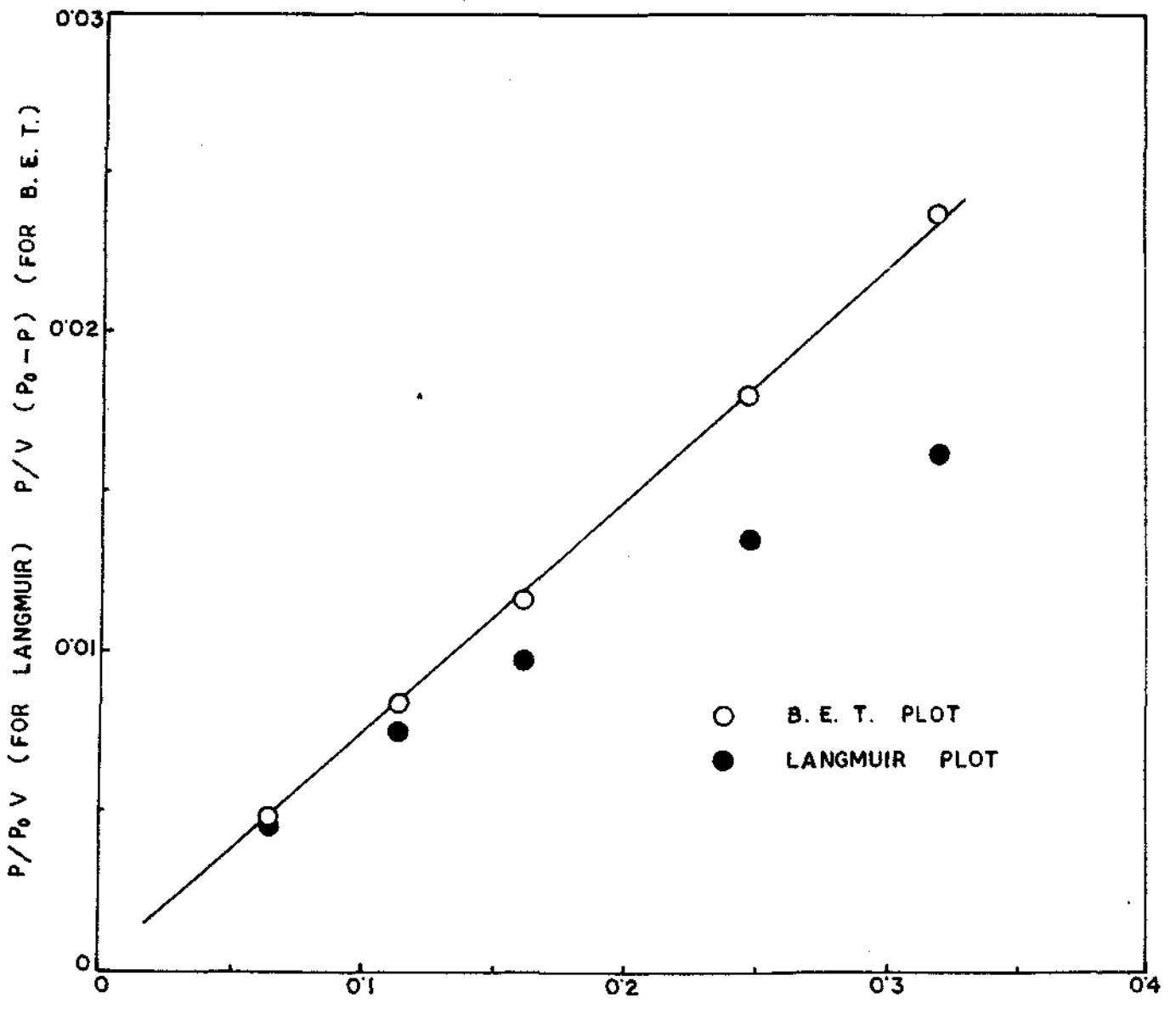
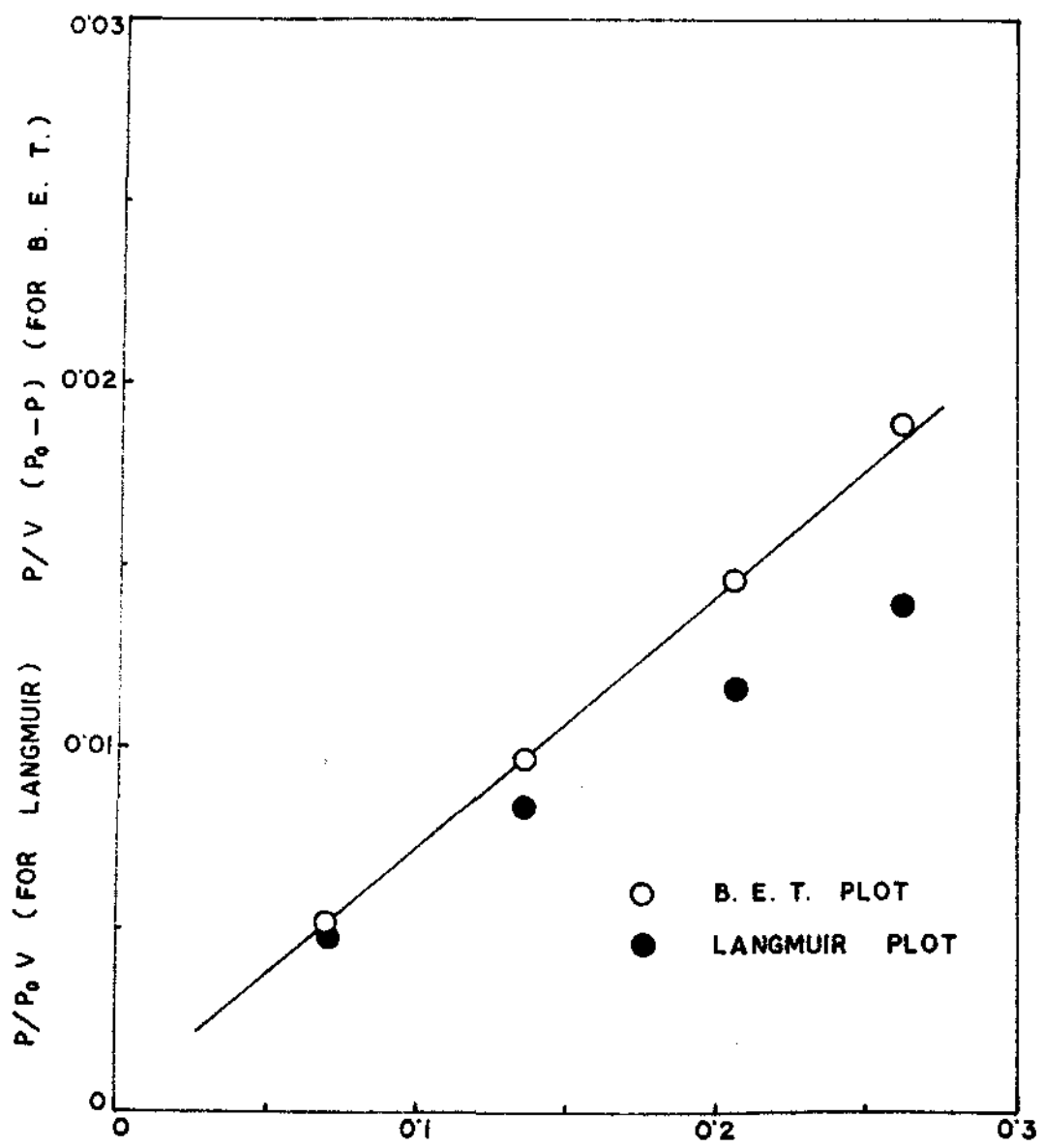


FIG. 6. NITROGEN SURFACE AREA — $71.46 \text{ m}^2/\text{gm}$.
 SORPTION DATA FOR $12.5\% \text{ Co}(\text{pH})_3, \text{H}^+$ BENTONITE.



SURFACE AREA — 74.09 m²/gm.
 FIG. 7. NITROGEN SORPTION DATA FOR 25% Co(pH)₃⁺ H⁺ BENTONITE.

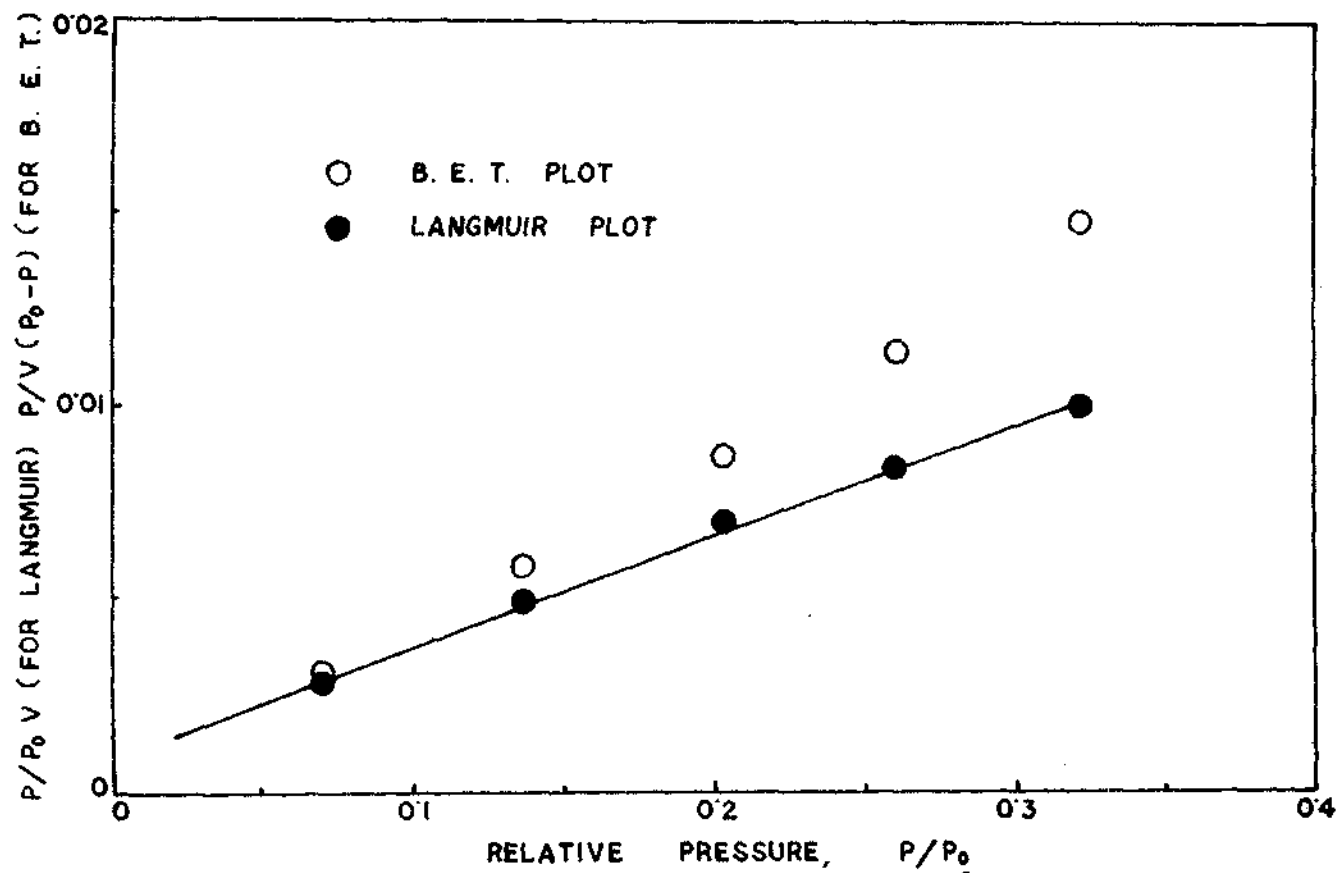


FIG. 8. NITROGEN SORPTION DATA FOR 50% $\text{Co}(\text{pn})_3^+ \text{H}^+$ BENTONITE.
SURFACE AREA — $153.32 \text{ m}^2/\text{gm}$

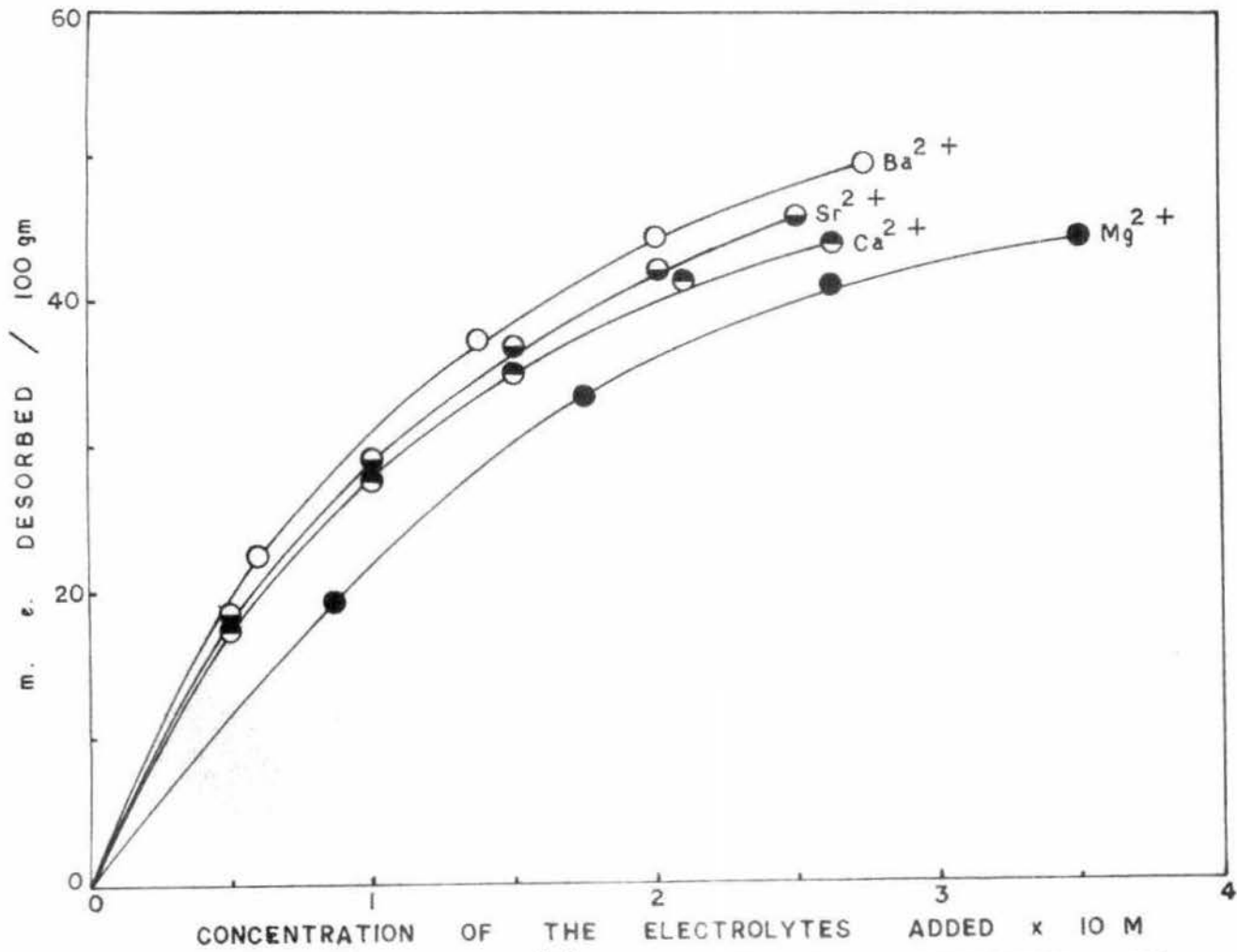


FIG. II. DESORPTION OF Copn_3^{3+} FROM H - Copn_3 - BENTONITE BY DIFFERENT IONS.

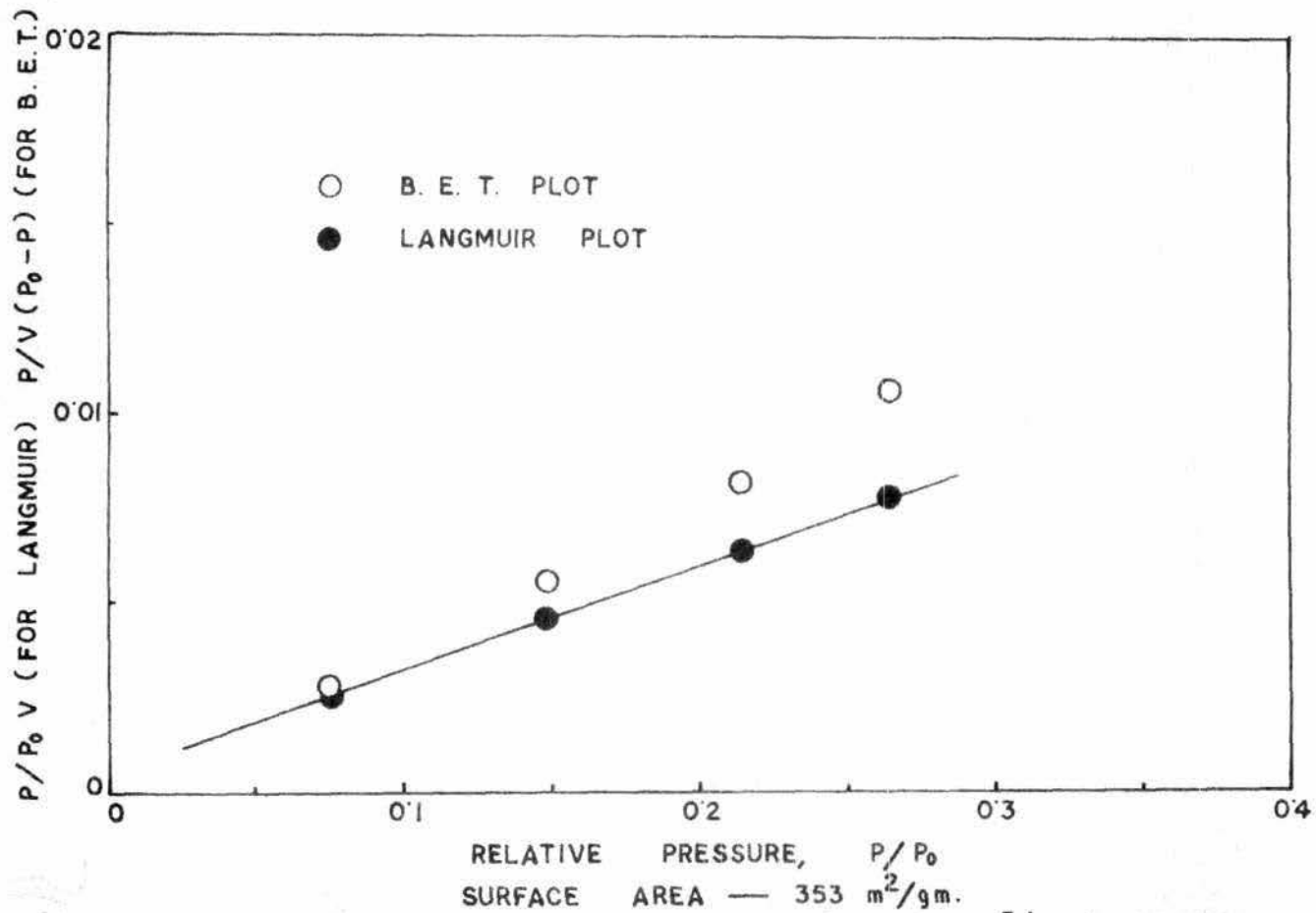


FIG. 9 . NITROGEN SORPTION DATA FOR 100 % $\text{Co}(\text{pn})_3^+ \text{H}^+$ BENTONITE.

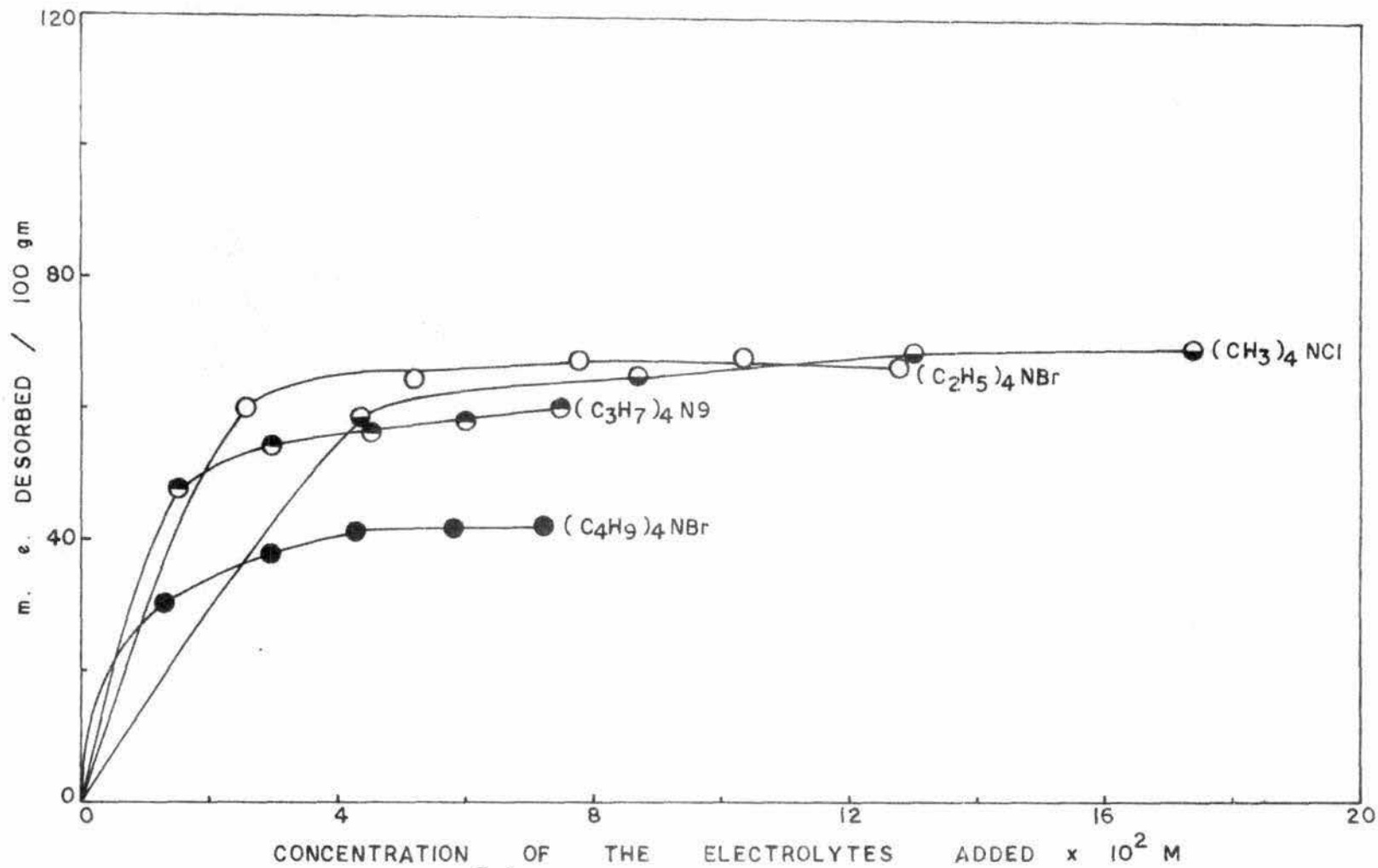


FIG.12. DESORPTION OF Copn_3^+ FROM H - Copn_3 -BENTONITE BY DIFFERENT IONS.

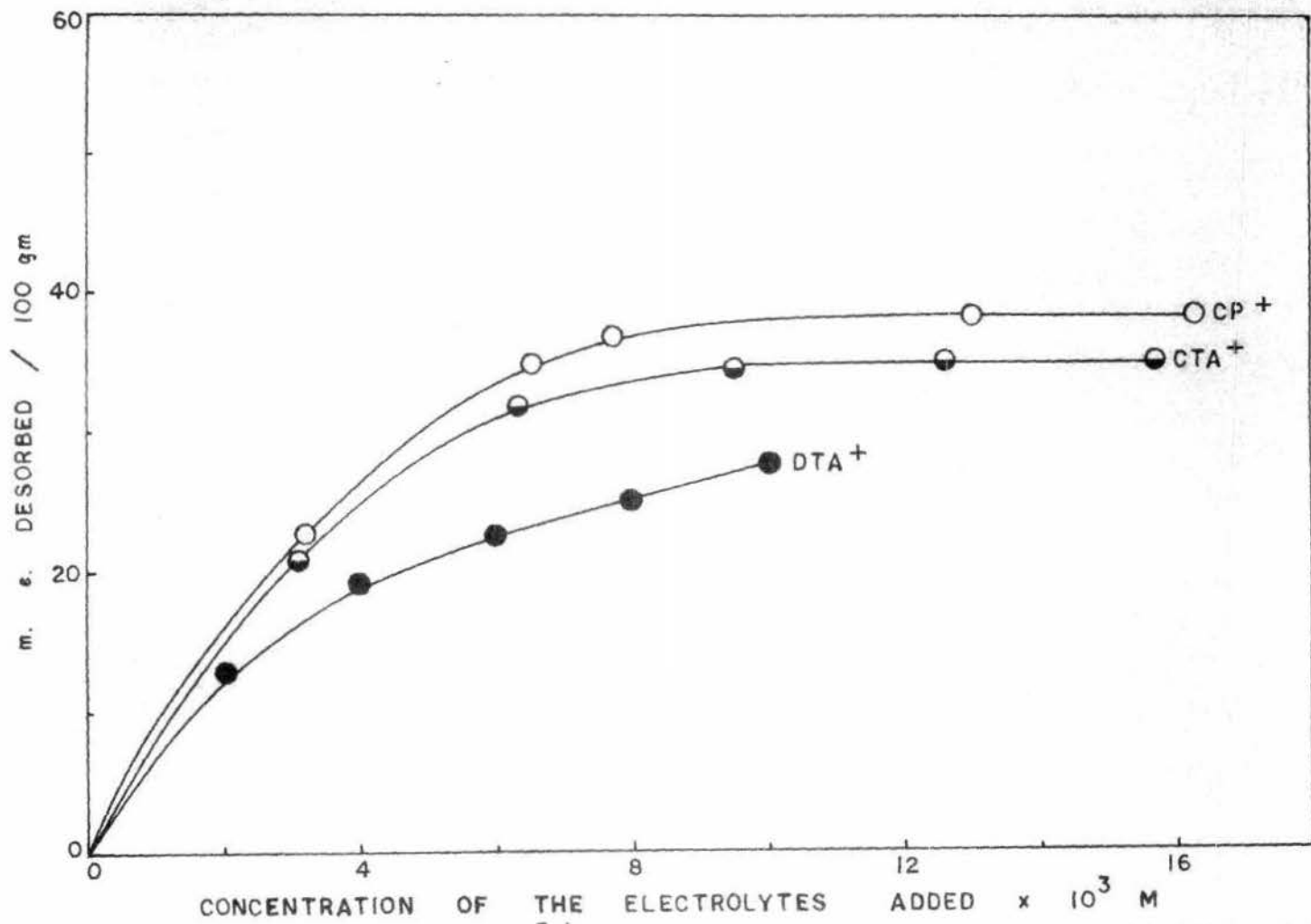


FIG.13. DESORPTION OF Copn_3^{3+} FROM H - Copn_3 - BENTONITE BY DIFFERENT IONS.

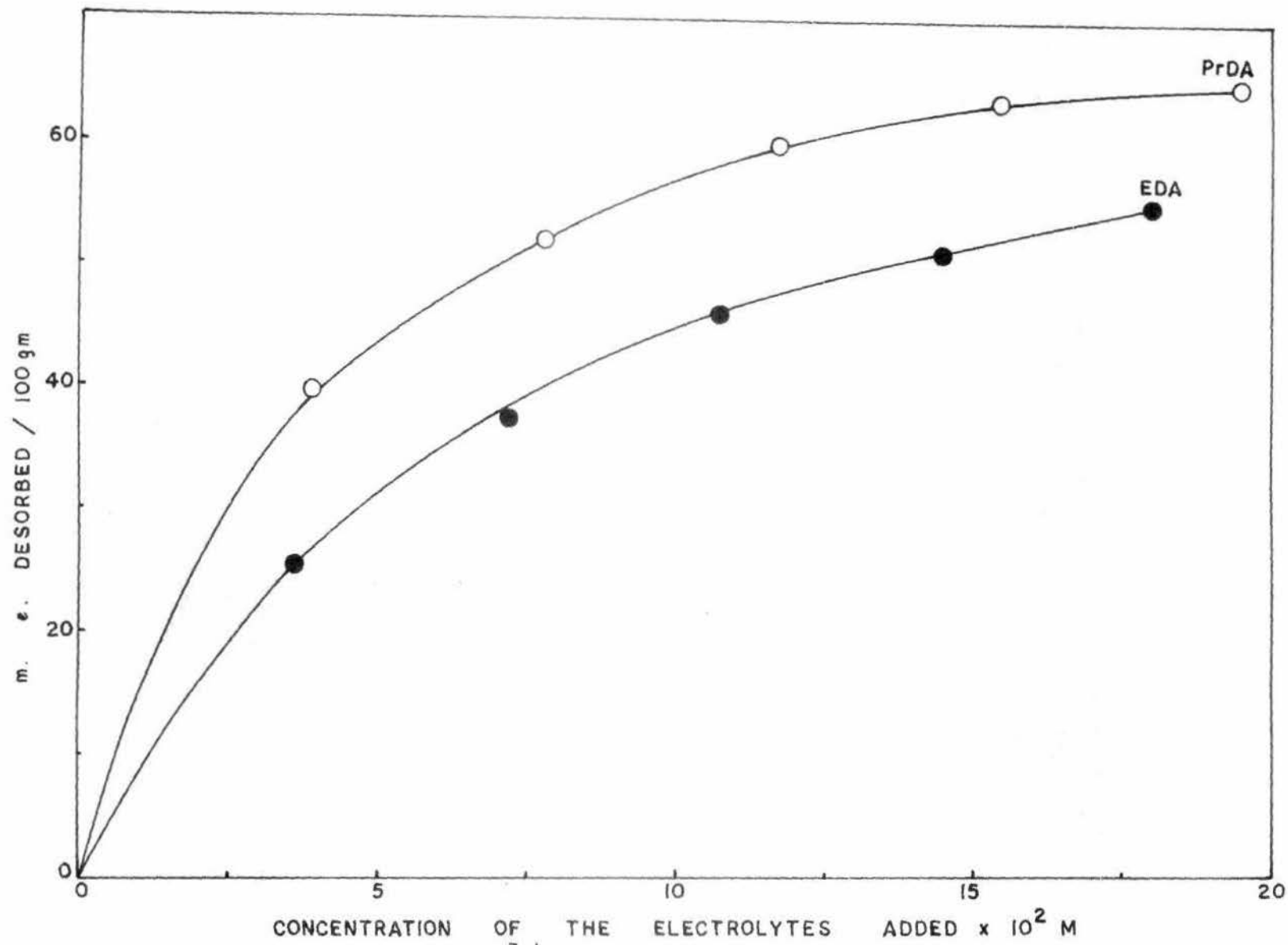


FIG. 14. DESORPTION OF Co^{3+} FROM H - Co^{3+} - BENTONITE BY DIFFERENT IONS.

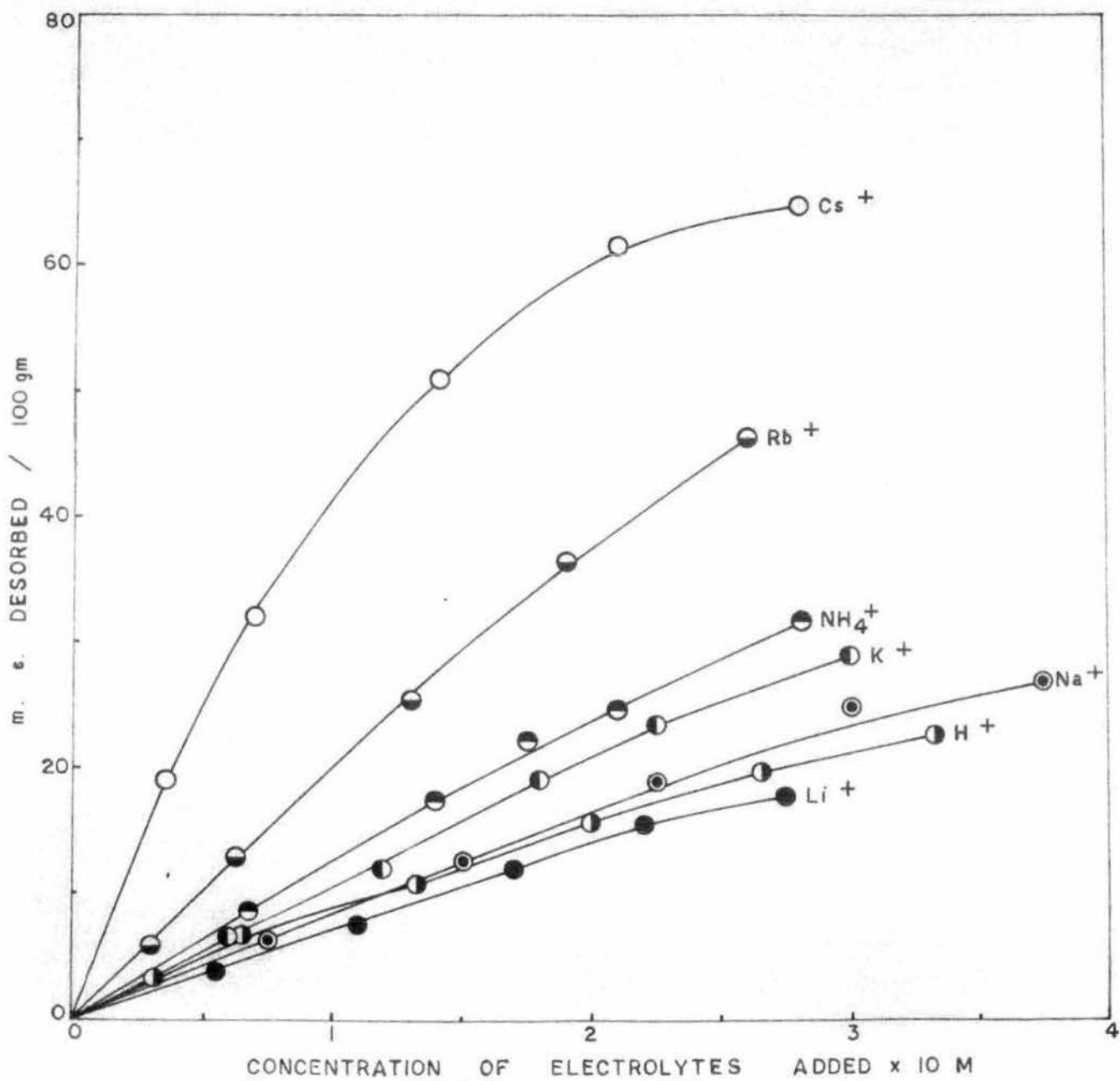


FIG. 10. DESORPTION OF Copn_3^+ FROM H - Copn_3 -BENTONITE BY DIFFERENT IONS.

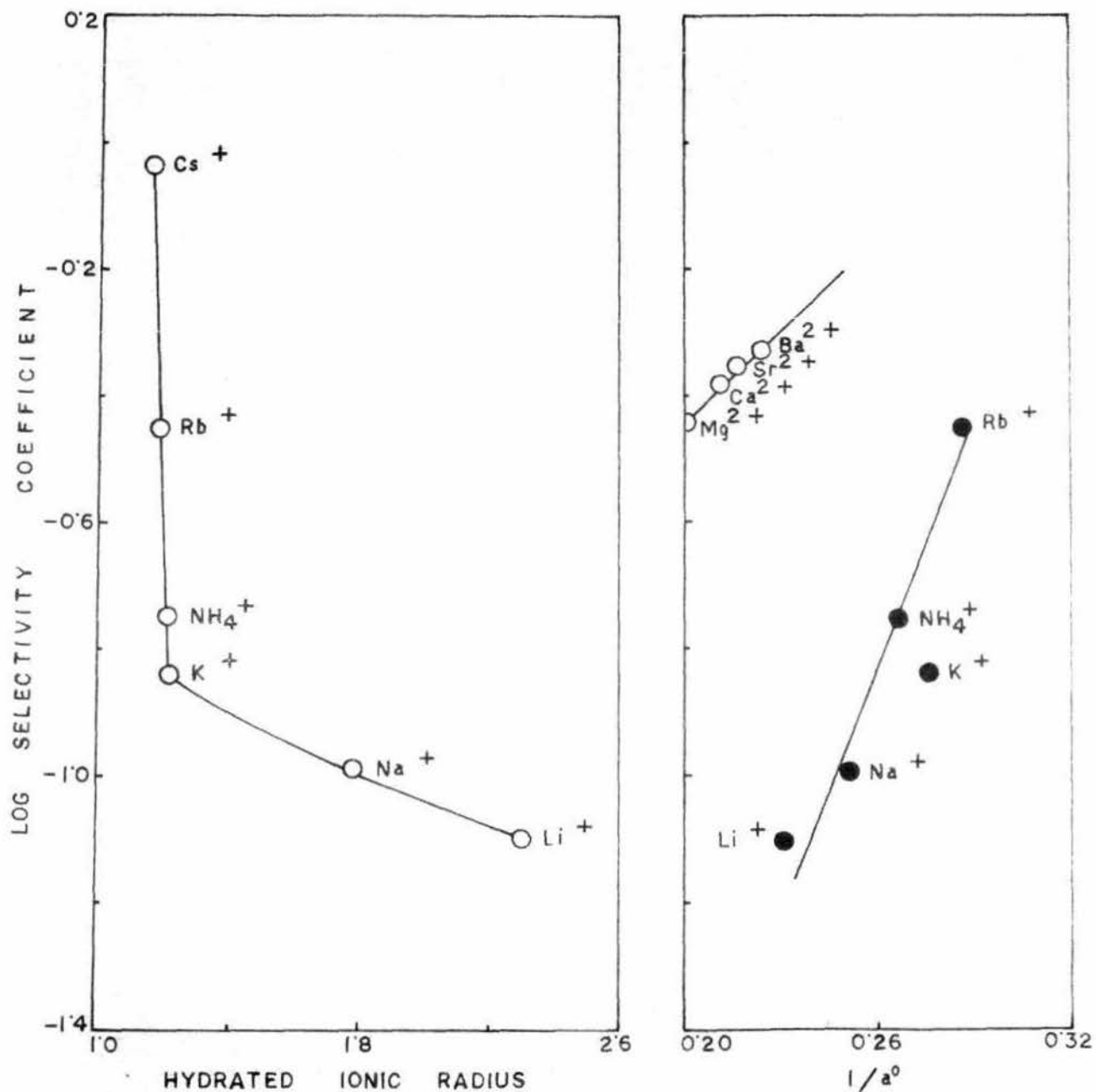


FIG.15. CORRELATION OF SELECTIVITY COEFFICIENT WITH HYDRATED IONIC RADIUS & DEBYE HÜCKEL PARAMETER a^0 IN THE DESORPTION OF H-Copn₃-BENTONITE.

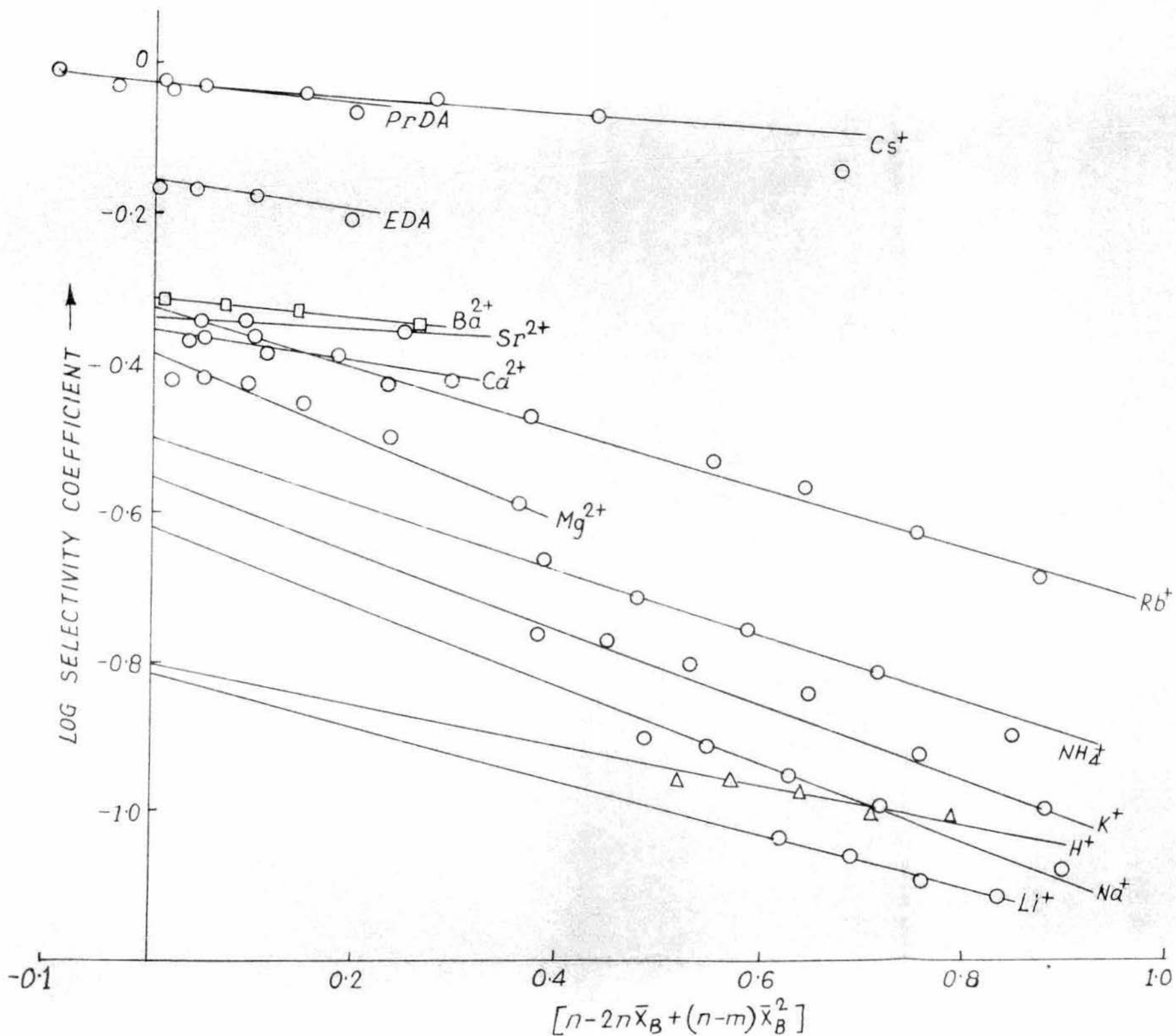


FIG. 16. PLOT OF LOG SELECTIVITY COEFFICIENT AGAINST $n-2n\bar{x}_B+(n-m)\bar{x}_B^2$ IN THE EXCHANGE OF $\text{Co}(\text{pn})_3^{3+}$ FROM H-Copn_3 -BENTONITE BY DIFFERENT IONS.

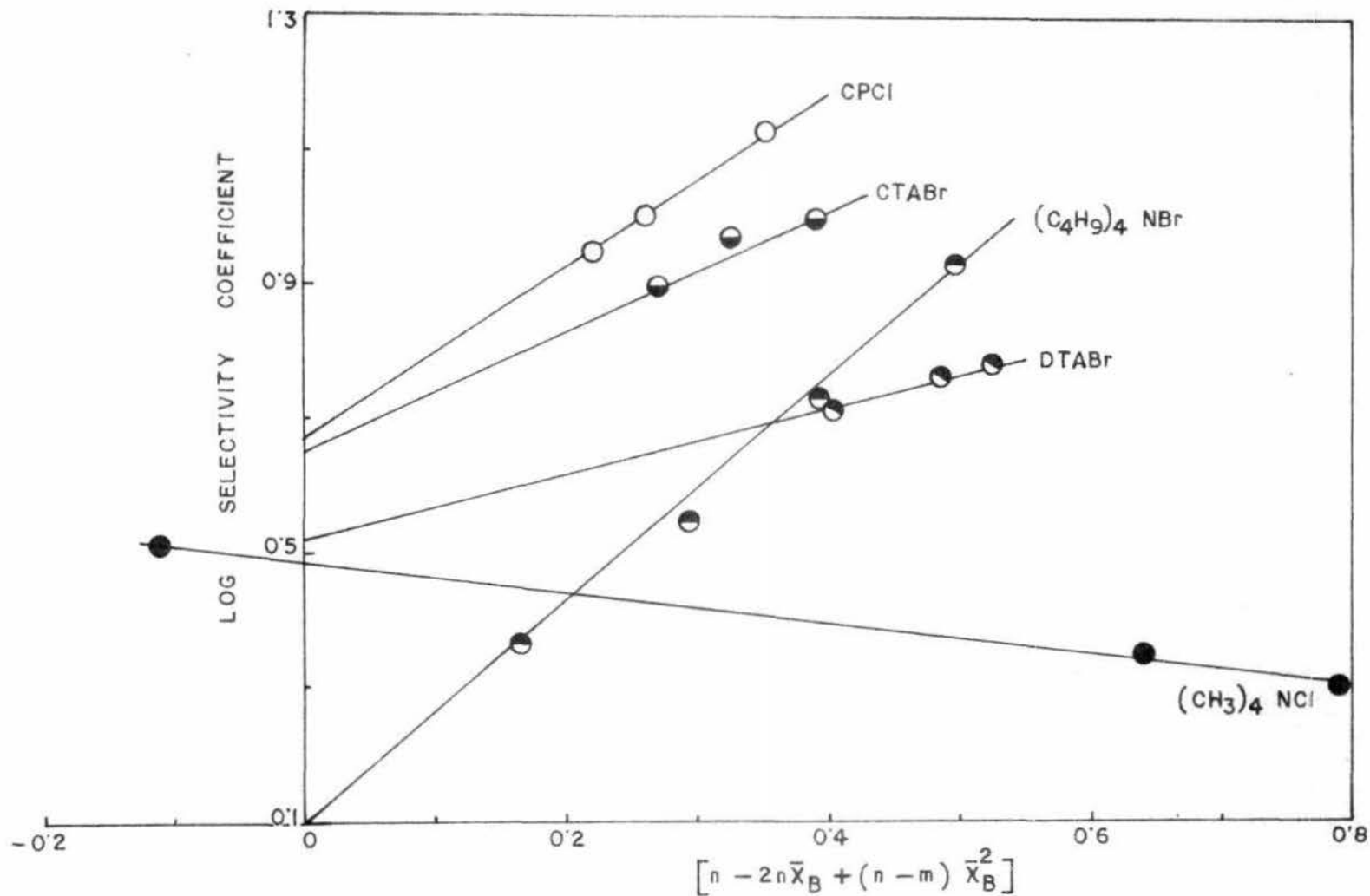


FIG. 17. PLOT OF LOG SELECTIVITY COEFFICIENT AGAINST $n - 2n\bar{X}_B + (n - m)\bar{X}_B^2$ IN THE EXCHANGE OF $\text{Co}(\text{pn})_3^{3+}$ FROM H-Copn₃-BENTONITE BY DIFFERENT IONS.

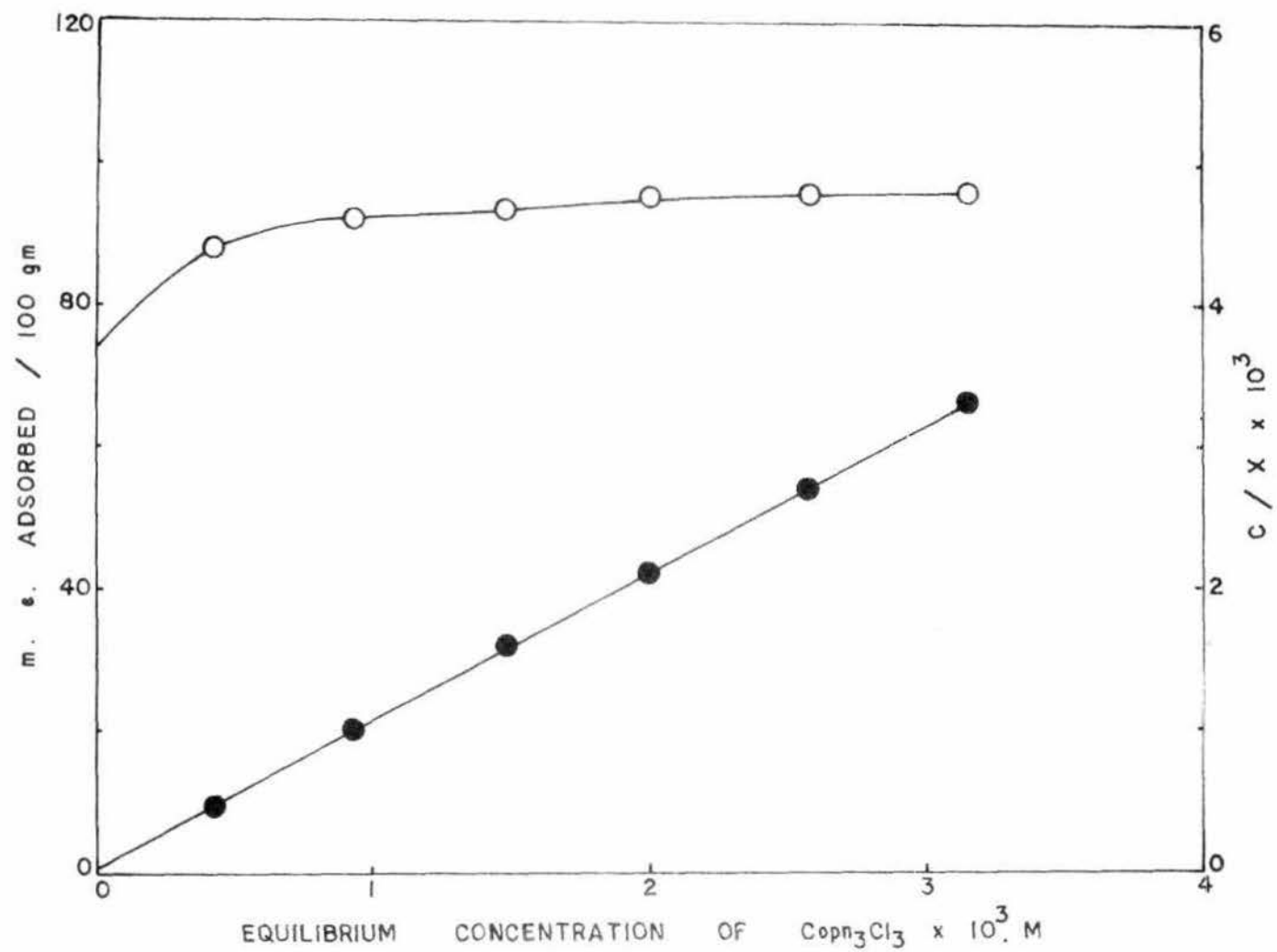


FIG. 18. ADSORPTION ISOTHERM OF Copn_3Cl_3 ON Na - BENTONITE.

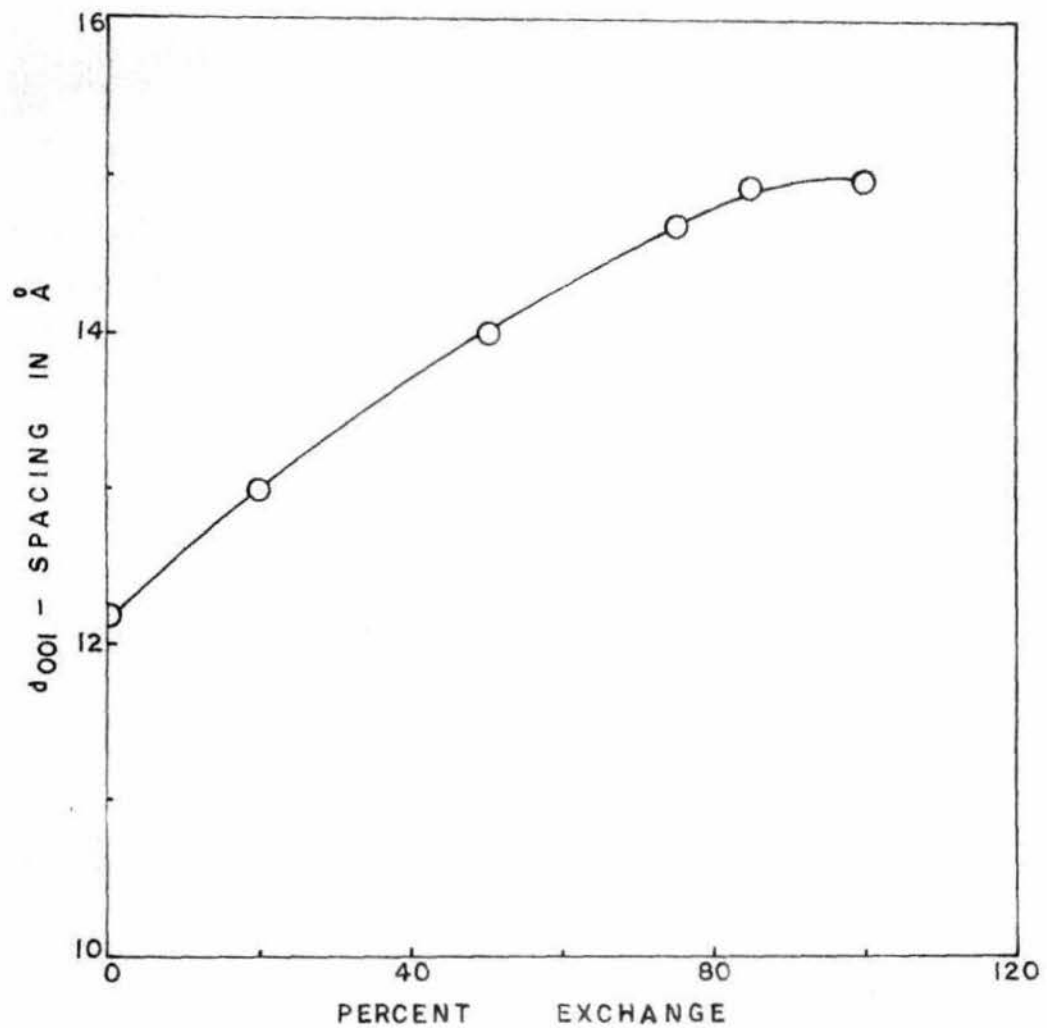


FIG. 19(a). d_{001} - SPACING VS PERCENT EXCHANGE
FOR Na - $\text{Co}(\text{pn})_3^{3+}$ - BENTONITE.

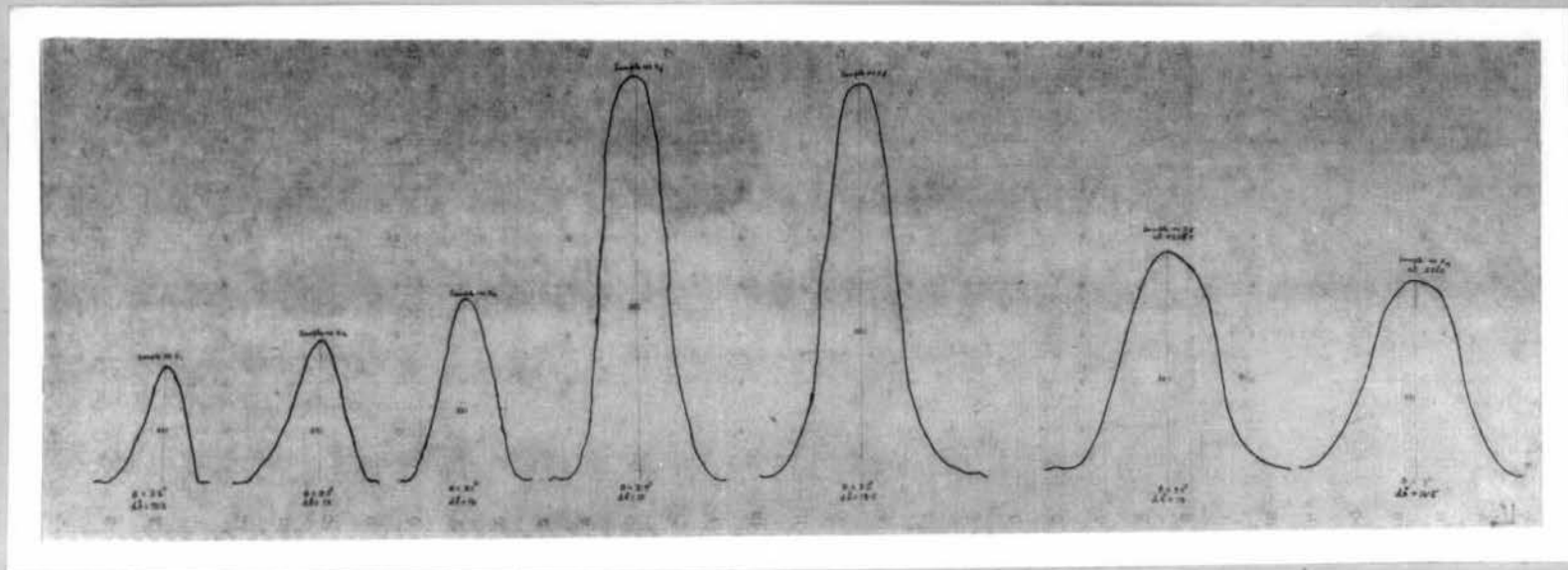


FIG. 19 (b). X-RAY DATA SHOWING CHANGES OF (001) DIFFRACTION PEAK:
 $X_1 = \text{Na-BENTONITE}$, $X_2 = 20\% \text{ EXCHANGED } \text{Co}(\text{pn})_3^{3+} \text{ CLAY}$, $X_3 = 55\% \text{ EXCHANGED } \text{Co}(\text{pn})_3^{3+} \text{ CLAY}$, $X_4 = 100\% \text{ EXCHANGED } \text{Co}(\text{pn})_3^{3+} \text{ CLAY AT ROOM TEMP. \& AT } 250^\circ \text{C.}$, $X_5 = 100\% \text{ EXCHANGED } \text{Co}(\text{tn})_3^{3+} \text{ CLAY AT ROOM TEMP. \& AT } 250^\circ \text{C.}$

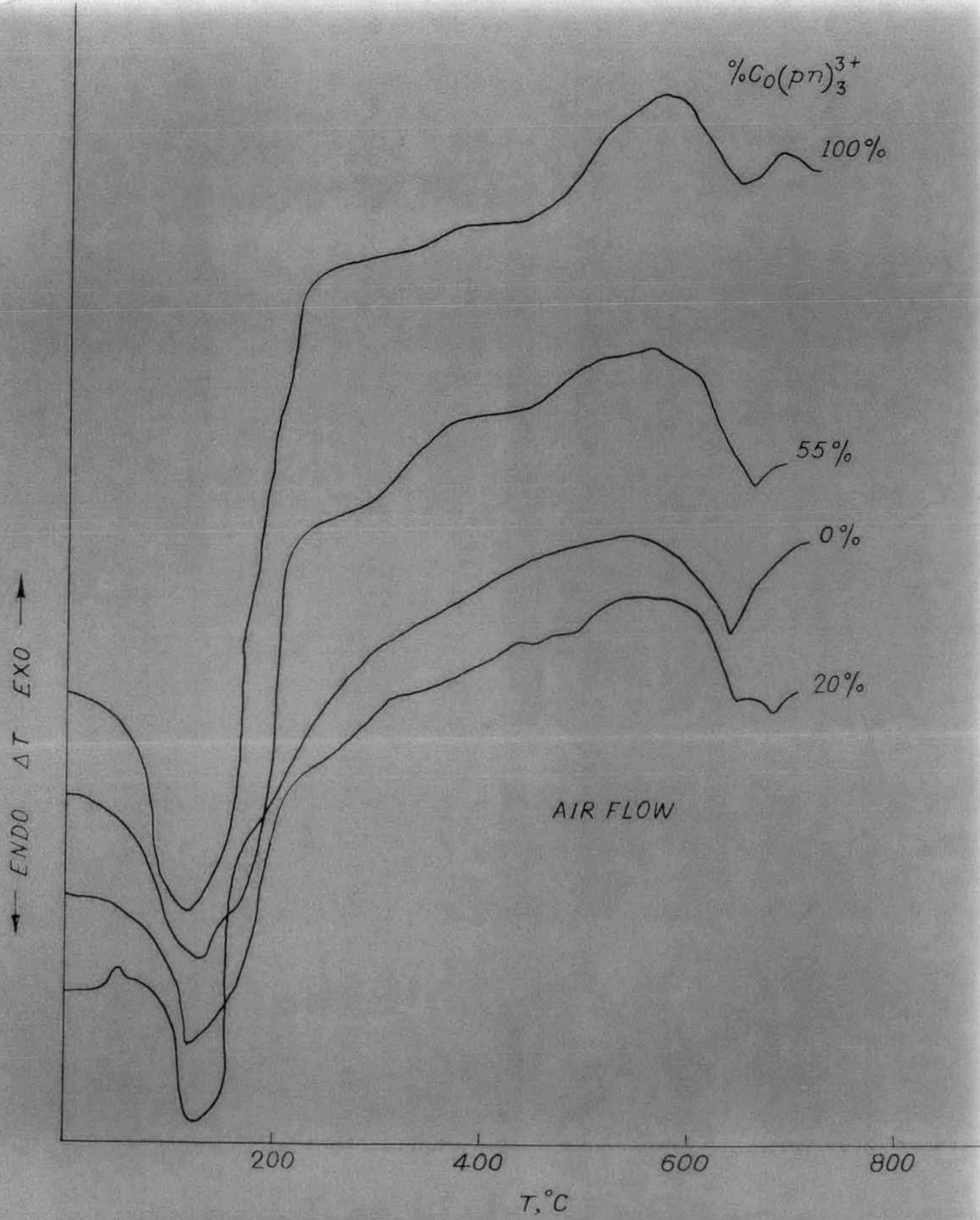


FIG. 20. D.T.A. CURVES FOR MIXED $\text{Co}(\text{pn})_3^{3+} - \text{Na}^+$ BENTONITES (PRETREATED OVER CONC. H_2SO_4) USING AIR FLOW; HEATING RATE $10^\circ\text{C}/\text{min}$.

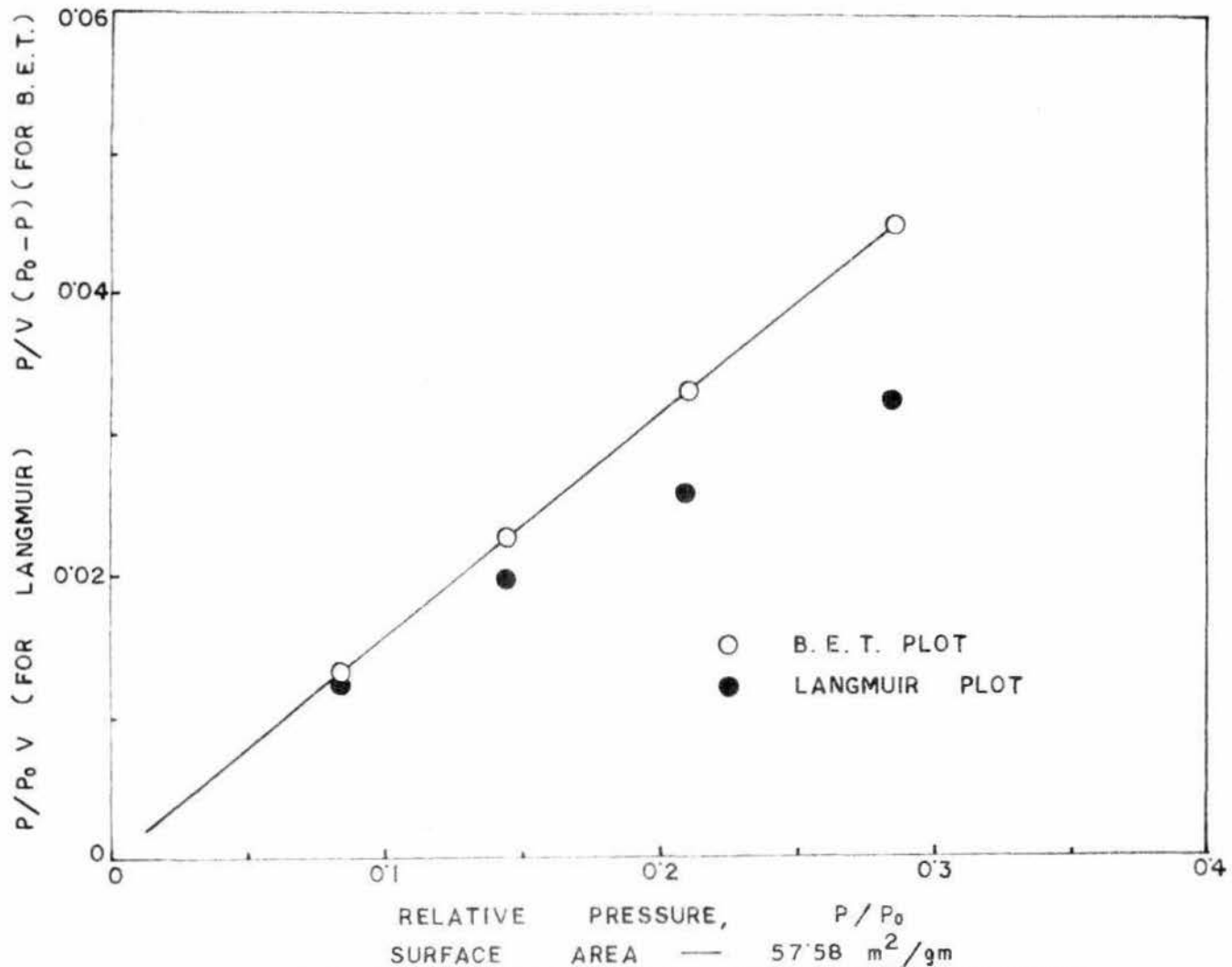


FIG. 21. NITROGEN SORPTION DATA FOR Na^+ BENTONITE.

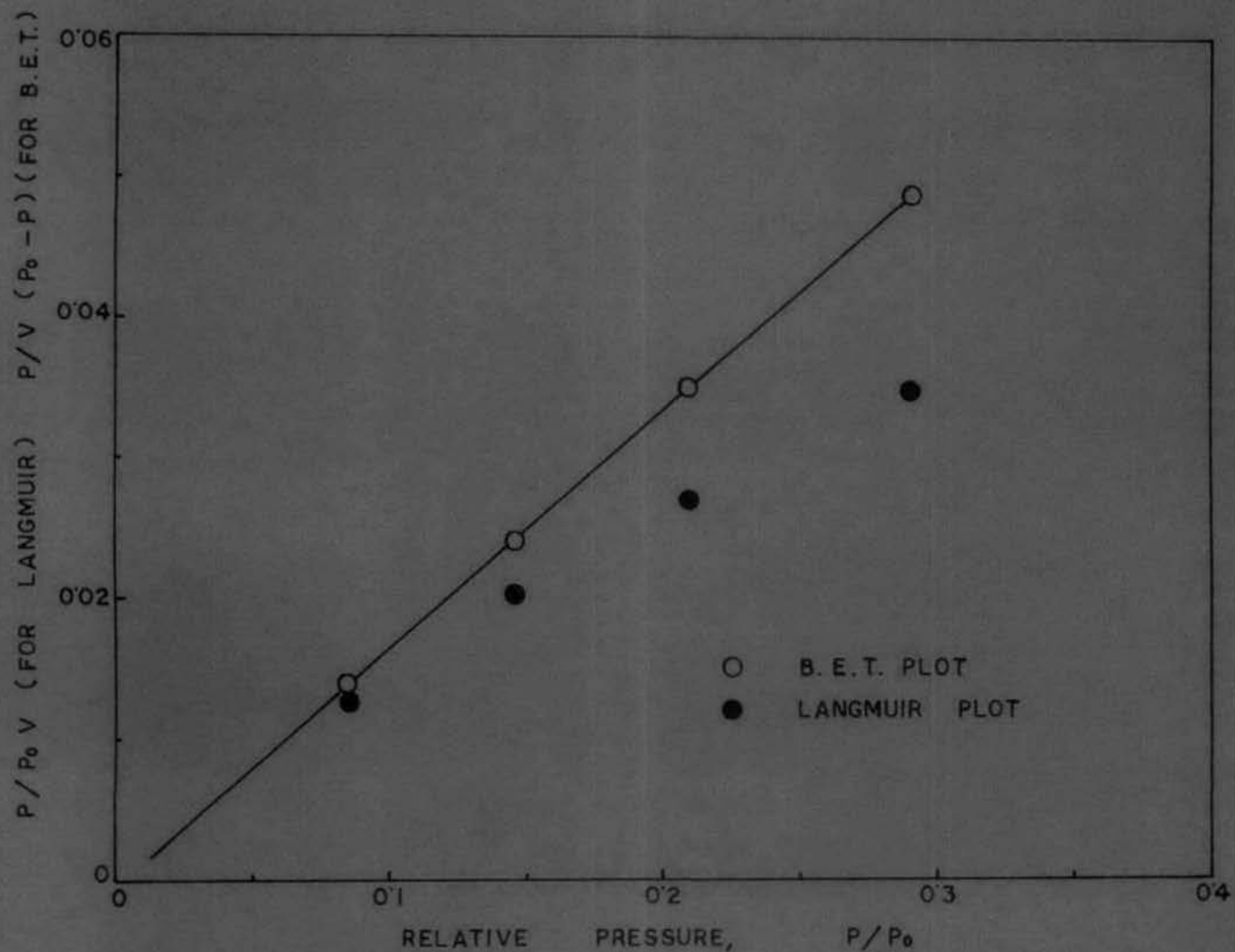


FIG. 22. NITROGEN SURFACE AREA — $43.34 \text{ m}^2/\text{gm}$
 SORPTION DATA FOR 12 PERCENT $\text{Co}(\text{pn})_3, \text{Na}^+$ BENTONITE

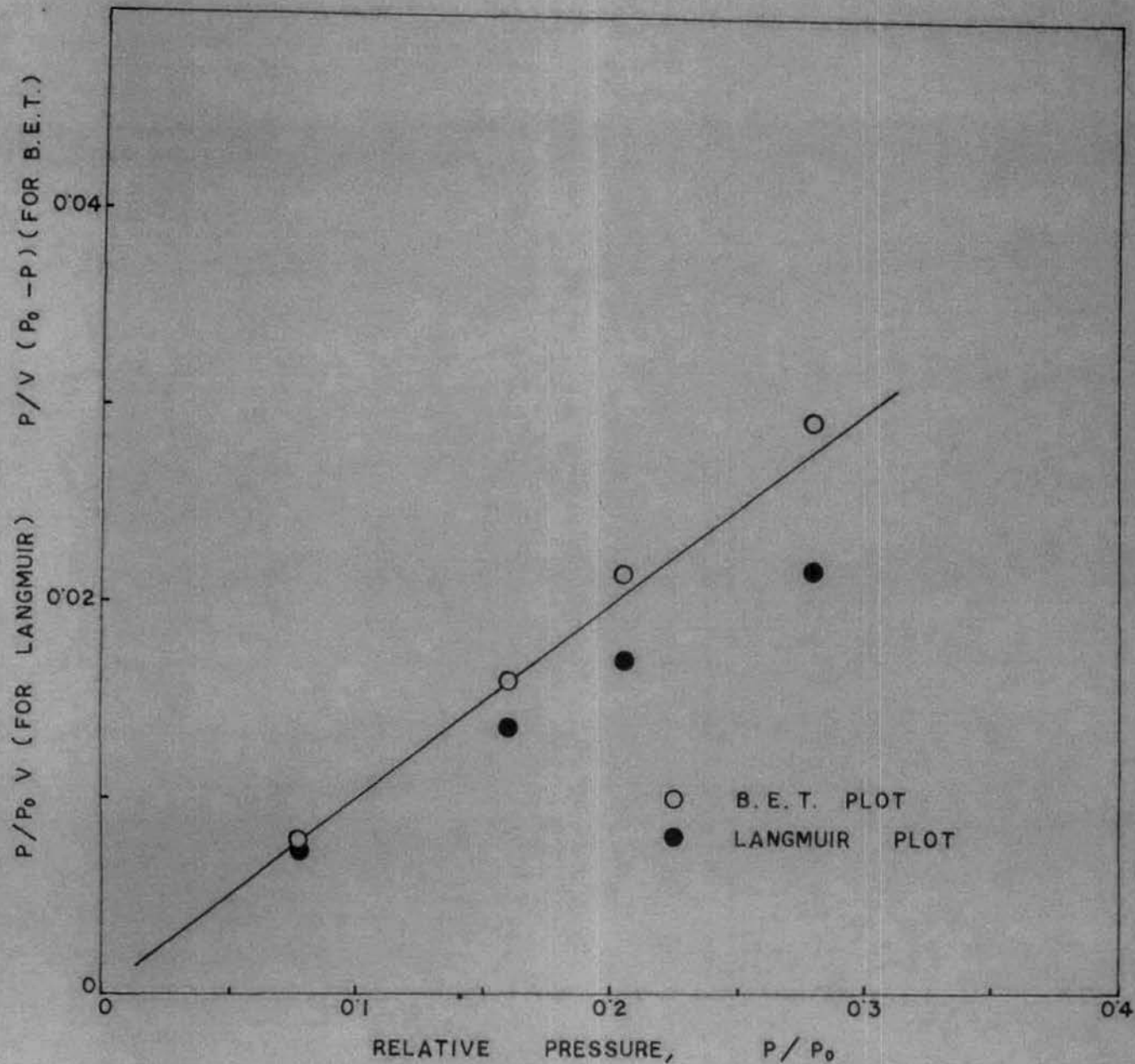


FIG. 23. NITROGEN SORPTION DATA FOR 20 PERCENT $\text{Co}(\text{pn})_3^+$
 Na^+ BENTONITE.

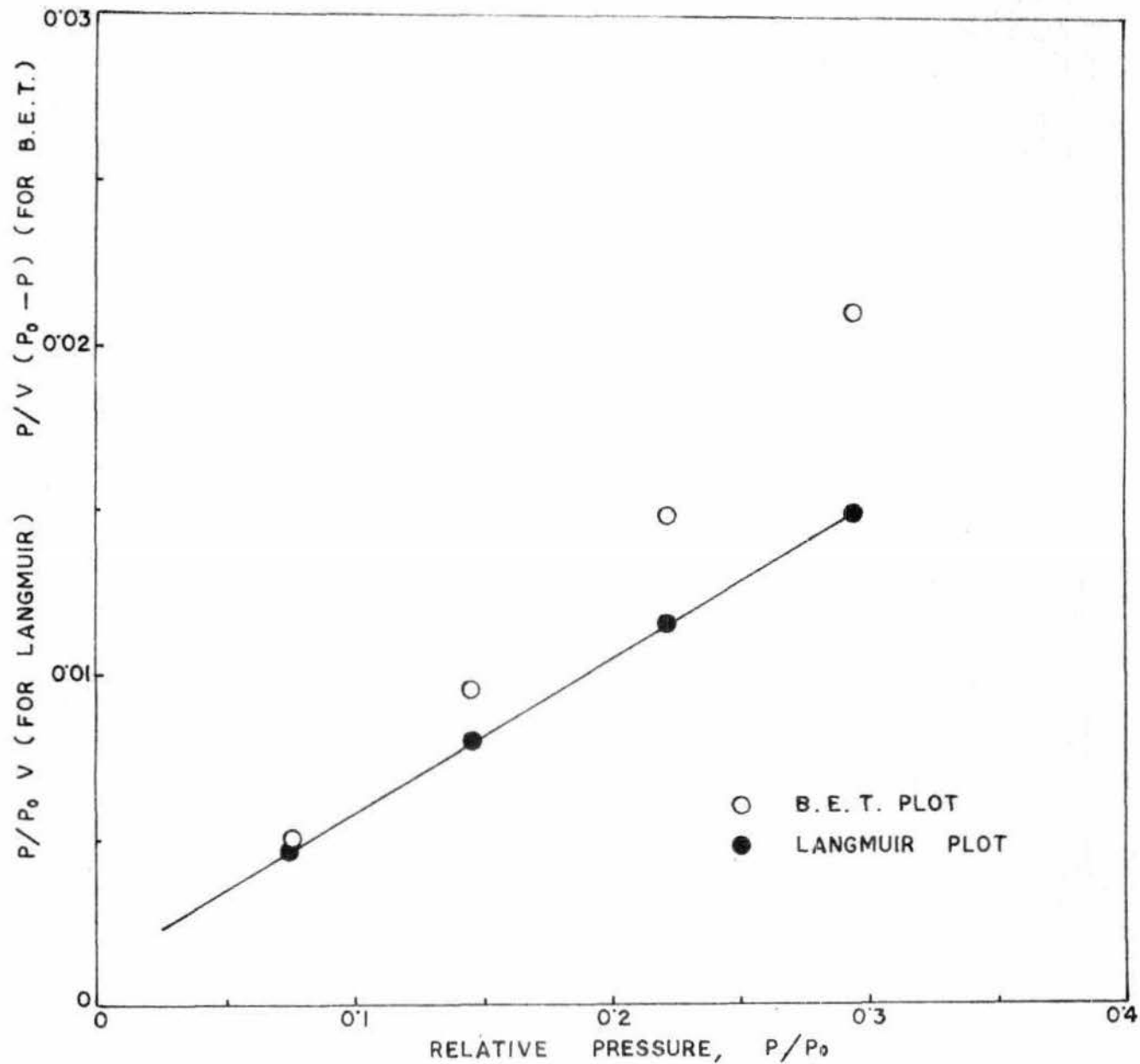


FIG. 24. NITROGEN SORPTION DATA FOR 45% $\text{Co}(\text{pn})_3, \text{Na}^+$ BENTONITE.
 SURFACE AREA — $108.32 \text{ m}^2/\text{gm}$

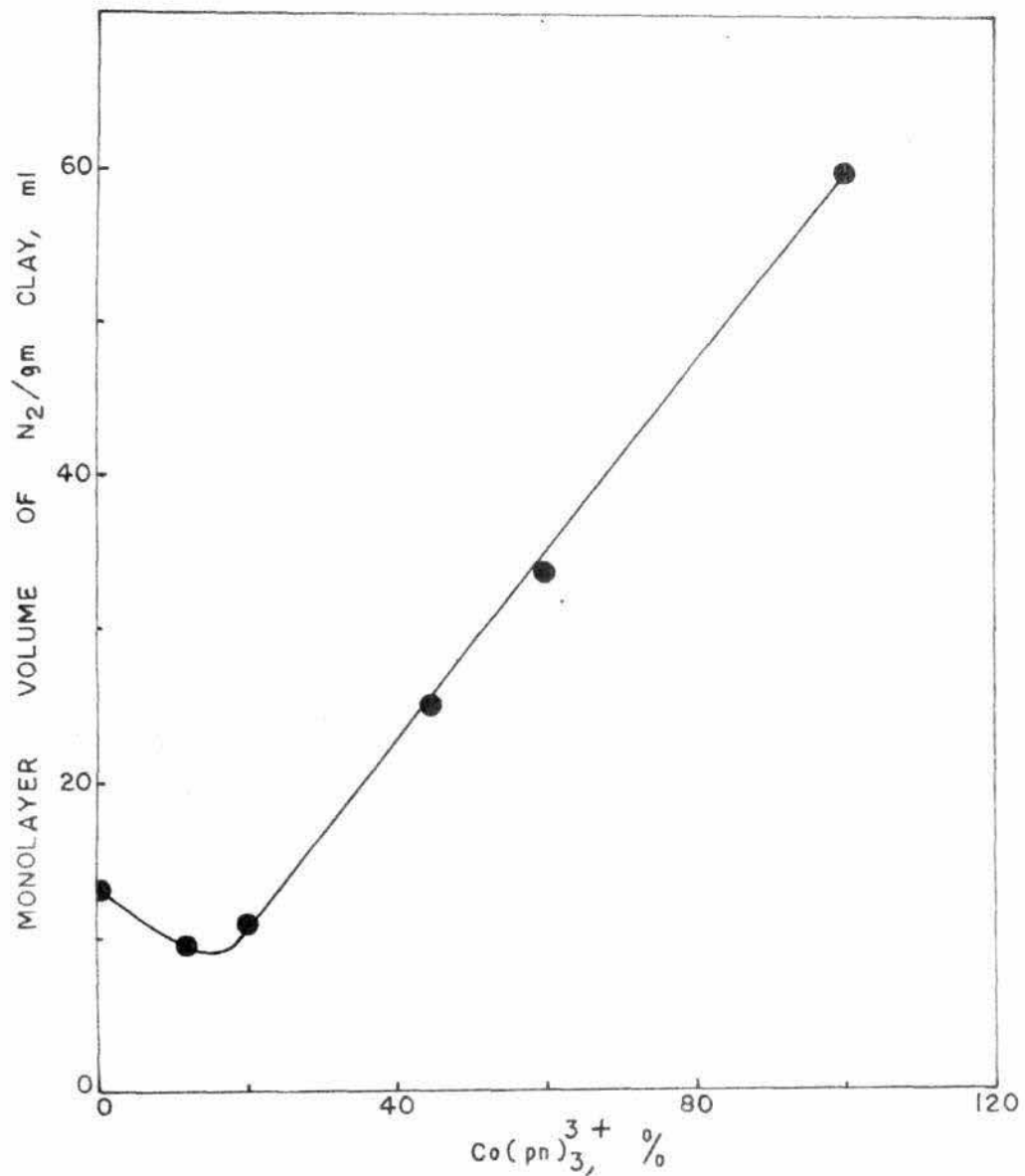


FIG. 25. NITROGEN MONOLAYER VOLUME (STP) AS A FUNCTION OF PERCENT $\text{Co}(\text{pn})_3^{3+}$ EXCHANGE, FOR MIXED $\text{Co}(\text{pn})_3^{3+}$ Na^+ BENTONITE.

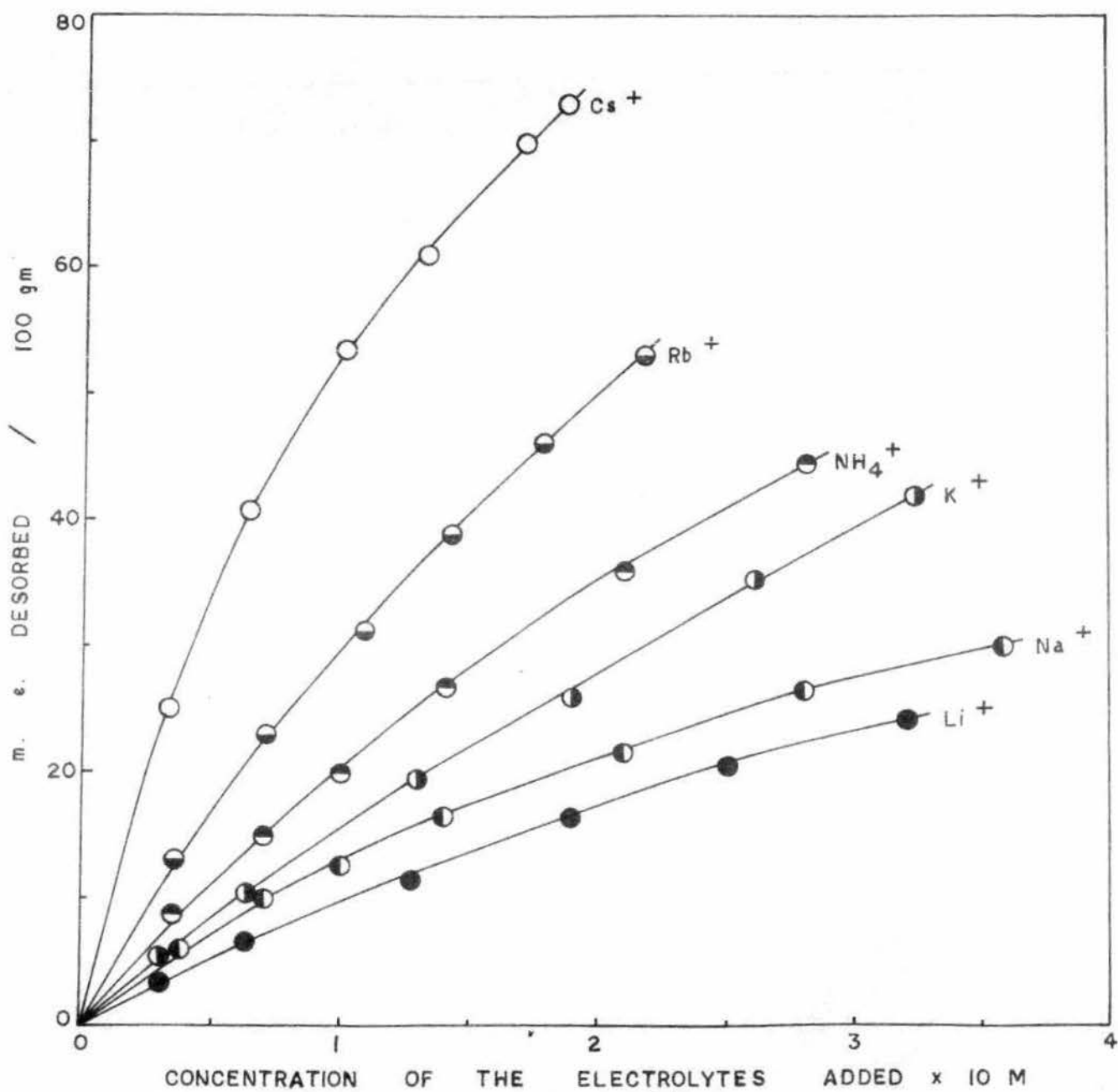
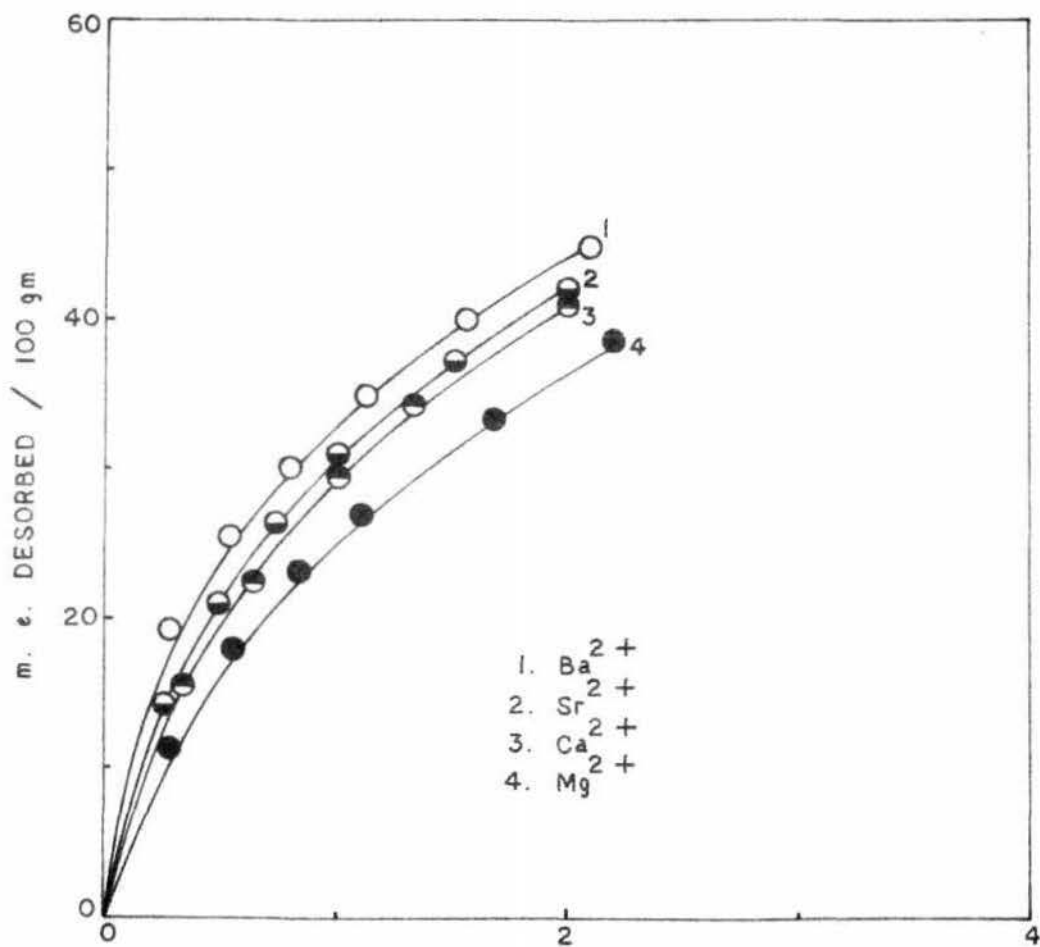


FIG. 26. DESORPTION OF $[Copr_3]^{3+}$ FROM Na - $Copr_3$ - BENTONITE BY DIFFERENT IONS.



CONCENTRATION OF THE ELECTROLYTES ADDED $\times 10 \text{ M}$
 FIG. 27. DESORPTION OF Copn_3^+ FROM Na-Copn_3 -
 BENTONITE BY DIFFERENT IONS.

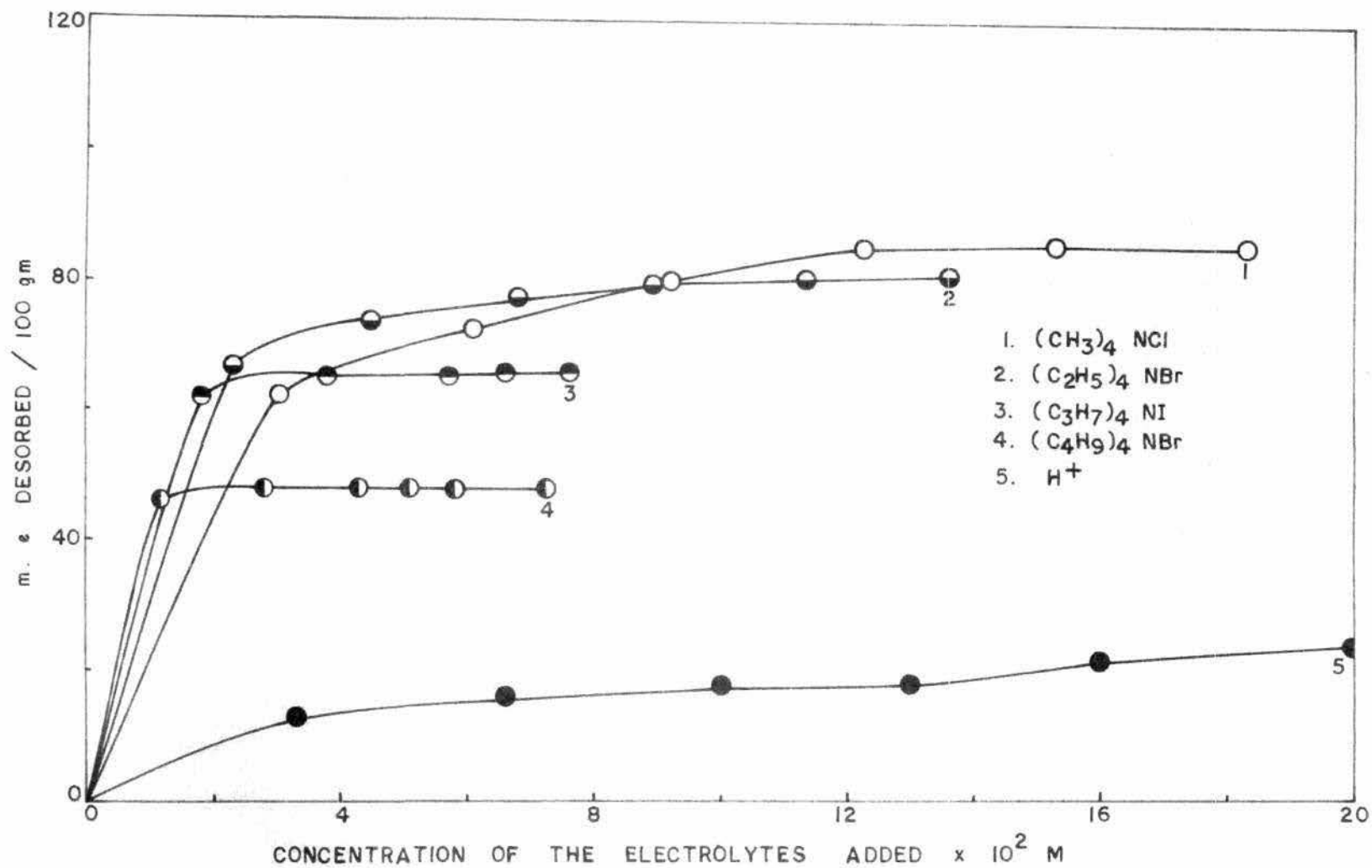


FIG. 28. DESORPTION OF Copn_3^+ FROM Na-Copn_3 -BENTONITE BY DIFFERENT IONS.

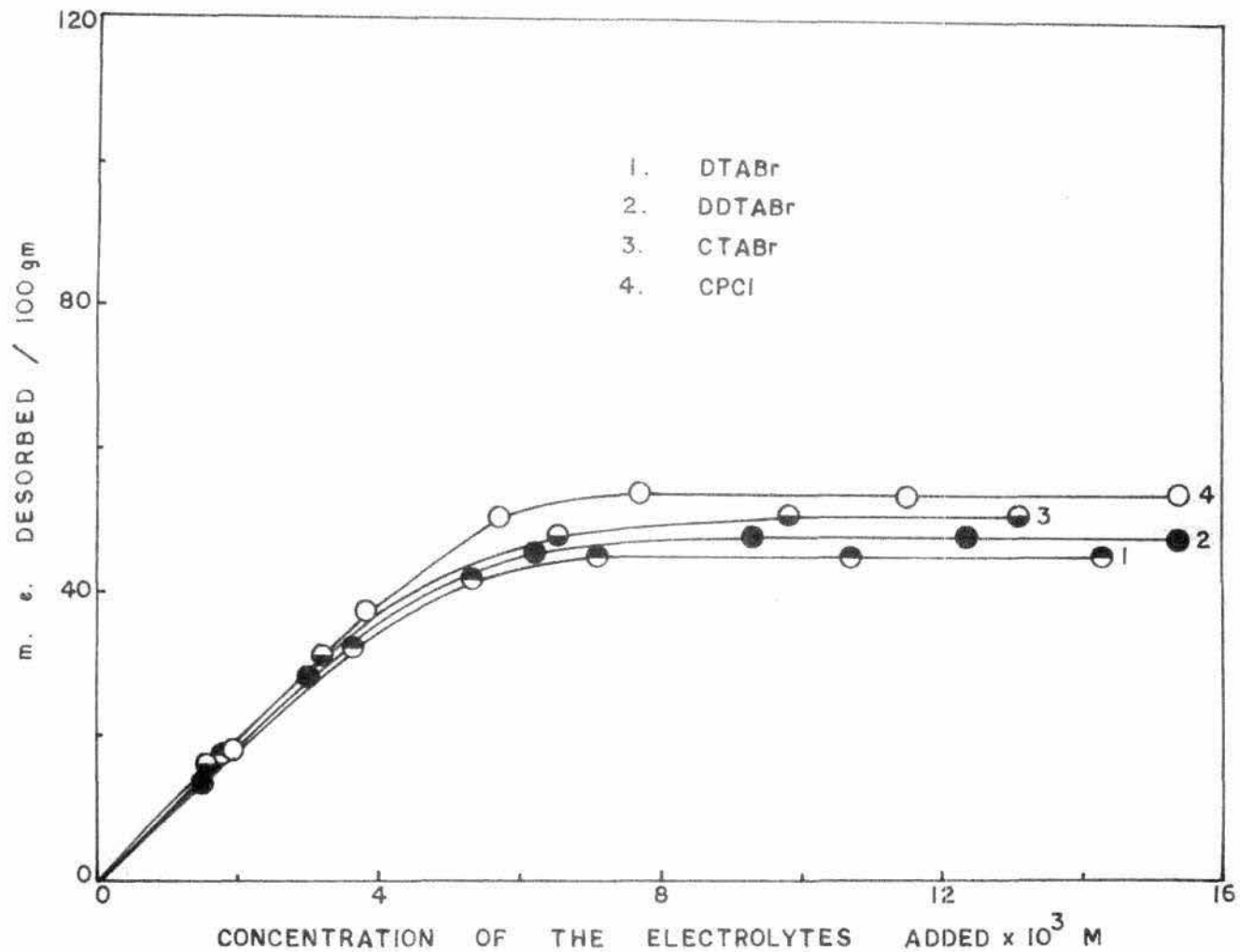


FIG. 29. DESORPTION OF Copn_3^{3+} FROM Na - Copn_3 - BENTONITE BY DIFFERENT IONS.

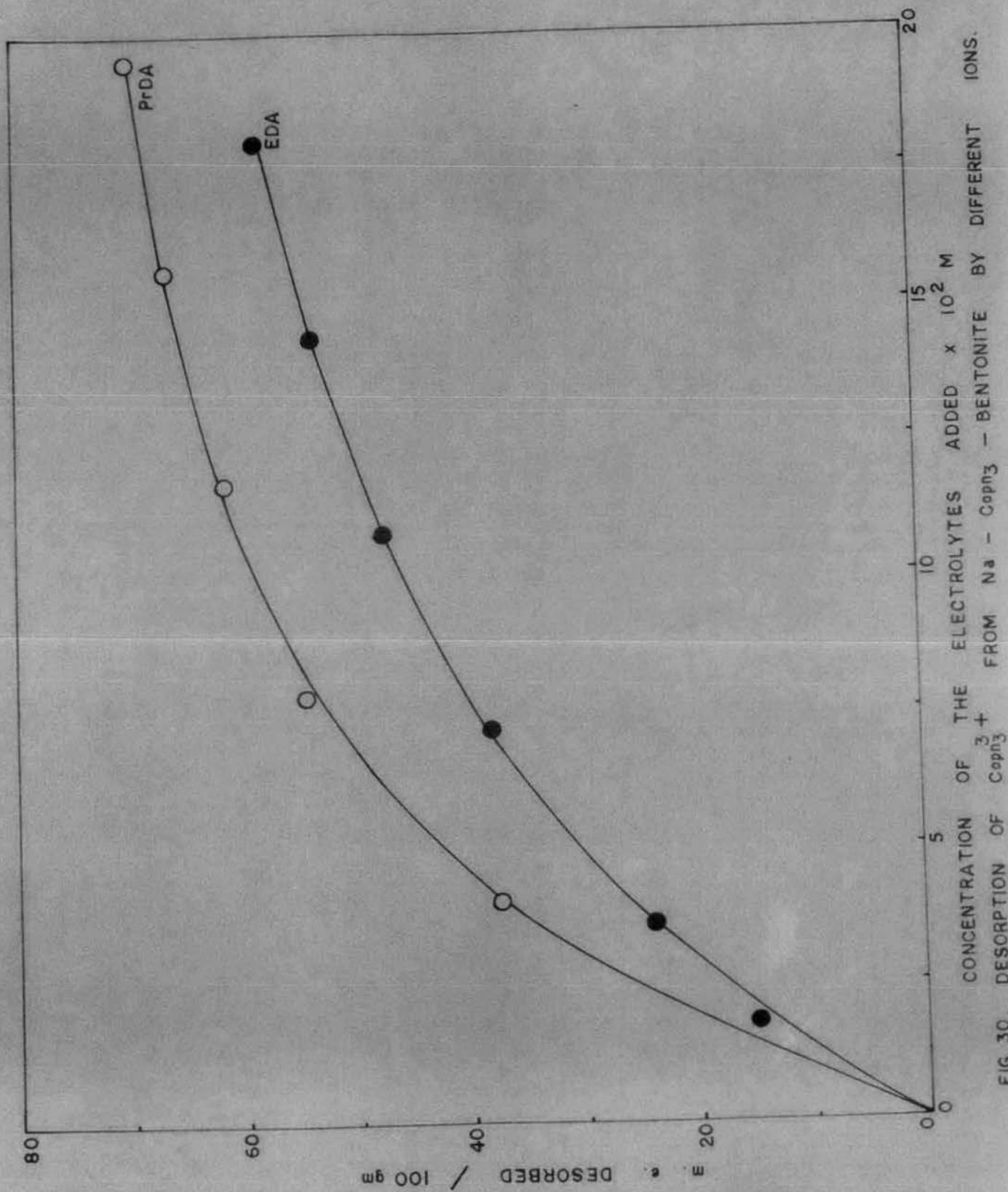


FIG. 30. DESORPTION OF Co^{3+} FROM Na - Cop³⁺ - BENTONITE BY DIFFERENT IONS.

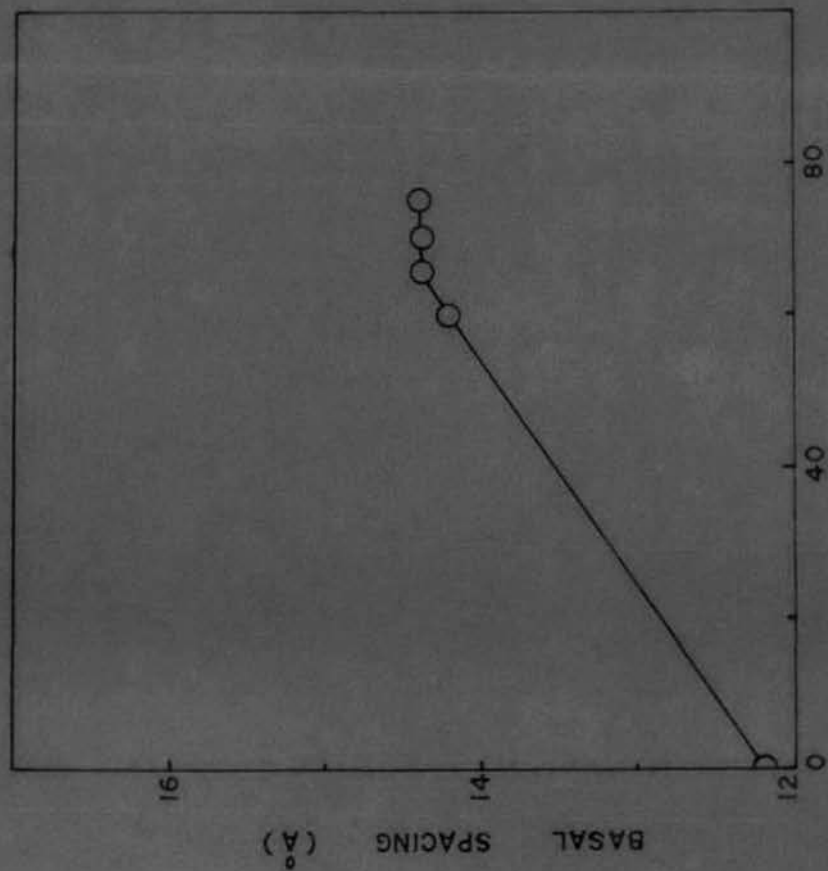


FIG. 31. BASAL SPACINGS OF MIXED $\text{NaCOPn}_3 - (\text{CH}_3)_4\text{N} - \text{BENTONITE}$.

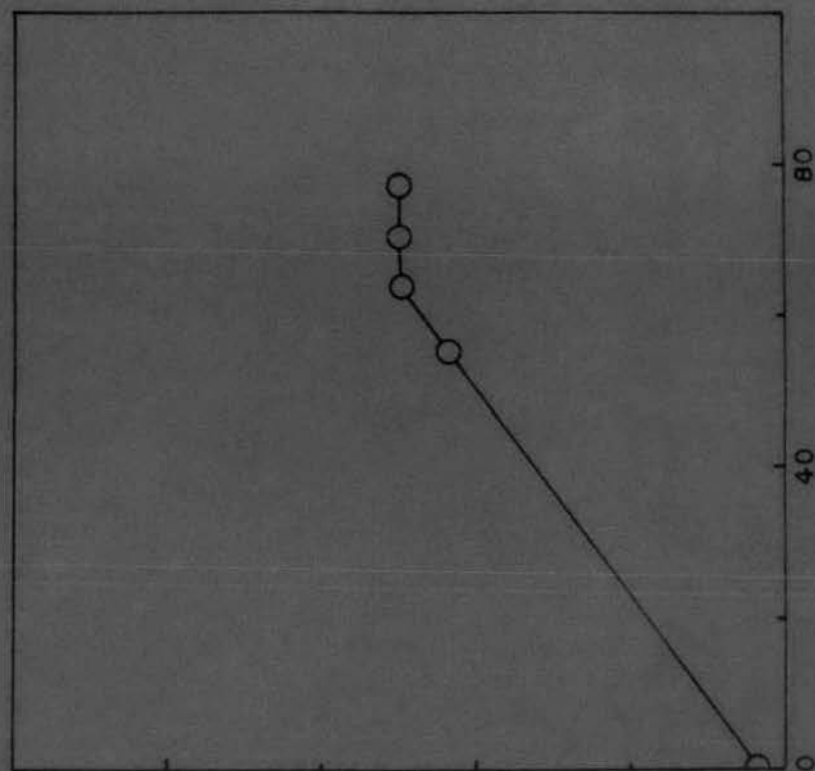
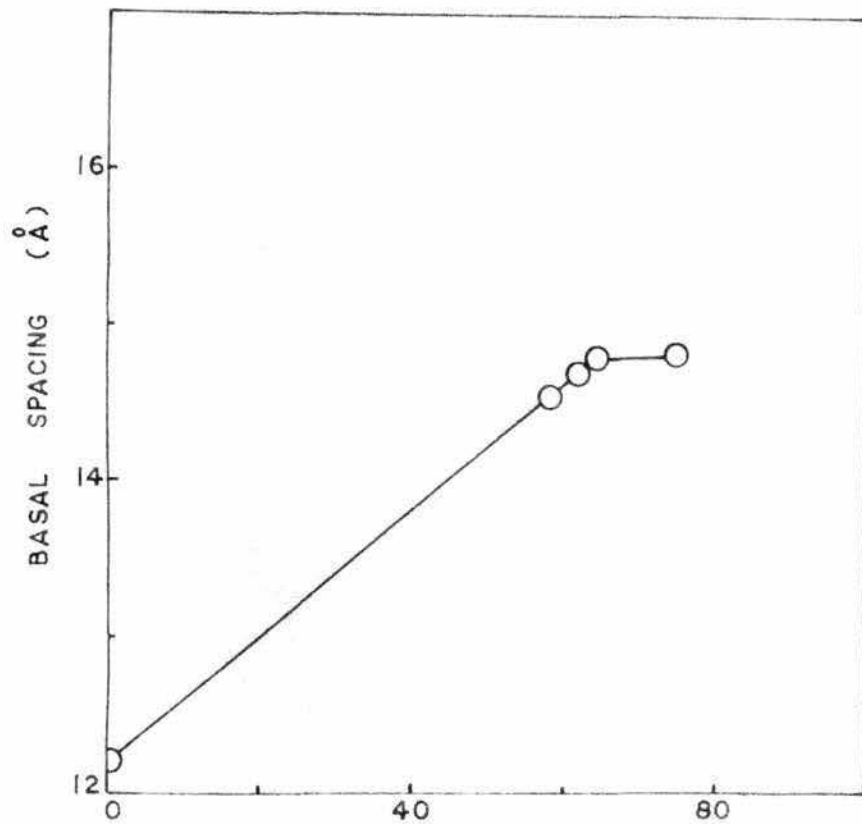
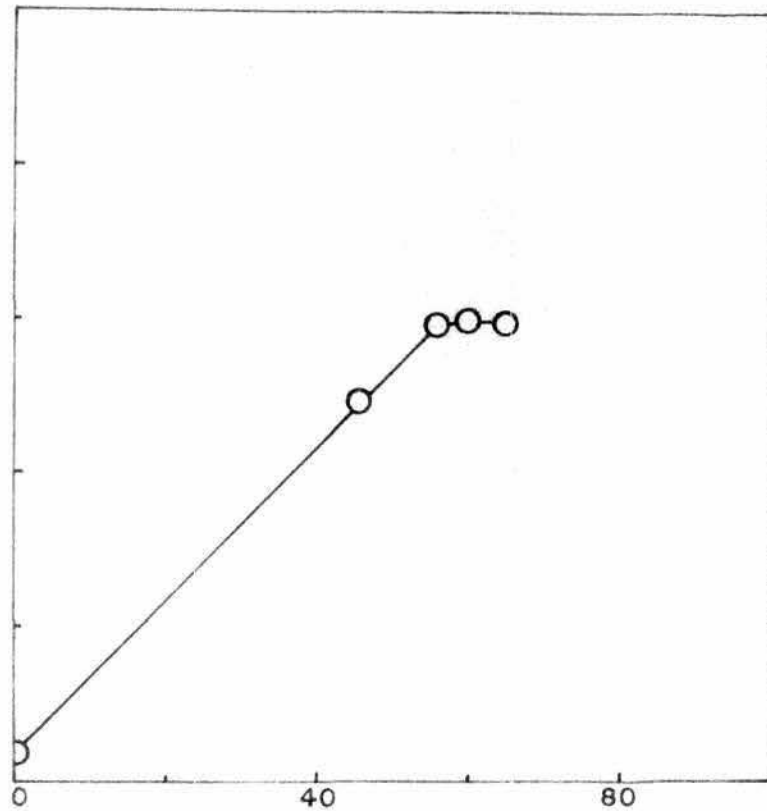


FIG. 32. BASAL SPACINGS OF MIXED $\text{NaCOPn}_3 - (\text{C}_2\text{H}_5)_4\text{N} - \text{BENTONITE}$.



% (C₃H₇)₄ NI ON BENTONITE
 FIG. 33. BASAL SPACINGS OF MIXED
 NaCOpn₃ - (C₃H₇)₄ N - BENTONITE.



% (C₄H₉)₄ NBr ON BENTONITE
 FIG. 34. BASAL SPACINGS OF MIXED
 NaCOpn₃ - (C₄H₉)₄ N - BENTONITE.

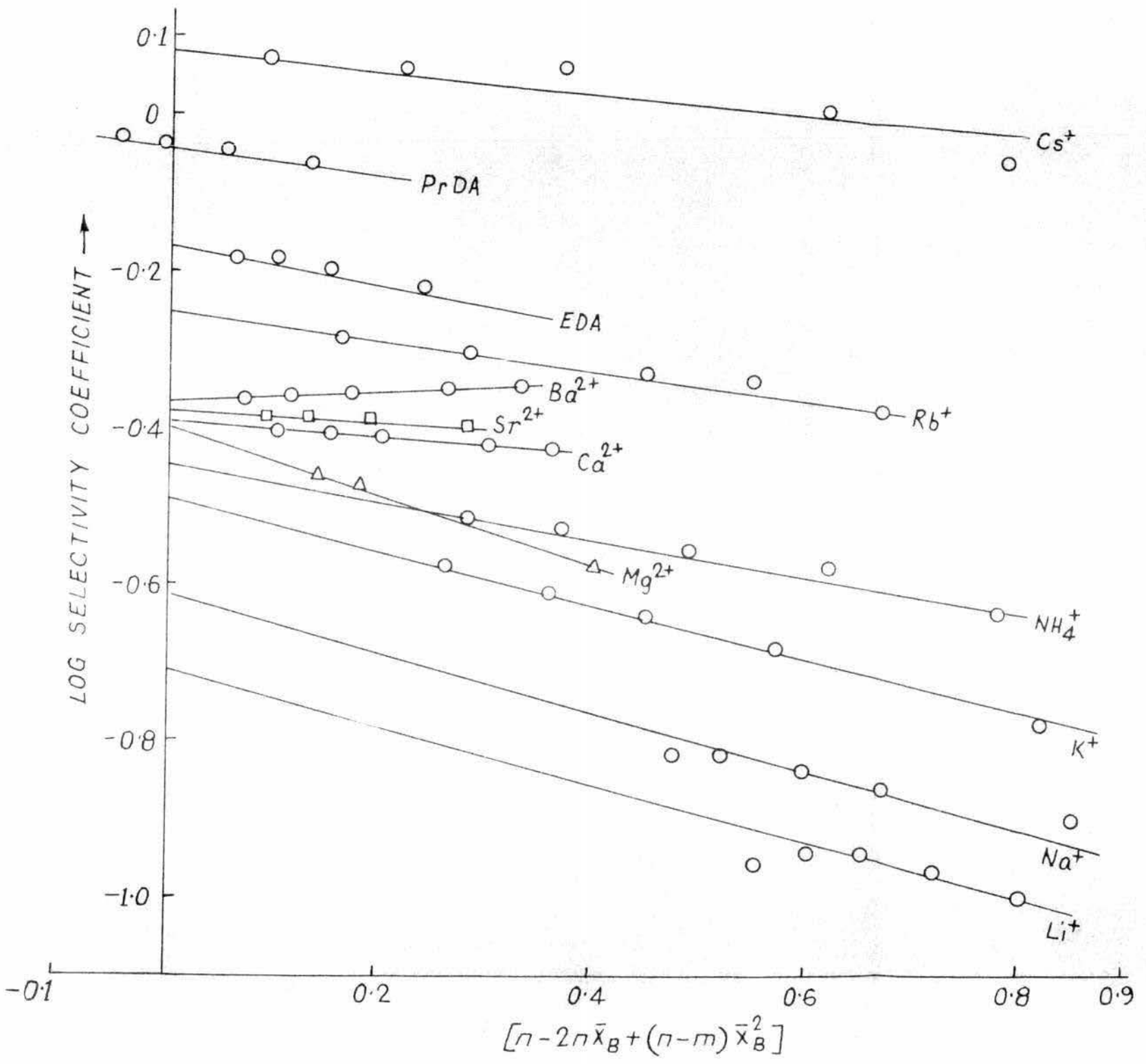


FIG. 35. PLOT OF LOG SELECTIVITY COEFFICIENT AGAINST $n-2n\bar{x}_B+(n-m)\bar{x}_B^2$ IN THE EXCHANGE OF $Co(pn)_3^{3+}$ FROM Na-Copn₃-BENTONITE BY DIFFERENT IONS.

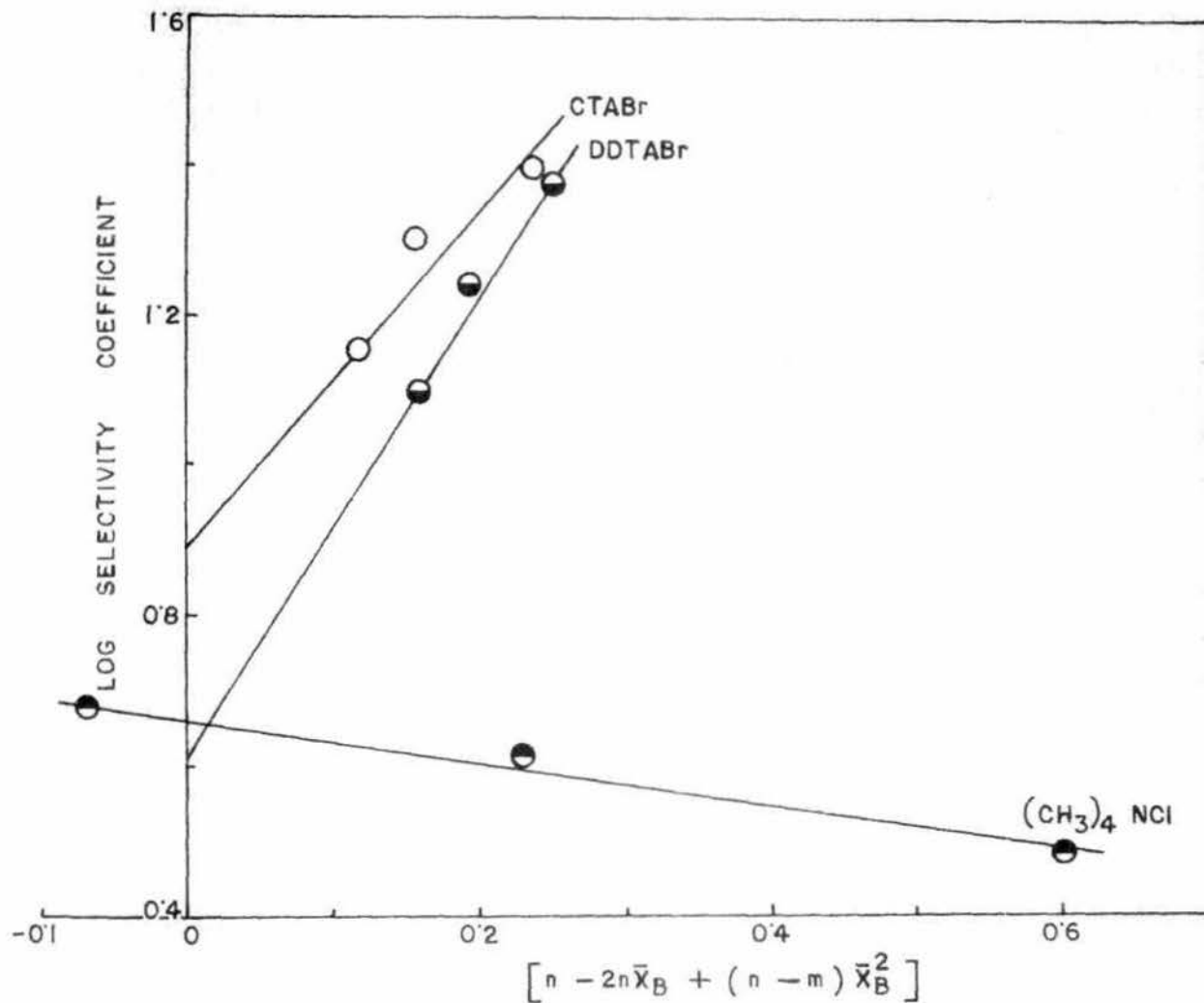


FIG. 36. PLOT OF LOG. SELECTIVITY COEFFICIENT AGAINST $n - 2n\bar{x}_B + (n - m)\bar{x}_B^2$ IN THE EXCHANGE OF $\text{Co}(\text{pn})_3^{3+}$ FROM Na - Cpn_3 - BENTONITE BY DIFFERENT IONS.

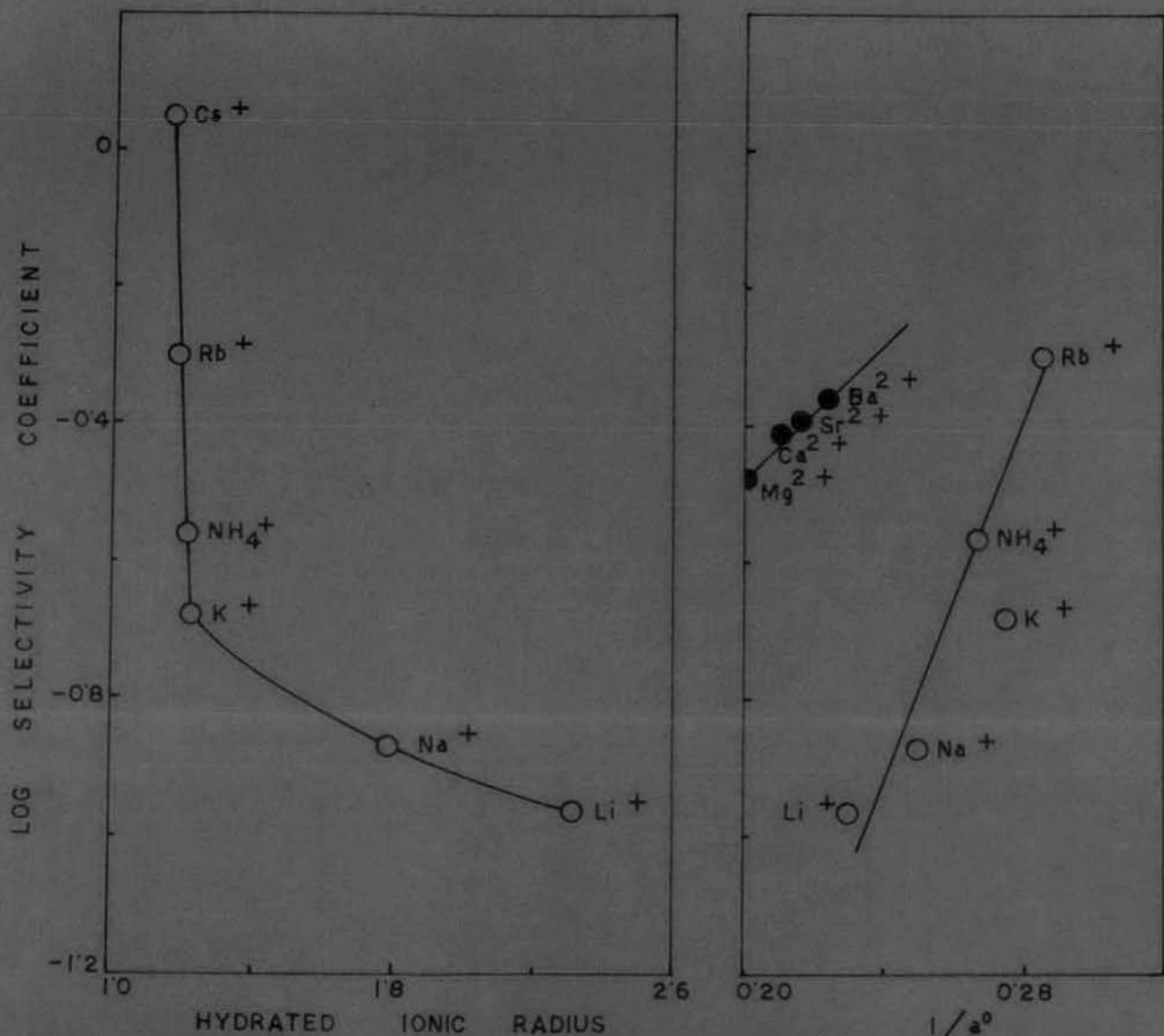


FIG. 37. CORRELATION OF SELECTIVITY COEFFICIENT WITH HYDRATED IONIC RADIUS & DEBYE HÜCKEL PARAMETER a° IN THE DESORPTION OF Na - Cop₃ - BENTONITE.

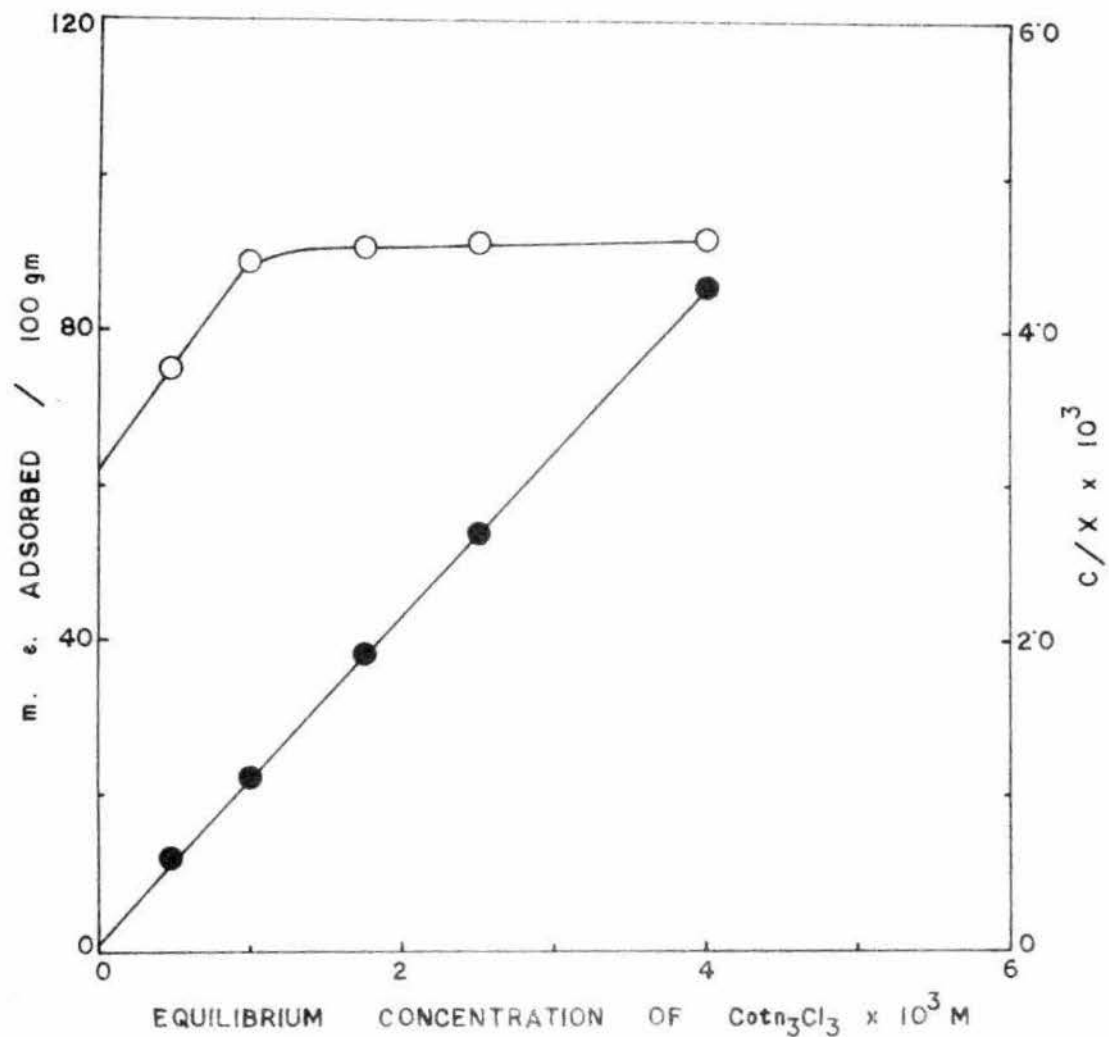


FIG. 38a. ADSORPTION ISOTHERM OF $\text{Co}(\text{NO}_3)_3$ ON H - BENTONITE.

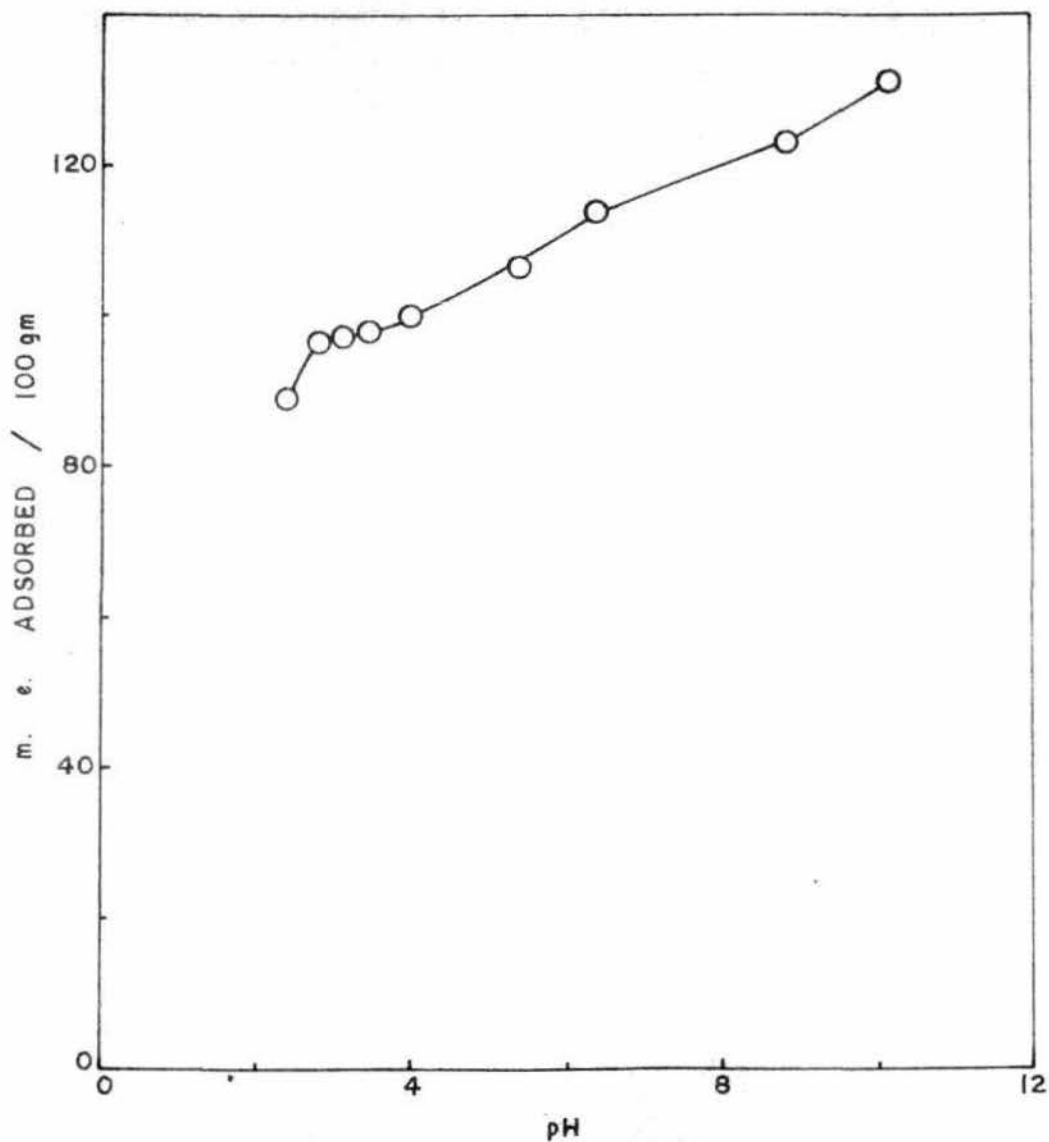


FIG. 38b. ADSORPTION OF $\text{Co}(\text{NO}_3)_3$ ON BENTONITE AT DIFFERENT pH.

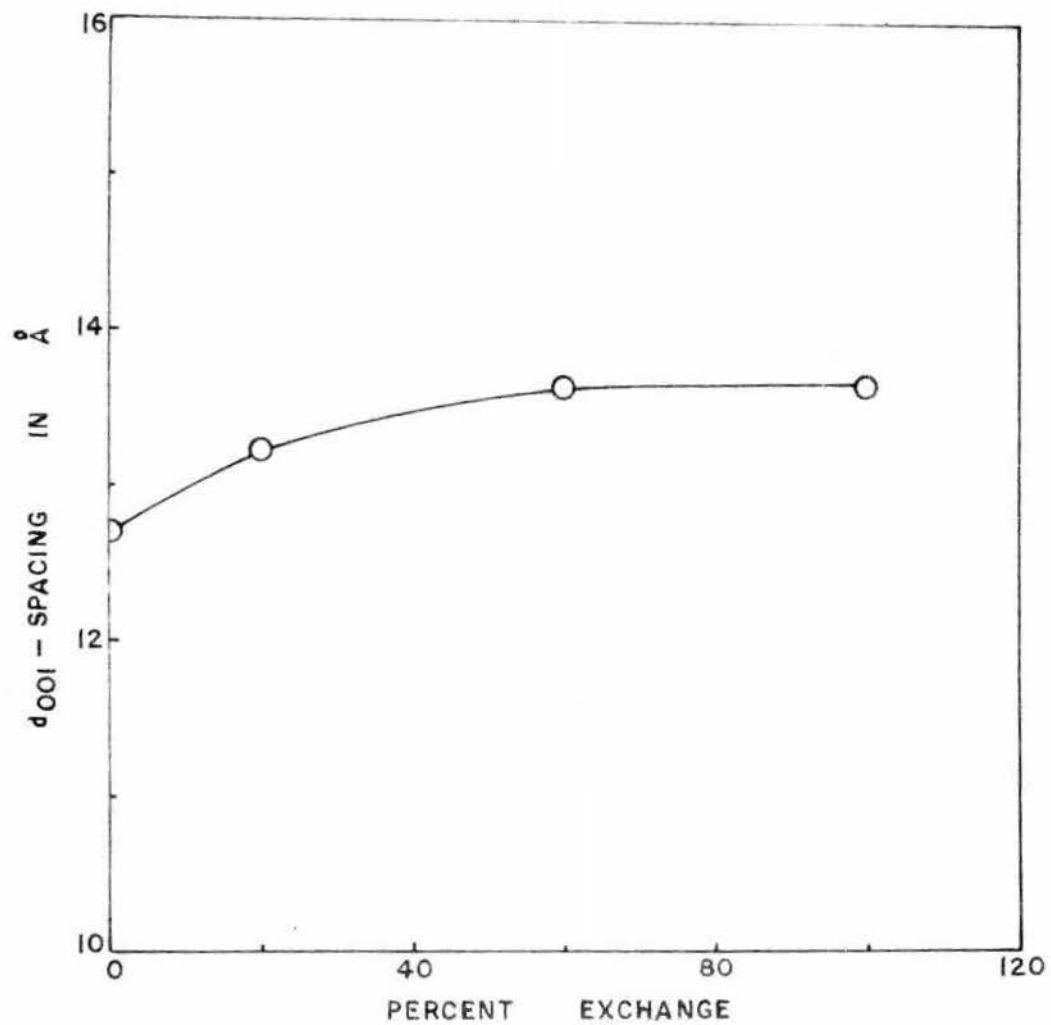


FIG. 39. d_{001} - SPACING VS. PERCENT EXCHANGE FOR $H - Coth_3^+$ - BENTONITE.

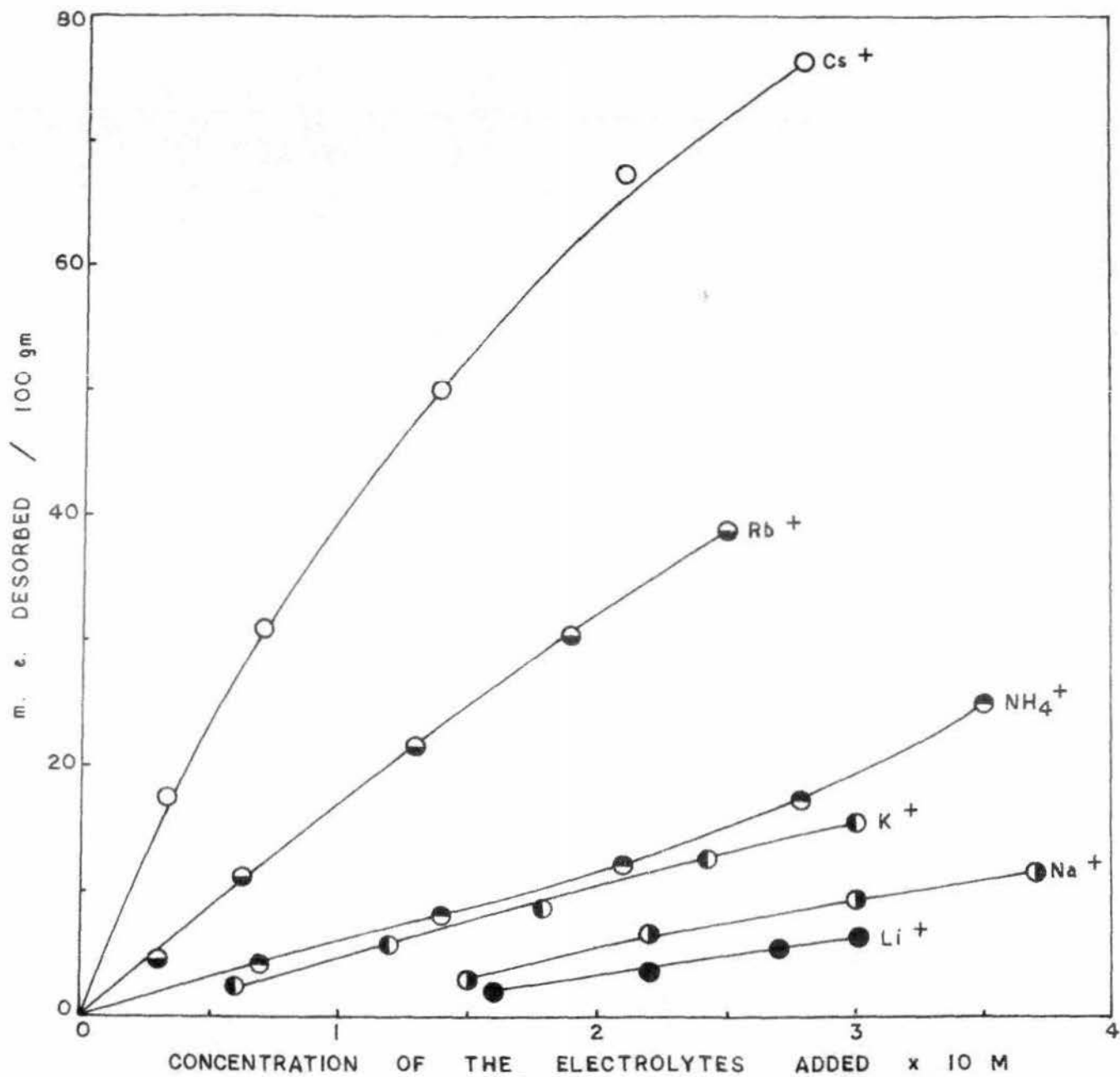


FIG. 40. DESORPTION OF $\text{Co}(\text{n}_3)_3^+$ FROM H - $\text{Co}(\text{n}_3)$ - BENTONITE BY DIFFERENT IONS.

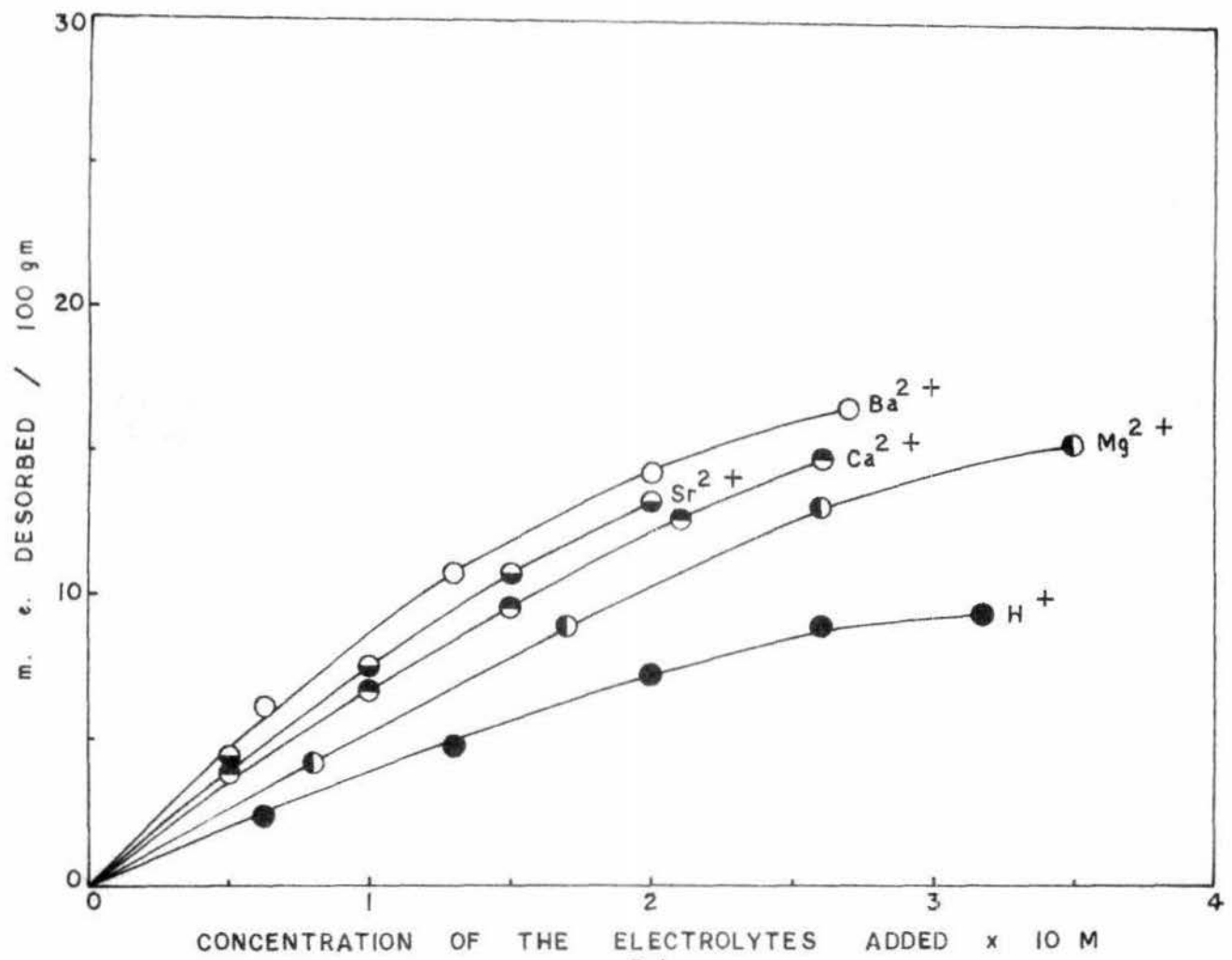


FIG. 41. DESORPTION OF Co^{2+} FROM H - Co^{2+} - BEN-TONITE BY DIFFERENT IONS.

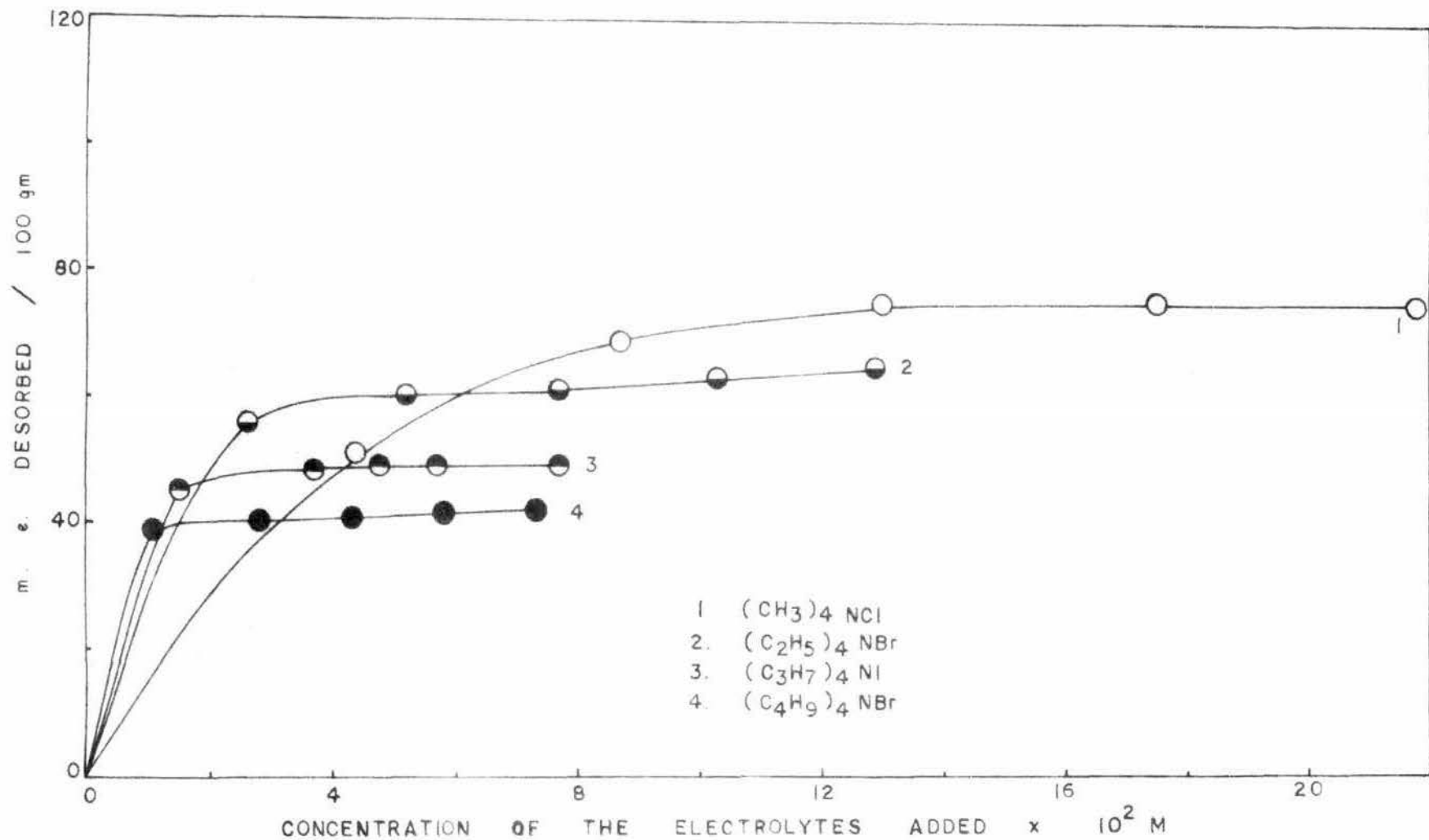


FIG 42. DESORPTION OF $\text{Co}(\text{n}_3)_3^+$ FROM H - $\text{Co}(\text{n}_3)$ - BENTONITE BY DIFFERENT IONS.

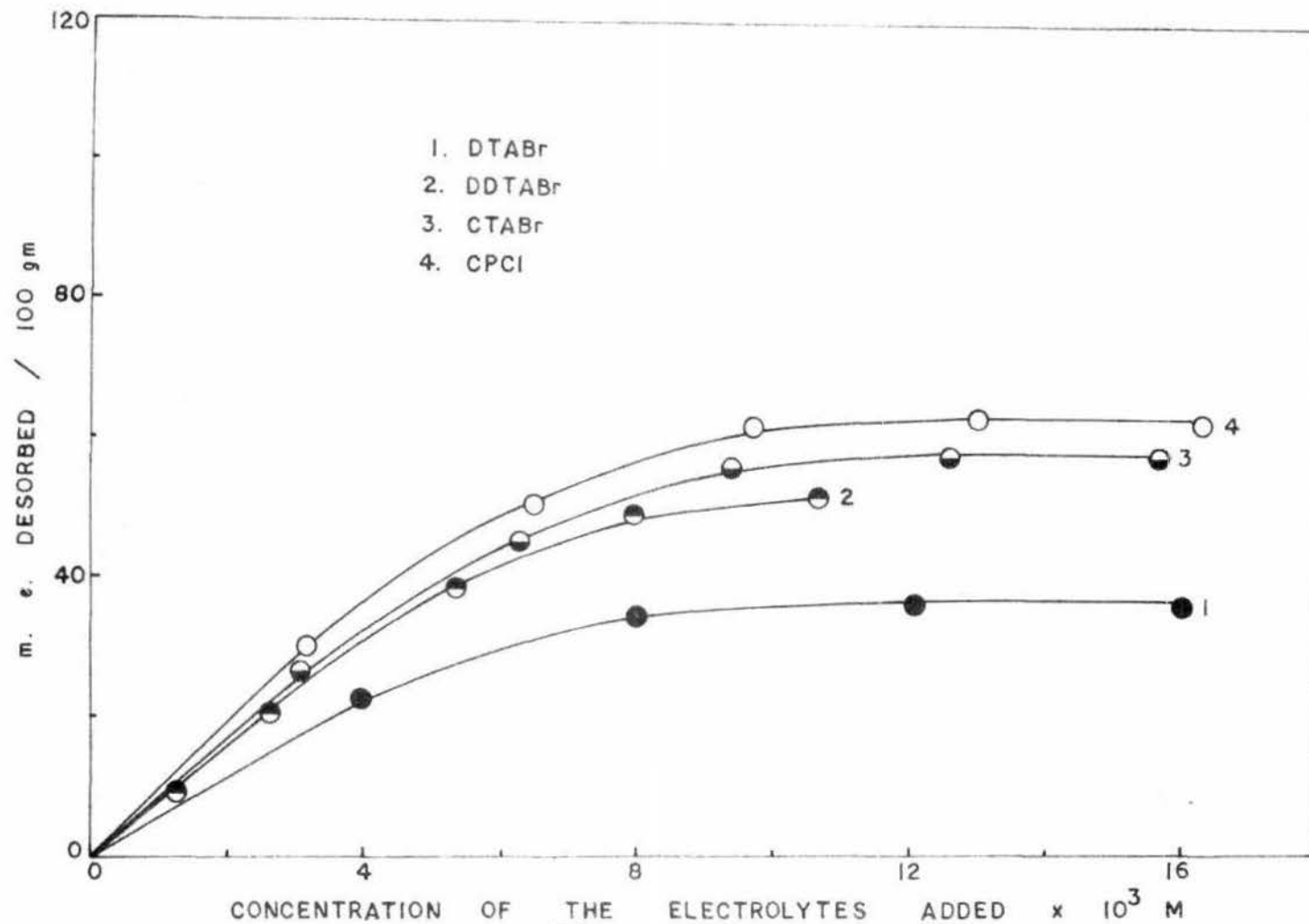


FIG. 43. DESORPTION OF Co^{3+} FROM H- Co^{3+} -BENTONITE BY DIFFERENT IONS.

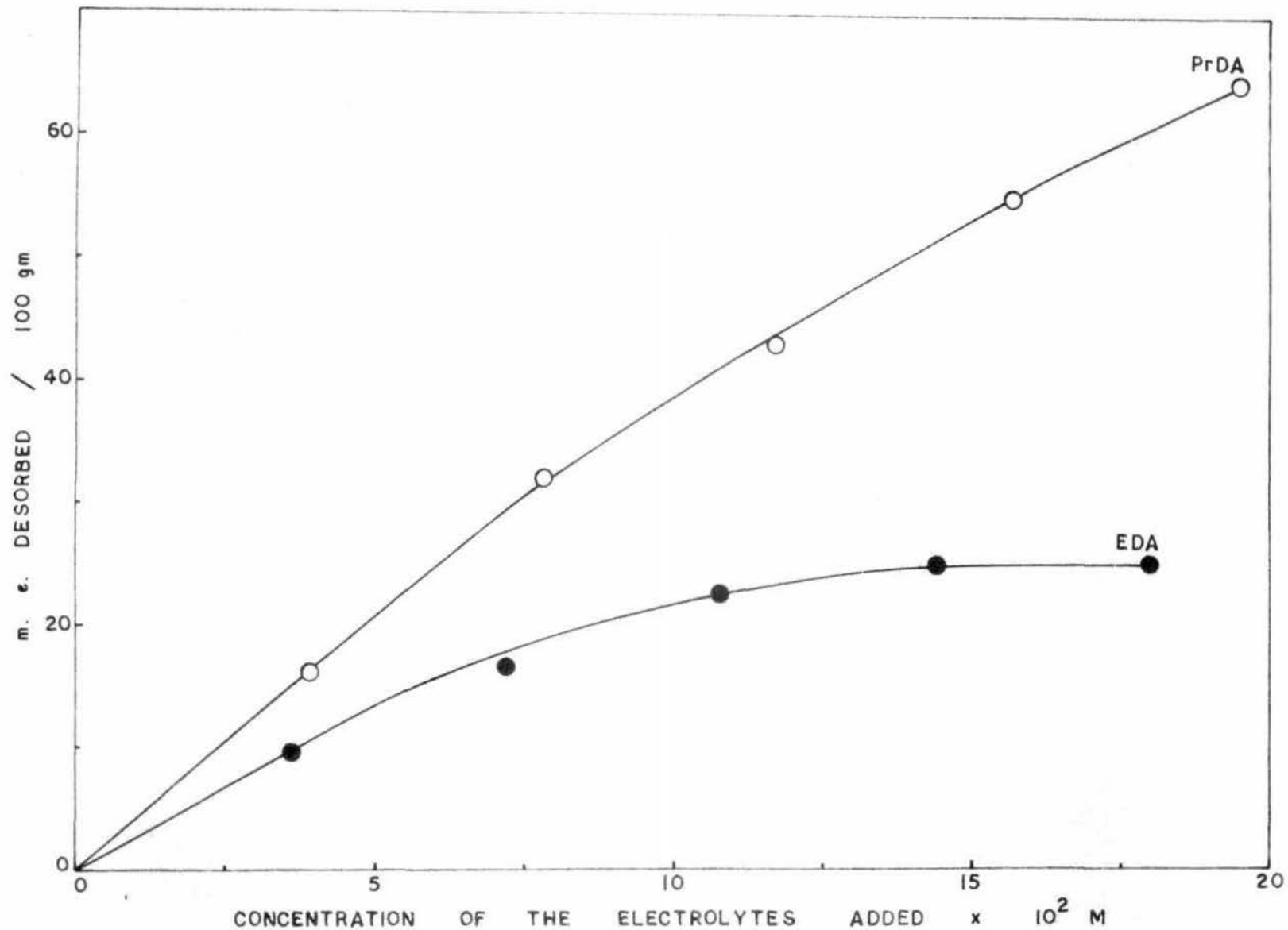


FIG. 44. DESORPTION OF $\text{Co}(\text{n}_3)_3^{3+}$ FROM H-Co(n₃)-BENTONITE BY DIFFERENT IONS.

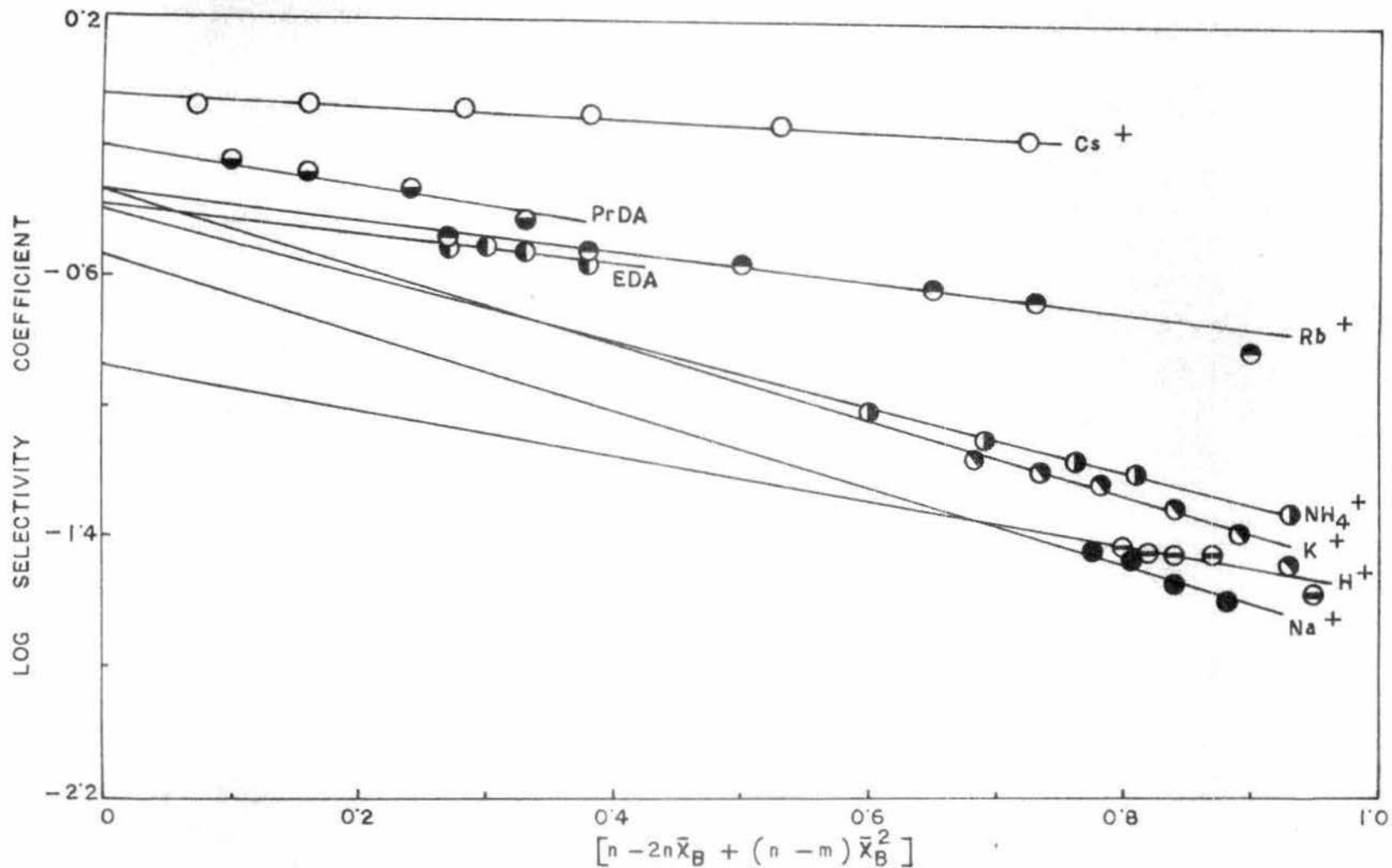


FIG. 45. PLOT OF LOG SELECTIVITY COEFFICIENT AGAINST $n - 2n\bar{X}_B + (n - m)\bar{X}_B^2$ IN THE EXCHANGE OF $\text{Co}(\text{tn})_3^{3+}$ FROM H - $\text{Co}(\text{tn})_3$ -BENTONITE BY DIFFERENT IONS.

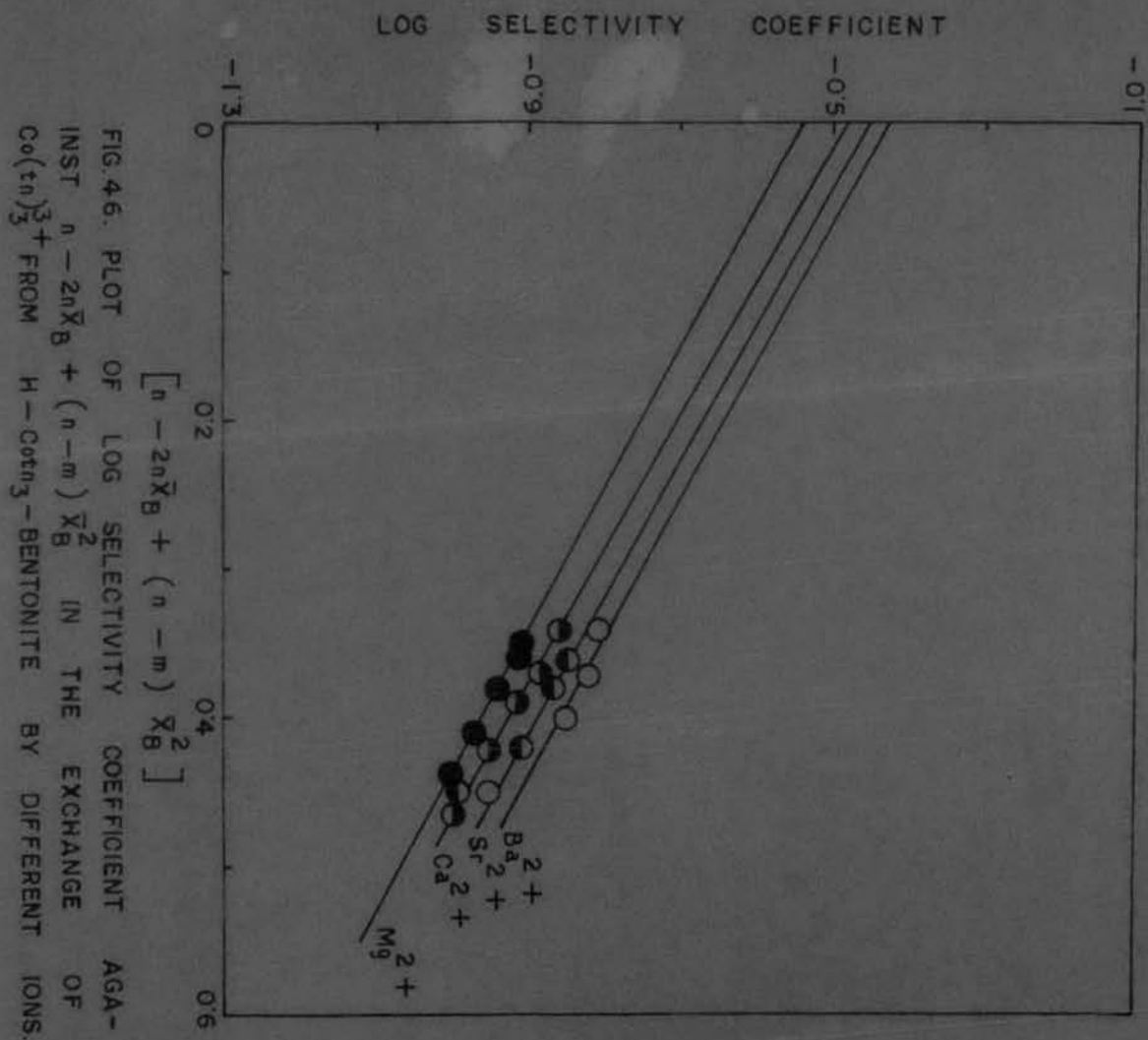


FIG.46. PLOT OF LOG SELECTIVITY COEFFICIENT AGA-
 INST $n - 2n\bar{X}_B + (n-m)\bar{X}_B^2$ IN THE EXCHANGE OF
 $Co(tn)_3^{3+}$ FROM H-Co(tn)₃-BENTONITE BY DIFFERENT IONS.

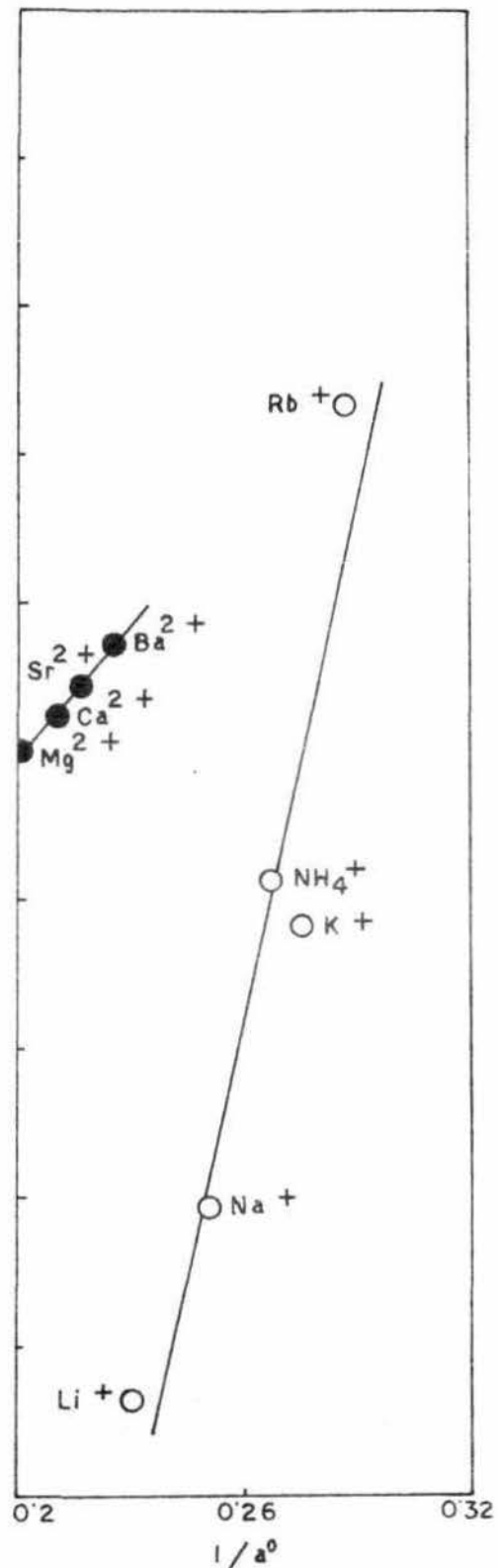
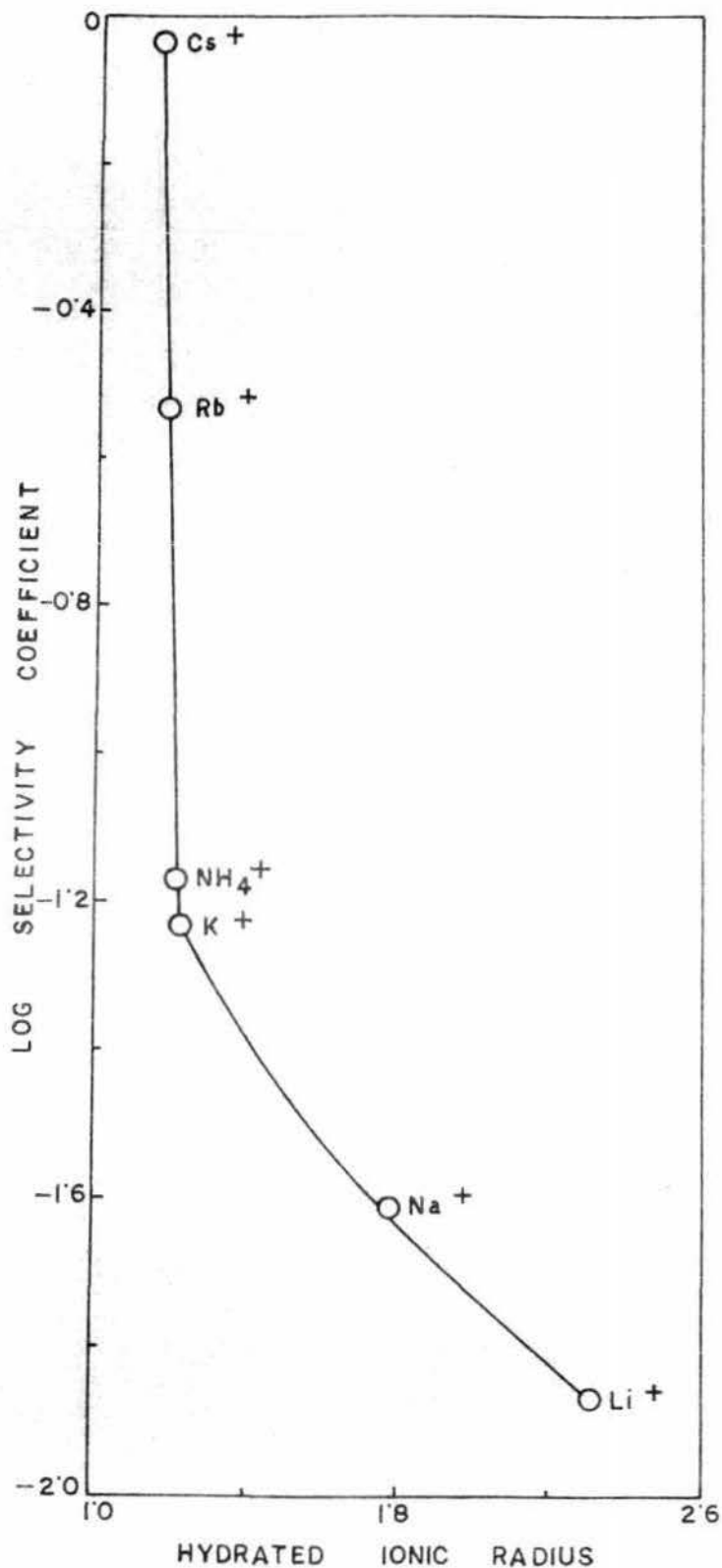


FIG. 47. CORRELATION OF SELECTIVITY COEFFICIENT WITH HYDRATED IONIC RADIUS AND DEBYE HÜCKEL PARAMETER a^0 IN THE DESORPTION OF H - Cotn₃ - BENTONITE.

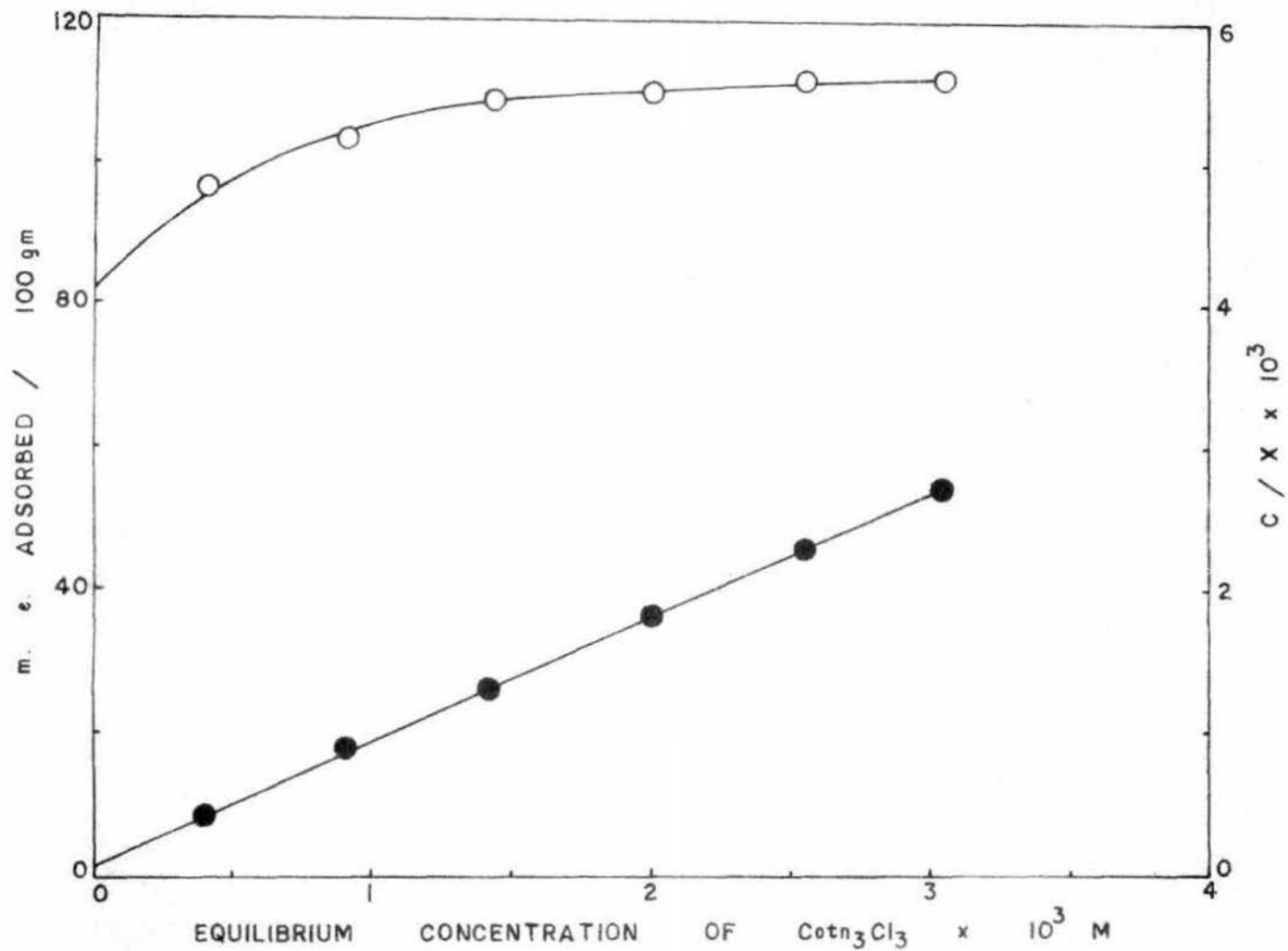


FIG. 48. ADSORPTION ISOTHERM OF $\text{Co}(\text{NO}_3)_3$ ON Na - BENTONITE.

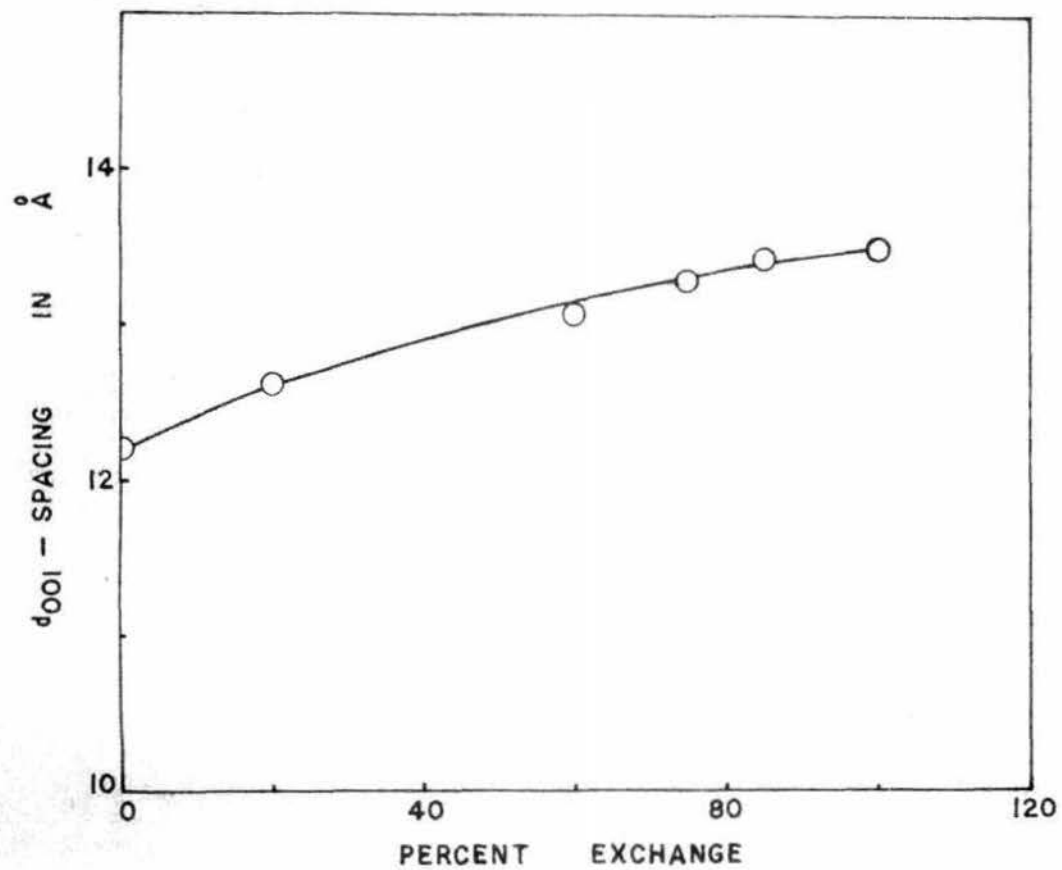


FIG. 49. d_{001} - SPACING VS. PERCENT EXCHANGE .
FOR Na - Cotn³⁺ - BENTONITE.

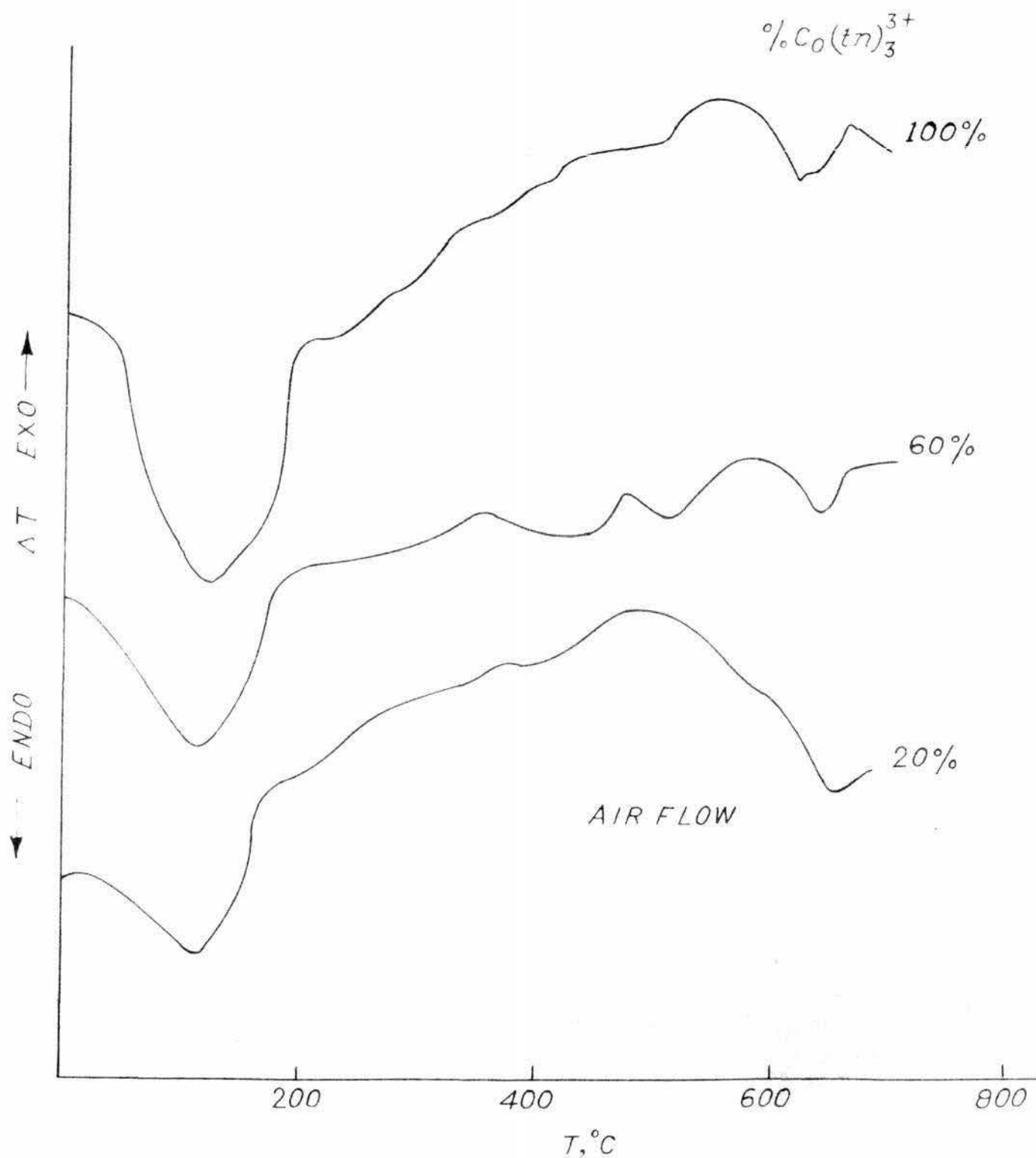


FIG. 50. D.T.A. CURVES FOR MIXED $\text{Co}(\text{tn})_3^{3+}\text{-Na}^+$ BENTONITES (PRETREATED OVER CONC. H_2SO_4) AIR FLOW; HEATING RATE $10^\circ\text{C}/\text{min}$.

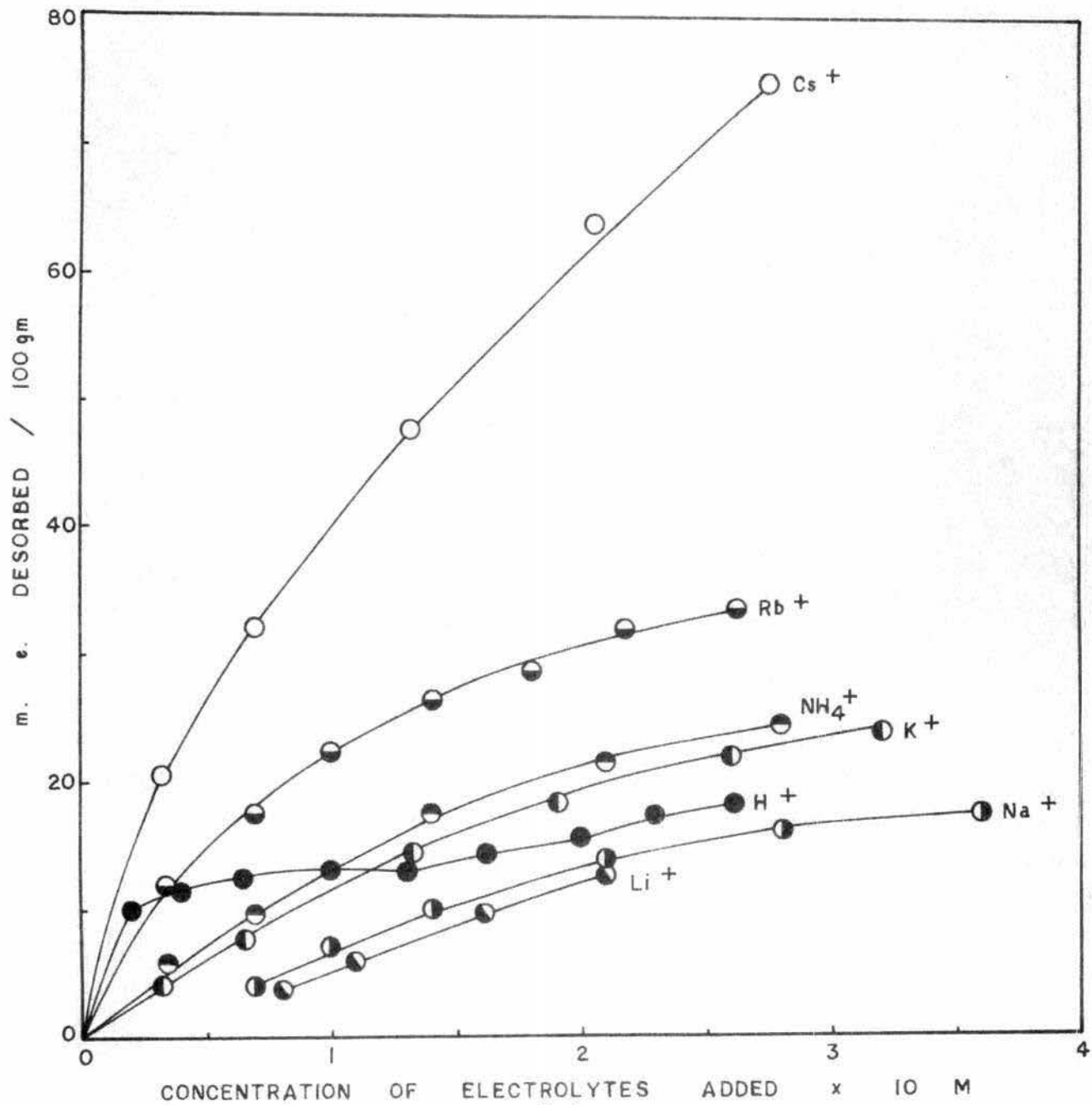
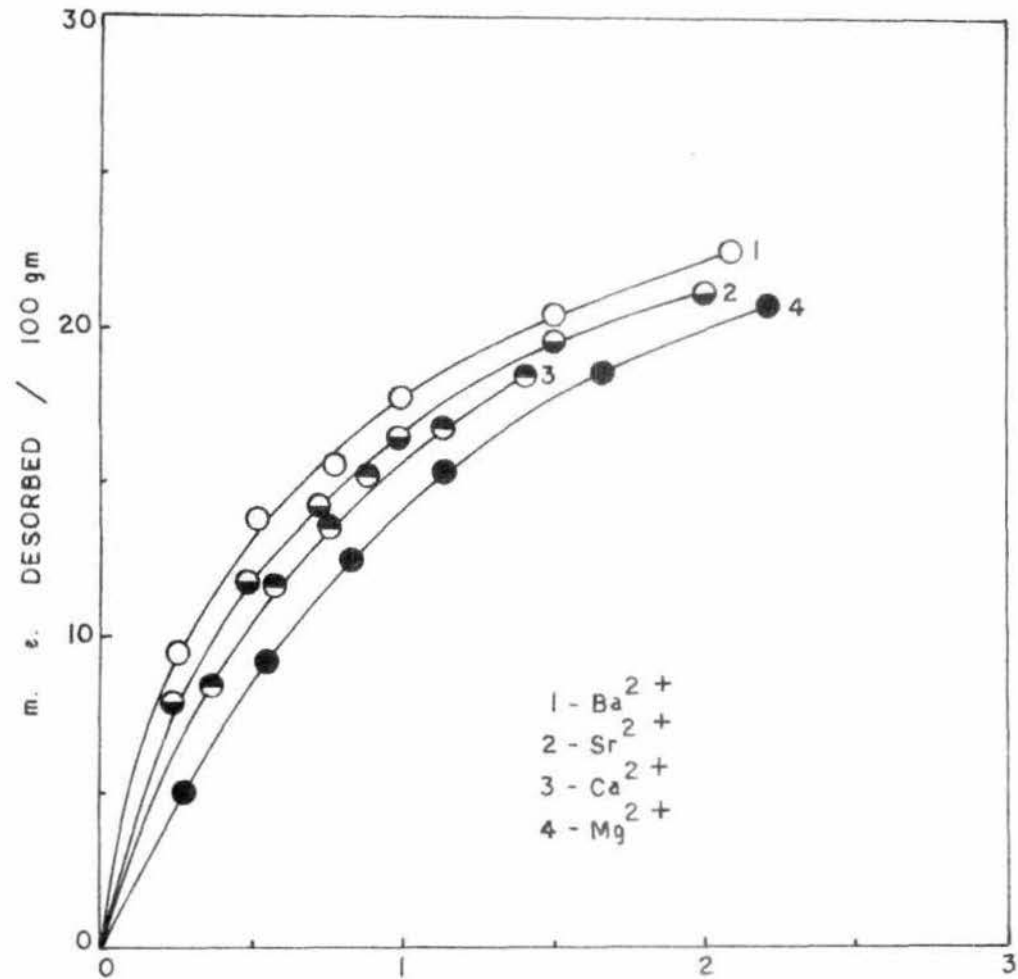


FIG. 51. DESORPTION OF $\text{Co(NO}_3)_3$ FROM Na - $\text{Co(NO}_3)_3$ - BENTONITE BY DIFFERENT IONS



CONCENTRATION OF THE ELECTROLYTES ADDED x 10 M

FIG. 52. DESORPTION OF Co^{3+} FROM Na-Cotn₃-BENTONITE BY DIFFERENT IONS.

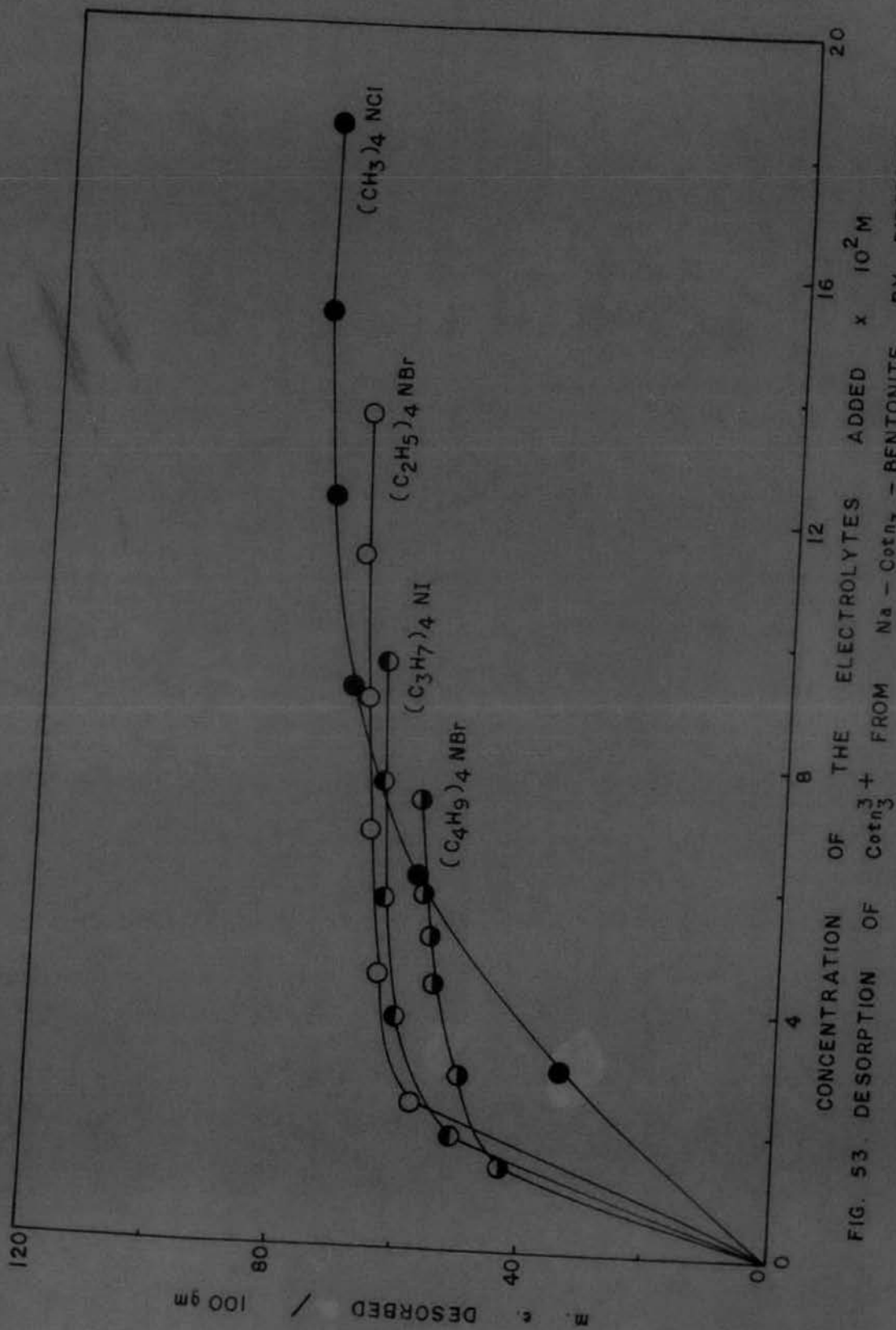


FIG. 53. DESORPTION OF Co^{3+} FROM Na - Co^{3+} - BENTONITE BY DIFFERENT IONS

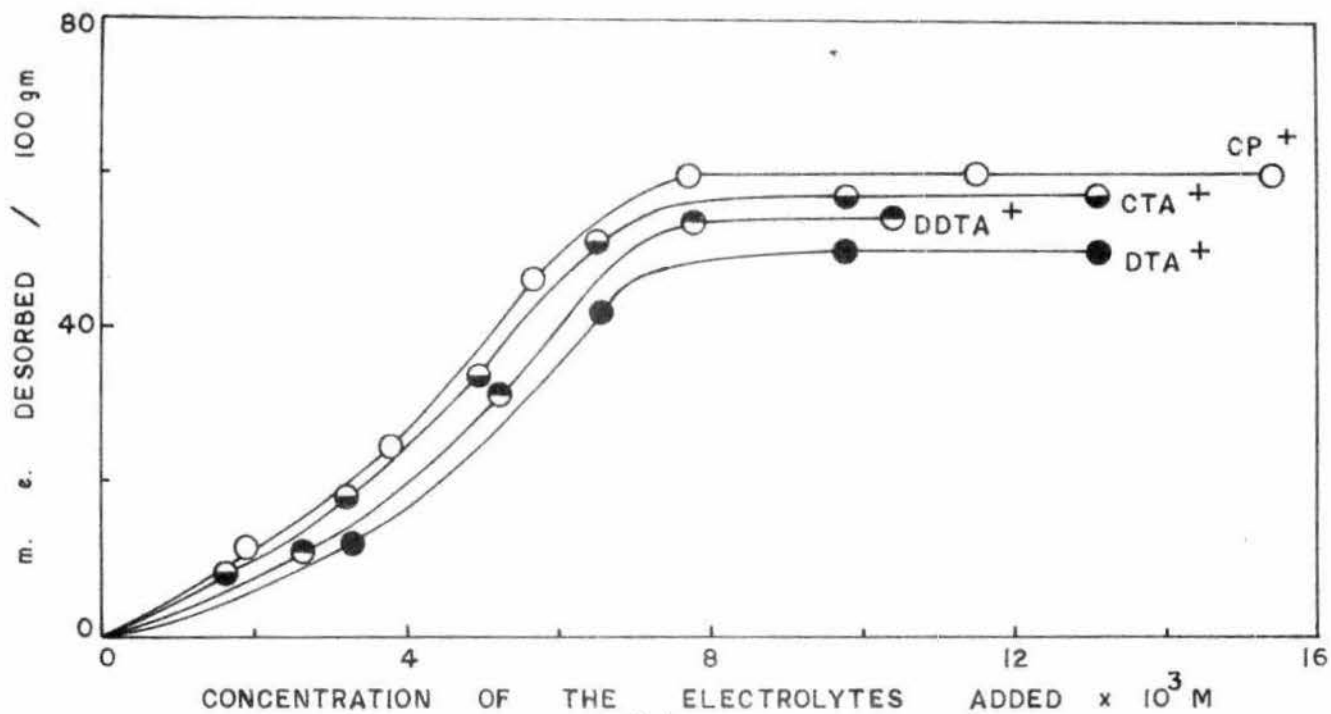


FIG. 54. DESORPTION OF $\text{Co}(\text{n}_3)^{3+}$ FROM Na - $\text{Co}(\text{n}_3)$ - BENTONITE BY DIFFERENT IONS.

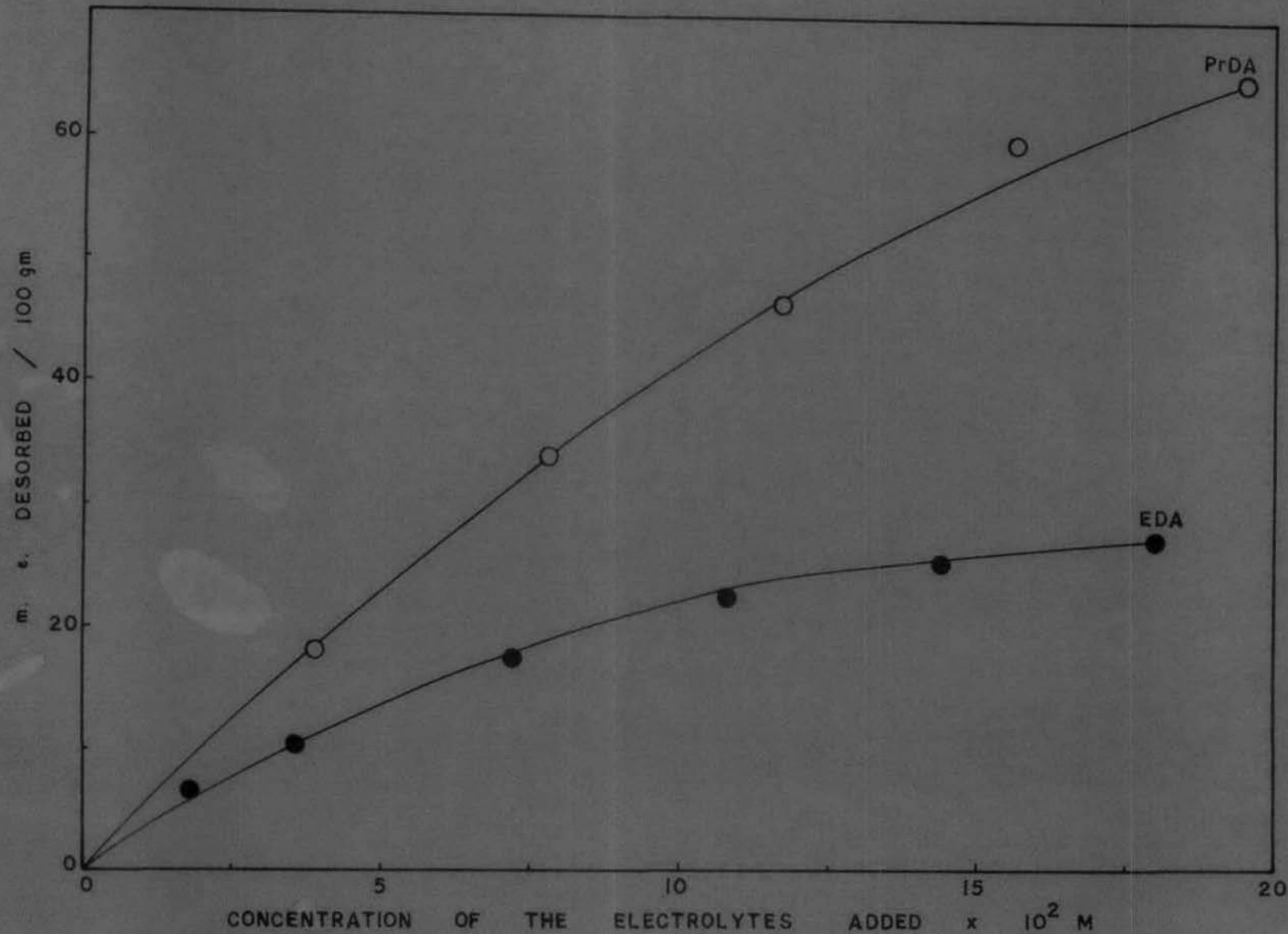


FIG. 55. DESORPTION OF $\text{Co}(\text{n}_3)_3^+$ FROM Na - $\text{Co}(\text{n}_3)$ - BENTONITE BY DIFFERENT IONS.

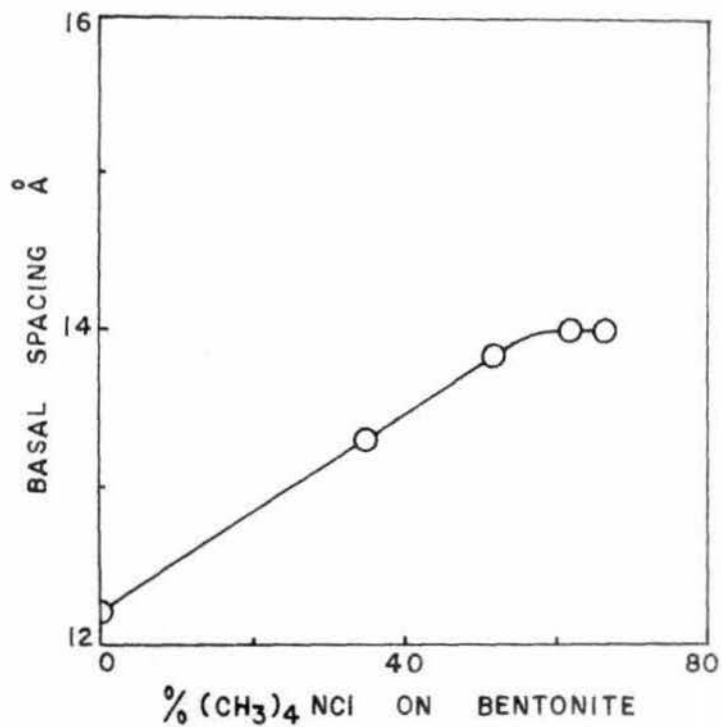


FIG.56. BASAL SPACINGS OF MIXED NaCotn₃ - (CH₃)₄ N - BENTONITE.

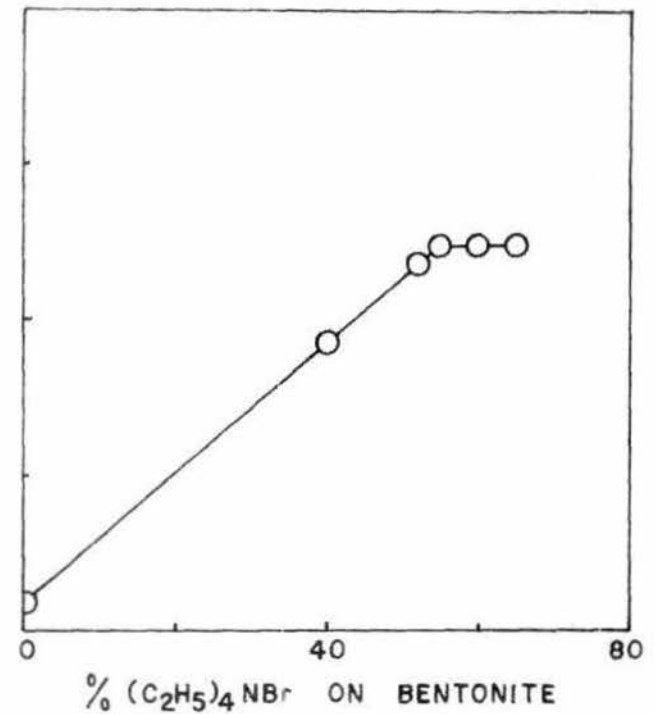


FIG.57. BASAL SPACINGS OF MIXED NaCotn₃ - (C₂H₅)₄ N - BENTONITE.

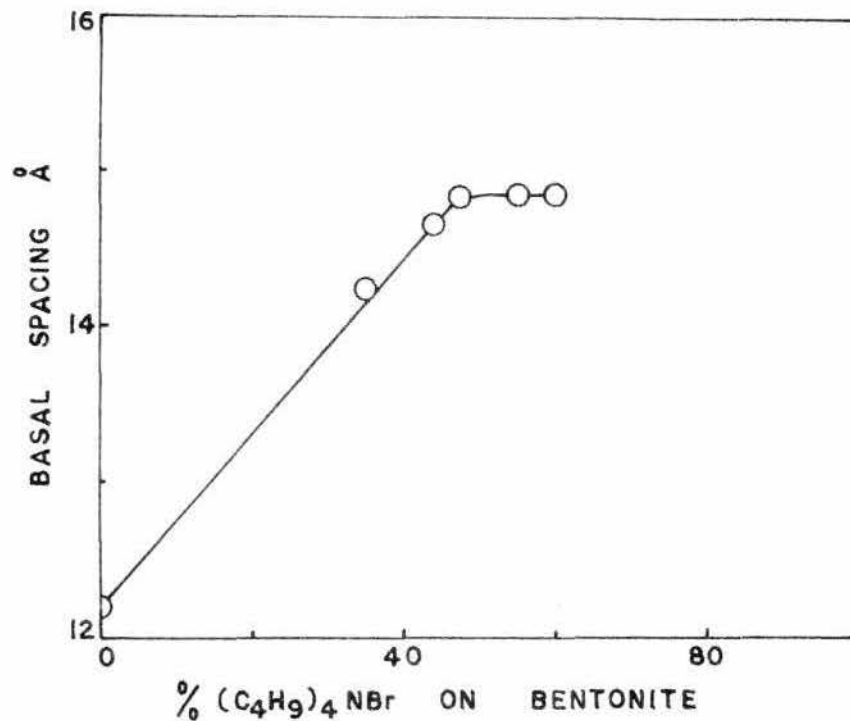


FIG. 58. BASAL SPACINGS OF MIXED $NaCotn_3 - (C_4H_9)_4N - BENTONITE$.

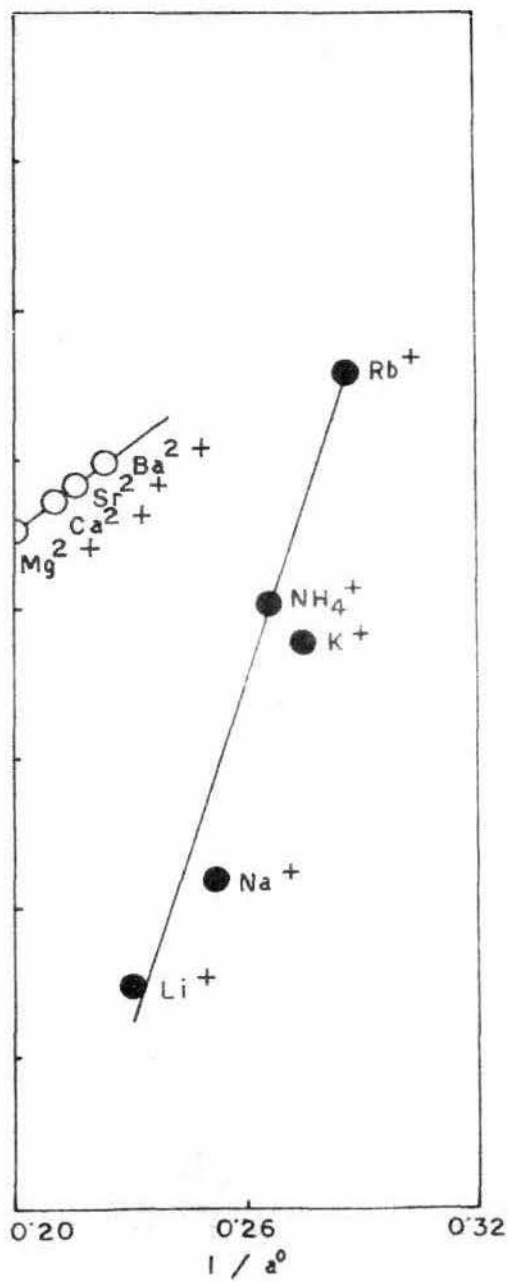
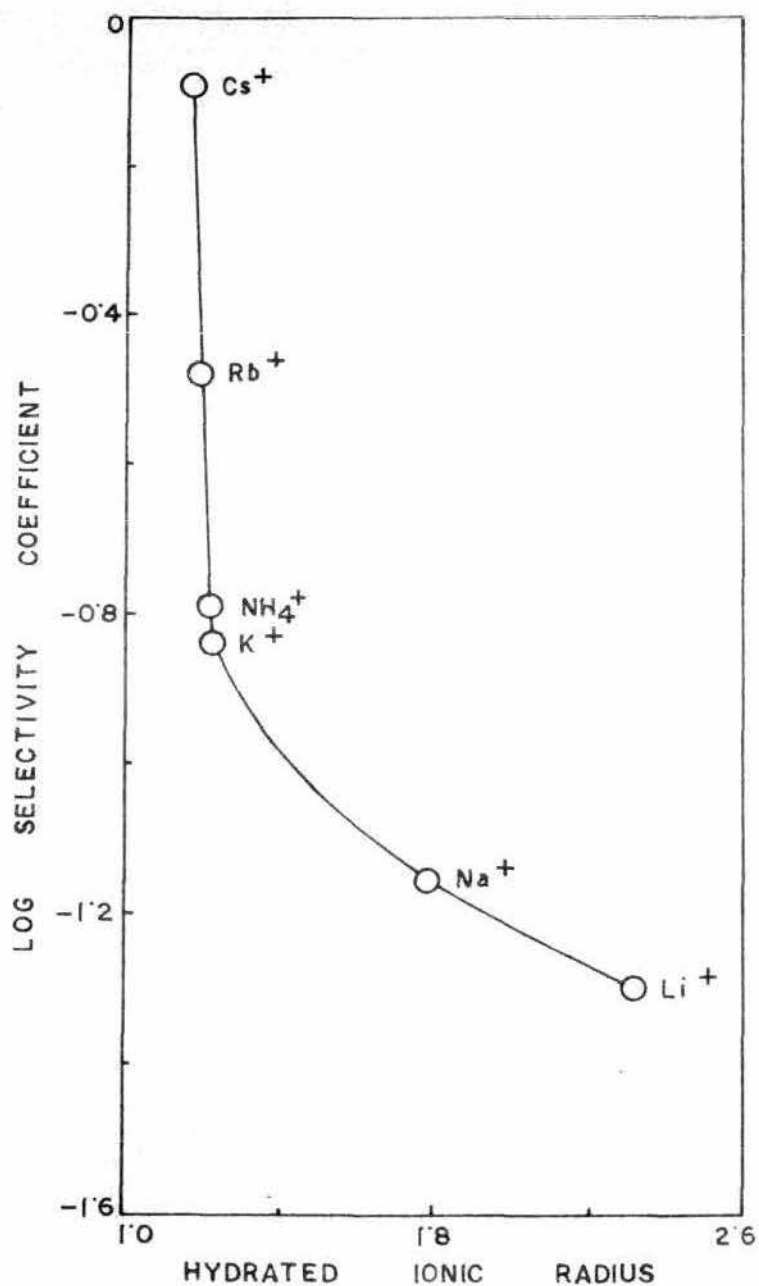


FIG. 59. CORRELATION OF SELECTIVITY COEFFICIENT WITH HYDRATED IONIC RADIUS AND DEBYE HÜCKEL PARAMETER a^0 IN THE DESORPTION OF Na - Co₃ - BENTONITE.

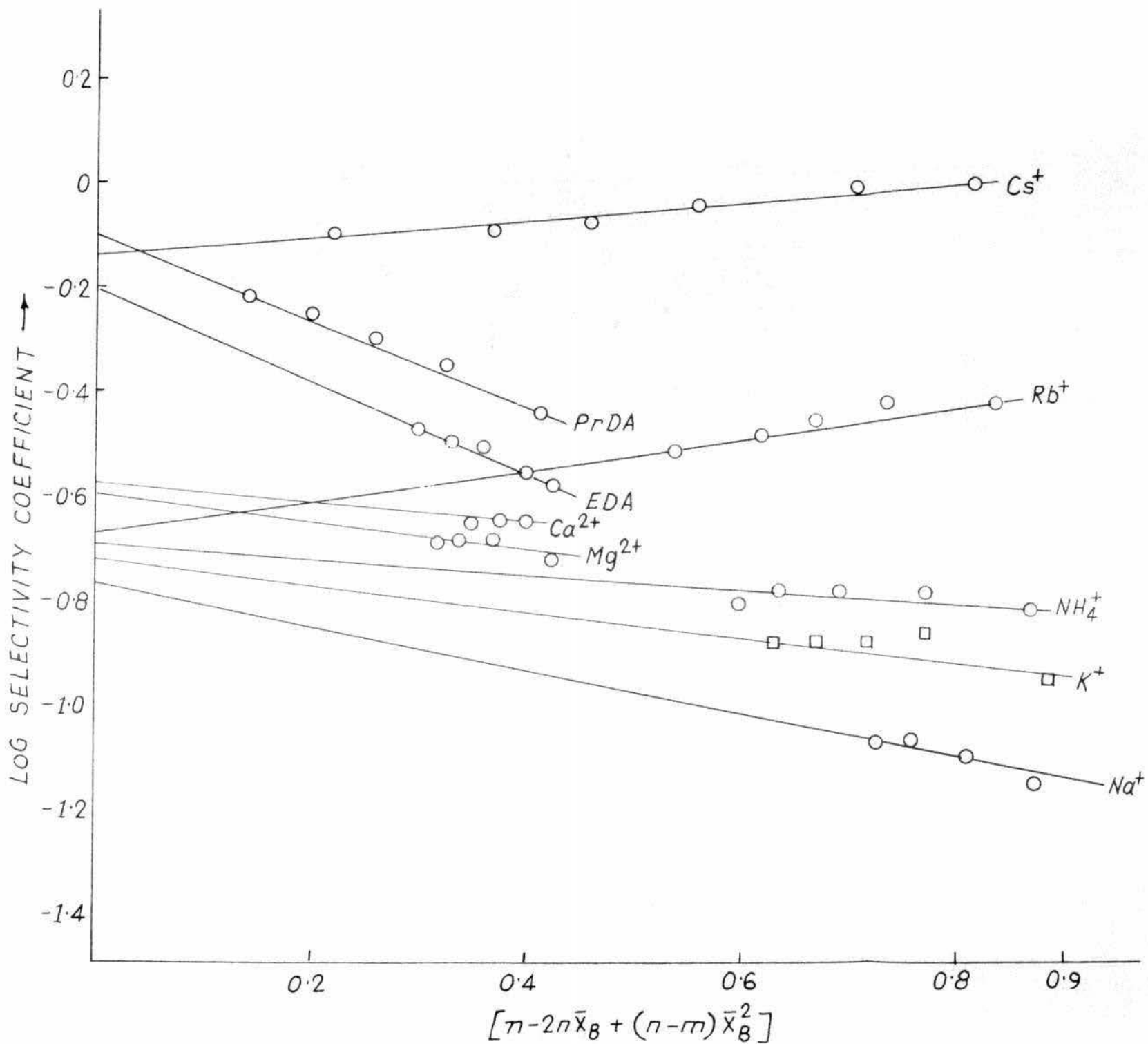


FIG.60. PLOT OF LOG SELECTIVITY COEFFICIENT AGAINST $n-2n\bar{x}_B + (n-m)\bar{x}_B^2$ IN THE EXCHANGE OF $Co(tn)_3^{3+}$ FROM $Na-Cotn_3^-$ BENTONITE BY DIFFERENT IONS.

CHAPTER V

Sorption and Desorption of $[Co^{3+}]$ and $[Co^{3+}]$ on Vermiculite system.

It has already been noted that vermiculites are closely related with the micas and are considered to be alteration products of biotites. These clay minerals have an expanding lattice differing from montmorillonite in that the expansion can take place only to a limited degree.

Vermiculite has not been so extensively used as other clay minerals for sorption and desorption studies of inorganic and organic ions. Walker *et al* (196) noted considerable swelling of vermiculite following amino acid sorption and referred to possible complex formation. The exchange of Na, Mg, Ca, Sr and Ba ions has been studied in the temperature range 25°C - 70°C by Wild and Keay (197) with vermiculite. They observed that vermiculite shows a preference for divalent ions over Na ions at 25°C and the preference increases very greatly at higher temperatures. The preference is largely determined by the increase in entropy which accompanies the replacement of monovalent ions by divalent ions in the vermiculite. Preference is less marked between divalent ions. The greater affinity of Mg^{2+} ions compared with other divalent ions is explained by these workers on the basis of their closer approach to the silicate surfaces. Exchange studies involving inorganic ions have been reviewed by Grim (23), Marshall (198) and others. But

the sorption characteristics of the trivalent inorganic complex cations and their subsequent desorption are not adequately investigated. In this section are presented the studies on sorption and desorption behaviour of two trivalent complex cations, namely, $\left[\text{Co}(\text{pn})_3 \right]^{3+}$ and $\left[\text{Co}(\text{tn})_3 \right]^{3+}$ with respect to vermiculite in line with similar studies reported earlier with bentonite systems.

SECTION A

Studies on Sorption

Sorption of $\text{Co}(\text{pn})_3^{3+}$ on Na-vermiculite at pH 7.

The adsorption isotherm of $\text{Co}(\text{pn})_3^{3+}$ on Na-vermiculite and the corresponding reciprocal graph are shown in Fig. 61. They are characteristic of the Langmuir type of isotherm. The value of V_m (Cf. P 46) calculated from the slope of the linear graph is equal to 133 m.e. and the amount corresponding to maximum adsorption (130 m.e.) are greater than the exchange capacity of the clay mineral, namely 112 m.e.

X-ray diffraction.

The X-ray diffraction data for Na-vermiculite and the partially exchanged $\text{Co}(\text{pn})_3^{3+}$ clays are reported in Fig. 62. The samples were prepared as described earlier (P 43) but here the samples were dried at about 70°C in an air oven and then powdered and stored in a desiccator over saturated $\text{Ca}(\text{NO}_3)_2$ (51% relative humidity). Each sample was allowed to equilibrate at 51% r.h. for 20 hours prior to analysis.

The basal spacings of Na-vermiculite was found to be 11.03\AA and that of the fully saturated $\text{Co}(\text{pn})_3^{3+}$ -clay, 12.84\AA . These results lead to the conclusion that segregation of $\text{Co}(\text{pn})_3^{3+}$ and Na^+ cations occurred in the partially exchanged

systems. The X-ray data also suggest that as $\text{Co}(\text{pn})_3^{3+}$ is added in increasing amounts, the basal spacing begins to increase thereby indicating interlamellar exchange.

Differential thermal analysis studies on $\text{Co}(\text{pn})_3^{3+}$ exchanged vermiculite.

The 0 percent, 20 percent, 60 percent and 100 percent $\text{Co}(\text{pn})_3^{3+}$ exchanged vermiculite clay samples were prepared and stored over concentrated sulphuric acid for 20 hours prior to analysis. Fig. 63 shows the D.T.A. curves. These curves were obtained under conditions of air flow. It will be noted that a strong endothermic peak was obtained at about 120°C which was probably related to adsorbed water. This was followed by a sharp exothermic peak at approximately 220°C for the 60 percent and 100 percent exchanged samples, but a very small exothermic peak appeared at about 250°C for the 20 percent exchanged sample. This exothermic peak probably corresponded to the melting point of the $\text{Co}(\text{pn})_3^{3+}$ as in the case of bentonite system. This was then followed by another weaker exothermic peak at about 310°C which was then followed by an exothermic peak starting at about 400°C and ending at about 460°C . The 460°C exothermic peak was not indicated for 20 percent exchanged samples. This curve indicated that the breakdown and pyrolysis of the organic portion of the complex takes place at about 450°C .

Sorption of $\text{Co}(\text{pn})_3^{3+}$ on H-vermiculite.

The adsorption isotherm of $\text{Co}(\text{pn})_3^{3+}$ on H-vermiculite and the corresponding reciprocal graph are shown in Fig. 64. They are characteristic of the Langmuir type of isotherm. The value of V_m calculated from the slope of the linear graph is equal to 117 m.e. and compares well both with the maximum of the isotherm 115 m.e. and exchange capacity of the mineral (112 m.e.). It may be noted that the pH of the clay suspension before and after adsorption is 4.5 and 3.0 respectively.

Differential thermal analysis of partially exchanged H-Copn₃-vermiculite.

D.T.A. curves of 20 percent and 100 percent $\text{Co}(\text{pn})_3^{3+}$ exchanged clay samples are shown in Fig. 65. The curves show a large endothermic peak at about 120°C probably due to adsorbed water. This was then followed by a broad exothermic peak at about 290°C for 20 percent exchanged clay which probably result from oxidation of the organic portion of $\text{Co}(\text{pn})_3^{3+}$. The supply of oxygen is probably sufficient in the case of lower percentage of the organic material in the clay and therefore the material is completely oxidised at a relatively low temperature. With increasing concentration, the amount of oxygen available becomes insufficient for complete oxidation. Probably for this reason, three exothermic peaks are obtained for fully

saturated $\text{Co}(\text{pn})_3^{3+}$ - clay at approximately 210°C , 285°C , 450°C representing melting and oxidation of the organic portion of the corresponding material. So the D.T.A. curve for the 20 percent sample was significantly different from that of 100 percent exchanged sample.

Sorption of $\text{Co}(\text{tn})_3^{3+}$ on Na-vermiculite at pH 7.

The adsorption isotherm and the reciprocal plot of $\text{Co}(\text{tn})_3^{3+}$ on vermiculite are given in Fig. 66. Both V_m (125 m.e) and the amount corresponding to maximum adsorption (125 m.e) are greater than the exchange capacity of the clay mineral, namely 112 m.e.

X-ray diffraction studies on partially exchanged Na- $\text{Co}(\text{tn})_3$ - vermiculite.

The X-ray diffraction data for the partially exchanged $\text{Co}(\text{tn})_3^{3+}$ clays are shown in Fig. 67. The samples were prepared as described earlier (P 43). The basal spacings of Na-vermiculite and that of the fully exchanged $\text{Co}(\text{tn})_3^{3+}$ - clay are 11.03\AA and 12.2\AA respectively. These results lead to the conclusion that segregation of $\text{Co}(\text{tn})_3^{3+}$ and Na^+ cations occurred in the partially exchanged systems.

X-ray diffraction data also indicate interstratification in the "clay vermiculite" sample. Since vermiculites are expanding lattice minerals, the lattice contracts on heat

treatment due to the exclusion of the interlayer water and the basal spacing was found to be 11.03\AA due to the presence of interlayer contaminants. The sample was dried at 70°C . Since the C.E.C. value (112 m.e./100 gm) found for the vermiculite is considerably lower than the C.E.C. of homogeneous vermiculites, it was obvious that the material still contained unexpanded layers, a conclusion which was confirmed by X-ray diffraction.

Differential thermal analysis studies on partially exchanged Na-Co₂tn₃ - vermiculite.

Fig. 68 shows the D.T.A. curves. These curves were obtained under conditions of air flow and heating rate was $10^{\circ}\text{C}/\text{minute}$. D.T.A. curves of 20%, 60% and 100% $\text{Co}(\text{tn})_3^{3+}$ exchanged vermiculite clay samples show a large endothermic peak at about 130°C which was probably related to adsorbed water. The exothermic peaks reflect the nature and binding of the interlamellar material. This endothermic peak was followed by several exothermic peaks at approximately 220°C , 300°C , 380°C and 480°C but the exothermic peak at 480°C was absent in the case of 20% $\text{Co}(\text{tn})_3^{3+}$ exchanged clay. Low and high temperature exothermic peaks probably result from the oxidation of the organic portion of $\text{Co}(\text{tn})_3^{3+}$. However, interpretation of the exothermic peaks is complex, since some of the oxidation reactions evidently occur inside the reaction

cell, but outside the clay phase, after partial liberation of the organic material. The course of oxidation reaction depends upon the supply of oxygen ; when sufficient oxygen is available, the material is entirely oxidised at a lower temperature, but with insufficient oxygen oxidation is completed at a higher temperature. So in the D.T.A. curves little difference was seen between the 60 and 100 percent $\text{Co}(\text{tn})_3^{3+}$ exchanged Na-vermiculite, but the D.T.A. curve for the 20 percent sample was significantly different from the former curves. This observation may also relate to the change in the environment of a $\text{Co}(\text{tn})_3^{3+}$ cation as the occupancy of clay exchange sites by $\text{Co}(\text{tn})_3^{3+}$ increases.

Sorption of $\text{Co}(\text{tn})_3^{3+}$ on H-vermiculite.

The adsorption isotherm of $\text{Co}(\text{tn})_3^{3+}$ on H-vermiculite and the corresponding reciprocal graph are given in Fig. 69. They are typical of the Langmuir type of isotherm. The value of V_m calculated from the slope of the linear graph is equal to 114 m.e. compares well with the maximum of the isotherm 112 m.e. and exchange capacity of the mineral 112 m.e.

It is observed that the pH of the clay suspension before and after adsorption varied between 4.5 and 3.0 respectively.

Differential thermal analysis of H-Co(tn)₃ - vermiculite.

D.T.A. curves of 20 percent and 100 percent Co(tn)₃³⁺ exchanged clay samples were shown in Fig. 65. The curves show an intense endothermic peak at 110-125°C which was probably related to the adsorbed water on the clay complex. Following the water loss peak there appeared a sharp exothermic peak at about 410°C, starting at about 360°C and ending at about 440°C in the D.T.A. curve for 20 percent Co(tn)₃³⁺ exchanged H-vermiculite. But the D.T.A. curve for 100 percent exchanged sample show much less intense three exothermic peaks at about 200°C, 270°C and 470°C respectively. The exothermic peaks were probably due to deamination, adsorption and desorption as the temperature is increased. So considerable differences appear in the D.T.A. curves for the 20 percent and 100 percent exchanged samples.

SECTION B

Studies on Desorption

Desorption of $\text{Co}(\text{pn})_3^{3+}$ from Na-Copn₃ - vermiculite.

The procedure for studying desorption has been described earlier (P 40). The results of desorption of $\text{Co}(\text{pn})_3^{3+}$ from its Na-Copn₃ -vermiculite complex are shown in Figs. 70, 71 and 72. Figs. 70 and 71 show the desorption by inorganic ions. The nature of the desorption curves with inorganic ions are almost similar as in the case of bentonite. Fig. 72 represents the desorption isotherm against $(\text{CH}_3)_4\text{N}^+$, $(\text{C}_2\text{H}_5)_4\text{N}^+$, $(\text{C}_3\text{H}_7)_4\text{N}^+$, $(\text{C}_4\text{H}_9)_4\text{N}^+$, EDA, PrDA, CTA and CP ions.

The influence of the size of the desorbing ions is more evident in the case of vermiculite than in montmorillonite. The latter swells considerably so that the sizes of the desorbing ions assume less importance, whereas in vermiculite the inter-lamellar space is limited to the thickness of about two water layers (4.98\AA) (Gruner, 228). Hence the influence of the size becomes more pronounced here. In this case it is observed that $(\text{CH}_3)_4\text{N}^+$, having an ionic diameter 6.94\AA (Ram Gopal and Rastogi, 229), desorbs larger amounts of $\text{Co}(\text{pn})_3^{3+}$ than $(\text{C}_2\text{H}_5)_4\text{N}^+$ with ionic diameter 8.00\AA (Ram Gopal and Rastogi, 229). Because ion exchange inherently requires a "two-way traffic" and cannot take place in a "one-way street" (Helfferich, 208), the inter-

lamellar space may be too narrow for a $(\text{CH}_3)_4\text{N}^+$ or $(\text{C}_2\text{H}_5)_4\text{N}^+$ to pass another ion and the results can be explained in terms of the space requirements as shown by Barrer, Buser and Grutter (1967). It is very likely that in this cation exchange process $(\text{C}_4\text{H}_9)_4\text{N}^+$, $(\text{C}_3\text{H}_7)_4\text{N}^+$ and $(\text{C}_2\text{H}_5)_4\text{N}^+$ experience more steric hindrance than $(\text{CH}_3)_4\text{N}^+$ and the exchange takes place from the edges and exterior surfaces of the mineral only.

The selectivity coefficients, as will be seen from the data given in Table 12, are smaller than 1.0 which indicates smaller affinity of the desorbing ions than $\text{Co}(\text{pn})_3^{3+}$ for the silicate minerals. According to the values of the selectivity coefficients the ions may be placed in the order: $\text{Li} < \text{Na} < \text{NH}_4 < \text{K} < \text{H} \leq \text{Rb} < \text{Cs}$ for the monovalent, $\text{Ca} < \text{Mg} < \text{Sr} < \text{Ba}$ for the bivalent inorganic ions and $(\text{C}_4\text{H}_9)_4\text{N} < (\text{C}_3\text{H}_7)_4\text{N} < (\text{C}_2\text{H}_5)_4\text{N} < (\text{CH}_3)_4\text{N} < \text{EDA} < \text{PrDA} \ll \text{CTA} < \text{CP}$ for the quaternary ammonium ions.

The variable position of H^+ in the series is well known. The greater exchangeability of H^+ than the bi or even the tri-valent ions has been explained by assuming H^+ to be present as a bare proton in the exchange reactions, as result of which it has got a greater accessibility to the exchange sites. Such an assumption may be made in the present case also.

The greater desorbing ability of Mg^{2+} than Ca^{2+} in vermiculite is attributable to the differences in stability of the water structures associated with these two inorganic cations adsorbed in vermiculite. The greater stability of Mg-system has

Table 12

Description characteristics of $\left[\text{Copn}_3 \right]^{3+}$ with respect
to different ions from Na-Copn₃-vermiculite.

Electrolyte used	Concentration of electrolyte	Distribution Coefficient	Selectivity Coefficient
<u>1:1 Electrolyte</u>			
LiCl	1.25 x 10 ⁻¹ (M)	0.12	0.00623
	1.50 "	0.15	0.00926
	2.0 "	0.175	0.012
	2.50 "	0.190	0.0148
NaCl	0.75 x 10 ⁻¹ (M)	0.200	0.0103
	1.0 "	0.200	0.0119
	1.25 "	0.200	0.0123
	1.50 "	0.200	0.0131
	2.0 "	0.237	0.0185
	2.50 "	0.240	0.02
	3.0 "	0.25	0.0225
NH ₄ Cl	0.50 x 10 ⁻¹ (M)	0.551	0.0361
	1.0 "	0.551	0.04459
	1.50 "	0.534	0.0493
	2.0 "	0.526	0.0535
	2.50 "	0.511	0.0558
	3.0 "	0.501	0.0578

(Contd..)

Table 12 (Contd..)

Electrolyte used	Concentration of electrolyte	Distribution Coefficient	Selectivity Coefficient
KCl	0.50 x 10 ⁻¹ (M)	0.651	0.0453
	1.0 "	0.626	0.0522
	1.50 "	0.601	0.05788
	2.0 "	0.576	0.06
	2.50 "	0.551	0.0619
	3.0 "	0.517	0.0605
RbCl	0.50 x 10 ⁻¹ (M)	1.256	0.104
	1.0 "	1.256	0.135
	1.50 "	1.17	0.143
	2.0 "	1.066	0.14
CsCl	0.25 x 10 ⁻¹ (M)	2.52	0.21
	0.50 "	2.37	0.253
	0.75 "	2.185	0.2595
	1.0 "	1.939	0.245
	1.50 "	1.61	0.2239

(Contd..)

Table 12 (Contd..)

Electrolyte used	Concentration of electrolyte	Distribution Coefficient	Selectivity Coefficient
HCl	0.50 x 10 ⁻¹ (M)	1.40	0.1218
	1.0 "	1.129	0.116
	1.50 "	0.936	0.105
	2.0 "	0.804	0.095
	2.50 "	0.722	0.0894
	3.0 "	0.652	0.0833
<u>2:1 Electrolyte</u>			
CaCl ₂	0.50 x 10 ⁻¹ (M)	1.585	0.1323
	1.0 "	1.417	0.1417
	1.50 "	1.29	0.140
	2.0 "	1.171	0.131
	2.50 "	1.076	0.123
MgCl ₂	0.50 x 10 ⁻¹ (M)	1.675	0.1475
	1.0 "	1.484	0.152
	1.50 "	1.33	0.145
	2.0 "	1.21	0.139
	2.50 "	1.11	0.129

(Contd..)

Table 12 (Contd..)

Electrolyte used	Concentration of electrolyte	Distribution Coefficient	Selectivity Coefficient
SrCl ₂	0.50 x 10 ⁻¹ (M)	1.71	0.154
	1.0 "	1.484	0.152
	1.50 "	1.34	0.148
	2.0 "	1.2	0.137
	2.50 "	1.09	0.126
BaCl ₂	0.50 x 10 ⁻¹ (M)	1.79	0.165
	1.0 "	1.55	0.165
	1.50 "	1.38	0.155
	2.0 "	1.269	0.15
<u>Quaternary ammonium salt</u>			
(CH ₃) ₄ NCl	4.0 x 10 ⁻² (M)	1.57	0.131
	6.0 "	1.38	0.127
	8.0 "	1.256	0.1256
(C ₂ H ₅) ₄ NBr	4.0 x 10 ⁻² (M)	1.25	0.0979
	6.0 "	1.13	0.0995
	8.0 "	1.00	0.0918

(Contd..)

Table 12 (Contd..)

**

Electrolyte used	Concentration of electrolyte	Distribution Coefficient	Selectivity Coefficient
$(C_3H_7)_4NI$	$4.0 \times 10^{-2}(M)$	0.816	0.0543
	6.0 "	0.752	0.0567
	8.0 "	0.689	0.0557
$(C_4H_9)_4NBr$	$4.0 \times 10^{-2}(M)$	0.626	0.0386
	6.0 "	0.501	0.0329
CTABr	$5.0 \times 10^{-3}(M)$	40.02	4.9
	7.0 "	35.48	4.76
	10.0 "	30.2	4.398
CPCl	$5.0 \times 10^{-3}(M)$	63.90	9.11
	7.0 "	50.00	7.54
	10.0 "	37.31	5.9
EDA	$0.25 \times 10^{-1}(M)$	2.849	0.2849
	0.50 "	2.50	0.2924
	0.75 "	2.26	0.2860
	1.0 "	2.05	0.270
	1.50 "	1.73	0.234

(Contd..)

Table 12 (Contd..)

Electrolyte used	Concentration of electrolyte	Distribution Coefficient	Selectivity Coefficient
PrDA	0.25 x 10 ⁻¹ (M)	3.16	0.342
	0.50 "	2.77	0.35
	0.75 "	2.44	0.327
	1.0 "	2.19	0.302
	1.50 "	1.83	0.258

been explained by Wild and Keay (197) and Peterson et al (199) by the smaller size of the Mg^{2+} , which could fit into the water structure of the vermiculite interlayer with less disruptive effect than could Ca^{2+} . Thus the exchanging Ca^{2+} would have a greater energy barrier to overcome than Mg^{2+} to form their respective vermiculite complexes. Here also CP^+ releases more $Co(pn)_3^{3+}$ than CTA^+ from the clay-complex, which is probably due to lower critical micelle concentration of the former. The detergent properties of these ions may also be operative in the exchange process.

Table 13 shows the values of the thermodynamic equilibrium constant, standard Gibbs free energy change calculated from the linear plot of Kielland's equation (Fig. 73).

Smooth linear curves are obtained in the case of Cs^+ , H^+ , Rb^+ , K^+ , NH_4^+ , Mg^{2+} , Ca^{2+} , and Ba^{2+} while curves obtained with Li^+ , Na^+ , $(CH_3)_4N^+$, $(C_2H_5)_4N^+$, $(C_3H_7)_4N^+$ and $(C_4H_9)_4N^+$ are not so. The failure of these ions may be traced to high hydration number of the first two and to the steric reasons for the alkyl quaternary ions as pointed out earlier.

As in other cases, the plot of \log (selectivity coefficient) vs. hydrated ionic radius curve (Fig. 74) is not linear but that against $\frac{1}{a_0}$ yields a good straight line. The behaviour of bivalent exchanging ions however is different from those of the monovalent ions in this respect. This deviation may result

Table 13

Evaluation of thermodynamic quantities
from Kielland's equation at 25°C

Exchange system	Thermodynamic equilibrium constant	ΔG° Cal/mole
$K_{\text{COPn}_3}^{\text{NH}_4}$	0.630	272.73
$K_{\text{COPn}_3}^{\text{K}}$	0.66	245.45
$K_{\text{COPn}_3}^{\text{Rb}}$	0.794	136.36
$K_{\text{COPn}_3}^{\text{Cs}}$	1.0	0
$K_{\text{COPn}_3}^{\text{H}}$	0.0398	1909.12
$K_{\text{COPn}_3}^{\text{Ca}}$	0.1	1363.66
$K_{\text{COPn}_3}^{\text{Mg}}$	0.109	1309.11
$K_{\text{COPn}_3}^{\text{Ba}}$	0.125	1227.29

from the irregular hydration as well as the characteristic behaviour (197,199) of Mg^{2+} towards the vermiculite surface. The results suggest that in such a process of desorption of $Co(pn)_3^{3+}$ by smaller inorganic cations, the parameter a^0 rather than the hydrated ionic radius may be used to correlate the affinities of the monovalent ions for the vermiculite.

Desorption of $Co(tn)_3^{3+}$ from Na- $Co(tn)_3$ -vermiculite.

The desorption isotherms of $Co(tn)_3^{3+}$ from its Na-vermiculite complex are shown in Figs. 75,76,77 and 78. The values of the selectivity coefficients are given in Table 14. The sequence of desorption is : $Li < Na < NH_4 \leq K < Rb < H < Cs$ for the monovalent, $Mg \leq Sr < Ca < Ba$ for the bivalent, and $(C_4H_9)_4N < (C_3H_7)_4N < (C_2H_5)_4N < (CH_3)_4N < EDA < PrDA < DTA < DDTA < CTA < OP$ for the organic ions, which is almost the same as in the desorption of $Co(pn)_3^{3+}$ from its vermiculite complex except in the relative position of H^+ and Sr^{2+} . This irregular behaviour of H^+ is however, well known, for which the idea of bare proton taking part in exchange has been invoked.

The desorption curve with Na^+ is S-shaped and may be placed in the S-group of curves of Giles et al (194). This is unlike that observed with the other silicate mineral studied in the present investigation with inorganic ions. The curve (Fig. 75) is initially convex towards the concentration axis, tending to

Table 14

Desorption characteristics of $[Co^{3+}]$ with respect to different ions from Na-Co₃-vermiculite.

Electrolyte used	Concentration of electrolyte	Distribution Coefficient	Selectivity Coefficient
<u>1:1 Electrolyte</u>			
LiCl	0.75 x 10 ⁻¹ (M)	0.266	0.0161
	1.0 "	0.280	0.195
	1.50 "	0.290	0.02319
	2.0 "	0.3	0.0267
	2.50 "	0.280	0.02617
NaCl	0.75 x 10 ⁻¹ (M)	0.534	0.0408
	1.0 "	0.451	0.0363
	1.50 "	0.400	0.0354
	2.0 "	0.417	0.0418
	2.50 "	0.474	0.053
	3.0 "	0.534	0.0675
NH ₄ Cl	0.50 x 10 ⁻¹ (M)	1.30	0.1188
	0.75 "	1.295	0.1356
	1.0 "	1.611	0.203
	1.50 "	1.228	0.1638
	2.0 "	1.193	0.175
	2.50 "	1.058	0.163

(Contd..)

Table 14 (Contd..)

Electrolyte used	Concentration of electrolyte	Distribution Coefficient	Selectivity Coefficient
KCl	0.50 x 10 ⁻¹ (M)	1.745	0.173
	1.0 "	1.61	0.203
	1.50 "	1.395	0.1962
	2.0 "	1.257	0.189
RbCl	0.25 x 10 ⁻¹ (M)	3.10	0.296
	0.50 "	2.90	0.352
	0.75 "	2.699	0.3718
	1.0 "	2.477	0.371
	1.50 "	1.97	0.319
CsCl	0.125 x 10 ⁻¹ (M)	5.74	0.5369
	0.25 "	5.95	0.724
	0.75 "	4.39	0.741
	1.0 "	3.48	0.6038
HCl	0.50 x 10 ⁻¹ (M)	3.384	0.436
	1.0 "	2.42	0.359
	1.50 "	1.95	0.313
	2.0 "	1.61	0.270
	2.50 "	1.006	0.169

(Contd..)

Table 14 (Contd..)

Electrolyte used	Concentration of electrolyte	Distribution Coefficient	Selectivity Coefficient
<u>2:1 Electrolyte</u>			
MgCl ₂	0.50 x 10 ⁻¹ (M)	1.96	0.205
	1.0 "	1.90	0.251
	1.50 "	1.731	0.249
	2.0 "	1.58	0.238
	2.50 "	1.49	0.235
CaCl ₂	0.50 x 10 ⁻¹ (M)	2.233	0.2569
	1.0 "	2.11	0.302
	1.50 "	1.94	0.306
	2.0 "	1.80	0.304
	2.50 "	1.678	0.293
SrCl ₂	0.50 x 10 ⁻¹ (M)	1.9	0.126
	1.0 "	1.9	0.251
	1.50 "	1.83	0.276
	2.0 "	1.73	0.282
	2.50 "	1.65	0.2849

(Contd..)

Table 14 (Contd..)

Electrolyte used	Concentration of electrolyte	Distribution Coefficient	Selectivity Coefficient
BaCl ₂	0.50 x 10 ⁻¹ (M)	2.35	0.282
	1.0 "	2.157	0.314
	1.50 "	1.99	0.322
	2.0 "	1.86	0.322
	2.50 "	1.75	0.318
<u>Quaternary ammonium salt</u>			
(CH ₃) ₄ NCl	4.0 x 10 ⁻² (M)	1.636	0.147
	7.0 "	1.47	0.156
(C ₂ H ₅) ₄ NBr	4.0 x 10 ⁻² (M)	1.38	0.118
	7.0 "	1.29	0.131
(C ₃ H ₇) ₄ NI	4.0 x 10 ⁻² (M)	1.19	0.099
	7.0 "	1.004	0.0939
(C ₄ H ₉) ₄ NBr	4.0 x 10 ⁻² (M)	1.004	0.0768
	7.0 "	0.846	0.0754
DTABr	5.0 x 10 ⁻³ (M)	16.09	1.53
	7.0 "	15.29	1.628
	10.0 "	13.81	1.61
	13.0 "	11.75	1.43

(Contd..)

Table 14 (Contd..)

Electrolyte used	Concentration of electrolyte	Distribution Coefficient	Selectivity Coefficient
DDTABr	5.0 x 10 ⁻³ (M)	24.44	2.68
	7.0 "	23.77	2.93
	10.0 "	21.40	2.92
	13.0 "	19.69	2.89
OTABr	5.0 x 10 ⁻³ (M)	55	7.87
	7.0 "	53.28	8.696
	10.0 "	49.69	9.32
	13.0 "	41.62	8.27
CPO1	5.0 x 10 ⁻³ (M)	88.48	14.76
	7.0 "	79.92	15.08
	10.0 "	65.58	13.81
	13.0 "	51.28	11.23
BDA	0.25 x 10 ⁻¹ (M)	4.10	0.564
	0.75 "	2.92	0.483
	1.0 "	2.58	0.439
	1.50 "	2.125	0.363

(Contd..)

Table 14 (Contd..)

Electrolyte used	Concentration of electrolyte	Distribution Coefficient	Selectivity Coefficient
PrDA	$0.25 \times 10^{-1}(M)$	4.44	0.653
	0.50 "	3.64	0.611
	0.75 "	3.09	0.541
	1.0 "	2.71	0.480
	1.50 "	2.22	0.395

change the curvature to that of a concave one at the latter stages. However, similar S-shaped curves have been observed by Daskanungo (200) in the desorption of $\text{Co}(\text{NH}_3)_6^{3+}$ from H- $\text{Co}(\text{NH}_3)_6$ -vermiculite by NH_4^+ , K^+ , Rb^+ and Cs^+ . The conditions of Giles et al (194) as observed in the case of CTA^+ and CP^+ are probably not applicable here and cannot be explained on the basis of the criteria laid down by these authors.

Their suggestion as to a lateral association between adsorbed molecules helping to hold them onto the surface seems to be valid only for surface active ions, viz., alkyl quaternary ammonium ions. The problem under consideration involves ion which is not surface active and where the lateral association is not probable. For this reason, an alternative suggestion may be made to explain the characteristic features of the desorption curves. It has already been pointed out in the case of similar studies with clay minerals that a water-proof character is developed in them when ions, like $\text{[Co}(\text{NH}_3)_6]^{3+}$ or $\text{Co}(\text{pn})_3^{3+}$ are present in the exchangeable form (P 54). Owing to the presence of a hydrophobic layer, ion such as Na is not easily accessible to the surface unless a considerable amount of the adsorbed ions get desorbed and replaced by hydrophillic ions. At lower concentrations of the desorbing ions, therefore, the amount of desorption is very small. This explains the initial rather flat part of the curve. At higher concentrations

of the electrolyte the hydrophobic ions are replaced by hydrophilic ones making the exchange-clay more accessible to water as well as to the desorbing ion with the result that desorption increases.

This brings out the important role of water molecules in desorption. The contributions of other factors, viz., ionic size, polarisability of the ions, distance of closest approach to the surface, geometric factor i.e., sieve action, architecture of the solid matrix, swelling pressure, sorption of electrolytes, binding energy of respective ions for the matrix, solubility of the electrolytes etc. cannot, however, be ignored.

The release of the Co(III) complex ions by quaternary ammonium ions was more difficult for vermiculite than for bentonite, and the effectiveness of exchange was inversely related to ionic size. Thus $(C_3H_7)_4N^+$ or $(C_4H_9)_4N^+$ ions are too large for entry into the higher charged vermiculite, although exchange of Co(III) complex from smectite of lower charge density occurred with little difficulty. This observation supports the view that the interlayer spacing of the clay in suspension is of crucial importance in explaining cation preference in exchange. This is especially true of the contracted, higher layer charge clays like vermiculite where the coulombic forces are too strong for layer expansion by organic ions and energy must be provided for interlayer expansion so that exchange by large organic cations can occur.

The values of the thermodynamic equilibrium constants have been evaluated from the linear plot of the experimental results by the use of Kielland's equation (Fig. 79). Gibbs free energy has been calculated from the relation $\Delta G^{\circ} = -RT \ln K$. The results are recorded in Table 15. Here the application of Kielland's equation seems to be very satisfactory in evaluating the thermodynamic equilibrium constants. Smooth linear curves are obtained in the case of H^{+} , Li^{+} , Na^{+} , NH_4^{+} , K^{+} , Rb^{+} , Cs^{+} , Mg^{2+} , Ca^{2+} and Ba^{2+} while curves obtained with $(CH_3)_4N^{+}$, $(C_2H_5)_4N^{+}$, $(C_3H_7)_4N^{+}$ and $(C_4H_9)_4N^{+}$ are not so. The failure of these ions may be traced to the steric reasons for the alkyl quaternary ions as pointed out earlier.

Fig. 80 shows the plot of log (selectivity coefficients) against the hydrated ionic radii (189) and $\frac{1}{a^{\circ}}$ (190) of the monovalent ions. It is observed that there is a sharp break in the log (selectivity coefficients) vs. hydrated ionic radius curve, whereas the plot of log (selectivity coefficients) vs. the reciprocal of the Debye Huckel parameter, a° , is linear. The behaviour of bivalent exchanging ions however is different from those of the monovalent ions in this respect. This deviation may result from the irregular hydration as well as the characteristic behaviour (197, 199) of Mg^{2+} towards the vermiculite surface.

The results strongly suggest that in such a process of desorption of $Co(tn)_3^{3+}$ by smaller inorganic cations the parameter a° rather than the hydrated ionic radius may be used to

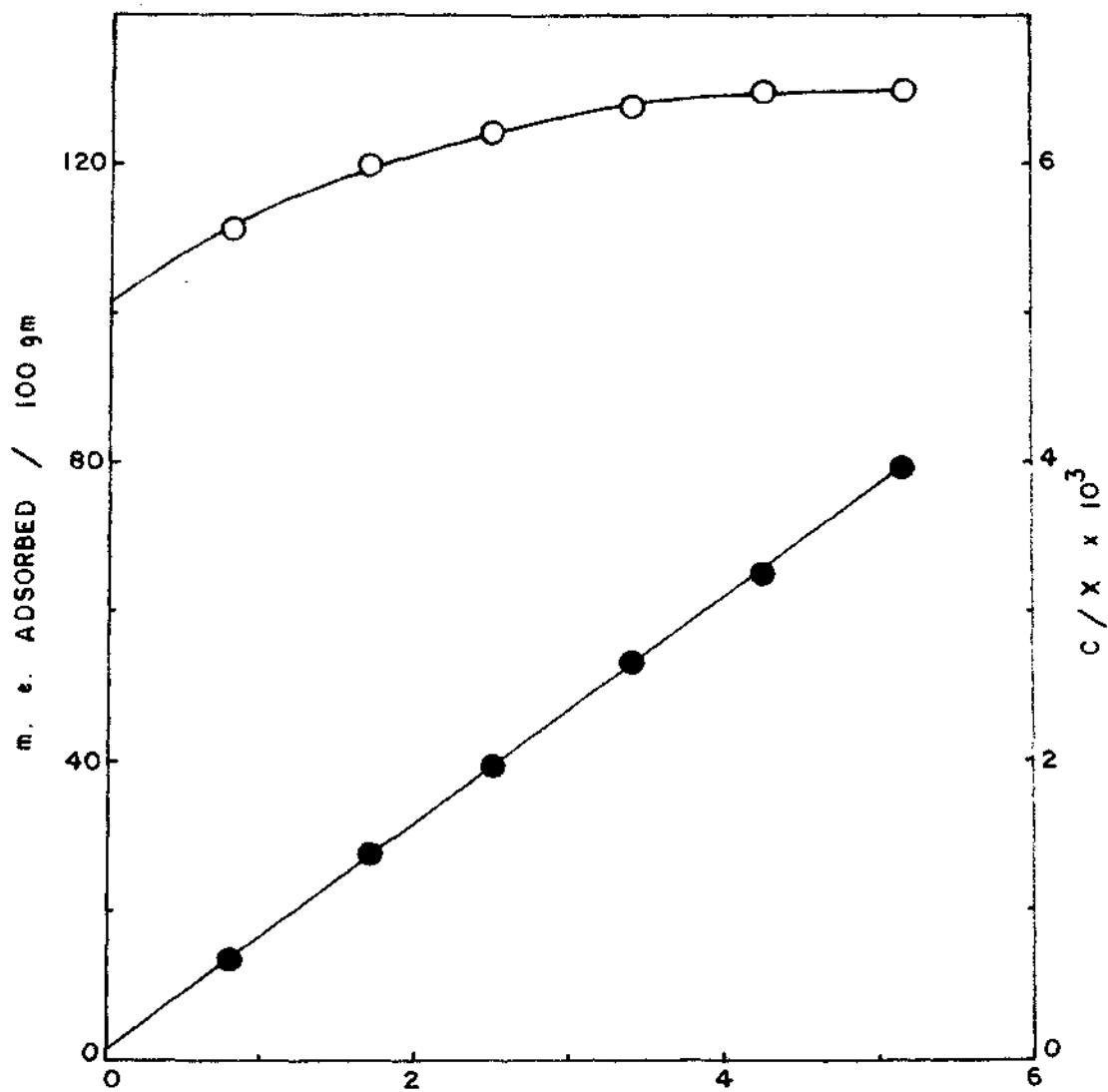
Table 15

Evaluation of thermodynamic quantities from
Kielland's equation at 25°C.

Exchange system	Thermodynamic equilibrium constant	ΔG° Cal/mole
$K_{\text{Co}^{\text{Li}}\text{tn}_3}$	0.501	409.09
$K_{\text{Co}^{\text{Na}}\text{tn}_3}$	0.831	109.09
$K_{\text{Co}^{\text{NH}_4}\text{tn}_3}$	0.912	54.54
$K_{\text{Co}^{\text{K}}\text{tn}_3}$	1.0	0
$K_{\text{Co}^{\text{Rb}}\text{tn}_3}$	1.148	-81.81
$K_{\text{Co}^{\text{Cs}}\text{tn}_3}$	1.258	-135.82
$K_{\text{Co}^{\text{H}}\text{tn}_3}$	0.1	1363.36
$K_{\text{Co}^{\text{Mg}}\text{tn}_3}$	0.281	750.01
$K_{\text{Co}^{\text{Ca}}\text{tn}_3}$	0.346	627.28
$K_{\text{Co}^{\text{Ba}}\text{tn}_3}$	0.416	567.28

correlate the affinities of the monovalent ions for the mineral.

The desorption curves of $\text{Co}(\text{pn})_3^{3+}$ and $\text{Co}(\text{tn})_3^{3+}$ from vermiculite together with the values of the selectivity coefficients, thermodynamic equilibrium constant and Gibbs free energy change (Tables 12-15) indicate that these are desorbed from the mineral surface in the sequence: $\text{Co}(\text{pn})_3^{3+} < \text{Co}(\text{tn})_3^{3+}$, which is the reverse as was observed in the case of bentonite system.



EQUILIBRIUM CONCENTRATION OF Copn₃Cl₃ x 10³ M
 FIG. 61. ADSORPTION ISOTHERM OF Copn₃Cl₃ ON
 Na - VERMICULITE.

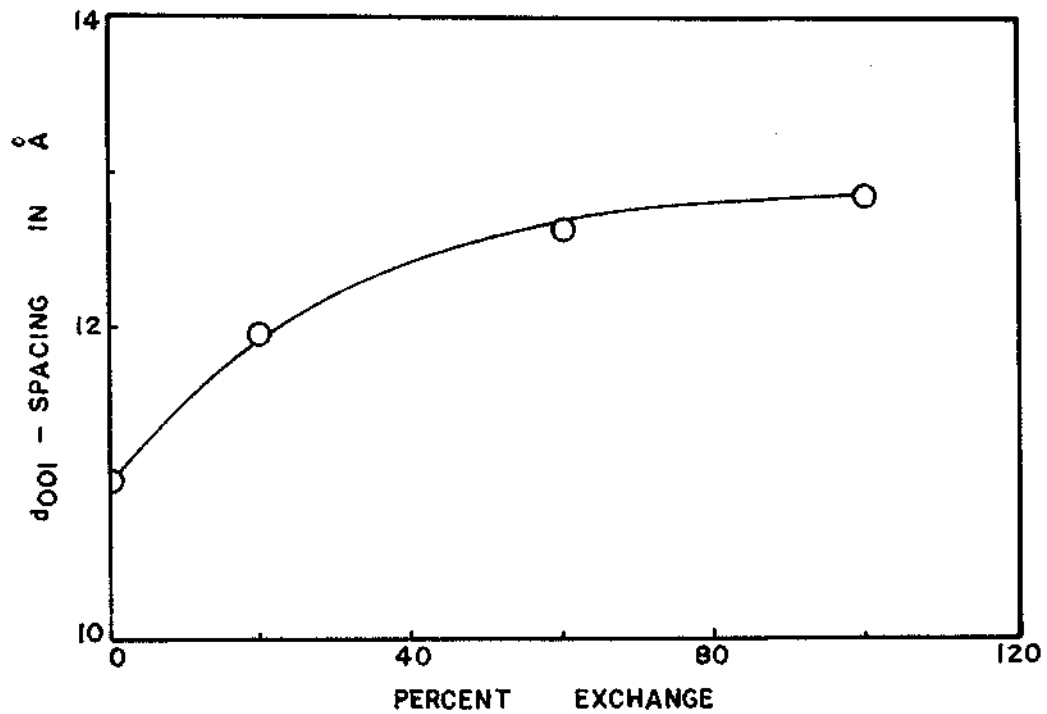


FIG. 62 . d₀₀₁ - SPACING VS. PERCENT EXCHANGE
FOR Na - Copn₃ - VERMICULITE .

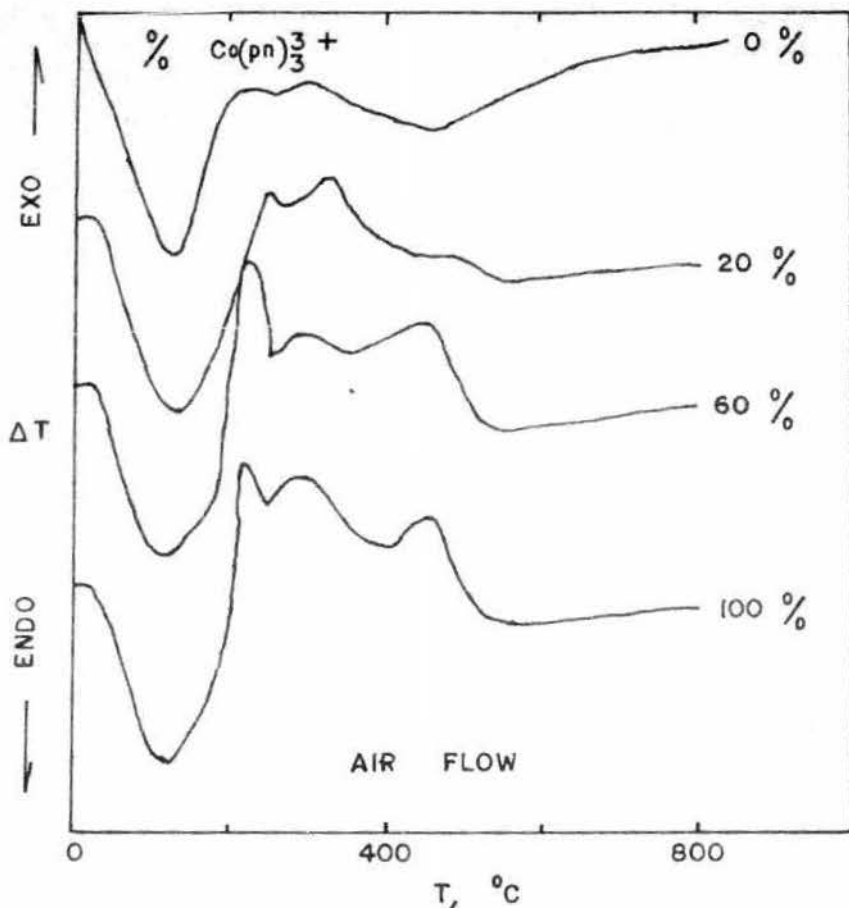
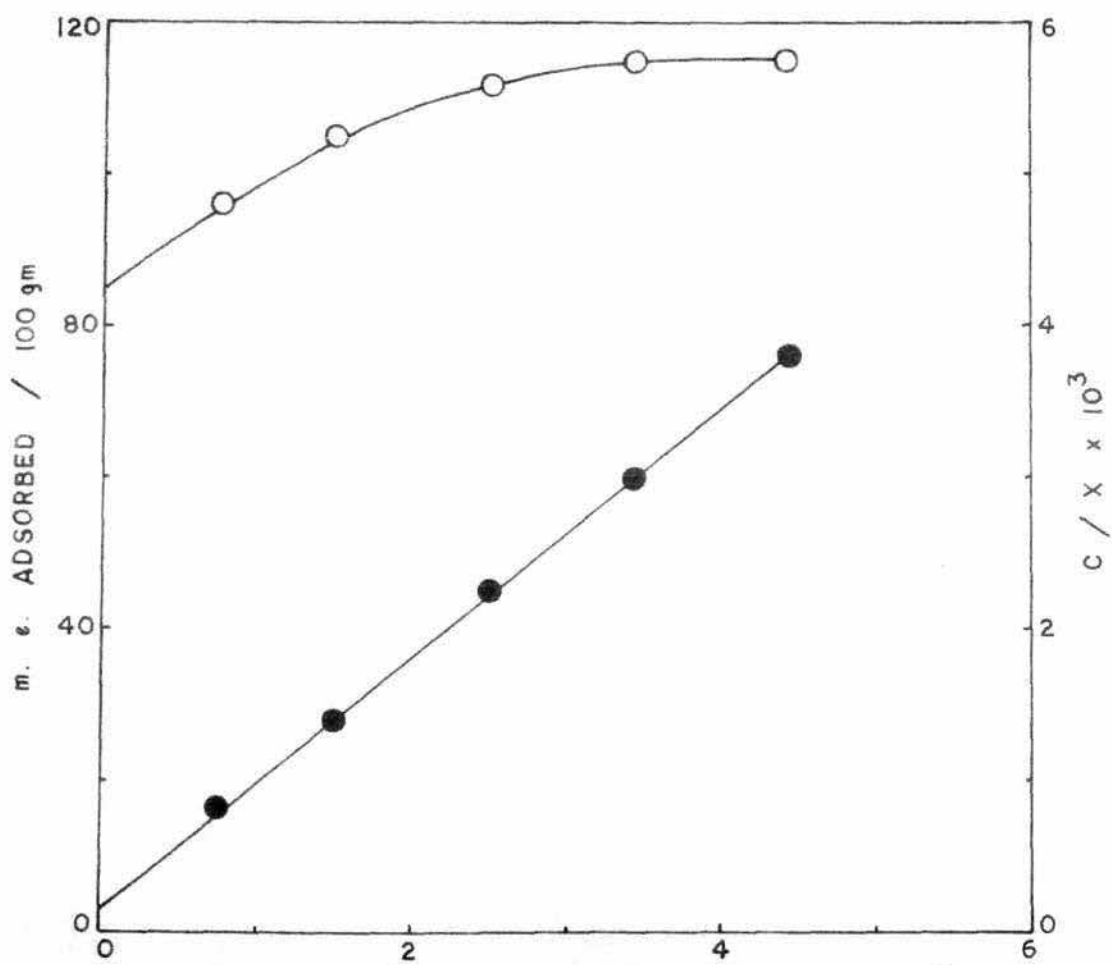


FIG. 63. D.T.A. CURVES FOR MIXED $\text{Co}(\text{pn})_3^+ \text{Na}^+$ VERMICULITES (PRETREATED OVER CONC. H_2SO_4) USING AIR FLOW, HEATING RATE $10^\circ \text{C}/\text{min}$.



EQUILIBRIUM CONCENTRATION OF $\text{Copn}_3\text{Cl}_3 \times 10^3 \text{ M}$
 FIG. 64. ADSORPTION ISOTHERM OF Copn_3Cl_3 ON
 H - VERMICULITE.

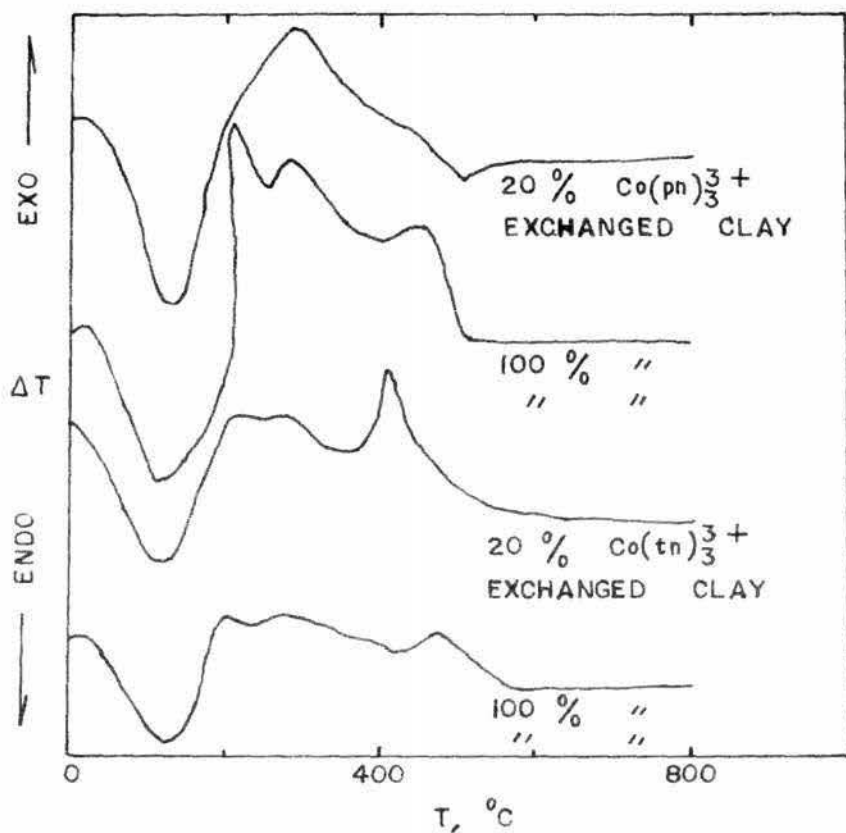


FIG. 65. D. T. A. CURVES FOR MIXED $\text{Co}(\text{pn})_3^+ - \text{H}^+$ VERMICULITE AND $\text{Co}(\text{tn})_3^+ - \text{H}^+$ VERMICULITE (PRETREATED OVER CONC. H_2SO_4) USING AIR FLOW, HEATING RATE $10^\circ \text{C}/\text{min}$.

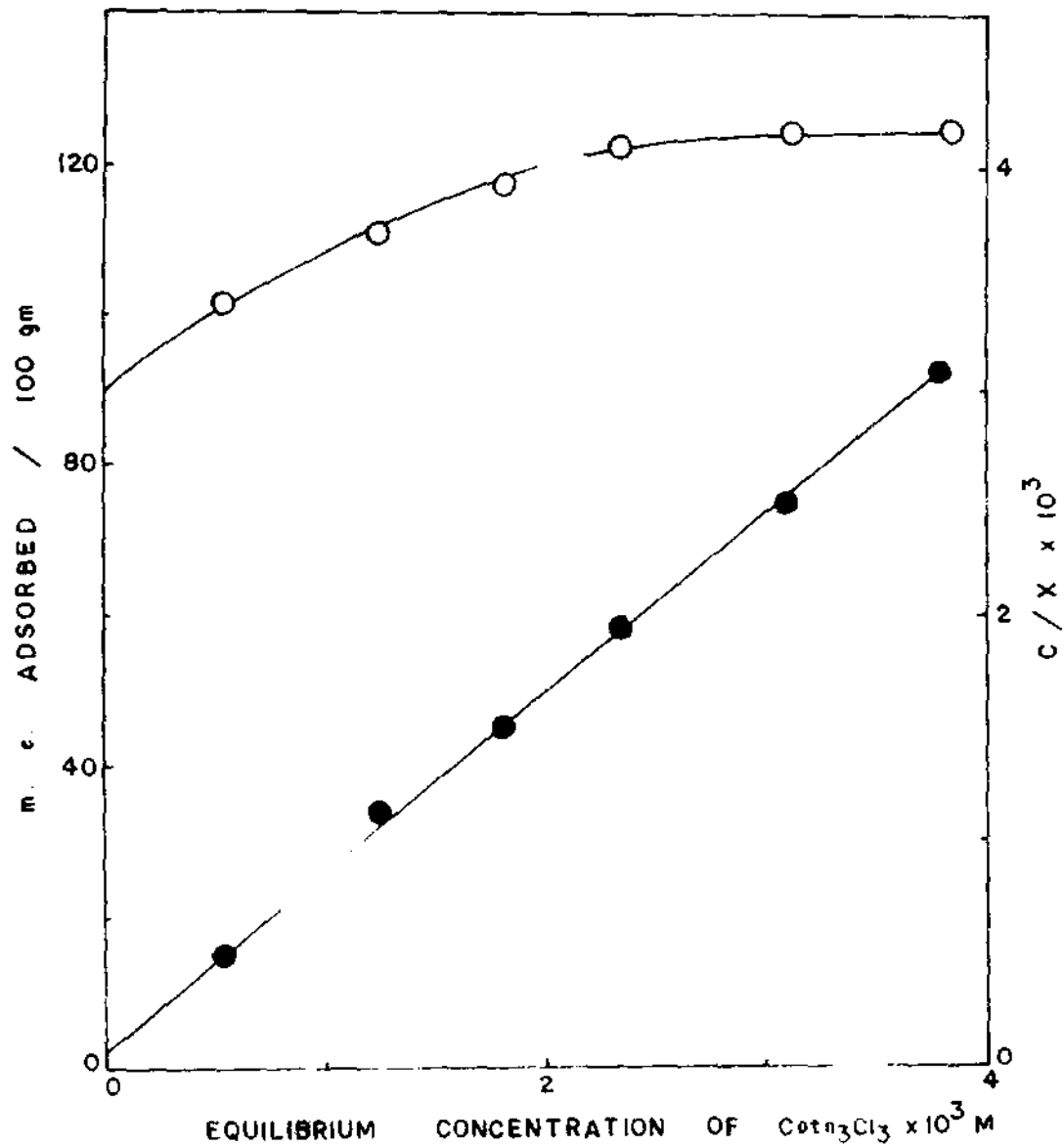


FIG. 66. ADSORPTION ISOTHERM OF $\text{Co}(\text{NO}_3)_3$ ON Na - VERMICULITE.

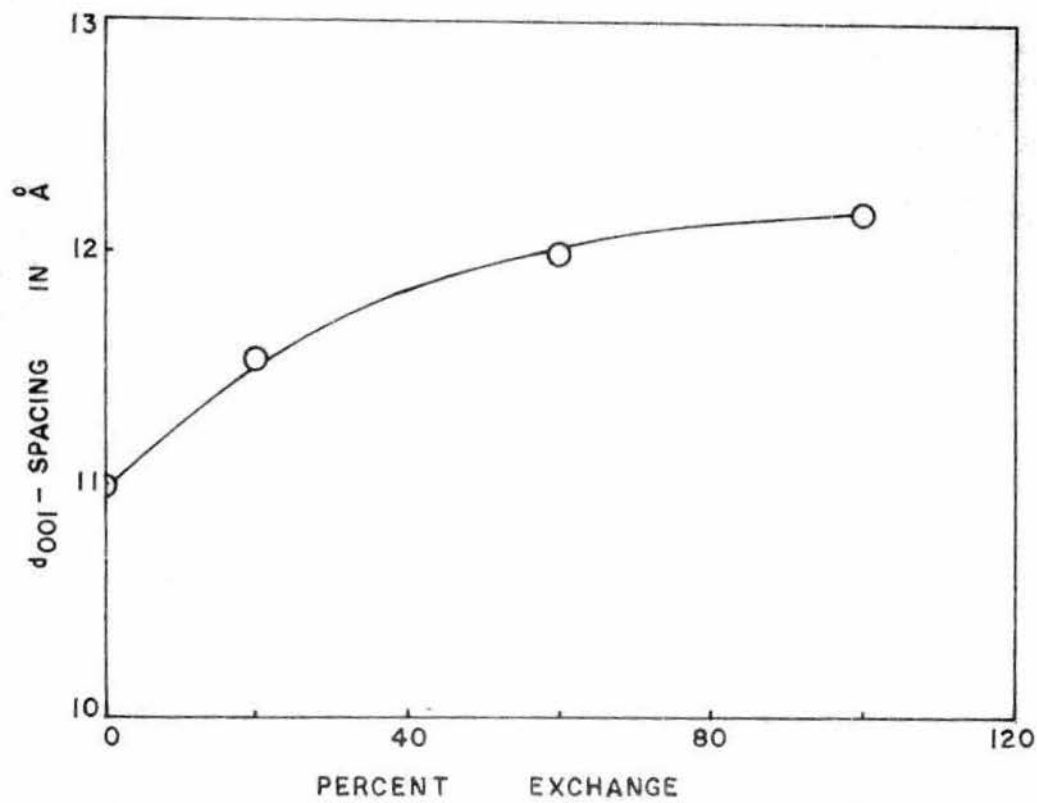


FIG. 67. d_{001} - SPACING VS. PERCENT EXCHANGE FOR Na - Cotn₃ - VERMICULITE.

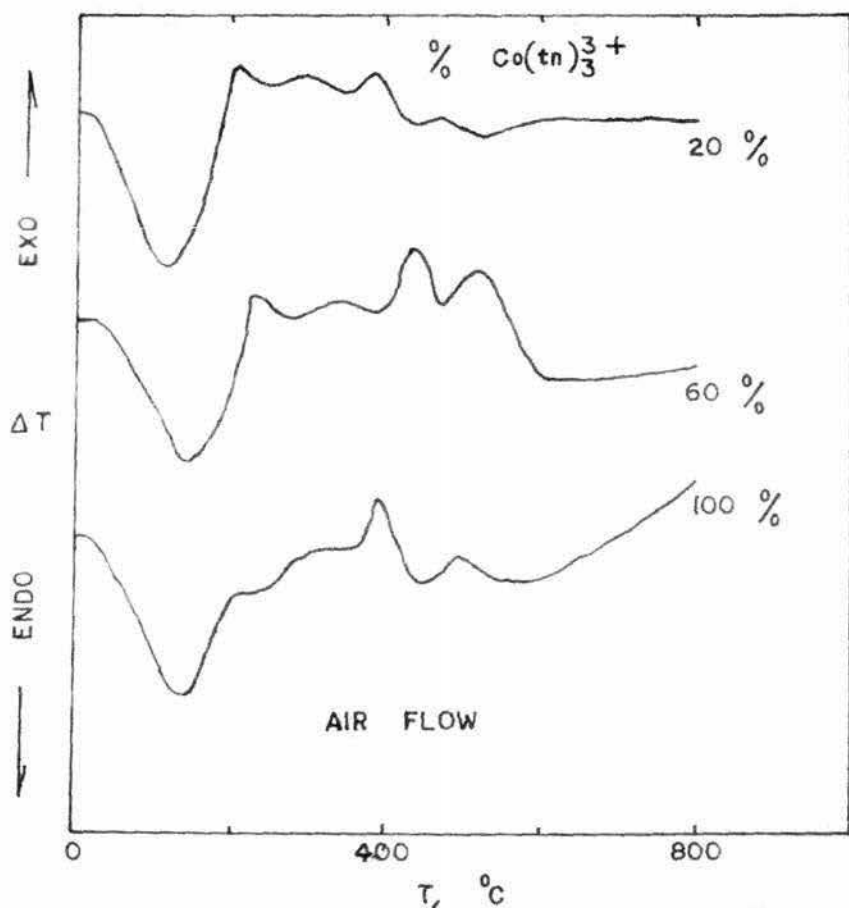
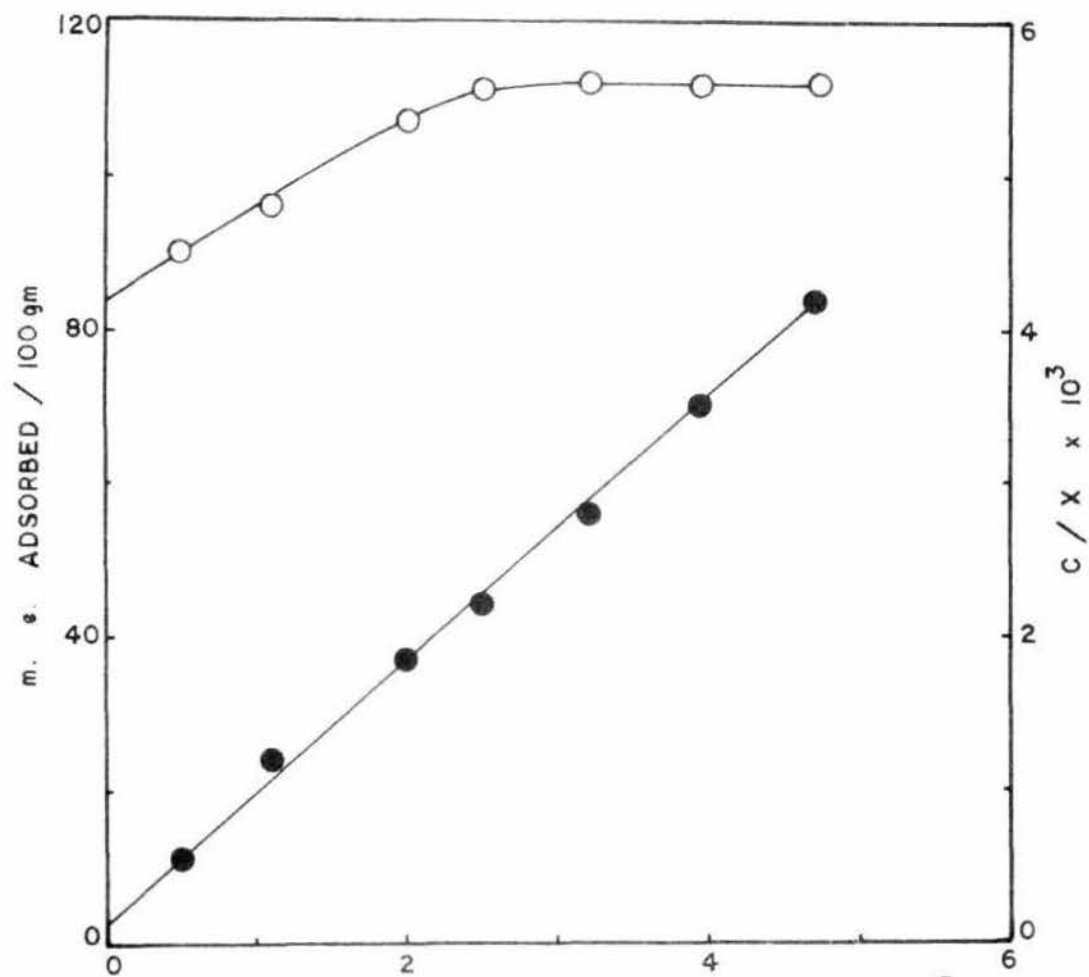


FIG. 68. D.T.A. CURVES FOR MIXED $\text{Co}(\text{tn})_3^+ \text{Na}^+$ VERMICULITES (PTREATED OVER CONC. H_2SO_4) USING AIR FLOW, HEATING RATE $10^\circ \text{C}/\text{min}$.



EQUILIBRIUM CONCENTRATION OF $\text{Co}(\text{NO}_3)_3 \times 10^3 \text{ M}$
 FIG. 69. ADSORPTION ISOTHERM OF $\text{Co}(\text{NO}_3)_3$ ON
 H - VERMICULITE.

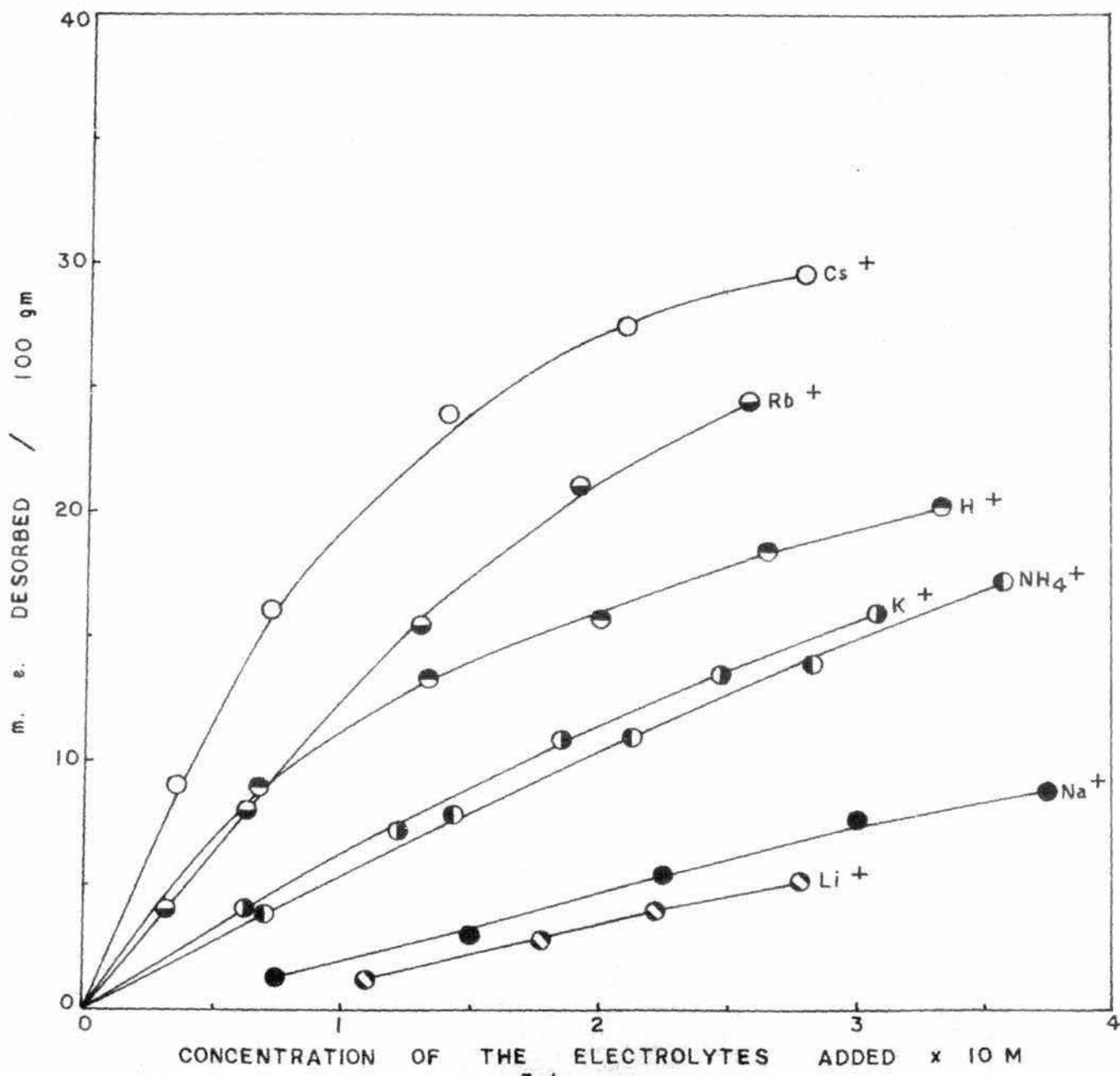


FIG. 70. DESORPTION OF $\text{Co}(\text{pn})_3^+$ FROM $\text{Na}-\text{Co}(\text{pn})_3$ -VERMICULITE BY DIFFERENT IONS.

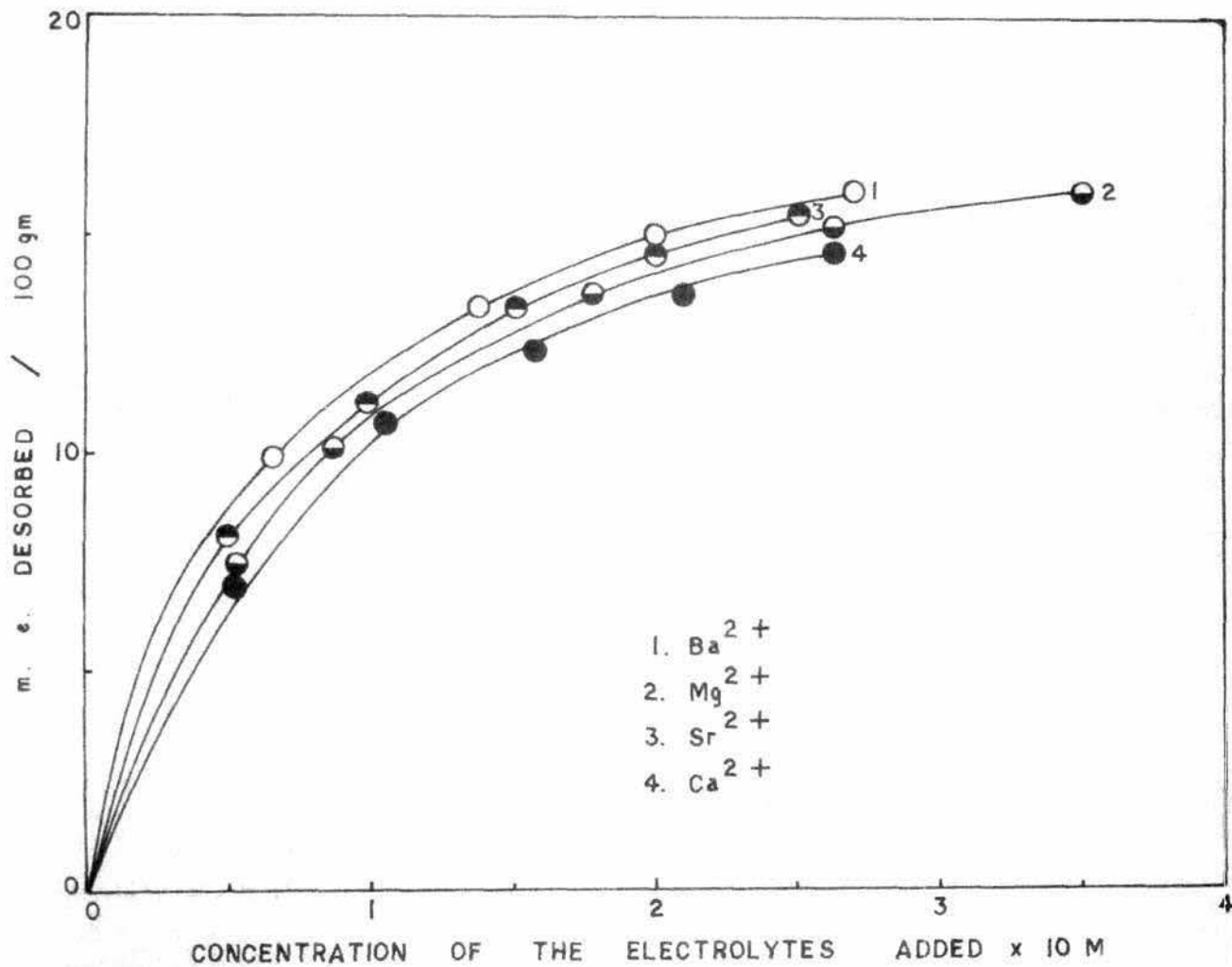


FIG. 71. DESORPTION OF $\text{Co}(\text{pn})_3^{3+}$ FROM Na-Copn_3 - VERMICULITE BY DIFFERENT IONS.

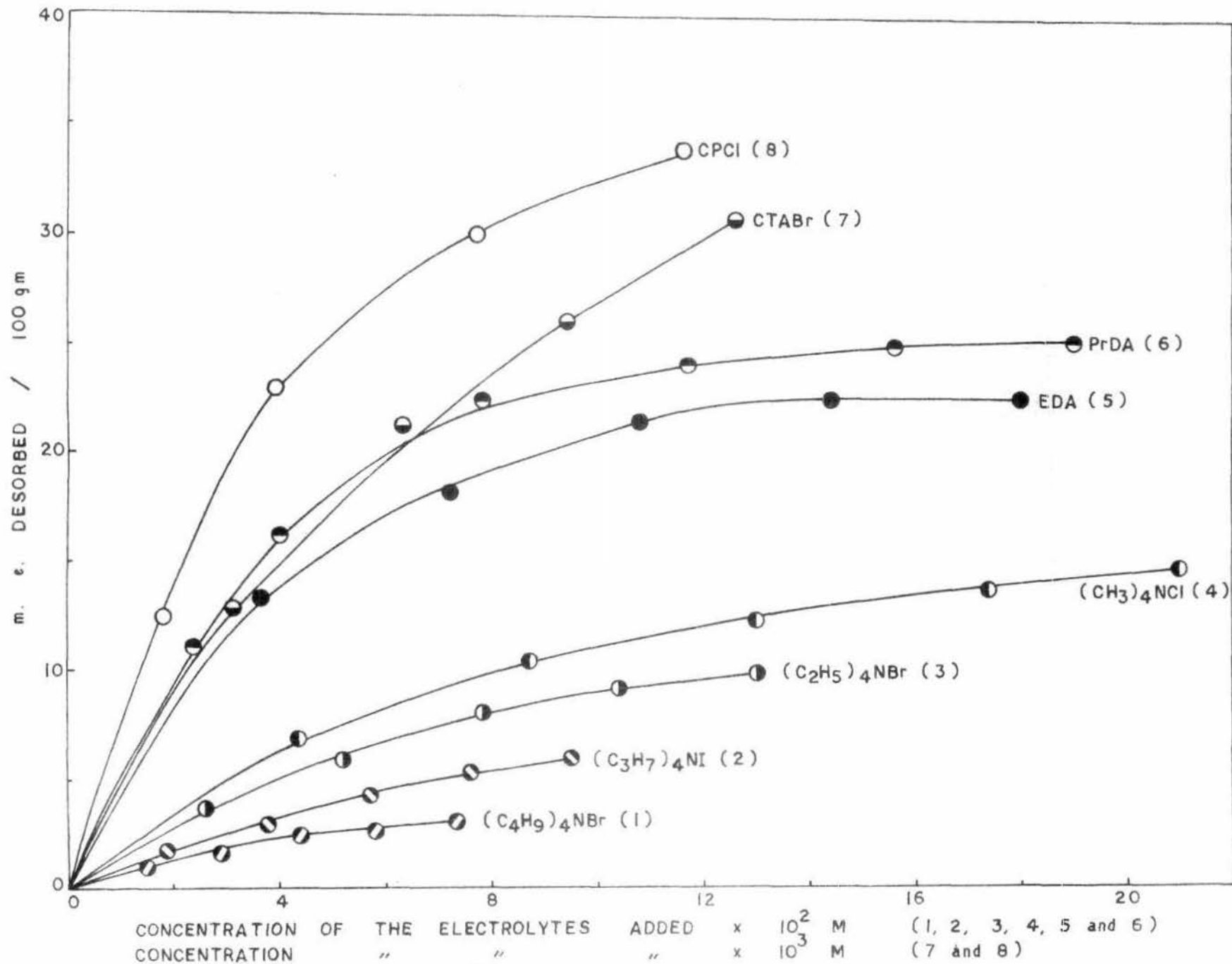


FIG. 7.2. DESORPTION OF $\text{Co}(\text{pn})_3^{3+}$ FROM Na-Copn_3 -VERMICULITE BY DIFFERENT IONS.

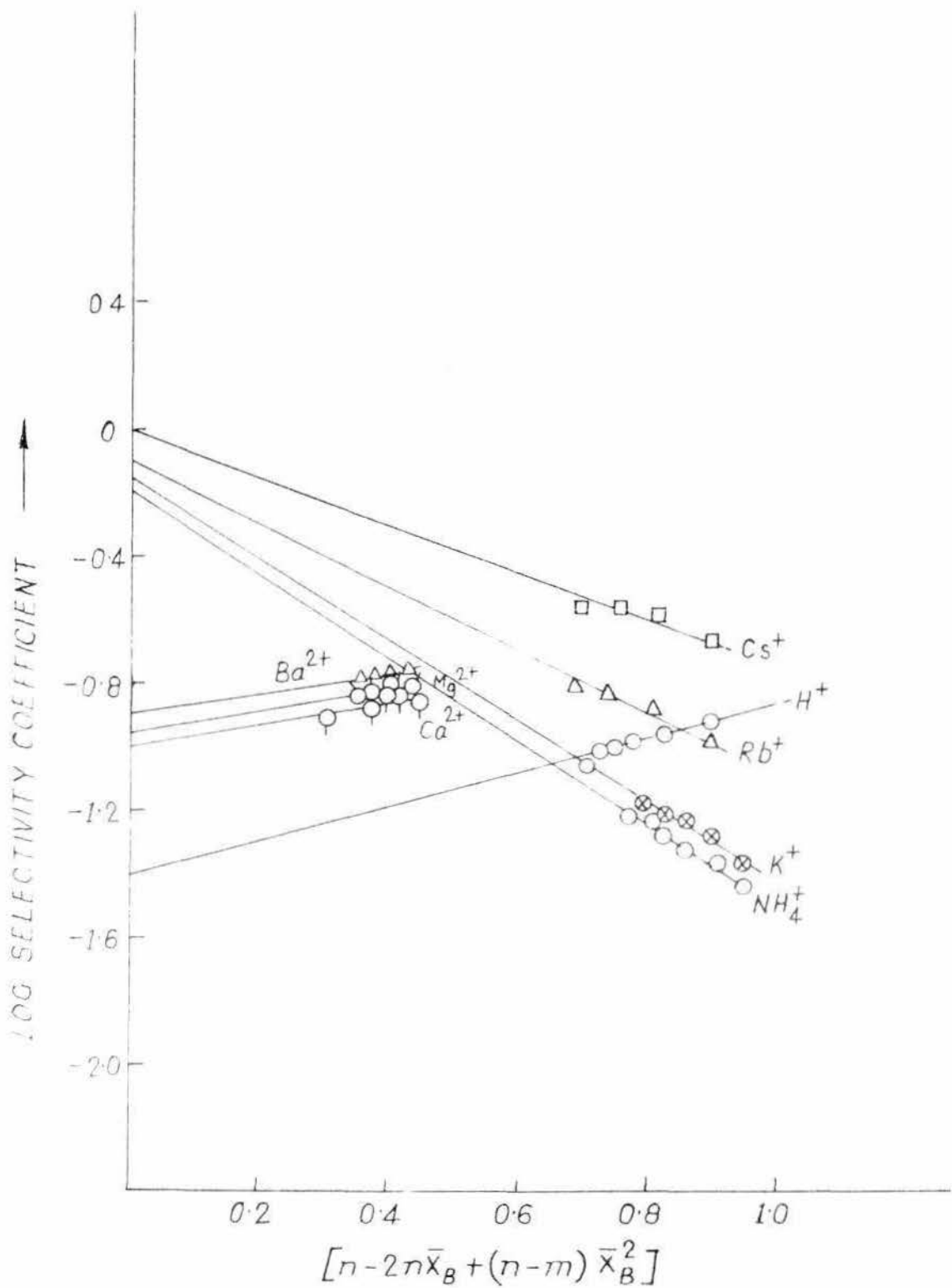


FIG. 73. PLOT OF LOG SELECTIVITY COEFFICIENT AGAINST $n - 2n\bar{x}_B + (n-m)\bar{x}_B^2$ IN THE EXCHANGE OF $\text{Co}(\text{pn})_3^{3+}$ FROM $\text{Na}-\text{Co}(\text{pn})_3$ -VERMICULITE BY DIFFERENT IONS.

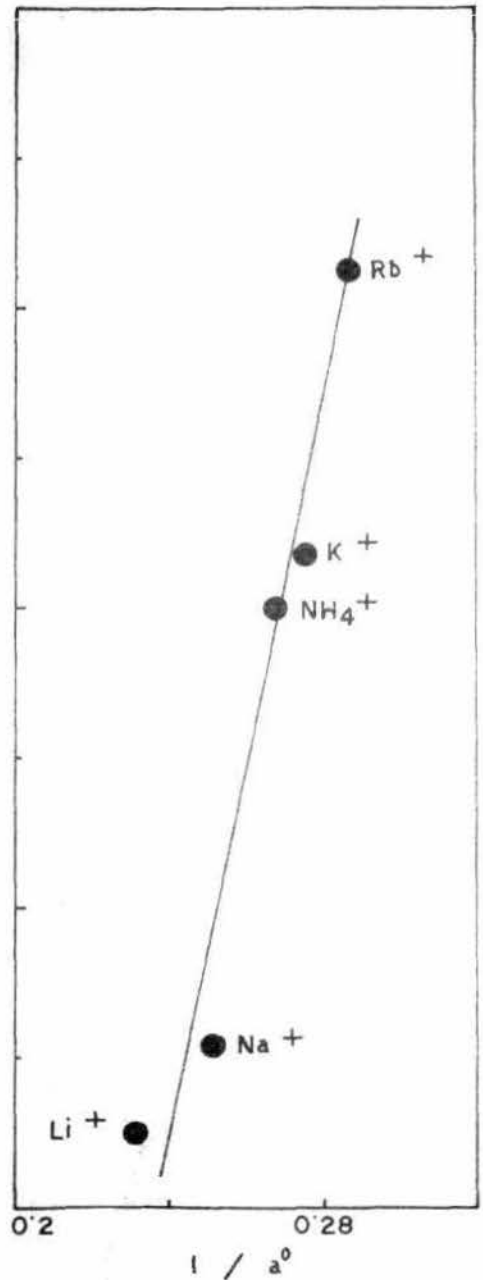
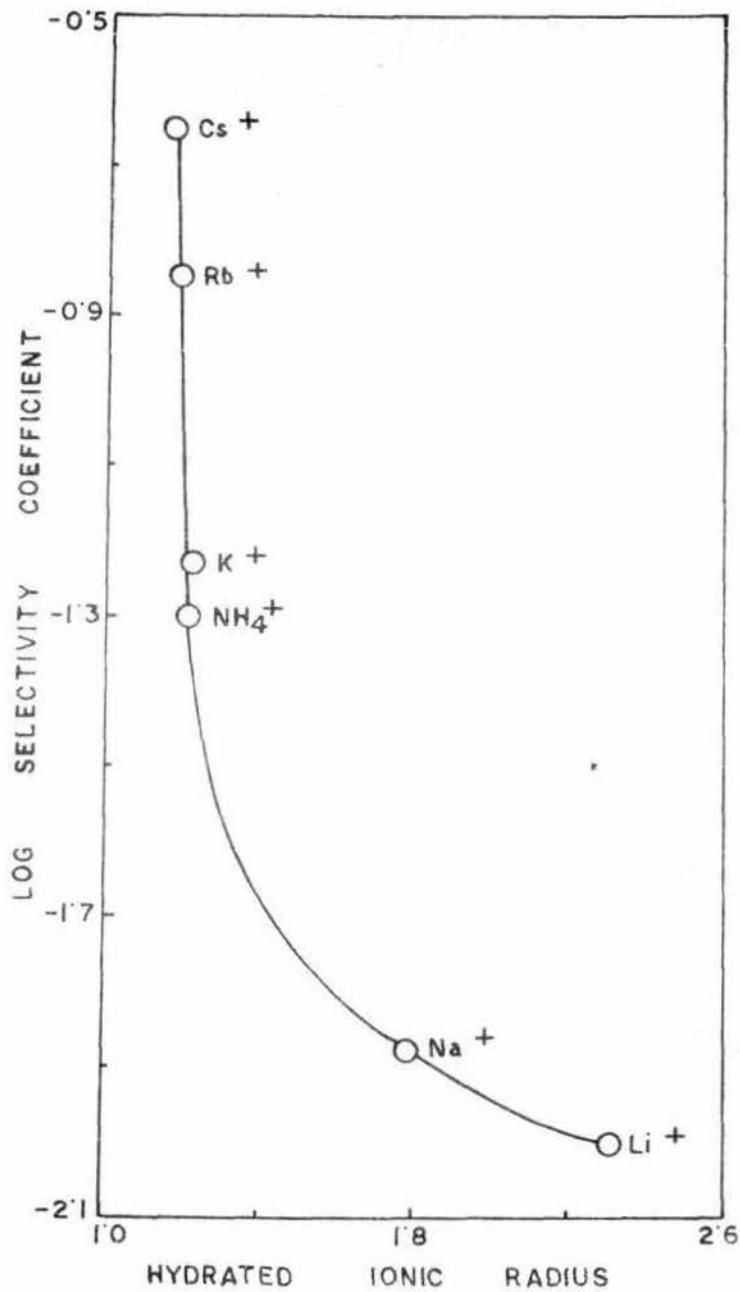


FIG. 74. CORRELATION OF SELECTIVITY COEFFICIENT WITH HYDRATED IONIC RADIUS AND DEBYE HÜCKEL PARAMETER a° IN THE DESORPTION OF Na - Copn₃ - VERMICULITE.

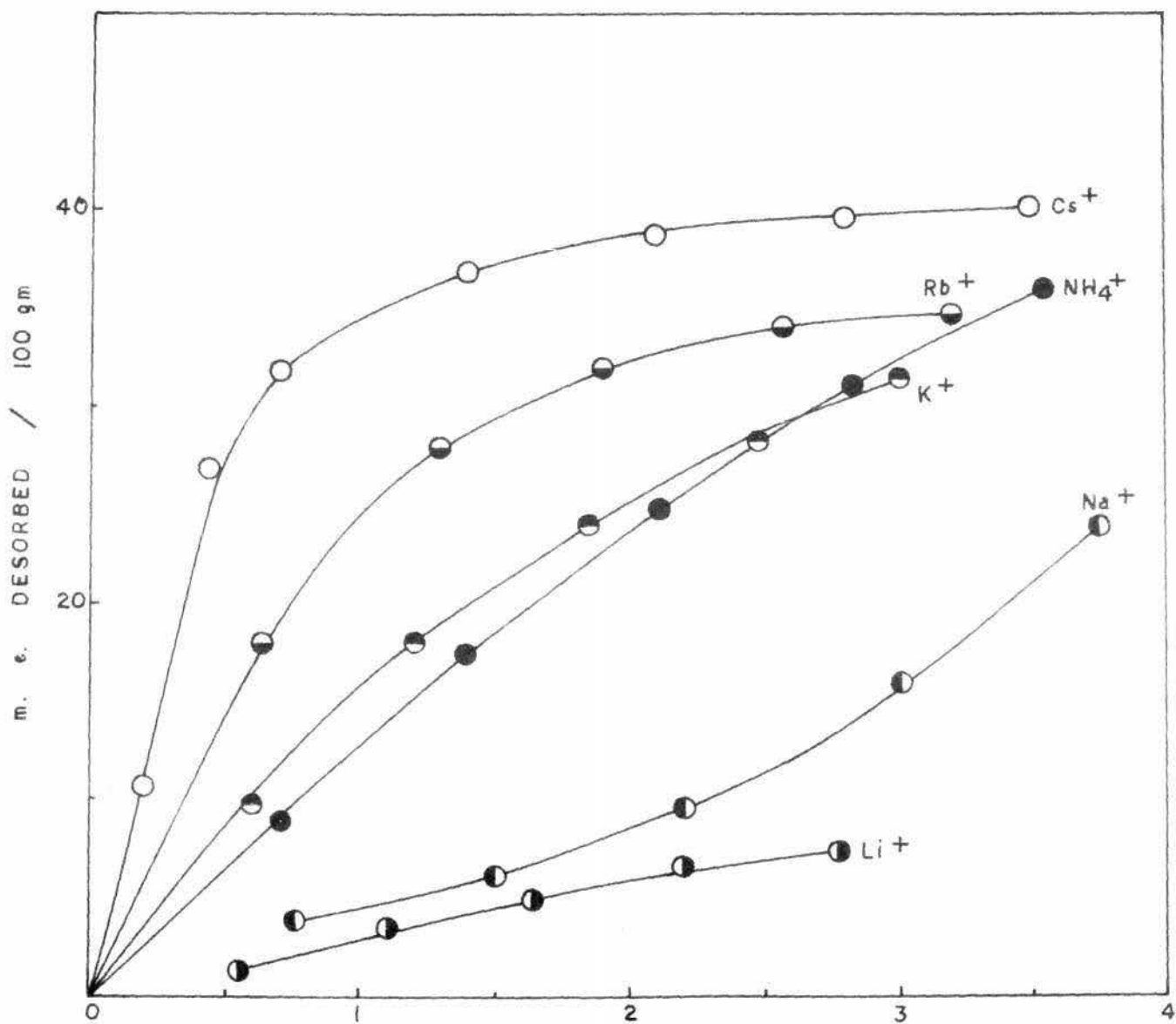


FIG. 75. DESORPTION OF Co^{3+} FROM Na-Cotn_3 -VERMICULITE BY DIFFERENT IONS.

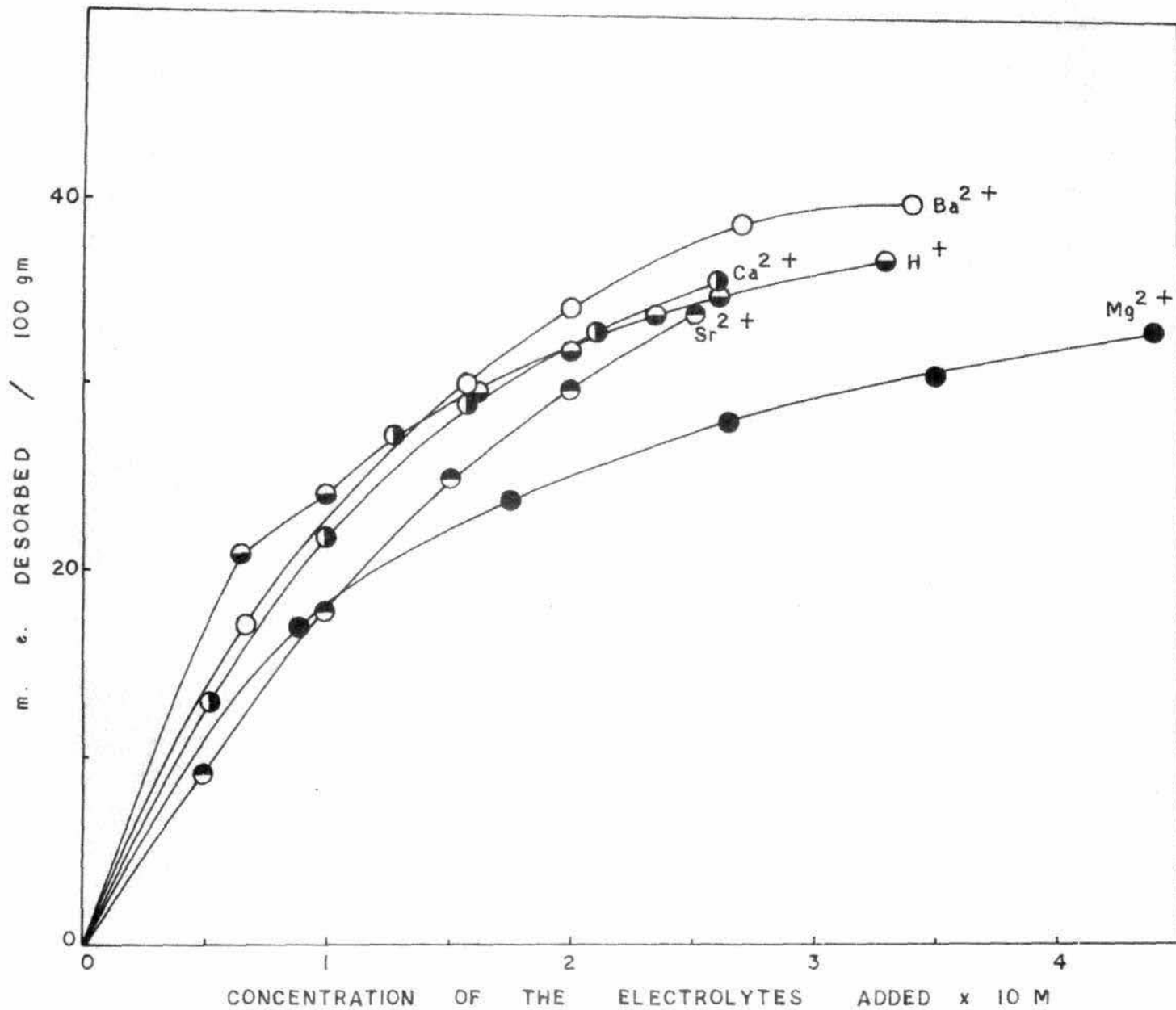


FIG. 76. DESORPTION OF Co^{3+} FROM $\text{Na} - \text{Co}_3$ - VERMICULITE BY DIFFERENT IONS.

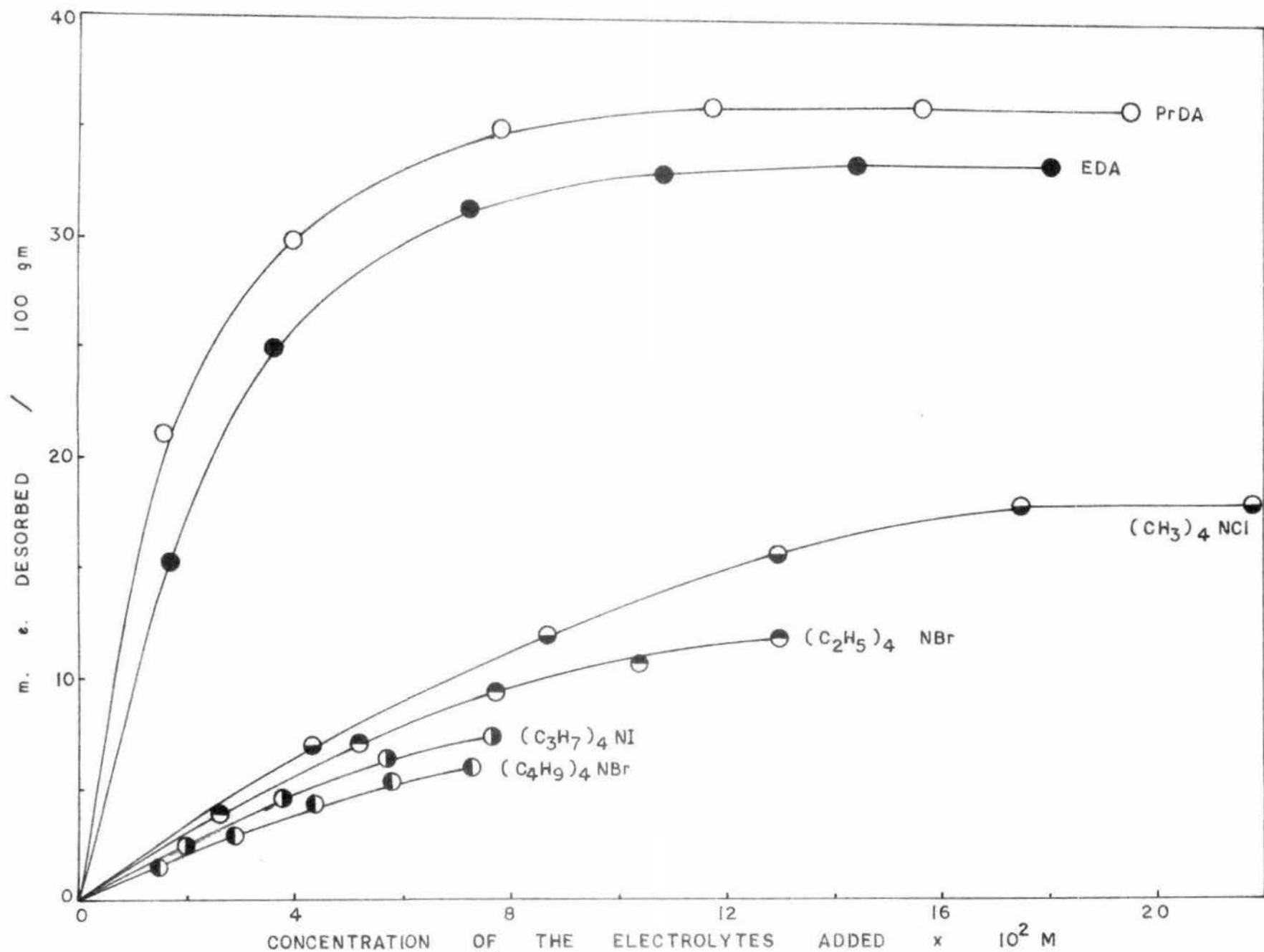


FIG. 77. DESORPTION OF Co^{3+} FROM Na - Co^{3+} - VERMICULITE BY DIFFERENT IONS.

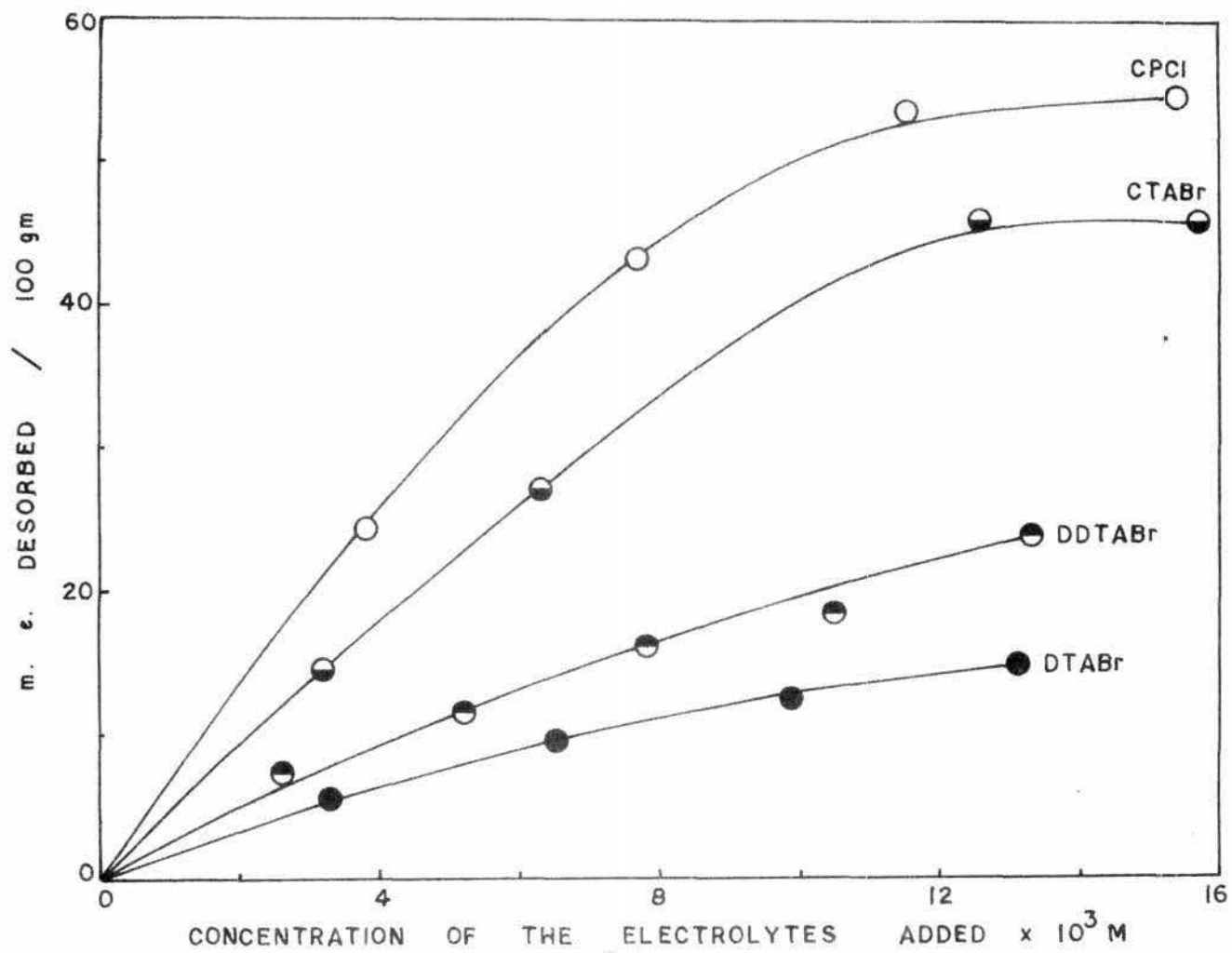


FIG. 78. DESORPTION OF Co^{3+} FROM Na - Co^{3+} - VERMICULITE BY DIFFERENT IONS.

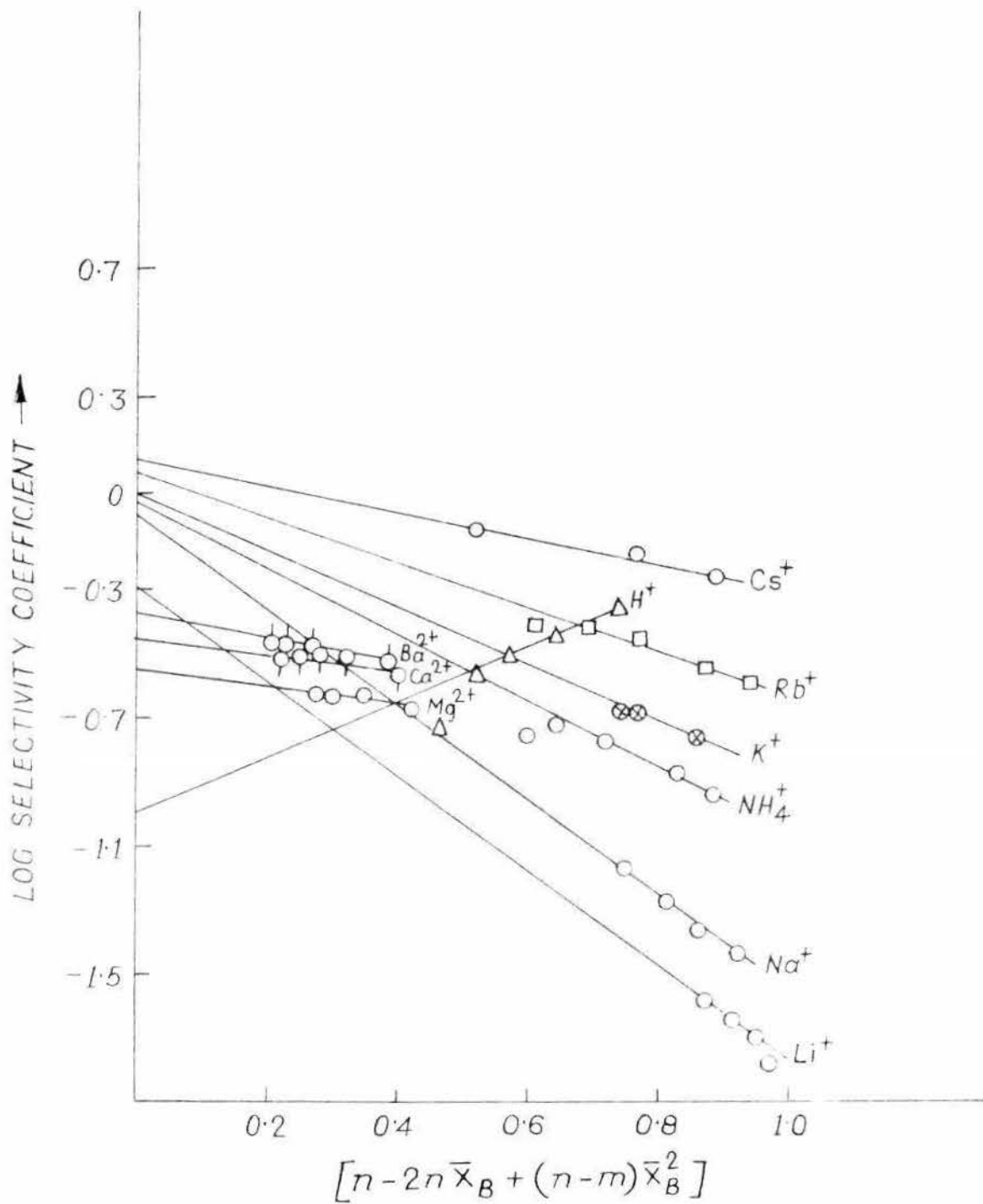


FIG. 79. PLOT OF LOG SELECTIVITY COEFFICIENT AGAINST $n - 2n\bar{x}_B + (n-m)\bar{x}_B^2$ IN THE EXCHANGE OF $\text{Co}(\text{tn})_3^{3+}$ FROM $\text{Na-Co}(\text{tn})_3$ -VERMICULITE BY DIFFERENT IONS.

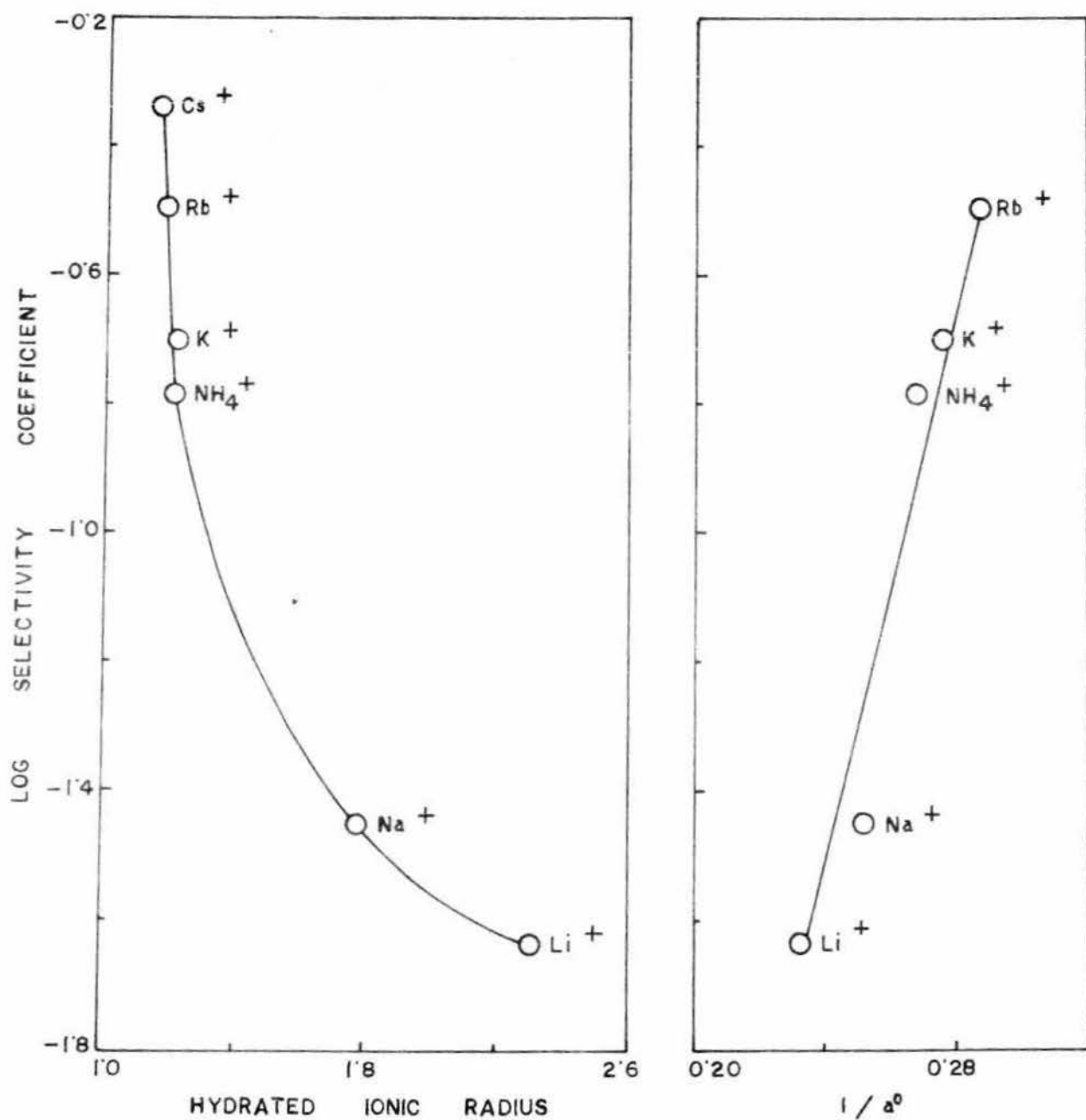


FIG. 80. CORRELATION OF SELECTIVITY COEFFICIENT WITH HYDRATED IONIC RADIUS & DEBYE HÜCKEL PARAMETER a° IN THE DESORPTION OF Na - Cotn₃ - VERMICULITE.

CHAPTER VI

Sorption and Desorption of $\text{Co}(\text{pn})_3^{3+}$ and $\text{Co}(\text{tn})_3^{3+}$ on Na-Laponite-system.

In order to investigate further the influence of clay mineral on ion exchange behaviour Na-Laponite XLG, a synthetic hectorite has been used for the sorption and desorption of complex ions viz. $\text{Co}(\text{pn})_3^{3+}$ and $\text{Co}(\text{tn})_3^{3+}$. The properties of this synthetic clay mineral has been described by Fripiat (201) and Neumann et al (202, 203). Stability of a Laponite CP sol in the presence of chlorides of lithium, sodium, potassium, ammonium, magnesium, calcium, barium, lanthanum and hexadecyl trimethyl ammonium bromide has been studied over a wide pH range by Perkins et al (204). They observed that the sols are stable over the pH range $\approx 7-12$ and Laponite CP particle charge becomes more negative as the pH increases. At $\text{pH} < 7$, sols are destabilized. Laponite CP clay suspensions behave quite differently with regard to the stability towards electrolytes as a function of pH than montmorillonite. Laponite was also chosen because it forms stable colloid solutions suitable for spectro photometric studies. So the present investigation was also carried out with the synthetic Laponite XLG, supplied by Laporte, England.

The sorption and desorption characteristics of $\text{Co}(\text{pn})_3^{3+}$ and $\text{Co}(\text{tn})_3^{3+}$ on Na-Laponite are discussed below on the basis of experimental results. The characteristics of sorption are presented in section A and those of desorption in section B.

SECTION A

Studies on Sorption

Sorption of $\text{Co}(\text{pn})_3^{3+}$ on Na-Laponite at pH 8.5

The adsorption isotherm of $\text{Co}(\text{pn})_3\text{Cl}_3$ on Na-Laponite is shown in Fig. 81. The plot of $\frac{C}{X}$ vs. C , where C is the equilibrium concentration of $\text{Co}(\text{pn})_3\text{Cl}_3$ and X is the amount adsorbed per 100 gm of adsorbent yields a good straight line. This indicates that the sorption data of $\text{Co}(\text{pn})_3\text{Cl}_3$ on Na-Laponite fits in with the Langmuir equation suggesting a unimolecular adsorption. From the slope of the line, the value of V_m (the amount required to form a complete monolayer) is found to be 81.4 m.e./100 gm and the maximum of the curve (79 m.e.) indicating here a monomolecular adsorption. It may be noted that the pH of the clay suspension before and after adsorption was 8.5 and 7.5 respectively.

Sorption of $\text{Co}(\text{tn})_3\text{Cl}_3$ on Na-Laponite at pH 8.5

The adsorption isotherm of $\text{Co}(\text{tn})_3\text{Cl}_3$ on Na-Laponite is shown in Fig. 82. The isotherm is similar to that observed earlier and conforms to the Langmuir type. Both V_m and the amount corresponding to maximum adsorption are found to be 86.95 m.e. and 85 m.e. respectively.

SECTION B

Desorption of $\text{Co}(\text{pn})_3^{3+}$ from Na-Copn₃-Laponite.

The results of desorption of $\text{Co}(\text{pn})_3^{3+}$ from Na-Copn₃-Laponite complex are shown in Figs. 83, 84, 85 and 86. The desorption curves for inorganic ions are very similar in nature to those obtained in the case of Na-Copn₃-bentonite. From Table 16 it can be seen that the selectivity coefficients increase in the order $\text{Li} < \text{Na} < \text{K} < \text{NH}_4 < \text{Rb} < \text{Cs} < \text{H}$ for the monovalent and $\text{Mg} < \text{Ca} < \text{Sr} < \text{Ba}$ for the bivalent cations. For the monovalent organic ions used the selectivity coefficients are in the following sequence: $(\text{CH}_3)_4\text{N} < (\text{C}_2\text{H}_5)_4\text{N} < (\text{C}_3\text{H}_7)_4\text{N} < (\text{C}_4\text{H}_9)_4\text{N} < \text{DTA} < \text{DDTA} < \text{CTA} < \text{CP}$ and for the bivalent organic ions used the selectivity coefficients are in the order: $\text{EDA} < \text{PrDA}$. It is noted that the efficiency of large organic cations in desorbing $\text{Co}(\text{pn})_3^{3+}$ from its Laponite complex is much greater than that of the inorganic cations.

It may be mentioned that the anomalous position of H^+ is well known. The greater exchangeability of H^+ has been explained by assuming H^+ to be present as a bare proton in the exchange reactions, as a result of which it has got a greater accessibility to the exchange sites. Such an assumption may be made in the present case also.

It is also observed that the amount of $\text{Co}(\text{pn})_3^{3+}$ desorbed from Na-Copn₃-Laponite complex by CTA or CP is greater than the

smaller ions $(\text{CH}_3)_4\text{N}$ or $(\text{C}_2\text{H}_5)_4\text{N}$. This is unlike that observed in the case of similar studies in bentonite system. Since Na-Laponite shows considerable interlamellar swelling in an aqueous medium, steric and space factors do not influence the extent of exchange. The observed isotherms (Fig. 85) reveal a regular increase in the affinity of alkyl ammonium ions for Laponite with increasing molecular weight, molecular size or chain length of the cations.

The selectivity coefficients and distribution coefficients are recorded in Table 16.

The thermodynamic equilibrium constants of some of the exchange reactions have been evaluated (Fig. 87 and Table 17) with the help of Kielland's equation. Gibbs free energy change at 25°C , which is a measure of the relative affinities of the ions for the mineral, has been calculated from the relation $\Delta G^\circ = -RT \ln K$ and is shown in Table 17.

As in the desorption of $\text{Co}(\text{pn})_3^{3+}$ from its Na-bentonite complex, here also (Fig. 88) the plot of log (selectivity coefficient) vs. hydrated ionic radius is a curved one but when the former is plotted against Debye Huckel parameter $\frac{1}{a_0}$, a linear curve is obtained.

Desorption of $\text{Co}(\text{tn})_3^{3+}$ from Na- $\text{Co}(\text{tn})_3$ - Laponite.

The results of desorption of $\text{Co}(\text{tn})_3^{3+}$ from Na- $\text{Co}(\text{tn})_3$ -Laponite are illustrated in Figs. 89, 90, 91, 92 and 93. The

Table 16

Desorption characteristics of $[\text{Co}(\text{pn}_3)]^{3+}$ with respect to different ions from Na-Co pn_3 -laponite.

Electrolyte used	Concentration of electrolyte	Distribution Coefficient	Selectivity Coefficient
<u>1:1 Electrolyte</u>			
LiCl	0.50 x 10 ⁻¹ (M)	1.003	0.0886
	1.0 "	0.953	0.106
	1.50 "	0.9027	0.1157
	2.0 "	0.852	0.120
NaCl	0.50 x 10 ⁻¹ (M)	1.2048	0.1129
	1.0 "	1.104	0.130
	1.50 "	1.0034	0.134
	2.0 "	0.9278	0.135
	2.50 "	0.862	0.134
	3.0 "	0.802	0.1316
KCl	0.50 x 10 ⁻¹ (M)	1.70	0.182
	1.0 "	1.482	0.197
	1.50 "	1.339	0.201
	2.0 "	1.217	0.200
	2.50 "	1.124	0.198

(Contd..)

Table 16 (Contd..)

Electrolyte used	Concentration of electrolyte	Distribution Coefficient	Selectivity Coefficient
NH ₄ Cl	0.50 x 10 ⁻¹ (M)	1.91	0.2129
	1.0 "	1.659	0.230
	1.50 "	1.50	0.2389
	2.0 "	1.3435	0.232
	2.50 "	1.20	0.220
	3.0 "	1.104	0.2137
RbCl	0.50 x 10 ⁻¹ (M)	2.01	0.2289
	1.0 "	1.81	0.261
	1.50 "	1.64	0.272
	2.0 "	1.5076	0.276
	2.50 "	1.366	0.268
CsCl	0.50 x 10 ⁻¹ (M)	3.849	0.567
	0.75 "	3.50	0.596
	1.0 "	3.18	0.599
	1.50 "	2.72	0.5979
	2.0 "	2.394	0.592
	2.50 "	2.054	0.541

(Contd..)

Table 16 (Contd..)

Electrolyte used	Concentration of electrolyte	Distribution Coefficient	Selectivity Coefficient
HCl	0.50 x 10 ⁻¹ (M)	5.71	1.009
	0.75 "	5.70	1.285
	1.0 "	5.30	1.42
	1.50 "	4.296	1.49
	2.0 "	3.43	1.367
<u>2:1 Electrolyte</u>			
MgCl ₂	0.50 x 10 ⁻¹ (M)	2.54	0.347
	1.0 "	2.25	0.375
	1.50 "	2.03	0.378
	2.0 "	1.9	0.387
	2.50 "	1.78	0.384
	3.0 "	1.66	0.370
CaCl ₂	0.25 x 10 ⁻¹ (M)	3.149	0.382
	0.50 "	2.92	0.430
	1.0 "	2.37	0.419
	1.50 "	2.158	0.428
	2.0 "	1.98	0.424
	2.50 "	1.84	0.419

(Contd..)

Table 16 (Contd..)

Electrolyte used	Concentration of electrolyte	Distribution Coefficient	Selectivity Coefficient
SrCl ₂	0.25 x 10 ⁻¹ (M)	3.45	0.454
	0.50 "	2.96	0.46
	1.0 "	2.46	0.451
	1.50 "	2.22	0.455
	2.0 "	2.01	0.441
	2.50 "	1.872	0.432
BaCl ₂	0.25 x 10 ⁻¹ (M)	3.69	0.513
	0.50 "	3.1	0.502
	1.0 "	2.56	0.490
	1.50 "	2.26	0.477
	2.0 "	2.06	0.469
	2.50 "	1.90	0.450
<u>Quaternary ammonium salt</u>			
(CH ₃) ₄ NCl	1.0 x 10 ⁻² (M)	11.42	1.345
	2.0 "	10.88	1.679
	4.0 "	9.28	1.89
	6.0 "	7.168	1.61
	8.0 "	6.05	1.496
	10.0 "	5.188	1.367
	12.0 "	4.56	1.272
	14.0 "	4.05	1.174

(Contd..)

Table 16 (Contd..)

Electrolyte used	Concentration of electrolyte	Distribution Coefficient	Selectivity Coefficient
$(C_2H_5)_4NBr$	$1.0 \times 10^{-2}(M)$	20.29	2.989
	2.0 "	16.35	3.05
	4.0 "	11.42	2.668
	6.0 "	8.57	2.22
	8.0 "	6.64	1.782
	10.0 "	5.39	1.479
	12.0 "	4.56	1.27
	14.0 "	4.212	1.175
$(C_3H_7)_4NI$	$1.0 \times 10^{-2}(M)$	47.50	10.52
	2.0 "	28.47	7.64
	4.0 "	14.41	4.10
	6.0 "	9.63	2.80
$(C_4H_9)_4NBr$	$1.0 \times 10^{-2}(M)$	57.21	14.29
	2.0 "	31.50	9.35
	4.0 "	15.23	4.60
	6.0 "	10.20	3.02

(Contd..)

Table 16 (Contd..)

Electrolyte used	Concentration of electrolyte	Distribution Coefficient	Selectivity Coefficient
DTABr	3.0 x 10 ⁻³ (M)	70.24	9.91
	5.0 "	71.96	12.96
	7.0 "	68.54	14.69
	10.0 "	57.21	14.30
DDTABr	3.0 x 10 ⁻³ (M)	80.50	11.86
	5.0 "	81.63	15.55
	7.0 "	72.82	16.13
	10.0 "	60.09	15.56
CTABr	3.0 x 10 ⁻³ (M)	97.34	15.31
	5.0 "	91.38	18.28
	7.0 "	81.96	19.44
	10.0 "	64.47	17.66
CPCl	3.0 x 10 ⁻³ (M)	115.74	19.34
	5.0 "	105.69	22.65
	7.0 "	96.40	25.41
	10.0 "	75.09	23.77

(Contd..)

Table 16 (Contd..)

Electrolyte used	Concentration of electrolyte	Distribution Coefficient	Selectivity Coefficient
EDA	0.2×10^{-1} (M)	4.43	0.697
	0.4 "	4.06	0.827
	0.6 "	3.69	0.855
	0.8 "	3.40	0.864
	1.0 "	3.14	0.849
	1.50 "	2.7	0.808
	2.0 "	2.38	0.741
PrDA	0.2×10^{-1} (M)	4.92	0.873
	0.4 "	4.34	0.939
	0.6 "	3.81	0.921
	0.8 "	3.47	0.914
	1.0 "	3.21	0.898
	1.50 "	2.76	0.861
	2.0 "	2.46	0.837

Table 17

Evaluation of thermodynamic quantities from
Kielland's equation at 25°C.

Exchange system	Thermodynamic equilibrium constant	ΔG° Cal/mole
$K_{\text{Copn}_3}^{\text{Li}}$	0.177	1022.74
$K_{\text{Copn}_3}^{\text{Na}}$	0.190	981.83
$K_{\text{Copn}_3}^{\text{K}}$	0.208	927.28
$K_{\text{Copn}_3}^{\text{NH}_4}$	0.221	893.19
$K_{\text{Copn}_3}^{\text{Rb}}$	0.331	654.55
$K_{\text{Copn}_3}^{\text{Cs}}$	0.602	300.00
$K_{\text{Copn}_3}^{\text{H}}$	1.348	-176.73
$K_{\text{Copn}_3}^{\text{Mg}}$	0.398	545.46
$K_{\text{Copn}_3}^{\text{Ca}}$	0.436	490.91
$K_{\text{Copn}_3}^{\text{Sr}}$	0.457	463.64
$K_{\text{Copn}_3}^{\text{Ba}}$	0.467	450.00

curves are almost alike to those obtained earlier. (Figs. 83, 84, 85 and 86). The data presented in Table 18 make it clear that according to the order of preference, the desorbing ions may be placed in the following sequence: $\text{Li} < \text{Na} < \text{K} < \text{NH}_4 < \text{Rb} < \text{Cs} < \text{H}$ for the monovalent, $\text{Mg} < \text{Ca} < \text{Sr} < \text{Ba}$ for the bivalent inorganic ions, $(\text{CH}_3)_4\text{N} < (\text{C}_2\text{H}_5)_4\text{N} < (\text{C}_3\text{H}_7)_4\text{N} < (\text{C}_4\text{H}_9)_4\text{N} < \text{DTA} < \text{DDTA} < \text{CTA} < \text{CP}$ for the monovalent organic ions and $\text{EDA} < \text{PrDA}$ for the bivalent organic ions.

H^+ is found to be more effective in desorption than the other monovalent inorganic cations. The idea of the bare proton taking part in the exchange reaction has been invoked to explain the peculiar behaviour of H^+ as observed here.

The lyotropic series as observed above has also been verified in a number of systems including resins (205) and inorganic ion-exchangers (206,207).

The observed isotherms for quaternary ammonium ions (Fig. 91) reveal a regular increase in the affinity of the alkyl ammonium ions for Laponite with increasing molecular weight, molecular size or chain length of the cations as described earlier (P 99). Since Na-Laponite shows considerable interlamellar swelling in an aqueous medium, steric and space factors do not influence the extent of exchange.

From a linear plot of Kielland's equation (Fig. 94), the values of thermodynamic equilibrium constants of some of the exchange reactions and standard Gibbs free energy change

Table 18

Description characteristics of $\left[\text{Co}(\text{OH})_3 \right]^{3+}$ with respect
to different ions from Na-Co(OH)₃-laponite.

Electrolyte used	Concentration of electrolyte	Distribution Coefficient	Selectivity Coefficient
<u>1:1 Electrolyte</u>			
LiCl	$1.0 \times 10^{-1} \text{ (M)}$	0.651	0.0595
	1.50 "	0.668	0.0717
	2.0 "	0.651	0.0771
	2.50 "	0.621	0.079
	3.0 "	0.584	0.0781
NaCl	$0.50 \times 10^{-1} \text{ (M)}$	0.802	0.062
	1.0 "	0.751	0.0727
	1.50 "	0.7015	0.0771
	2.0 "	0.676	0.0816
	2.50 "	0.681	0.090
	3.0 "	0.651	0.0912
KCl	$0.50 \times 10^{-1} \text{ (M)}$	1.204	0.108
	1.0 "	1.103	0.1228
	1.50 "	1.003	0.126
	2.0 "	0.927	0.127
	2.25 "	0.891	0.1266

(Contd..)

Table 18 (Contd..)

Electrolyte used	Concentration of electrolyte	Distribution Coefficient	Selectivity Coefficient
NH ₄ Cl	0.50 x 10 ⁻¹ (M)	1.70	0.171
	1.0 "	1.456	0.180
	1.50 "	1.271	0.176
	2.0 "	1.128	0.169
RbCl	0.50 x 10 ⁻¹ (M)	1.91	0.202
	1.0 "	1.608	0.208
	1.50 "	1.40	0.203
	2.0 "	1.28	0.203
	2.50 "	1.164	0.1968
CsCl	0.50 x 10 ⁻¹ (M)	2.92	0.362
	1.0 "	2.519	0.3948
	1.50 "	2.215	0.400
	2.0 "	1.96	0.389
HCl	0.50 x 10 ⁻¹ (M)	4.872	0.749
	0.75 "	4.878	0.924
	1.0 "	4.82	1.096
	1.50 "	4.22	1.245
	2.0 "	3.25	1.001

(Contd..)

Table 18 (Contd..)

Electrolyte used	Concentration of electrolyte	Distribution Coefficient	Selectivity Coefficient
<u>2:1 Electrolyte</u>			
MgCl ₂	0.50 x 10 ⁻¹ (M)	1.98	0.210
	1.0 "	1.82	0.238
	1.50 "	1.67	0.242
	2.0 "	1.55	0.238
	2.50 "	1.45	0.234
	3.0 "	1.37	0.227
CaCl ₂	0.50 x 10 ⁻¹ (M)	2.24	0.306
	1.0 "	1.936	0.310
	1.50 "	1.74	0.303
	2.0 "	1.6	0.295
	2.50 "	1.49	0.286
	3.0 "	1.40	0.277
SrCl ₂	0.50 x 10 ⁻¹ (M)	2.31	0.322
	1.0 "	2.00	0.33
	1.50 "	1.79	0.321
	2.0 "	1.66	0.317

(Contd..)

Table 18 (Contd..)

Electrolyte used	Concentration of electrolyte	Distribution Coefficient	Selectivity Coefficient
BaCl ₂	0.50 x 10 ⁻¹ (M)	2.51	0.373
	1.0 "	2.07	0.350
	1.50 "	1.83	0.335
	2.0 "	1.67	0.322
	2.50 "	1.55	0.310
<u>Quaternary</u>			
<u>ammonium salt</u>			
(CH ₃) ₄ NCl	1.0 x 10 ⁻² (M)	12.5	1.438
	2.0 "	11.38	1.68
	4.0 "	9.79	1.92
	6.0 "	8.2	1.87
	8.0 "	6.89	1.74
(C ₂ H ₅) ₄ NBr	1.0 x 10 ⁻² (M)	33.07	5.68
	2.0 "	22.45	4.68
	4.0 "	14.36	3.69
	6.0 "	10.17	2.25
	8.0 "	7.68	2.16

(Contd..)

Table 18 (Contd..)

Electrolyte used	Concentration of electrolyte	Distribution Coefficient	Selectivity Coefficient
$(C_3H_7)_4NI$	1.0×10^{-2} (M)	59.17	13.15
	2.0 "	31.86	8.64
	4.0 "	16.31	4.76
	6.0 "	10.86	3.24
$(C_4H_9)_4NBr$	1.0×10^{-2} (M)	67.71	17.71
	2.0 "	33.33	9.36
	4.0 "	16.84	5.13
	5.0 "	13.56	4.22
DTABr	5.0×10^{-3} (M)	117.1	24.8
	7.0 "	98.33	24.63
	10.0 "	73.61	20.69
	14.0 "	54.62	17.00
DDTABr	5.0×10^{-3} (M)	124.65	27.25
	7.0 "	103.77	26.68
	10.0 "	77.5	22.64
	11.0 "	71.11	21.62

(Contd..)

Table 18 (Contd..)

Electrolyte used	Concentration of electrolyte	Distribution Coefficient	Selectivity Coefficient
CTABr	5.0 x 10 ⁻³ (M)	140.4	32.65
	7.0 "	111.5	30.20
	10.0 "	84.81	27.60
	12.0 "	71.42	25.06
OPCl	5.0 x 10 ⁻³ (M)	152.9	37.32
	7.0 "	124.0	36.22
	10.0 "	89.74	31.48
	12.0 "	75.25	28.97
EDA	0.2 x 10 ⁻¹ (M)	2.85	0.330
	0.4 "	2.76	0.405
	0.6 "	2.67	0.45
	0.8 "	2.57	0.479
	1.0 "	2.46	0.492
	1.4 "	2.30	0.512
	1.8 "	2.14	0.512
	2.0 "	2.07	0.507

(Contd..)

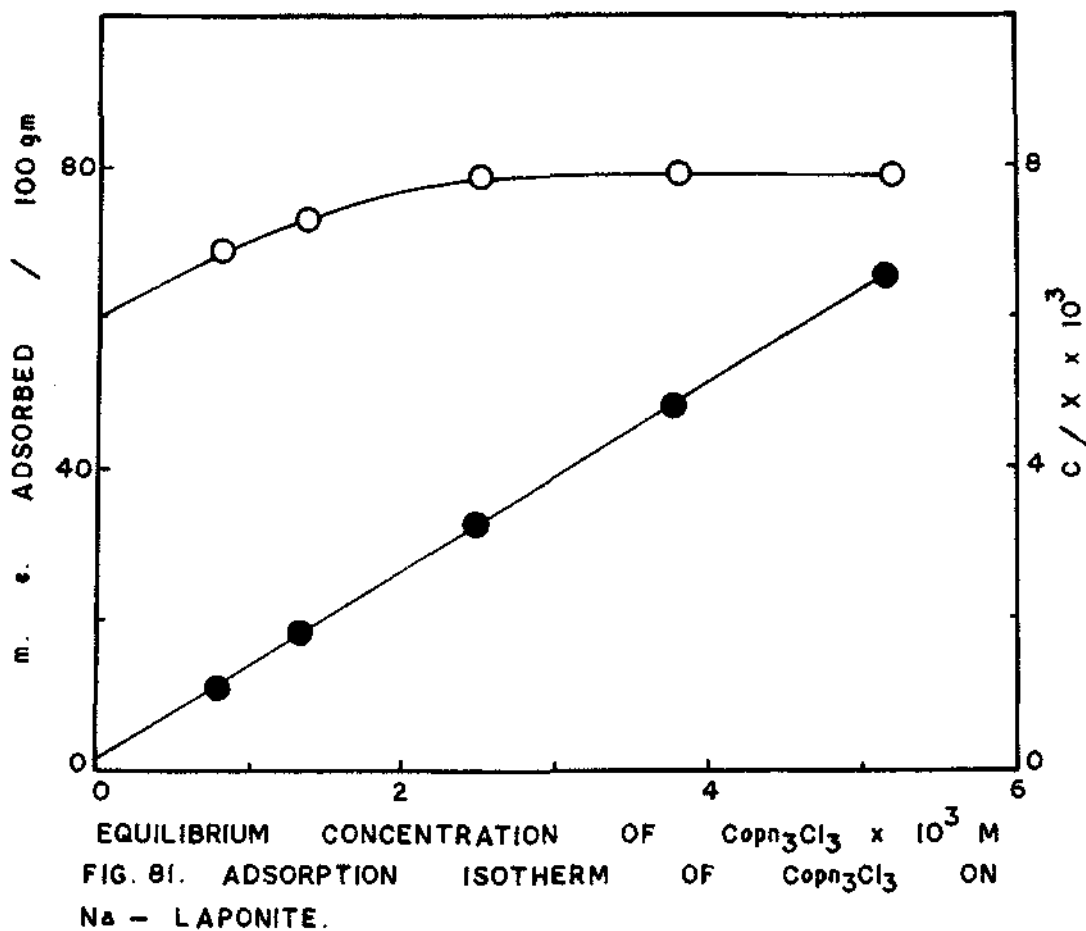
Table 18 (Contd..)

Electrolyte used	Concentration of electrolyte	Distribution Coefficient	Selectivity Coefficient
PrDA	0.2×10^{-1} (M)	3.94	0.579
	0.4 "	3.59	0.657
	0.6 "	3.32	0.687
	0.8 "	3.08	0.691
	1.0 "	2.89	0.691
	1.2 "	2.73	0.685
	1.4 "	2.61	0.687
	1.8 "	2.40	0.671
	2.0 "	2.30	0.659

have been evaluated and are presented in Table 19. The results are similar to those obtained with bentonite system.

The plot of $\log(\text{selectivity coefficient})$ vs. hydrated ionic radius is a curved one but when the former is plotted against Debye Huckel parameter $\frac{1}{a^0}$, a linear curve is obtained (Fig. 95).

The desorption curves of $\text{Co}(\text{pn})_3^{3+}$ and $\text{Co}(\text{tn})_3^{3+}$ from Laponite as well as the selectivity coefficients and thermodynamic equilibrium constants suggest that they are desorbed in the order : $\text{Co}(\text{tn})_3^{3+} < \text{Co}(\text{pn})_3^{3+}$, which is the same as observed in the case of bentonite.



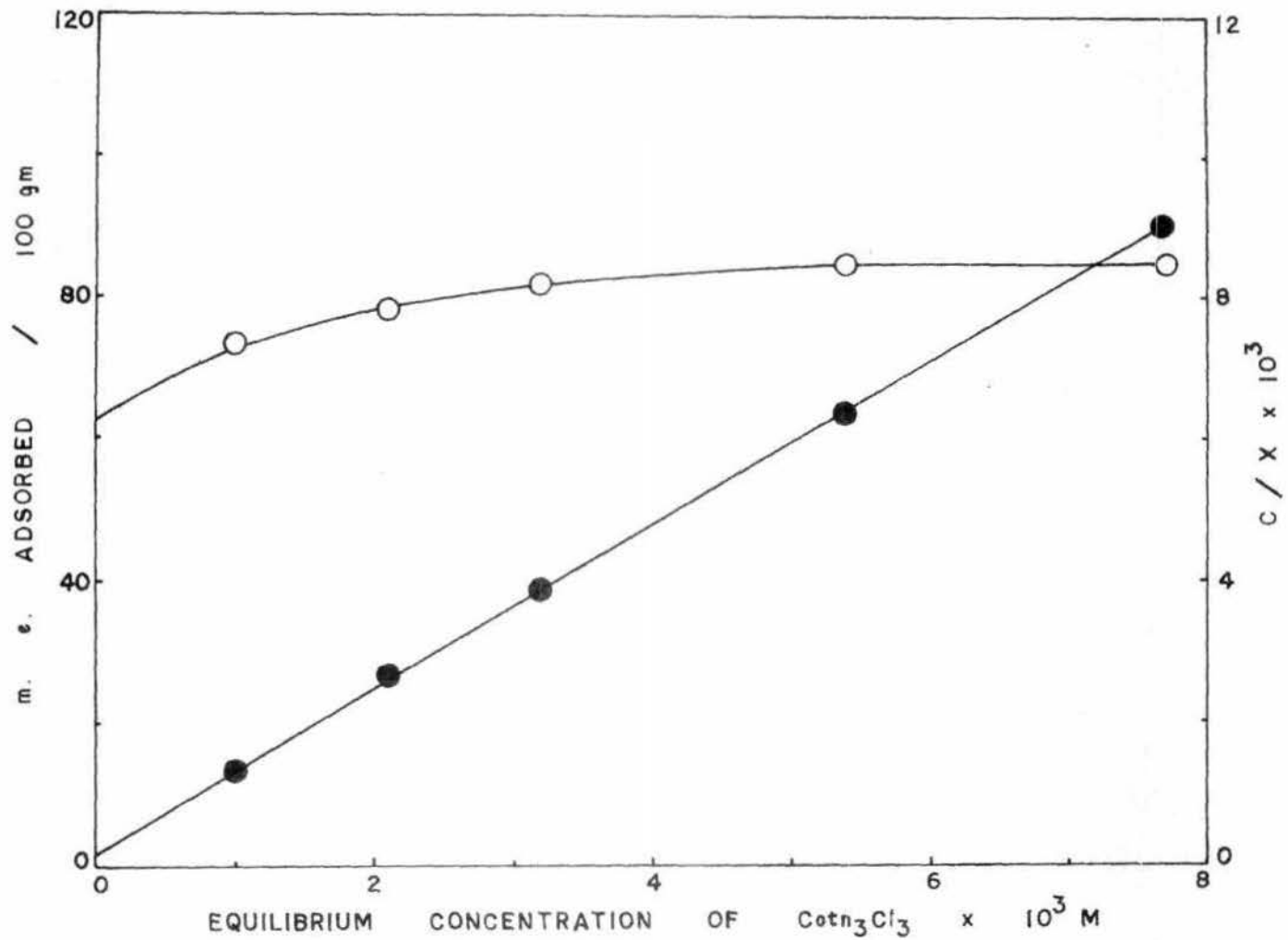


FIG. 82 . ADSORPTION ISOTHERM OF $\text{Co}(\text{NO}_3)_3$ ON Na - LAPONITE.

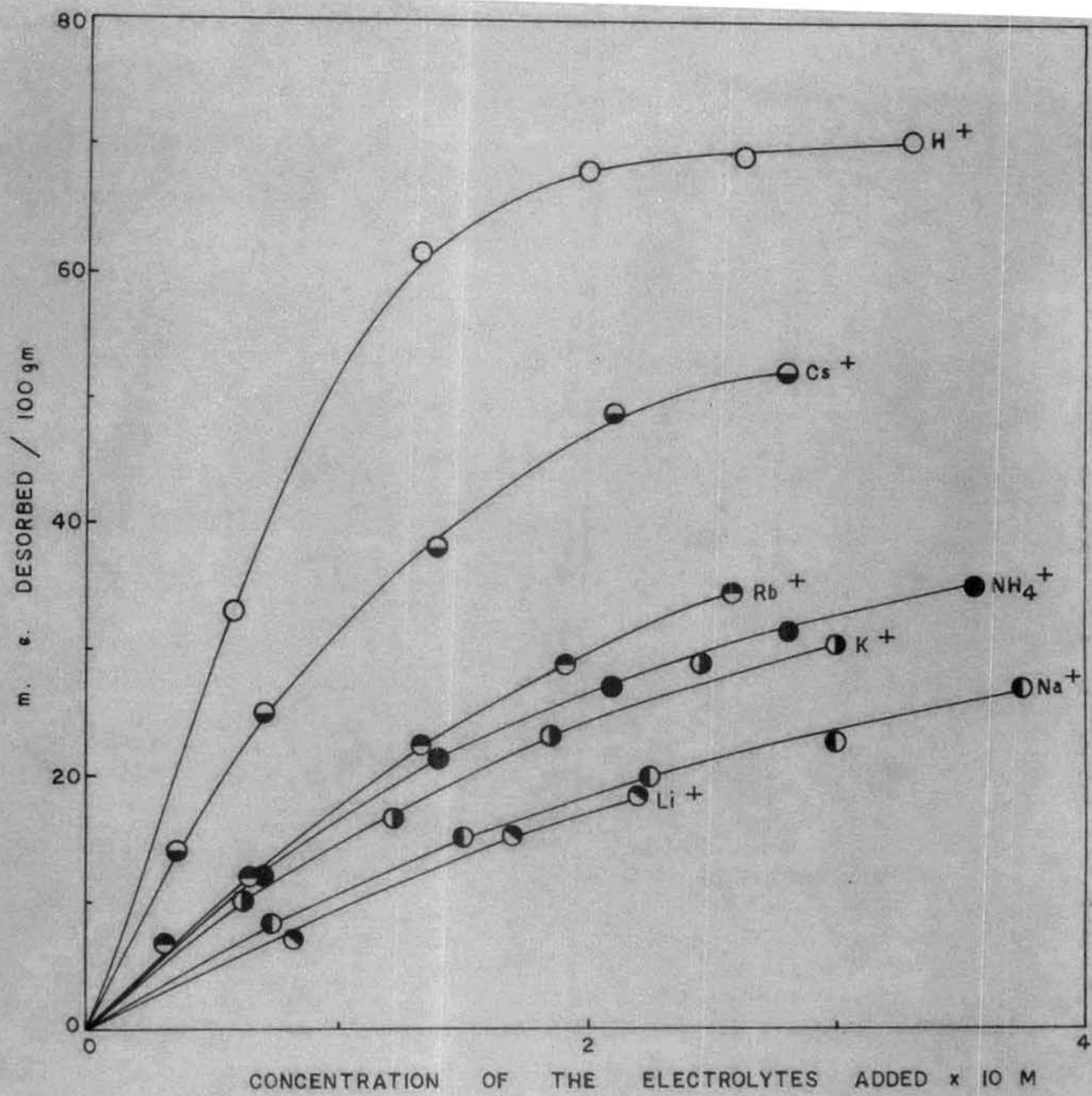


FIG. B3. DESORPTION OF Copn_3^+ FROM Na - Copn_3 - LAPONITE BY DIFFERENT IONS.

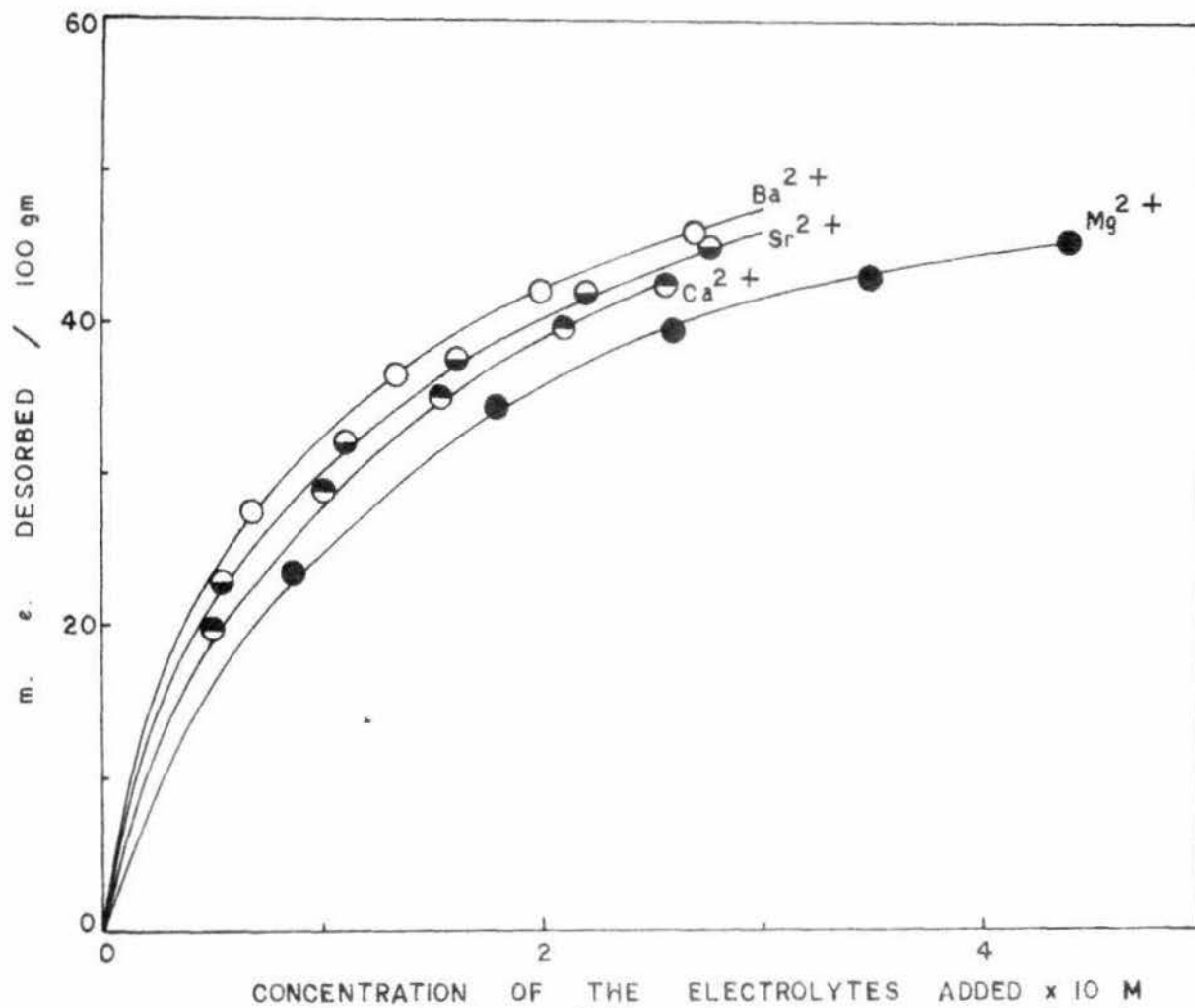


FIG. 84. DESORPTION OF Copn_3^+ FROM Na - Copn_3 - LAPONITE BY DIFFERENT IONS.

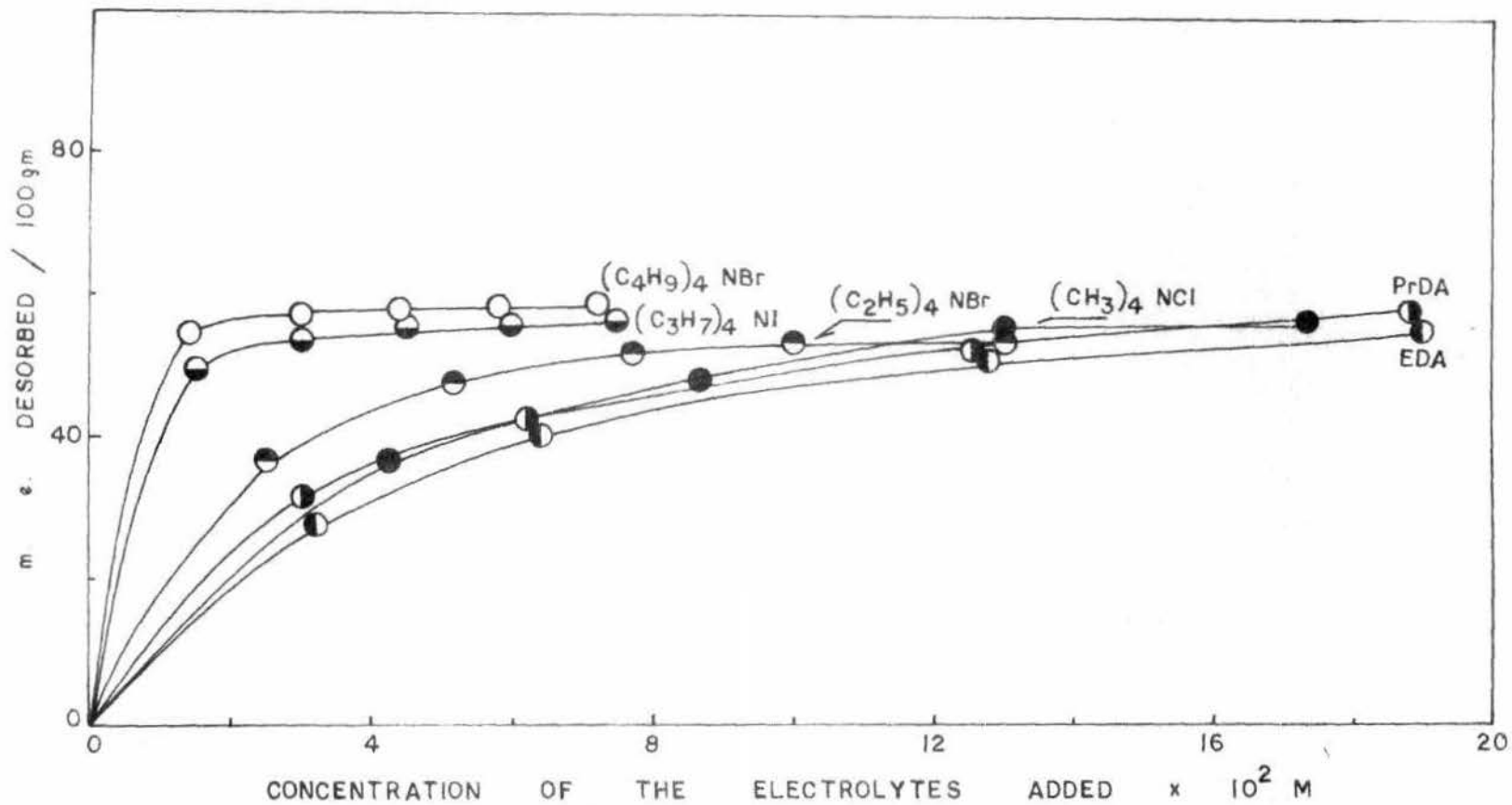


FIG. 85. DESORPTION OF Copn_3^+ FROM Na - Copn_3 - LAPONITE BY DIFFERENT IONS.

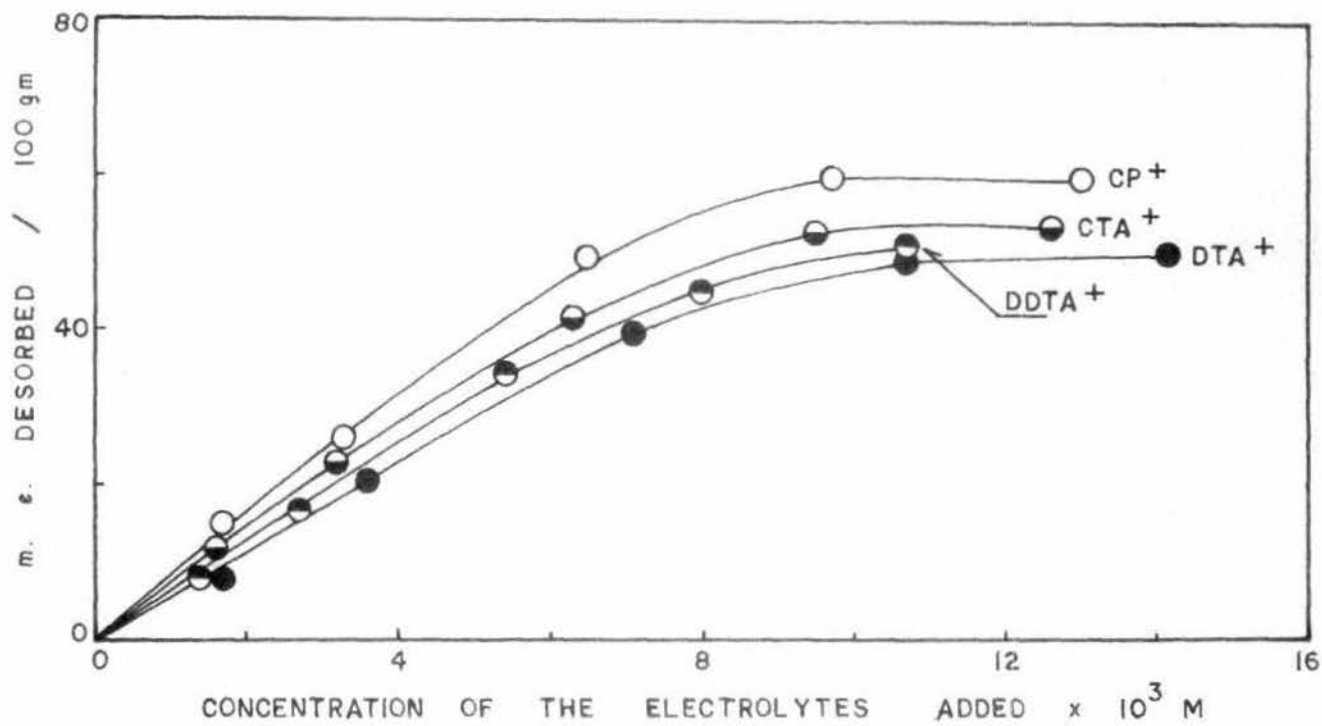


FIG. 86. DESORPTION OF Copn_3 FROM Na-Copn_3 -LAPONITE BY DIFFERENT IONS.

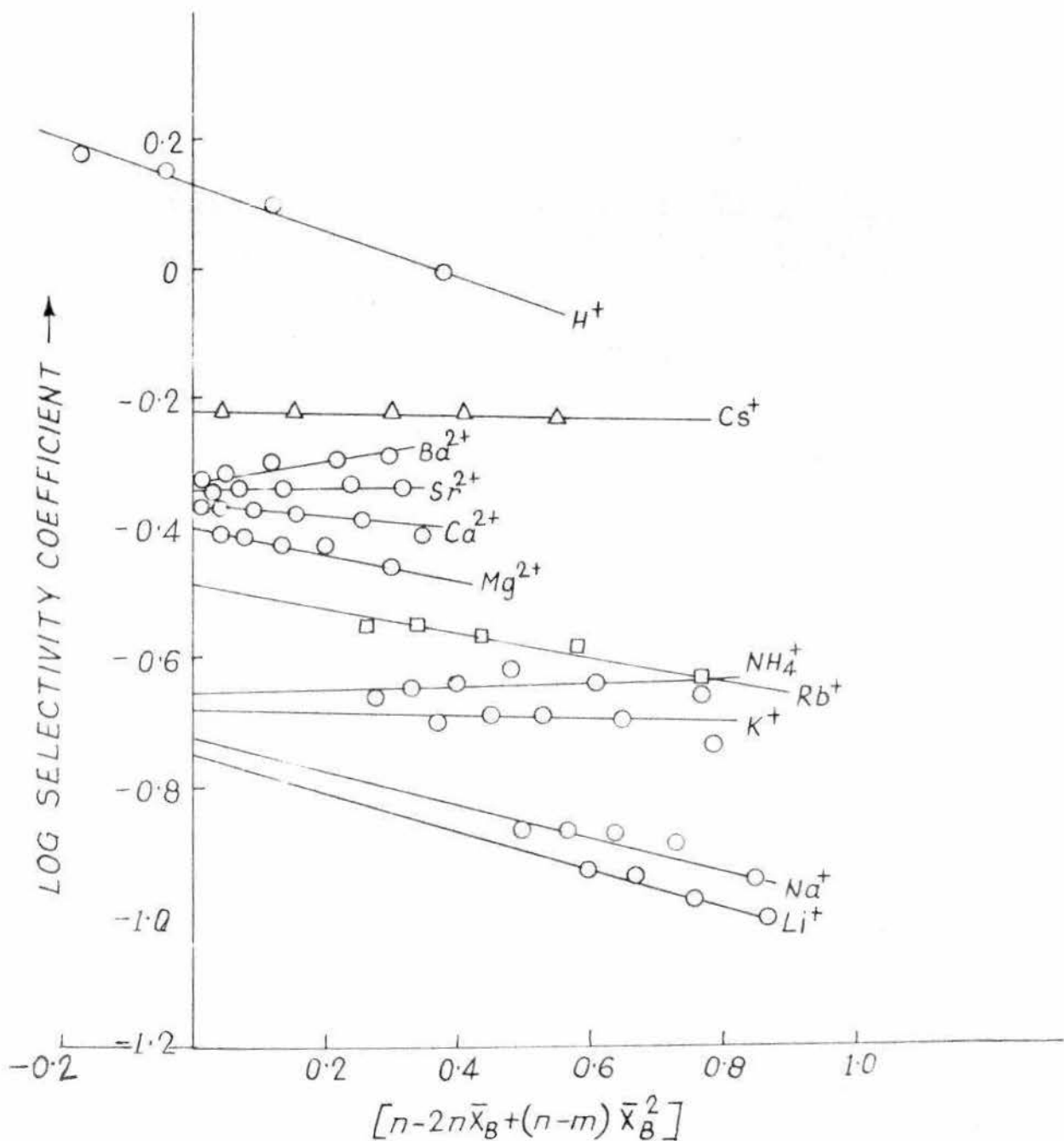


FIG. 87. PLOT OF LOG SELECTIVITY COEFFICIENT AGAINST $n-2n\bar{x}_B+(n-m)\bar{x}_B^2$ IN THE EXCHANGE OF $Co(pn)_3^{3+}$ FORM Na-Copn₃-LAPONITE BY DIFFERENT IONS.

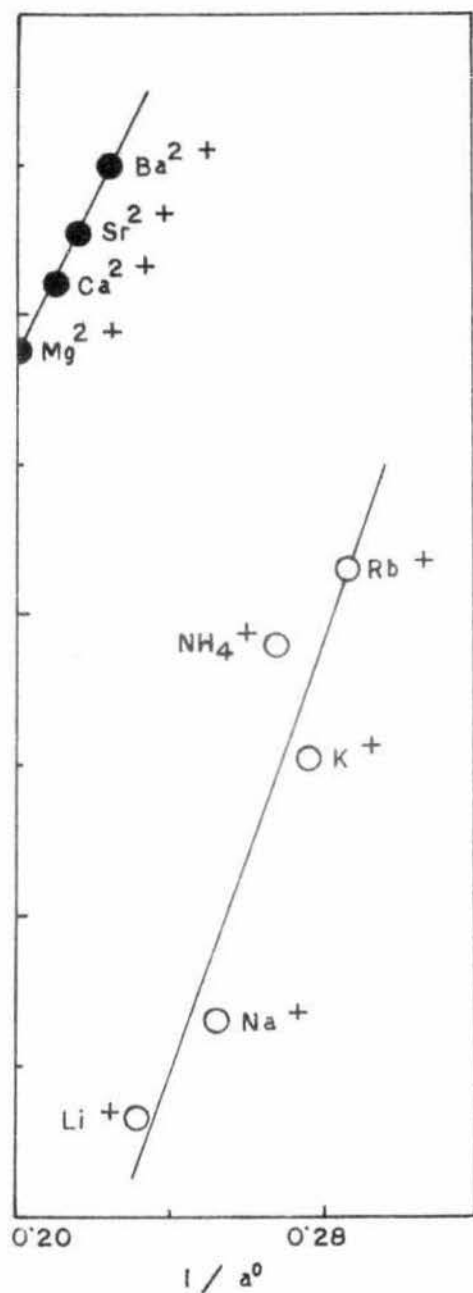
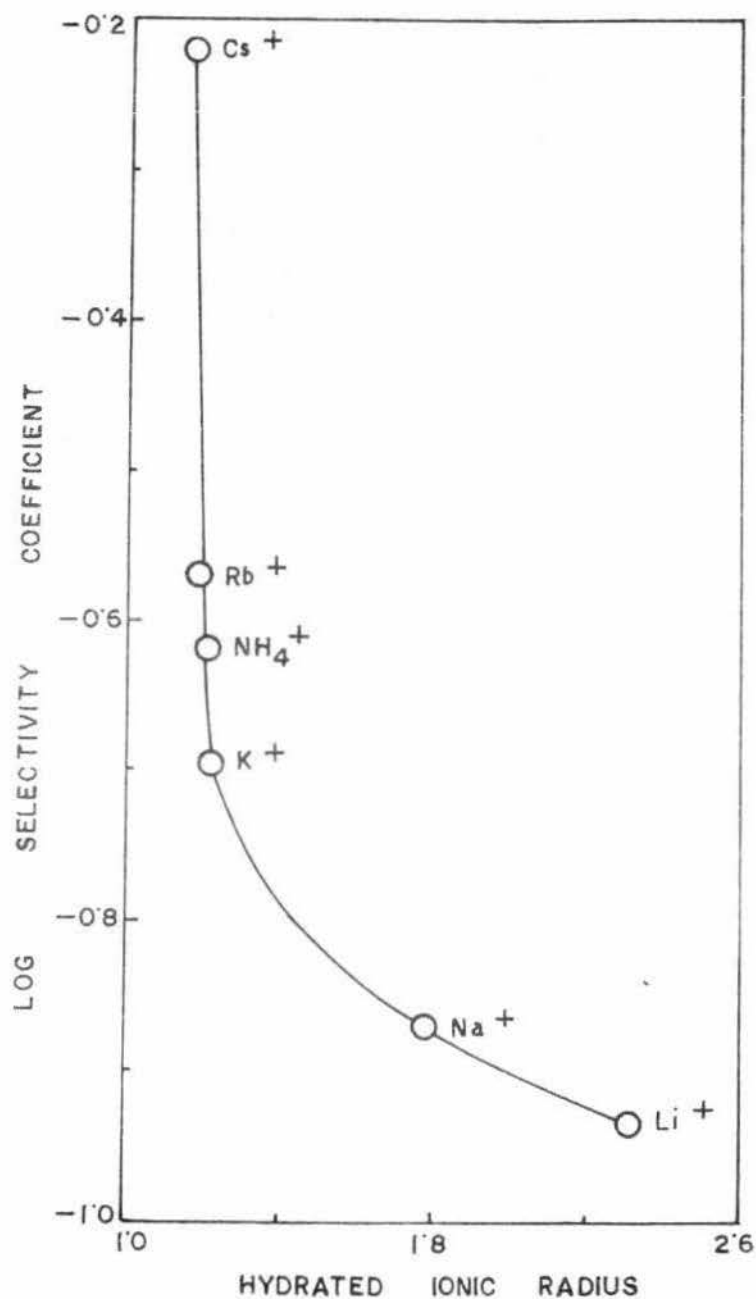


FIG. 88. CORRELATION OF SELECTIVITY COEFFICIENT WITH HYDRATED IONIC RADIUS AND DEBYE HÜCKEL PARAMETER a^0 IN THE DESORPTION OF Na - Copn₃ - LAPONITE.

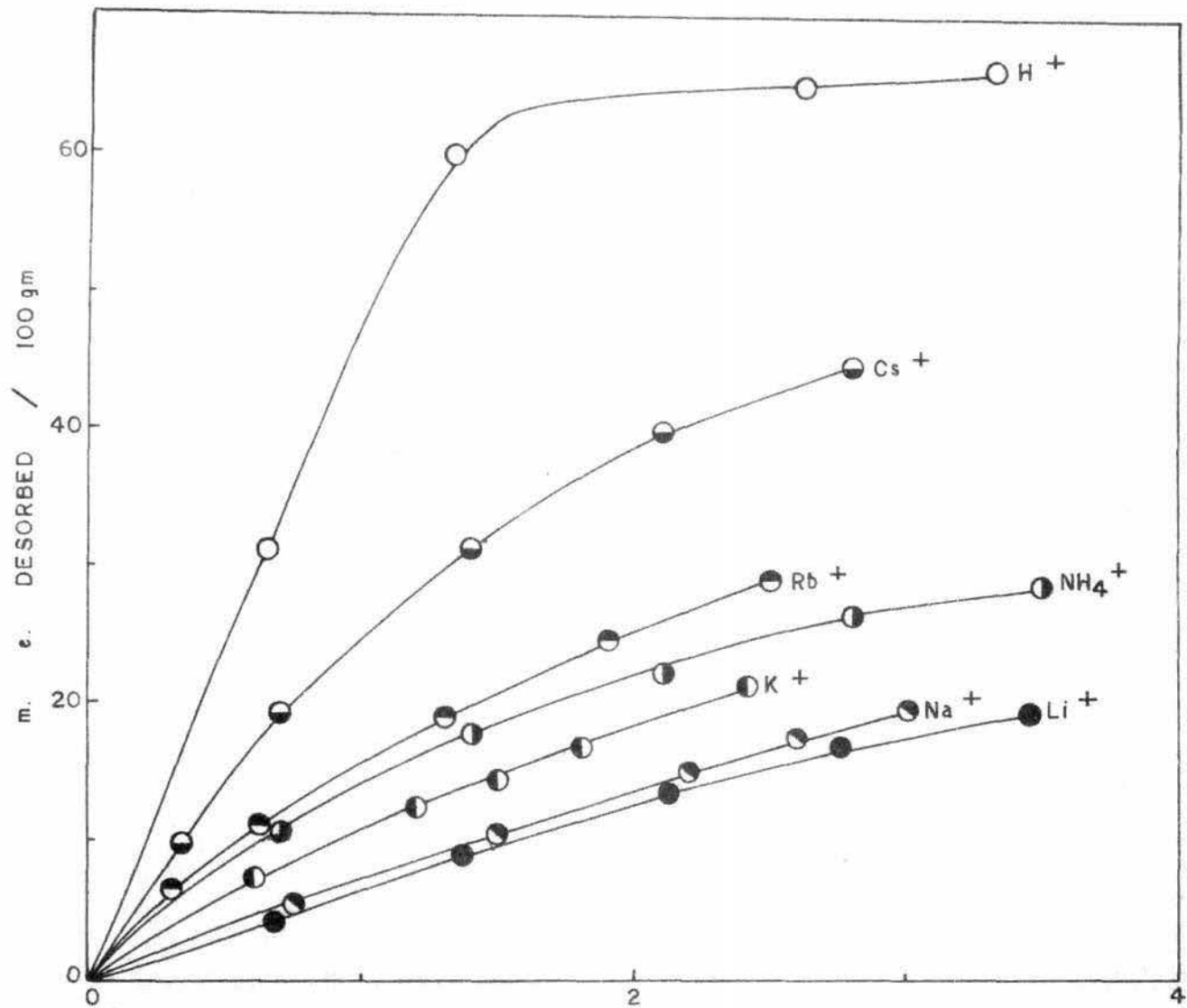


FIG. 89. DESORPTION OF Co^{3+} FROM Na - Co^{3+} - LAPONITE BY DIFFERENT IONS.

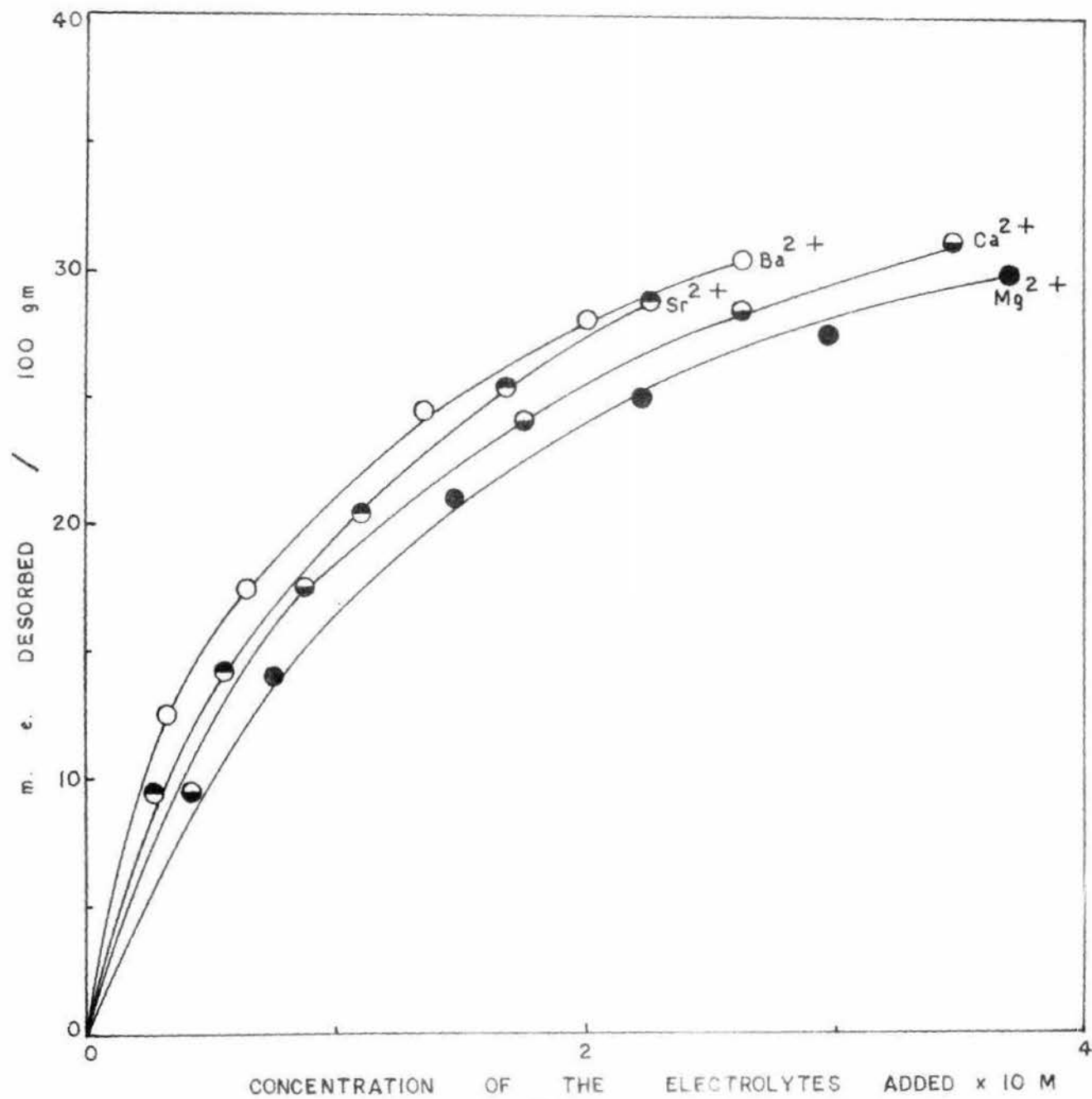


FIG. 90. DESORPTION OF $\text{Co(NO}_3)_3$ FROM Na - $\text{Co(NO}_3)_3$ - LAPO-NITE BY DIFFERENT IONS.

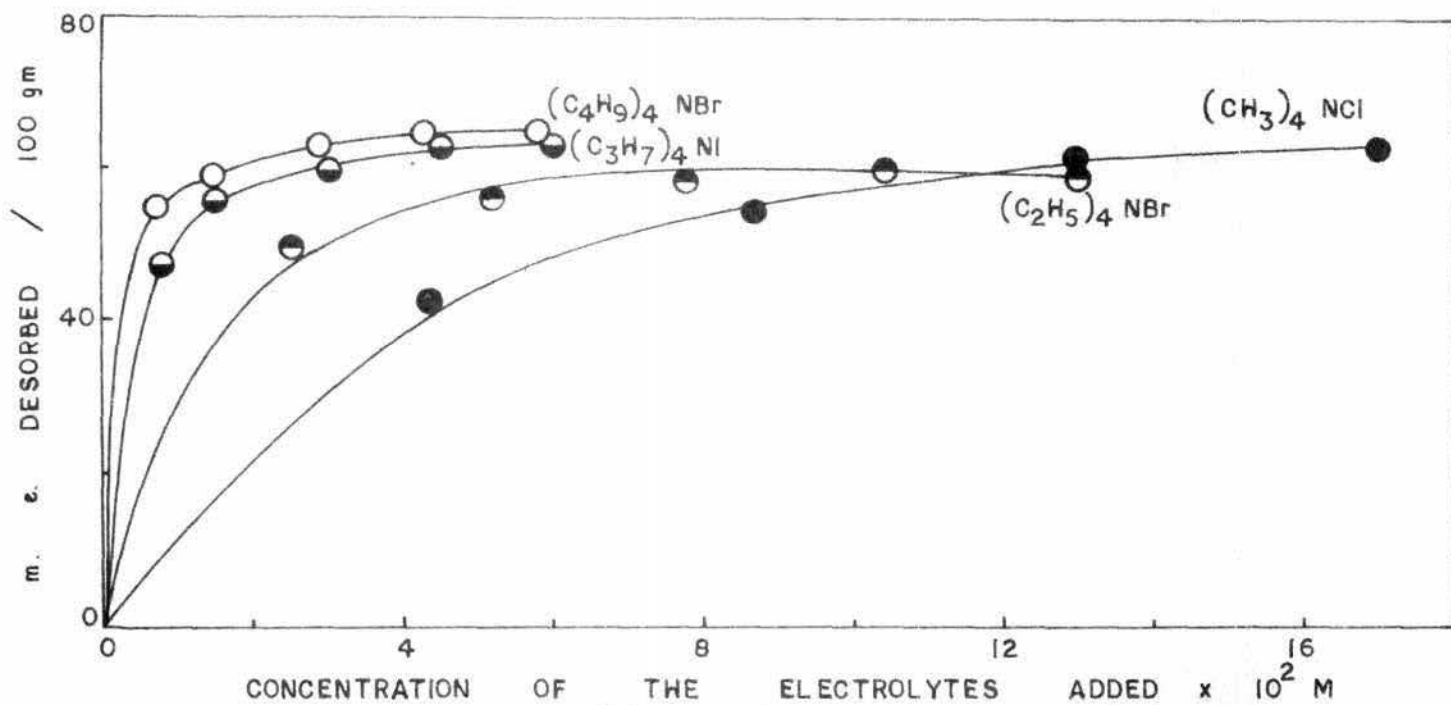


FIG. 91. DESORPTION OF $\text{Co}(\text{n}_3)^{3+}$ FROM $\text{Na} - \text{Co}(\text{n}_3) - \text{LAPONITE}$ BY DIFFERENT IONS.

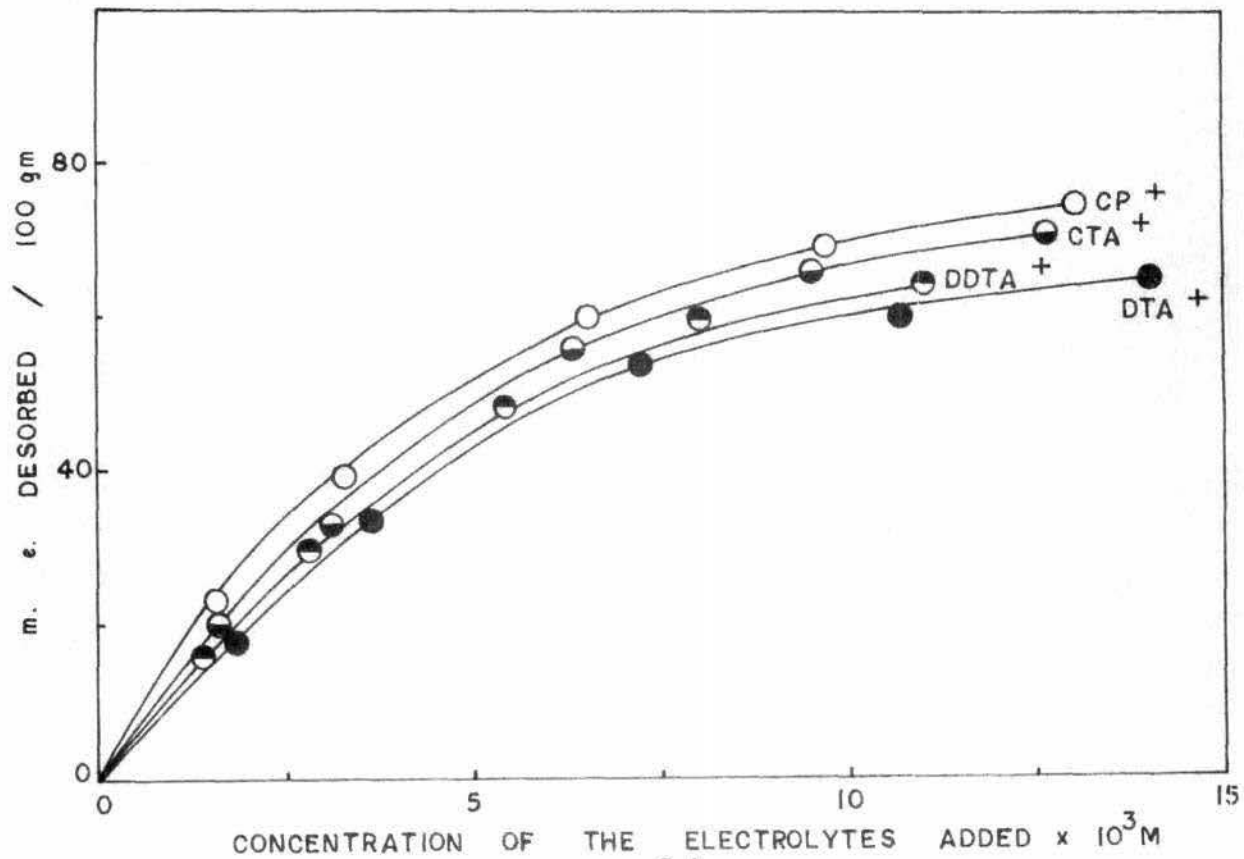


FIG. 92. DESORPTION OF Co^{3+} FROM Na - Co^{3+} - LA - PONITE BY DIFFERENT IONS.

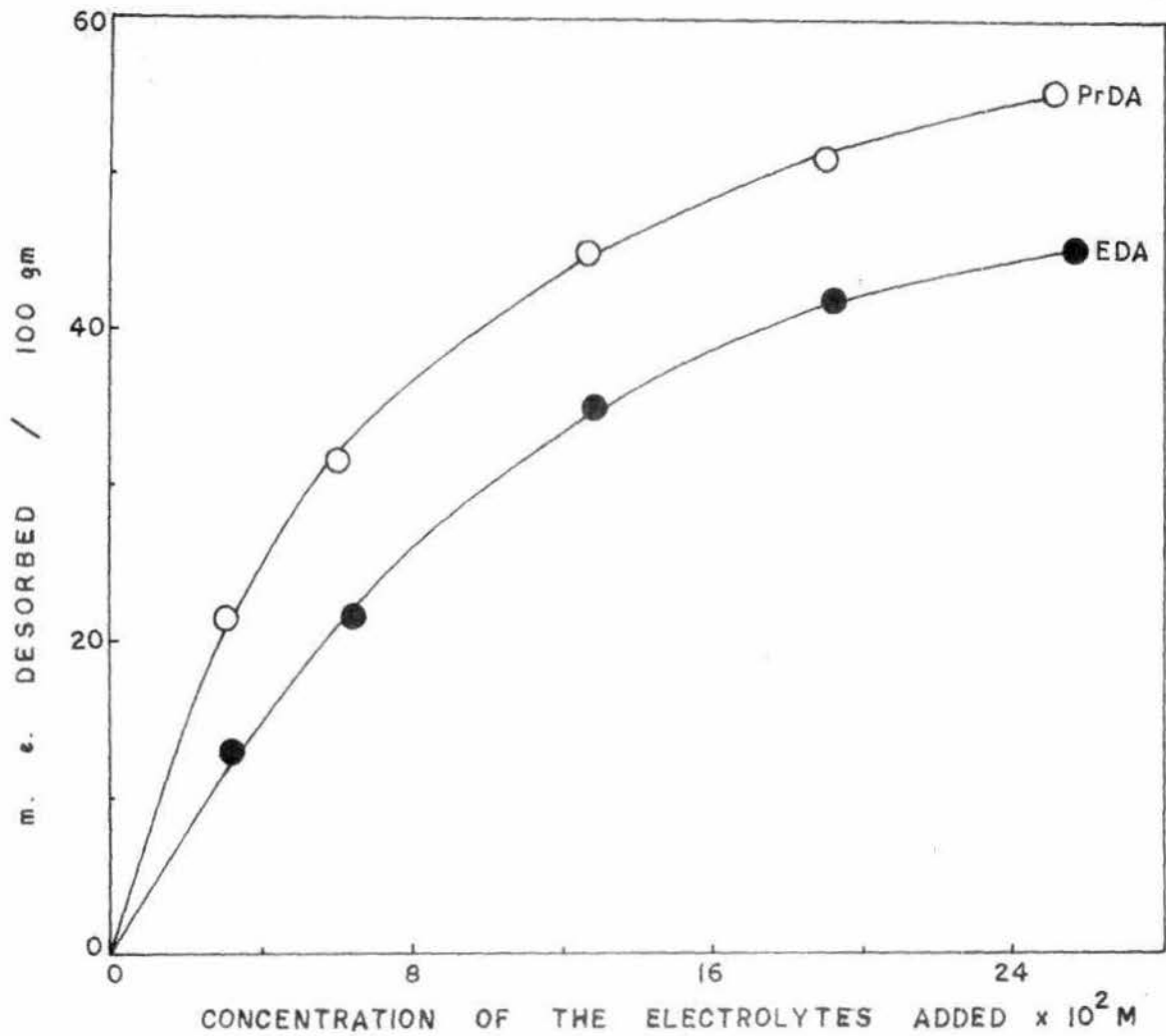


FIG. 93. DESORPTION OF $Co(n_3)^{3+}$ FROM Na - $Co(n_3)$ - LAPONITE BY DIFFERENT IONS.

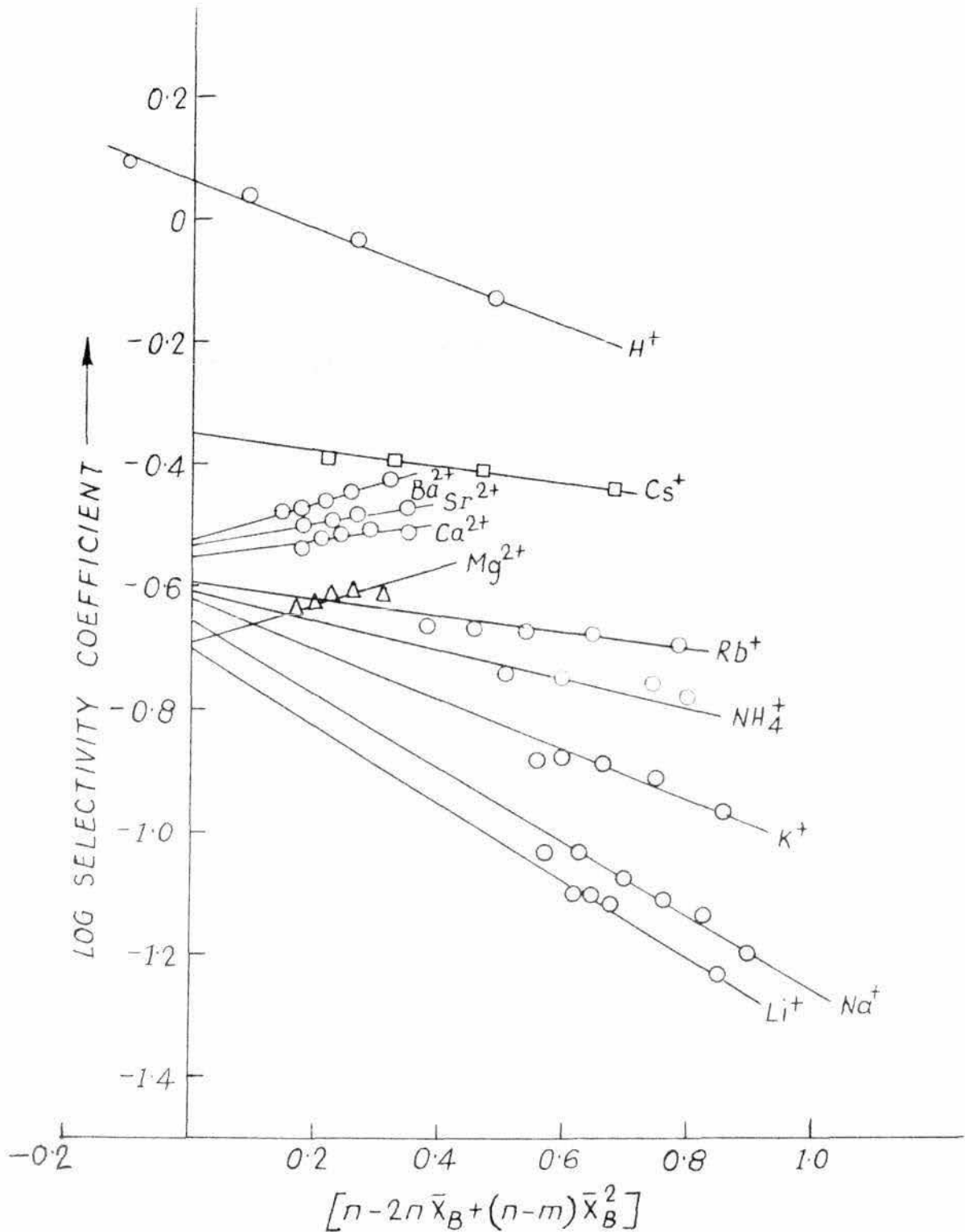


FIG. 94. PLOT OF LOG SELECTIVITY COEFFICIENT AGAINST $n - 2n\bar{x}_B + (n-m)\bar{x}_B^2$ IN THE EXCHANGE OF $\text{Co}(\text{tn})_3^{3+}$ FROM Na - $\text{Co}(\text{tn})_3$ - LAPONITE BY DIFFERENT IONS.

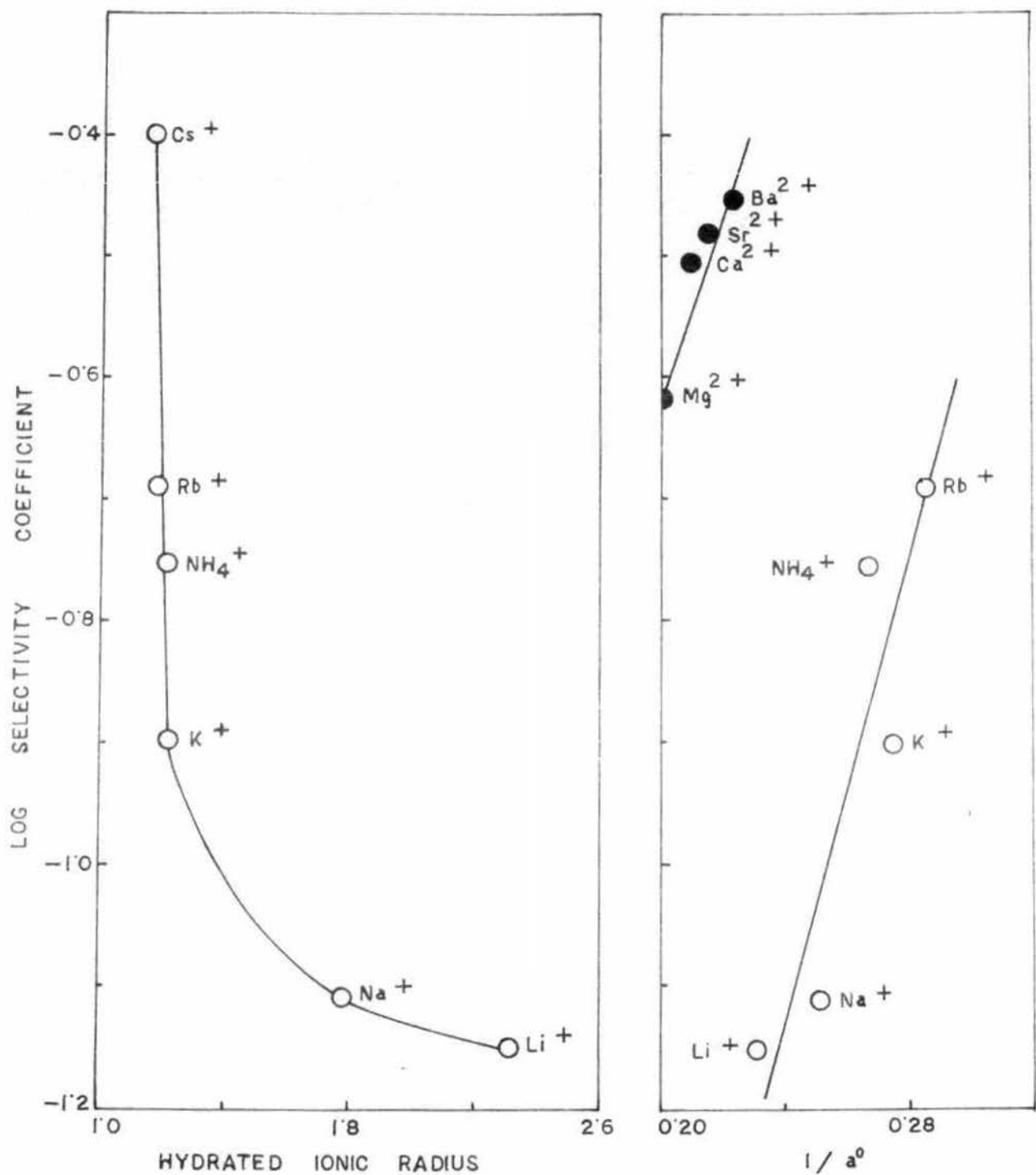


FIG. 95. CORRELATION OF SELECTIVITY COEFFICIENT WITH HYDRATED IONIC RADIUS AND DEBYE HÜCKEL PARAMETER a° IN THE DESORPTION OF Na - Cotn₃ - LAPONITE.

CHAPTER VII

Sorption and Desorption of $\text{Co}(\text{pn})_3^{3+}$ and $\text{Co}(\text{tn})_3^{3+}$ on Amberlite IRC-50 Resin-System.

Amberlite-IRC-50 (Rohm and Haas Co), a carboxylic acid type exchanger, is commercially available in the form of white, opaque, near spherical particles of approximately 50+ mesh and is a copolymer of methacrylic acid crosslinked with divinyl benzene. It is insoluble in water and is unaffected by strong acids and alkalies, oxidising and reducing agents.

This weak cation exchanger was converted into its H-form by leaching the exchanger with 1.0 N HCl until the leachate composition was constant. It was washed free of chloride ions and air dried. All solutions used in the experiment are from reagent grade chemicals and distilled water. The resin was then kept in a desiccator over saturated NH_4Cl solution (r.h. 79.5%). The ion-exchange capacity of this resin was determined by shaking its acid form with a measured excess of standard NaOH solution and back-titrating an aliquot of the supernatant solution with standard HCl. The exchange capacity of the H-resin was found to be 1020 m.e. per 100 gm of the dry resin. For exchange study it was converted into the Na-form by adding an equivalent amount of NaOH. The Na-resin was then air-dried and placed in a desiccator over saturated NH_4Cl . After seven days it was used for the exchange of $\text{Co}(\text{pn})_3\text{Cl}_3$ and $\text{Co}(\text{tn})_3\text{Cl}_3$. A

known weight of the resin was dried overnight in an air oven at 105°C and after drying its weight was recorded. The difference gave the moisture content per gm. resin. The calculations were done on the basis of dried resin at 105°C. The Na-Copn₃-resin and Na-Cotn₃-resin were used for desorption studies.

The experimental procedures for studying adsorption of Copn₃Cl₃ and Cotn₃Cl₃ were almost alike as in the case of clay minerals. About 0.1 gm of Na-IRC-50 was weighed into pyrex bottles to which increasing amount of Copn₃Cl₃ or Cotn₃Cl₃ were added. The total volume was kept constant (10 ml) in each case by adding the requisite amount of water. The system was allowed to equilibrate overnight with occasional shaking. After centrifugation, for about 15 minutes, the Copn₃Cl₃ or Cotn₃Cl₃ contents of the supernatant liquids were estimated by Beckman DU-2 Spectrophotometer.

To study desorption, the Na-Copn₃-resin or Na-Cotn₃-resin was weighed accurately (~0.1 gm) in pyrex bottles to which varying amounts of desorbing electrolytes were added. The volume was kept constant (10 ml) in each case by quantitatively adding distilled water. They were shaken for about two hours, kept overnight and Copn₃Cl₃ or Cotn₃Cl₃ content of the solution was estimated colorimetrically as above.

SECTION A

Sorption Studies.

Sorption of $\text{Co}(\text{pn})_3\text{Cl}_3$ on Na-IRC-50

The exchange isotherm of Na-IRC-50 with $\text{Co}(\text{pn})_3\text{Cl}_3$ is given in Fig. 96 which is typically of the Langmuir type. Accordingly, the plot of $\frac{C}{X}$ against C (Fig. 96) is linear. From the slope of the line, the value of V_m (the amount required to form a complete monolayer) is found to be 914 m.e./100 gm, which is less than the exchange capacity (1020 m.e./100 gm). The lower value may be caused by the physical inaccessibility of the resin to the large-sized $\text{Co}(\text{pn})_3^{3+}$ ions. The latter are attached so strongly (Fig. 96) on the resin surface at low concentration that the equilibrium concentration becomes almost negligible. This is reflected in the initial portion of the exchange isotherm.

Sorption of $\text{Co}(\text{tn})_3\text{Cl}_3$ on Na-IRC-50.

The exchange isotherm of Na-IRC-50 with $\text{Co}(\text{tn})_3\text{Cl}_3$ obtained as usual is shown in Fig. 97. V_m from the linear plot is equal to 704 m.e./100 gm as against the exchange capacity of the resin (1020 m.e.). The lower value of V_m may be due to the physical inaccessibility of the resin to the large-sized $\text{Co}(\text{tn})_3^{3+}$ ions.

SECTION B

Desorption studies

Desorption of $\text{Co}(\text{pn})_3^{3+}$ from Na-Copn₃-IRC-50

The results of desorption of $\text{Co}(\text{pn})_3^{3+}$ from its resin complex are shown in Figs. 98, 99, 100 and 101. It is interesting to note that (Fig. 98) all the isotherms obtained with monovalent inorganic ions except H^+ are S-shaped and is identical with that obtained in the desorption of $\text{Co}(\text{tn})_3^{3+}$ from Na-Cotn₃-vermiculite by Na^+ (P 90). The isotherms may be placed in the S-group of curves in the classification of isotherms of Giles et al(1949). However, recent theoretical treatment for the classification of sorption isotherms by Giles, Smith and Huitson (195) shows that S-curve occurs when the activation energy for the desorption of the solute is concentration dependent, and/or is markedly reduced by large negative contributions of the solvent or a second solute.

It is clear from Fig. 98 that in the initial part of the S-curves, the more the desorbing ions adsorbed, the easier it is for additional amounts to be taken up by the resin matrix. The explanation put forward for the characteristic feature of the desorption curve of Cotn₃ by Na in vermiculite (P 91) seems to be applicable here also. Among different factors involved, the hydrophobic nature of the complex ions as well as

their bigger sizes and the peculiarity in the structural pattern of the resin architecture seem to be predominant. The sequence in the desorption curves obtained by different ions is then understood on the basis of this qualitative picture. The following data in Table 20 suggest that a hydrophilic character is exhibited when H^+ is replaced by Na^+ or Mg^{2+} but a hydrophobic character if H^+ is exchanged by $Co(pn)_3^{3+}$. It has also been noted in the present study in bentonite (P 55) from X-ray diffraction studies that when $Co(pn)_3^{3+}$ or $Co(tn)_3^{3+}$ ions are adsorbed in bentonite a distinct water-proof character is developed in the clay-complex. A similar conclusion has been reached for ion exchange processes on the zeolites (208), in which the dehydration is attributed to crystal lattice forces and the same forces may also be important in the present system. Recently, Lindenbaum and Boyd (209) and Becker, Lindenbaum and Boyd (210) have obtained positive ΔS values for the exchange of caesium with lithium on weak acid organic exchangers. They also postulated water removal from the ingoing alkali metal ion, Li^+ , accompanying site-binding of this ion by the exchanger and this conclusion was supported by the results of dilatometric measurements (211). The sizes of the unhydrated ions seem to play predominant role in the desorption process. A reversed preference series, such as that found in the present work, was also observed for the alkali metal ions on weak acid carboxylate and phosphonate resins by Gregor et al (212),

Table 20

Intake of water by resins

Form	ml of water per gm of the resinate.
Na^+	3.6
Mg^{2+}	3.3
H^+	2.1
$\text{[Co(ph)}_3\text{]}^{3+}$	1.65
$\text{[Co(tn)}_3\text{]}^{3+}$	1.78

Bregman (213) and also for hydrous Zirconia, a weak acid exchanger, by Britz and Nancollas (214).

The bivalent ions however, desorb more strongly and hence the isotherms show their typical features. The distribution and selectivity coefficients shown in Table 21 are in the order: $Cs < Rb < K < Na < Li < NH_4 < Mg < Ca < Sr < Ba < H$ for the inorganic ions and $(C_4H_9)_4N < (C_3H_7)_4N < (C_2H_5)_4N < (CH_3)_4N < DDTA < CTA < CP < PrDA < EDA$ for the quaternary ammonium ions.

It is interesting to note that the general lyotrope series is reversed for the monovalent ions although the behaviour is somewhat different with NH_4^+ and H^+ . This reversal is unlike what has been observed with clay minerals. The divalent ions, Mg^{2+} , Ca^{2+} , Sr^{2+} and Ba^{2+} however, show the normal behaviour.

The higher desorbing power of NH_4^+ is probably due to the low pH of NH_4Cl solution in the concentration range studied so that the high exchangeability of H^+ comes into play. The anomalous position of H^+ in the series is to be particularly noticed. This may be explained by assuming H^+ to be present as a bare proton in the exchange reactions as a result of which it has greater accessibility to the exchange sites.

The results of the desorption by quaternary ammonium ions are very interesting. The values of the selectivity coefficients are found to be much smaller than those observed with similar studies in clay minerals (P 70). This is probably

Table 21

Desorption characteristics of $[\text{Co}(\text{pn})_3]^{3+}$ with respect to different ions from Na-Copn₃-IRC-50.

Electrolyte used	Concentration of electrolyte	Distribution Coefficient	Selectivity Coefficient
<u>1:1 Electrolyte</u>			
LiCl	2.5×10^{-1} (M)	2.90	0.265
	3.0 "	2.97	0.294
	4.0 "	3.02	0.336
	5.0 "	3.05	0.369
	7.0 "	3.28	0.478
NaCl	4.0×10^{-1} (M)	2.45	0.250
	5.0 "	2.53	0.285
	6.0 "	2.67	0.332
	7.0 "	2.85	0.389
KCl	4.0×10^{-1} (M)	1.884	0.175
	5.0 "	1.86	0.187
	6.0 "	1.93	0.210
	7.0 "	2.04	0.242
RbCl	4.0×10^{-1} (M)	1.65	0.145
	5.0 "	1.74	0.170
	6.0 "	1.80	0.191

(Contd..)

Table 21 (Contd..)

Electrolyte used	Concentration of electrolyte	Distribution Coefficient	Selectivity Coefficient
CsCl	2.5 x 10 ⁻¹ (M)	1.264	0.087
	4.0 "	1.43	0.120
	5.0 "	1.50	0.139
	6.0 "	1.60	0.163
HCl	1.0 x 10 ⁻² (M)	1056	164.6
	2.0 "	308.4	53.71
	3.0 "	184.26	33.92
	4.0 "	134.48	25.78
NH ₄ Cl	2.0 x 10 ⁻¹ (M)	3.78	0.351
	3.0 "	3.99	0.439
	4.0 "	4.02	0.500
	5.0 "	4.12	0.570
<u>2:1 Electrolyte</u>			
MgCl ₂	2.0 x 10 ⁻² (M)	9.57	0.919
	4.0 "	9.29	1.136
	6.0 "	8.83	1.233
	10.0 "	7.73	1.229

(Contd..)

Table 21 (Contd..)

Electrolyte used	Concentration of electrolyte	Distribution Coefficient	Selectivity Coefficient
CaCl ₂	4.0 x 10 ⁻² (M)	10.43	1.39
	6.0 "	9.679	1.459
	10.0 "	8.313	1.41
SrCl ₂	4.0 x 10 ⁻² (M)	11.0	1.52
	6.0 "	9.87	1.518
	10.0 "	8.53	1.48
BaCl ₂	4.0 x 10 ⁻² (M)	11.3	1.60
	6.0 "	10.18	1.59
	10.0 "	8.65	1.53
<u>Quaternary ammonium salt</u>			
(CH ₃) ₄ NCl	2.0 x 10 ⁻¹ (M)	0.60	0.0284
	3.0 "	0.60	0.0337
	4.0 "	0.582	0.0367
	6.0 "	0.601	0.0429
(C ₂ H ₅) ₄ NBr	1.5 x 10 ⁻¹ (M)	0.40	0.0141
	2.5 "	0.30	0.01418

(Contd..)

Table 21 (Contd..)

Electrolyte used	Concentration of electrolyte	Distribution Coefficient	Selectivity Coefficient
$(C_3H_7)_4NI$	$1.0 \times 10^{-1}(M)$	0.30	0.00982
	2.0 "	0.30	0.0118
$(C_4H_9)_4NBr$	$1.0 \times 10^{-1}(M)$	0.226	0.0126
	2.0 "	0.225	0.00736
DDTABr	$1.0 \times 10^{-2}(M)$	3.03	0.0991
	2.0 "	3.40	0.133
	3.0 "	2.01	0.083
CTABr	$1.0 \times 10^{-2}(M)$	34.23	2.855
	2.0 "	27.41	2.20
	3.0 "	21.73	1.87
CPCl	$1.0 \times 10^{-2}(M)$	36.26	2.498
	2.0 "	30.00	2.47
	3.0 "	23.40	2.059
EDA	$0.50 \times 10^{-1}(M)$	9.52	1.309
	1.0 "	7.72	1.222
	1.50 "	6.83	1.189
	2.0 "	6.16	1.13
	2.50 "	5.68	1.086

(Contd..)

Table 21 (Contd..)

Electrolyte used	Concentration of electrolyte	Distribution Coefficient	Selectivity Coefficient
PrDA	0.50×10^{-1} (M)	7.68	0.893
	1.0 "	6.68	0.933
	1.50 "	6.12	0.955
	2.0 "	5.63	0.941
	2.50 "	5.26	0.921

due to the physical inaccessibility of the exchange sites in the resin matrix by the large organic ions.

In order to ascertain the role of hydration (215-217) of ions the desorption experiments have also been carried out in 50% aqueous ethanolic medium (Fig. 98) with Li^+ , Na^+ , K^+ , Rb^+ and Cs^+ . It is observed that for Li^+ , Na^+ , K^+ , Rb^+ and Cs^+ the amount of $\text{Co}(\text{pn})_3^{3+}$ desorbed is larger than in aqueous medium, and the order of preference is $\text{Cs}^+ < \text{Rb}^+ < \text{Li}^+ < \text{K}^+ < \text{Na}^+$. This behaviour may be explained on the basis of solvation of these ions, the resulting ionic sizes, their activities and the dielectric properties of the solvent mixture.

It appears that the experimental data with Cs^+ do not fit in Kielland's equation. The values corresponding to Li^+ , Na^+ , K^+ , Rb^+ , NH_4^+ , Ca^{2+} , Mg^{2+} , Sr^{2+} and Ba^{2+} may however be analysed and explained in the language of this equation (Fig. 102). The thermodynamic equilibrium constant, ΔG° , calculated on the basis of the equation are shown in Table 22. The values of the thermodynamic equilibrium constants are in the order: $\text{NH}_4^+ > \text{Li}^+ > \text{Na}^+ > \text{K}^+ > \text{Rb}^+$ for the monovalent ions. For divalent ions, however, the values are in the order: $\text{Ba}^{2+} > \text{Sr}^{2+} > \text{Ca}^{2+} > \text{Mg}^{2+}$. Compared to other monovalent ions NH_4^+ shows a higher value of the thermodynamic equilibrium constant and negative free energy change. This is probably caused by H^+ present in appreciable concentration in the solutions of NH_4Cl used as a desorbing electrolyte.

Table 22

Evaluation of thermodynamic quantities

from Kielland's equation at 25°C.

Exchange system	Thermodynamic equilibrium constant	ΔG° Cal/mole
$K_{\text{COPn}_3}^{\text{NH}_4}$	1.412	-204.54
$K_{\text{COPn}_3}^{\text{Li}}$	1.12	- 68.183
$K_{\text{COPn}_3}^{\text{Na}}$	1.0	0
$K_{\text{COPn}_3}^{\text{K}}$	0.891	68.183
$K_{\text{COPn}_3}^{\text{Rb}}$	0.794	136.36
$K_{\text{COPn}_3}^{\text{Mg}}$	0.724	190.91
$K_{\text{COPn}_3}^{\text{Ca}}$	1.445	-218.18
$K_{\text{COPn}_3}^{\text{Sr}}$	1.513	-245.45
$K_{\text{COPn}_3}^{\text{Ba}}$	1.584	-272.73

It can be seen from figure 103 that the plot of the hydrated ionic radius as well as reciprocal of the Debye Huckel parameter a° against logarithm of the selectivity coefficient is, unlike that observed with clay minerals, linear. This suggests that both the parameters may be utilised to correlate the affinities of the ions for the resin matrix.

Desorption of $\text{Co}(\text{tn})_3^{3+}$ from Na-Cotn₃-IRC-50.

The results of the exchange of $\text{Co}(\text{tn})_3^{3+}$ ions from the Na-Cotn₃ - resin by inorganic and organic ions are shown in Figs. 104, 105 and 106. The cations can be arranged in the following order: $\text{H} > \text{NH}_4 > \text{Li} > \text{Na} > \text{K} > \text{Rb} > \text{Cs}$ for the monovalent, $\text{Ba} > \text{Sr} > \text{Ca} > \text{Mg}$ for the bivalent and $\text{EDA} > \text{PrDA} > \text{CP} > \text{CTA} > \text{DDTA} > (\text{CH}_3)_4\text{N} > (\text{C}_2\text{H}_5)_4\text{N} > (\text{C}_3\text{H}_7)_4\text{N}$ for the quaternary ammonium ions.

It is interesting to note that as in the desorption of $\text{Co}(\text{pn})_3^{3+}$ from the resin, in the present case also the general lyotrope series is reversed for the monovalent ions, and the isotherms are S-shaped, although the behaviour is somewhat different with H^+ . The divalent ions, Ba^{2+} , Sr^{2+} , Ca^{2+} and Mg^{2+} however, show the normal behaviour. This reversal is unlike what has been observed with clay minerals and can be explained in the same way as in the desorption of $\text{Co}(\text{pn})_3^{3+}$ from the corresponding resin complex (P106).

The results of the desorption of $\text{Co}(\text{tn})_3^{3+}$ by quaternary ammonium ions are shown in Fig. 106. The values of the selectivity coefficients (Table 23) are much smaller than those observed in clay minerals. As mentioned earlier (P 108) this is probably due to big size of the quaternary ions as well as some geometrical relationship of the ion to the resin surface. It is also observed that $(\text{C}_2\text{H}_5)_4\text{N}^+$ desorbs a much smaller amount of $\text{Co}(\text{tn})_3^{3+}$ than $(\text{CH}_3)_4\text{N}^+$. A similar behaviour observed in the desorption of $\text{Co}(\text{pn})_3^{3+}$ and $\text{Co}(\text{tn})_3^{3+}$ from vermiculite was explained on the basis of its limited swelling. This may be so in the case of the resin system.

To ascertain the role of ionic hydration some desorption experiments have been carried out in 50% aqueous ethanolic medium with Li^+ , Na^+ , K^+ , Rb^+ and Cs^+ (Fig. 104). It is observed that in each case the amount of $\text{Co}(\text{tn})_3^{3+}$ desorbed is larger than in purely aqueous medium and the order of preference is $\text{Cs}^+ < \text{Rb}^+ < \text{Li}^+ < \text{K}^+ < \text{Na}^+$. This sequence, which is a deviation from the lyotrope series, may be explained on the basis of solvation of these ions, the resulting ionic sizes, their activities and the dielectric properties of the solvent mixture.

Table 24 shows the values of the thermodynamic equilibrium constant and standard Gibbs free energy change calculated from the linear plot on the basis of Kielland's equation (Fig. 107).

Table 23

Desorption characteristics of $\left[\text{Co}(\text{tn})_3 \right]^{3+}$ with respect to different ions from Na-Co₃-IRC-50.

Electrolyte used	Concentration of electrolyte	Distribution Coefficient	Selectivity Coefficient
<u>1:1 Electrolyte</u>			
LiCl	1.5 x 10 ⁻¹ (M)	4.25	0.406
	2.5 "	4.12	0.472
	4.0 "	3.86	0.520
	5.0 "	3.88	0.583
NaCl	2.5 x 10 ⁻¹ (M)	2.66	0.259
	4.0 "	3.02	0.369
	5.0 "	3.27	0.453
KCl	1.5 x 10 ⁻¹ (M)	2.01	0.144
	2.5 "	2.05	0.179
	4.0 "	2.18	0.236
	5.0 "	2.47	0.305
RbCl	1.5 x 10 ⁻¹ (M)	1.60	0.109
	2.5 "	1.80	0.153
	4.0 "	1.96	0.202
	5.0 "	2.11	0.245

(Contd..)

Table 23 (Contd..)

Electrolyte used	Concentration of electrolyte	Distribution Coefficient	Selectivity Coefficient
CsCl	1.5 x 10 ⁻¹ (M)	1.40	0.0909
	2.5 "	1.68	0.134
	4.0 "	1.80	0.179
	5.0 "	2.05	0.235
NH ₄ Cl	2.0 x 10 ⁻¹ (M)	6.1	0.745
	2.5 "	5.85	0.772
	3.0 "	5.89	0.847
	4.0 "	6.10	1.01
HCl	1.0 x 10 ⁻² (M)	381.25	55.89
	2.0 "	364.28	77.23
	3.0 "	233.3	56.03
	4.0 "	168.8	43.76
<u>2:1 Electrolyte</u>			
MgCl ₂	4.0 x 10 ⁻² (M)	11.14	1.74
	6.0 "	10.54	1.93
	10.0 "	8.95	1.90
	14.0 "	7.94	1.84

(Contd..)

Table 23 (Contd..)

Electrolyte used	Concentration of electrolyte	Distribution Coefficient	Selectivity Coefficient
CaCl ₂	4.0 x 10 ⁻² (M)	11.47	1.84
	8.0 "	10.93	2.09
	10.0 "	9.476	2.18
	14.0 "	8.56	2.24
SrCl ₂	4.0 x 10 ⁻² (M)	11.85	1.96
	6.0 "	11.1	2.152
	10.0 "	9.76	2.34
	14.0 "	8.67	2.33
BaCl ₂	4.0 x 10 ⁻² (M)	12.39	2.11
	6.0 "	11.38	2.28
	10.0 "	10.0	2.49
	14.0 "	8.872	2.499
<u>Quaternary ammonium salt</u>			
(CH ₃) ₄ NCl	2.0 x 10 ⁻¹ (M)	0.676	0.038
	4.0 "	0.676	0.0484
	6.0 "	0.626	0.0501
(C ₂ H ₅) ₄ NBr	1.0 x 10 ⁻¹ (M)	0.60	0.0268
	2.0 "	0.601	0.0324

(Contd..)

Table 23 (Contd..)

Electrolyte used	Concentration of electrolyte	Distribution Coefficient	Selectivity Coefficient
$(C_3H_7)_4NI$	$1.0 \times 10^{-1}(M)$	0.300	0.0106
	2.0 "	0.375	0.0167
DDTAbR	$1.0 \times 10^{-2}(M)$	4.54	0.160
	2.0 "	3.03	0.145
	3.0 "	4.56	0.257
CTAbR	$1.0 \times 10^{-2}(M)$	42.13	3.37
	1.5 "	37.5	3.28
	2.0 "	32.78	3.07
	3.0 "	25.71	2.56
CPCL	$1.0 \times 10^{-2}(M)$	53.44	4.54
	1.5 "	45.11	4.23
	2.0 "	38.33	3.81
	3.0 "	28.7	3.006
EDA	$1.0 \times 10^{-2}(M)$	16.20	1.90
	2.0 "	13.21	1.72
	3.0 "	11.57	1.635
	4.0 "	10.53	1.57

(Contd..)

Table 23 (Contd..)

Electrolyte used	Concentration of electrolyte	Distribution Coefficient	Selectivity Coefficient
PrDA	1.0 x 10 ⁻² (M)	11.42	1.02
	2.0 "	10.90	1.27
	3.0 "	10.17	1.30
	4.0 "	9.56	1.32

Both the hydrated ionic radius and the reciprocal of the Debye Huckel parameter a^0 when plotted against logarithm of the selectivity coefficient (Fig. 108) give a linear graph as observed earlier in the desorption of $\text{Co}(\text{pn})_3^{3+}$ from this resin (Fig. 103).

It can be observed from Table 21 and 23 that the values of the selectivity coefficient are low with $\text{Co}(\text{pn})_3^{3+}$ and higher with $\text{Co}(\text{tn})_3^{3+}$. The order of the affinity of the trivalent complex ions for the resin is : $\text{Co}(\text{pn})_3^{3+} > \text{Co}(\text{tn})_3^{3+}$ which is the reverse order of their desorption.

Table 23 (Contd..)

Electrolyte used	Concentration of electrolyte	Distribution Coefficient	Selectivity Coefficient
CaCl ₂	4.0 x 10 ⁻² (M)	11.47	1.84
	5.0 "	10.93	2.09
	10.0 "	9.476	2.18
	14.0 "	8.56	2.24
SrCl ₂	4.0 x 10 ⁻² (M)	11.85	1.96
	6.0 "	11.1	2.152
	10.0 "	9.76	2.34
	14.0 "	8.67	2.33
BaCl ₂	4.0 x 10 ⁻² (M)	12.39	2.11
	6.0 "	11.38	2.28
	10.0 "	10.0	2.49
	14.0 "	8.872	2.499
<u>Quaternary ammonium salt</u>			
(CH ₃) ₄ NCl	2.0 x 10 ⁻¹ (M)	0.676	0.038
	4.0 "	0.676	0.0484
	6.0 "	0.626	0.0501
(C ₂ H ₅) ₄ NBr	1.0 x 10 ⁻¹ (M)	0.60	0.0268
	2.0 "	0.601	0.0324

(Contd..)

Table 23 (Contd..)

Electrolyte used	Concentration of electrolyte	Distribution Coefficient	Selectivity Coefficient
CsCl	1.5 x 10 ⁻¹ (M)	1.40	0.0909
	2.5 "	1.68	0.134
	4.0 "	1.80	0.179
	5.0 "	2.05	0.235
NH ₄ Cl	2.0 x 10 ⁻¹ (M)	6.1	0.745
	2.5 "	5.85	0.772
	3.0 "	5.89	0.847
	4.0 "	6.10	1.01
HCl	1.0 x 10 ⁻² (M)	381.25	55.39
	2.0 "	364.28	77.23
	3.0 "	233.3	56.03
	4.0 "	168.8	43.76
<u>2:1 Electrolyte</u>			
MgCl ₂	4.0 x 10 ⁻² (M)	11.14	1.74
	6.0 "	10.54	1.93
	10.0 "	8.95	1.90
	14.0 "	7.94	1.84

(Contd..)

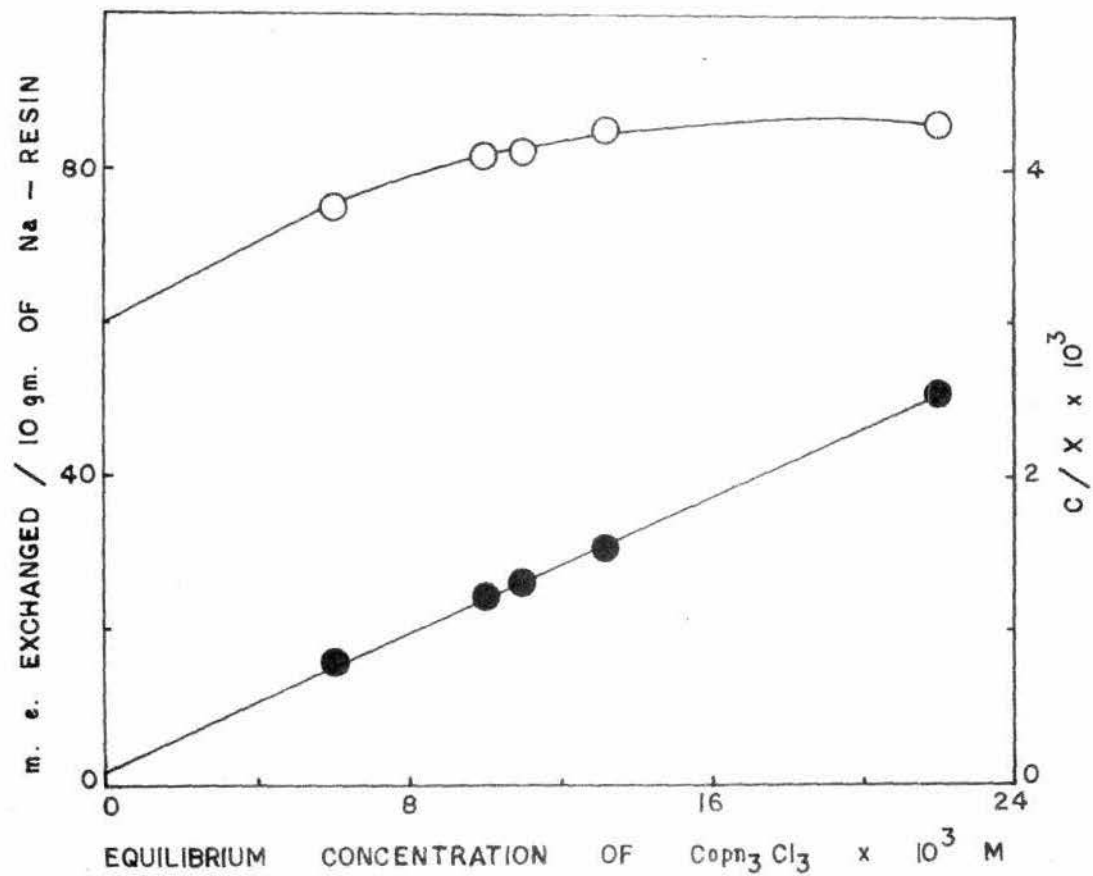
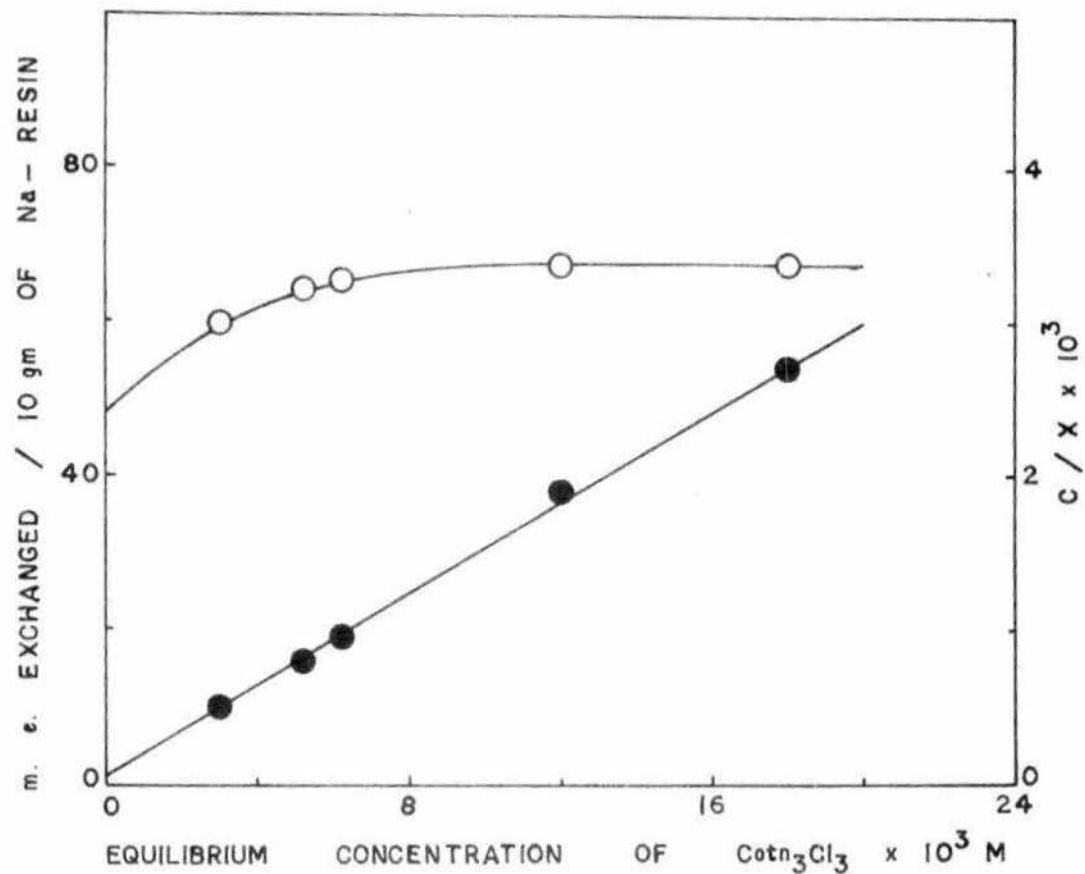


FIG.96. EXCHANGE ISOTHERM OF Copn₃Cl₃ ON Na - IRC - 50 - RESIN.



EQUILIBRIUM CONCENTRATION OF $\text{Co(NO}_3)_3 \times 10^3 \text{ M}$
 FIG. 97. EXCHANGE ISOTHERM OF $\text{Co(NO}_3)_3$ ON Na-
 IRC - 50 - RESIN.

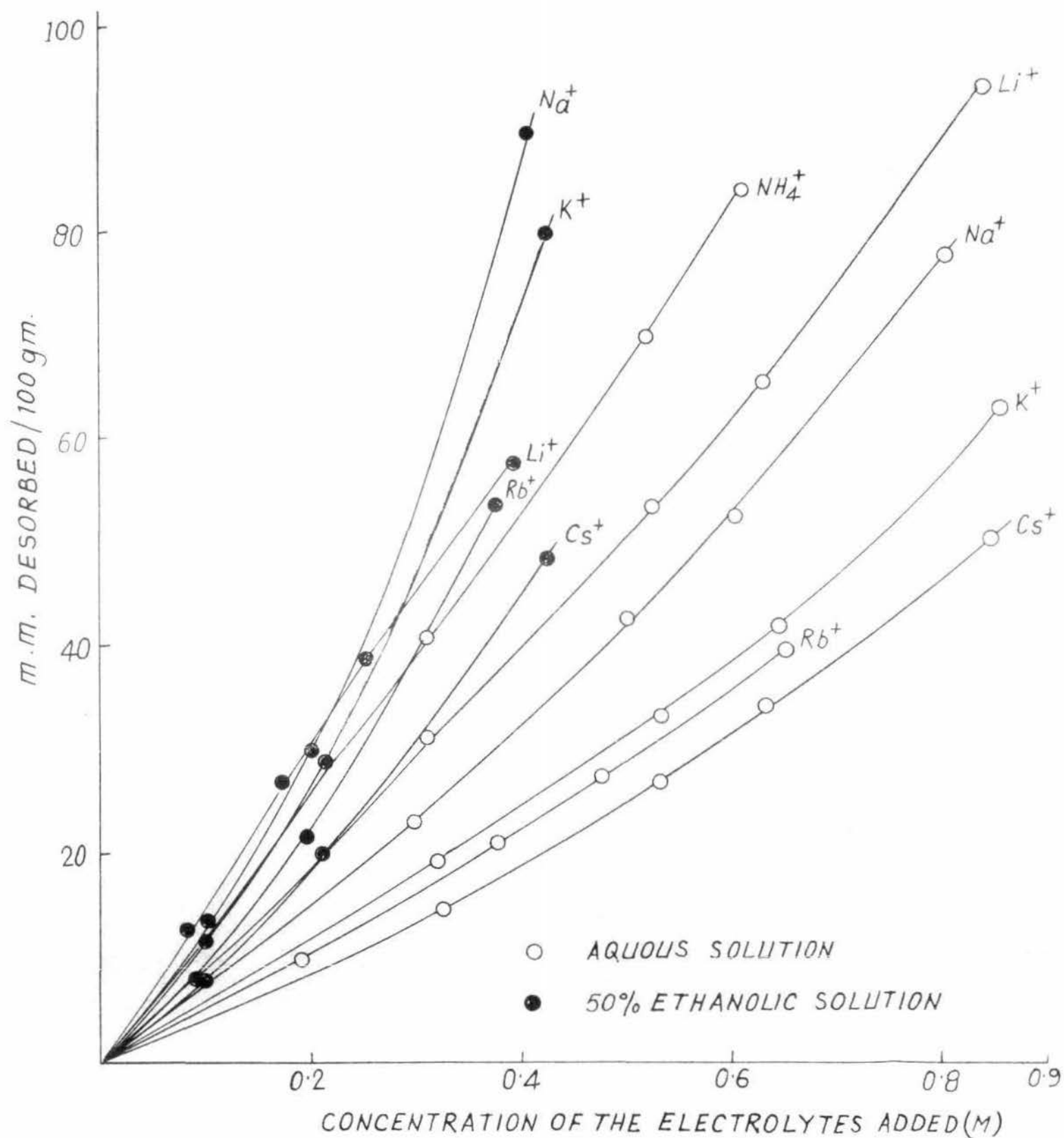


FIG. 98. DESORPTION OF $\text{Co}(\text{pn})_3^{3+}$ FROM $\text{Na-Copn}_3\text{-IRC-50}$ BY DIFFERENT IONS.

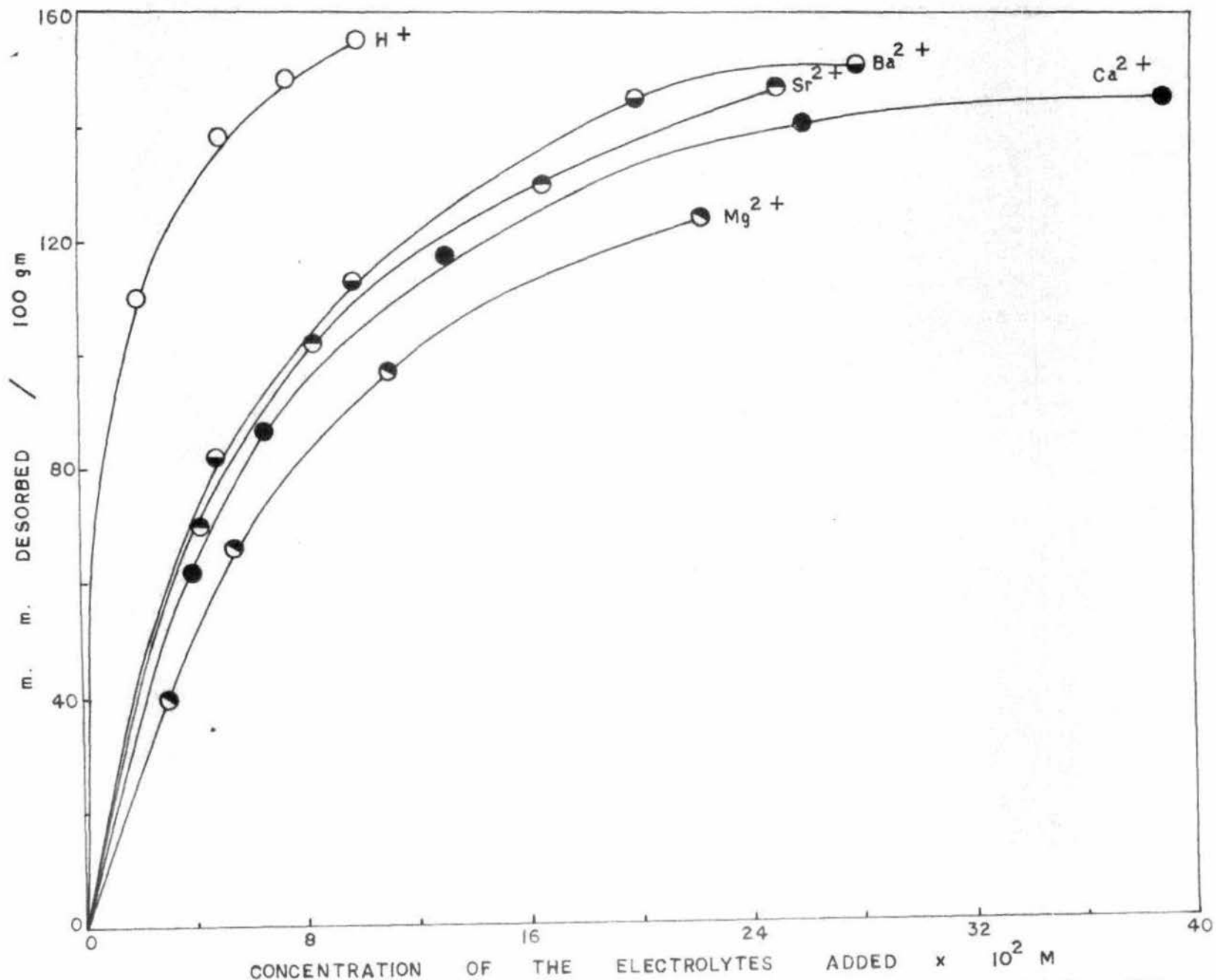


FIG. 99. DESORPTION OF Copn_3^{3+} FROM Na - Copn_3 - IRC - 50 BY DIFFERENT IONS.

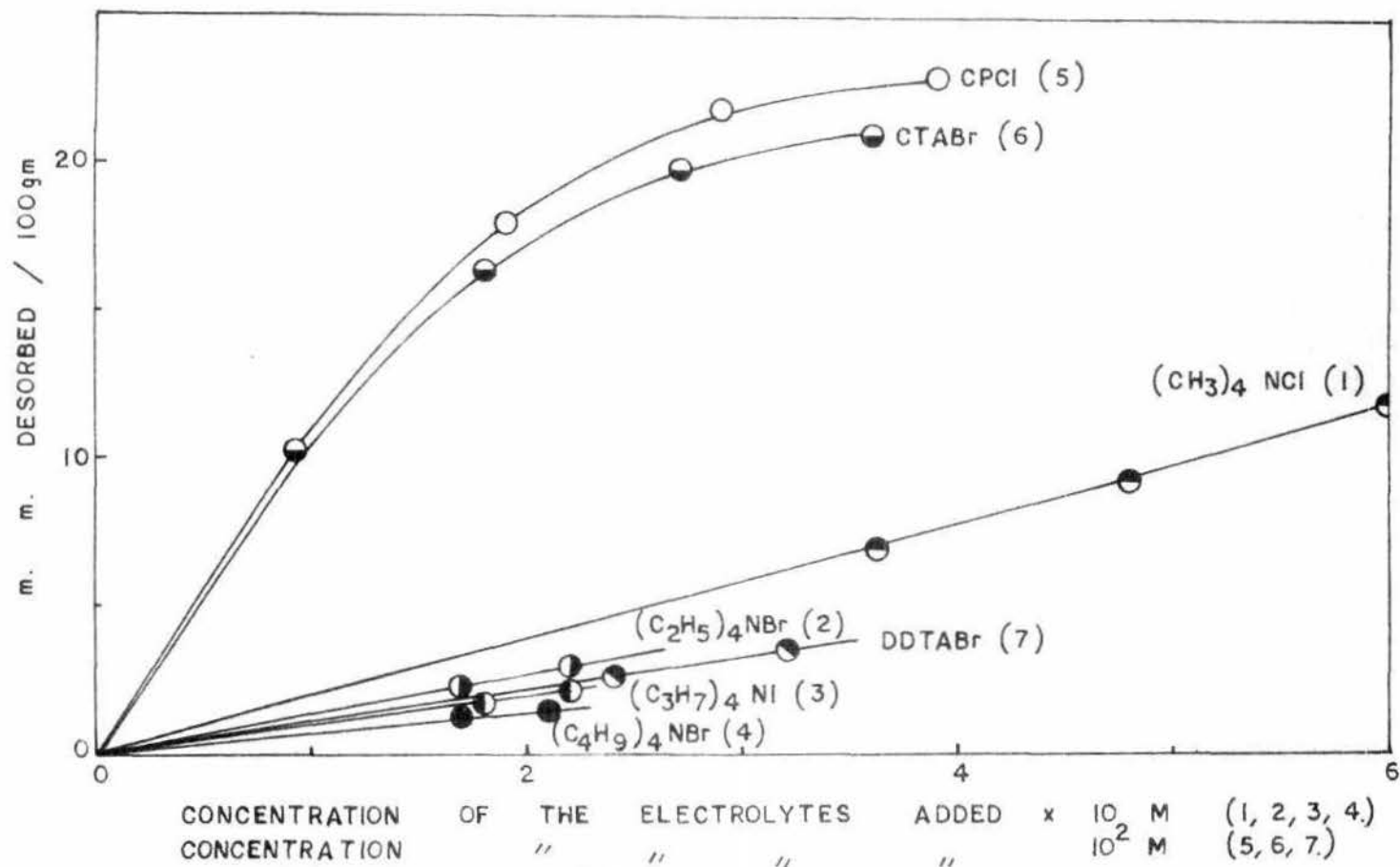


FIG. 100. DESORPTION OF Co(pn)_3^+ FROM $\text{Na-Copn}_3\text{-IRC-50}$ BY DIFFERENT IONS.

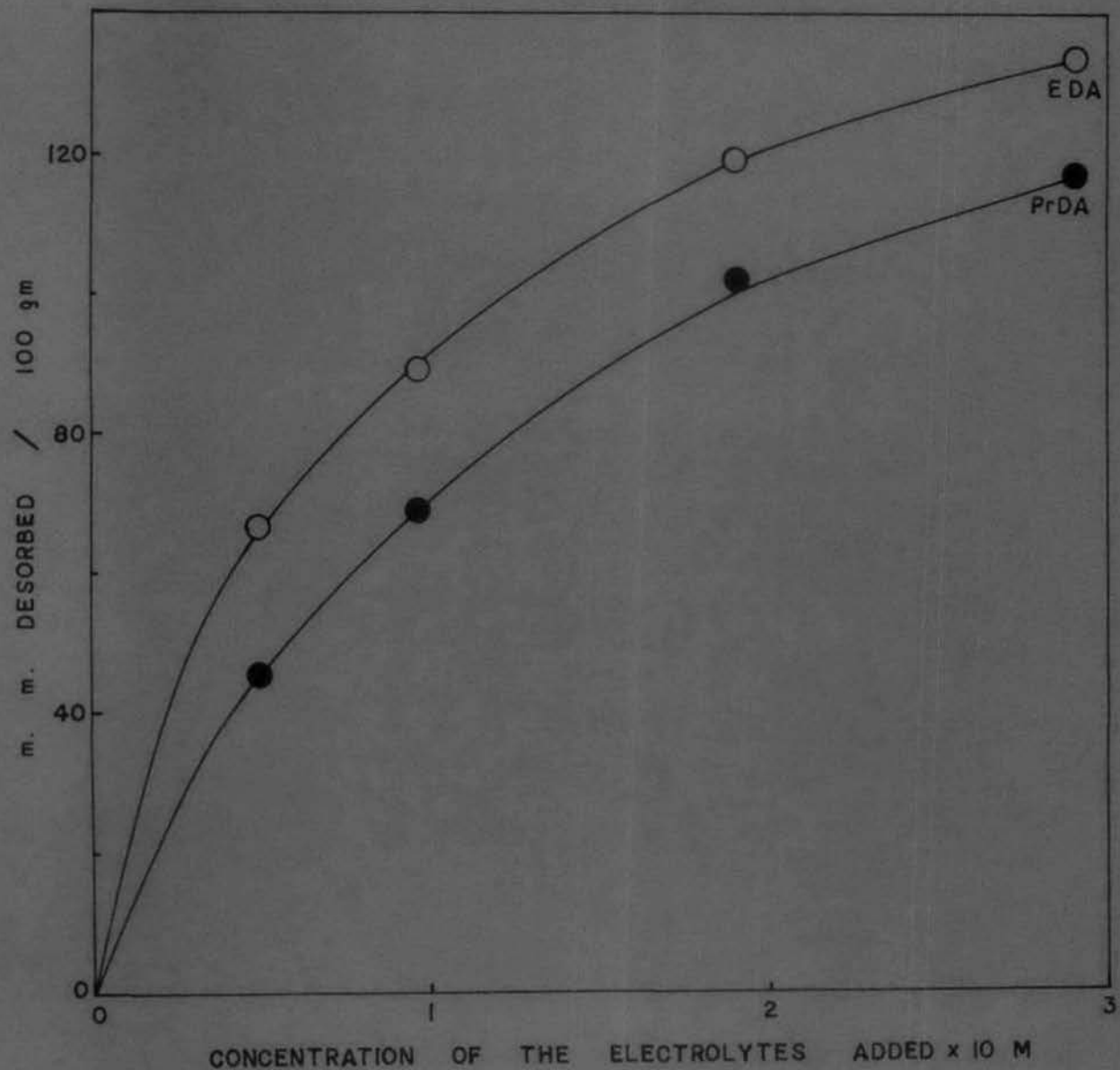


FIG. 101. DESORPTION OF $\text{Co}(\text{pn})_3^+$ FROM $\text{Na} - \text{Co}(\text{pn})_3 - \text{IRC} - 50$ BY DIFFERENT IONS.

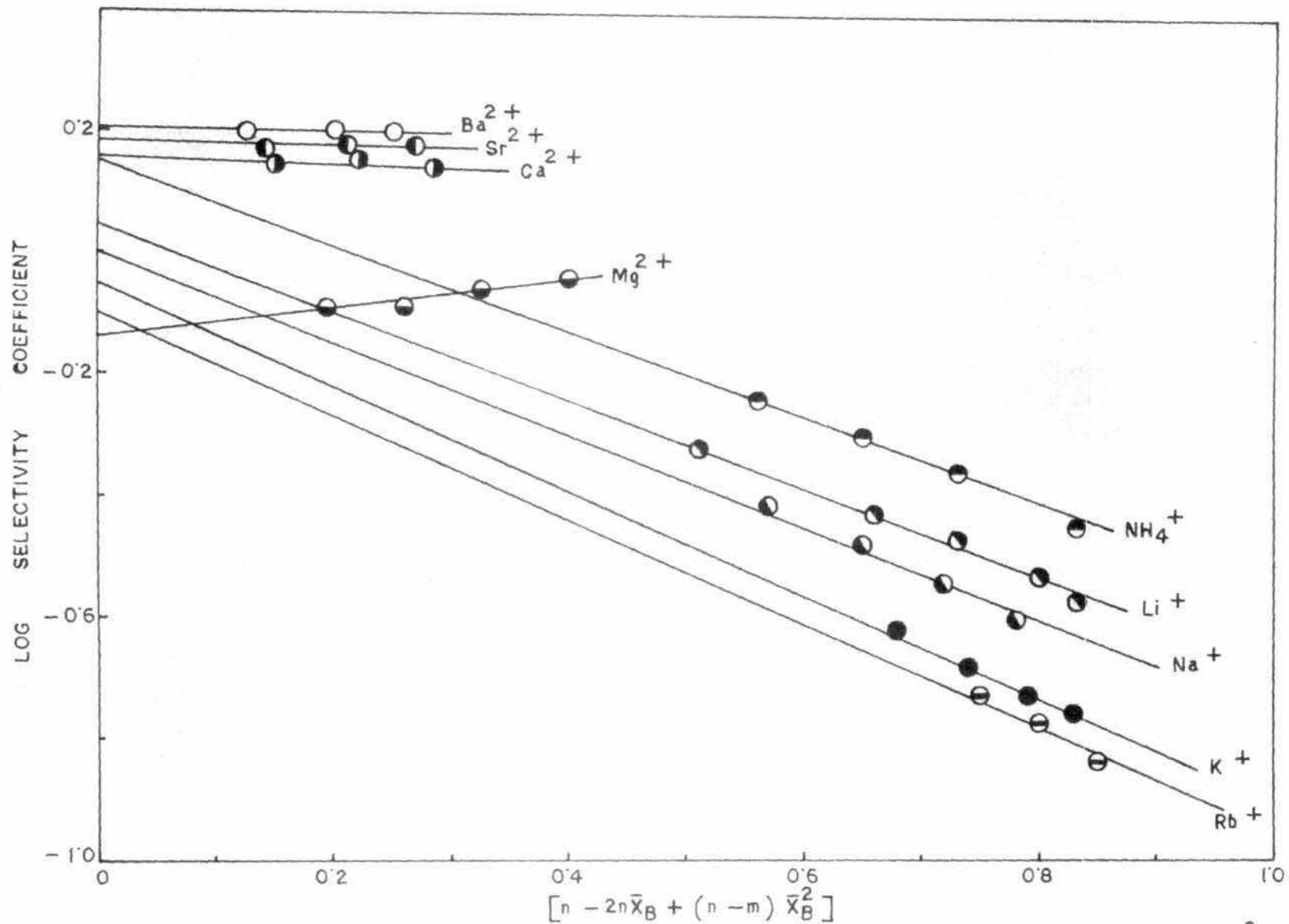


FIG. 102. PLOT OF LOG SELECTIVITY COEFFICIENT AGAINST $n - 2n\bar{X}_B + (n - m)\bar{X}_B^2$ IN THE EXCHANGE OF $Co(pn)_3^{3+}$ FROM Na - Copn₃ - IRC - 50 BY DIFFERENT IONS.

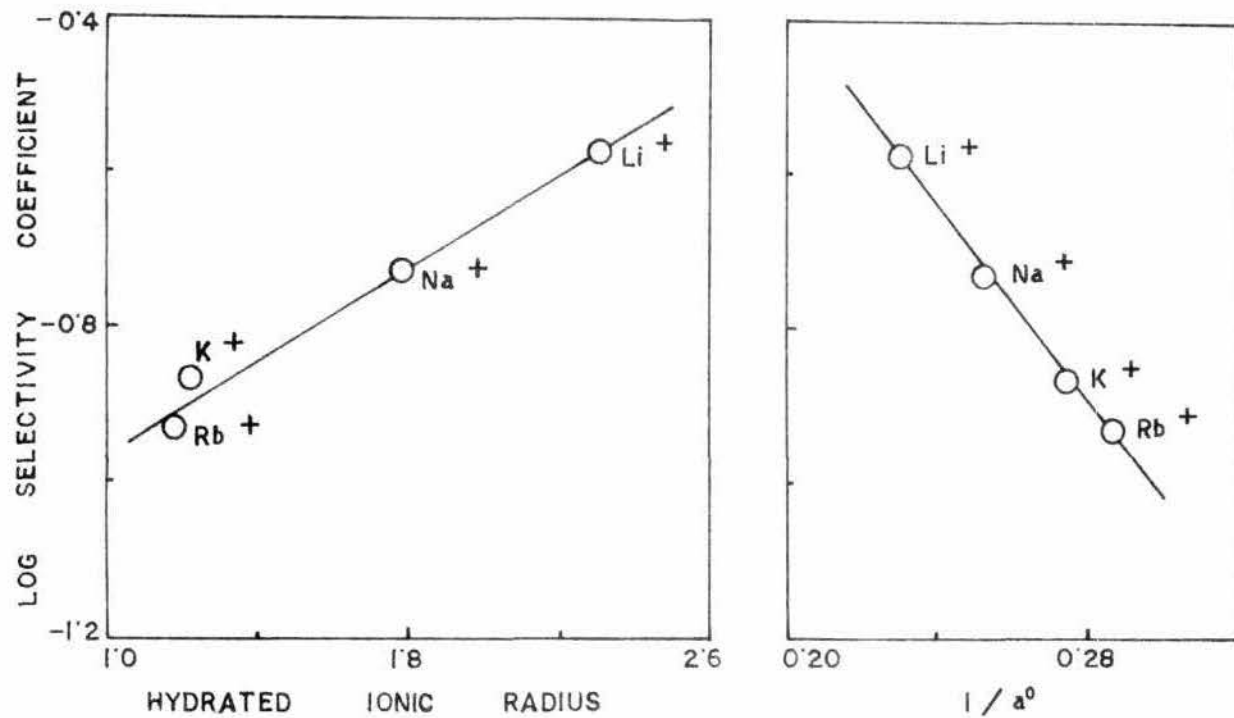


FIG.103. CORRELATION OF SELECTIVITY COEFFICIENT WITH HYDRATED IONIC RADIUS AND DEBYE HÜCKEL PARAMETER a° IN THE DESORPTION OF Na - Corn₃ - RESIN.

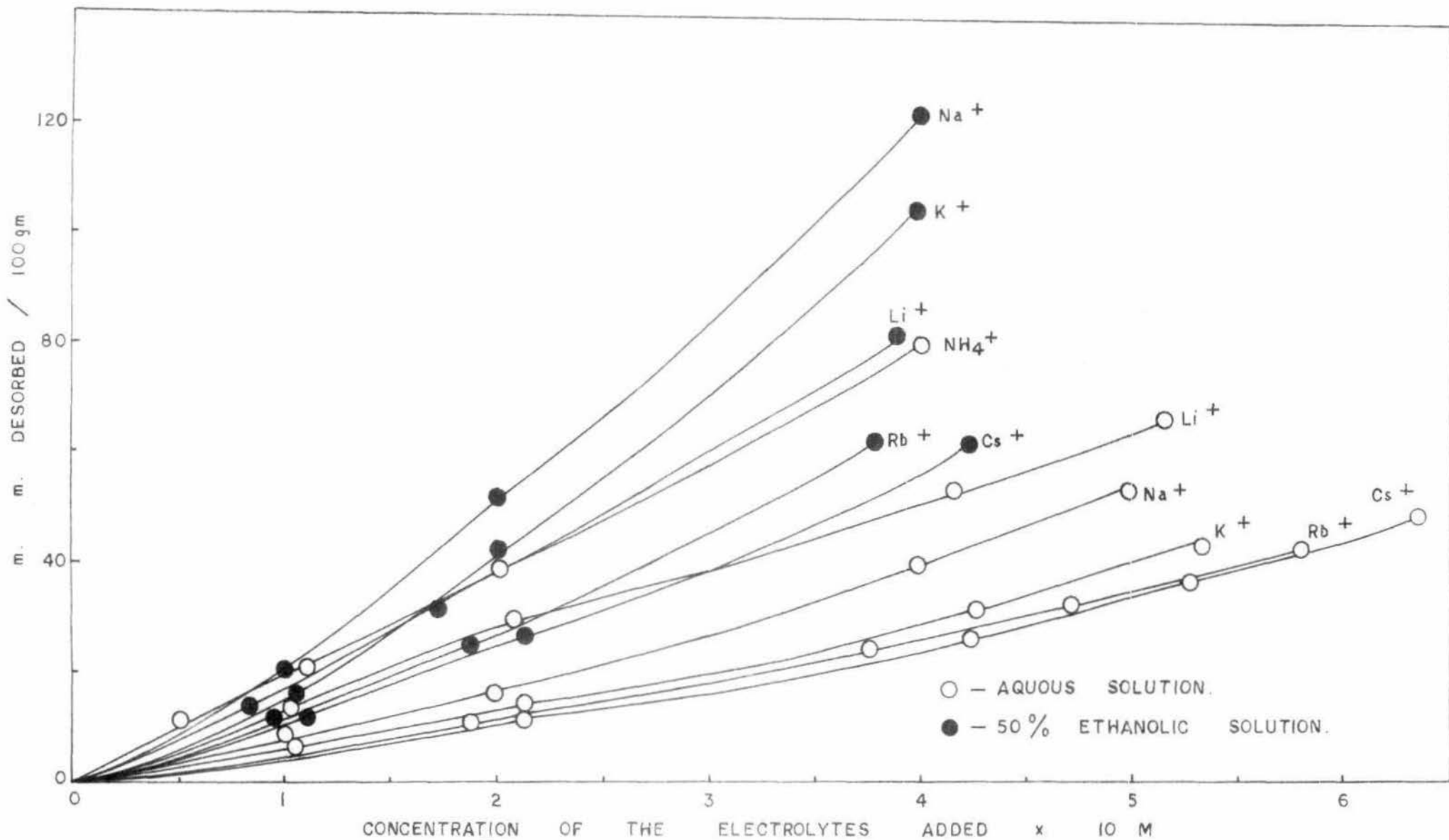


FIG. 104. DESORPTION OF $\text{Co}(\text{tn})_3^+$ FROM $\text{Na} - \text{Co}(\text{tn})_3 - \text{IRC} - 50$ BY DIFFERENT IONS.

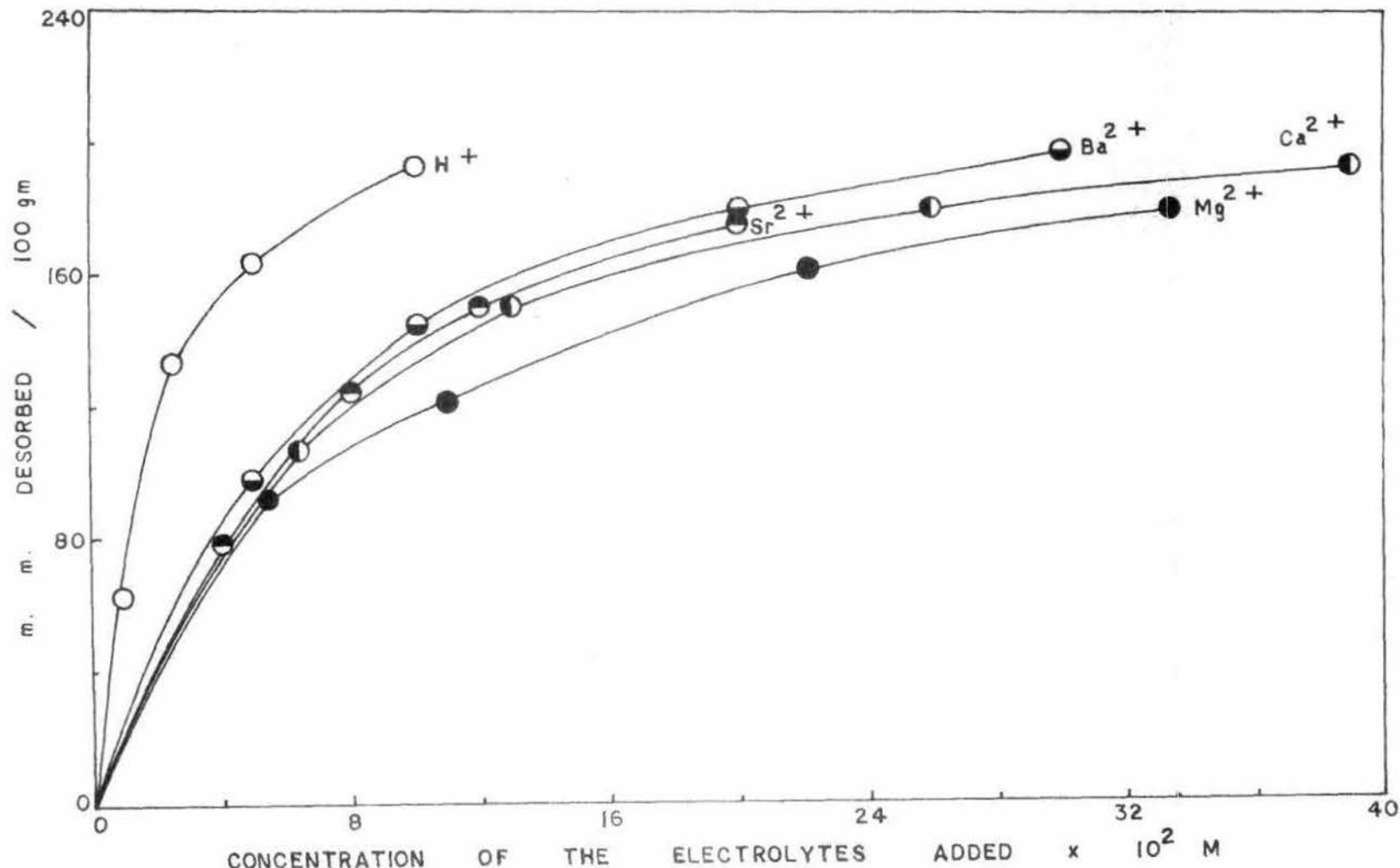


FIG. 105. DESORPTION OF $\text{Co}(\text{tn})_3^{3+}$ FROM $\text{Na} - \text{Co}(\text{tn})_3 - \text{IRC} - 50$ BY DIFFERENT IONS.

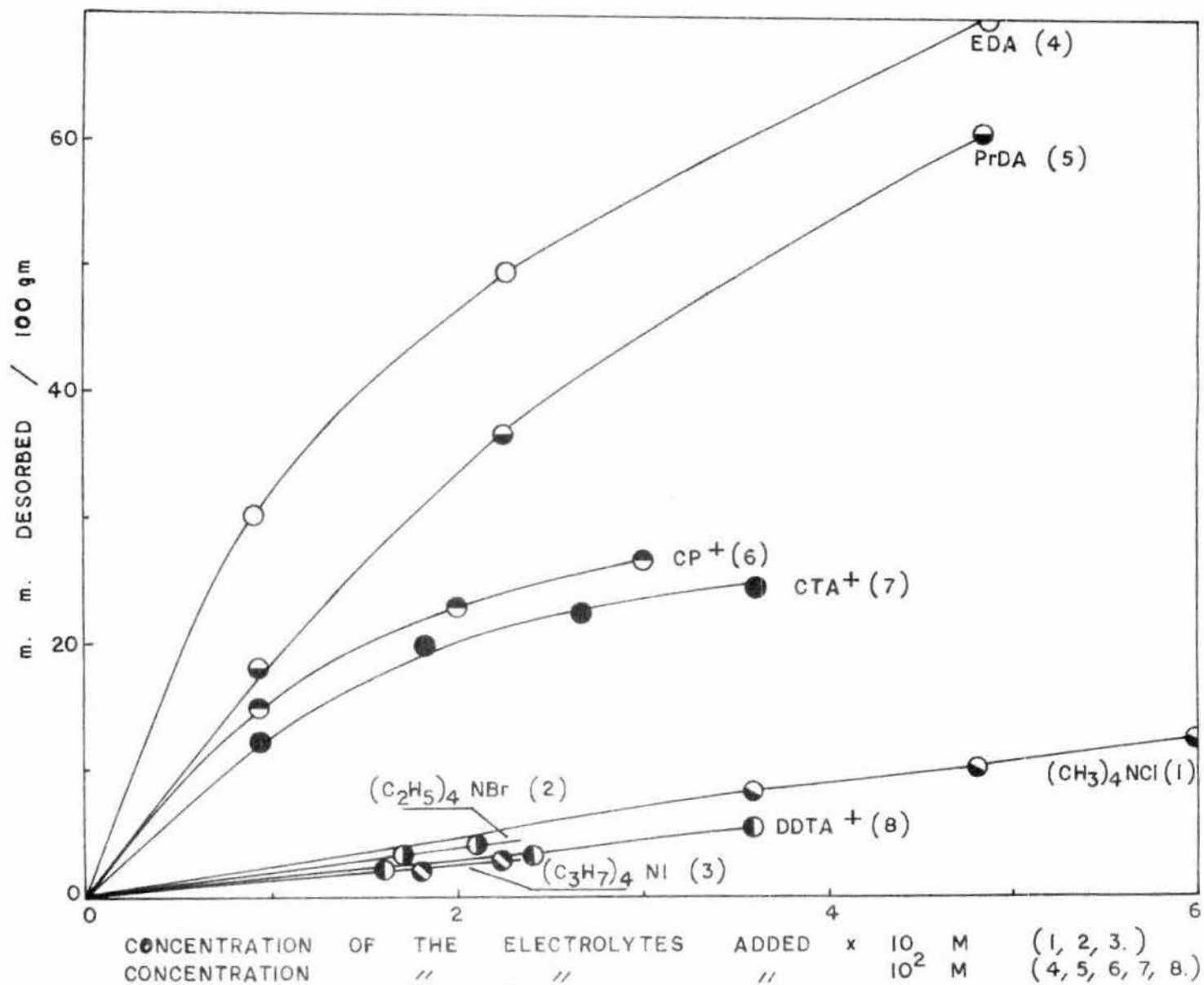


FIG. 106. DESORPTION OF $\text{Co}(\text{tn})_3^{3+}$ FROM $\text{Na-Cotn}_3\text{-IRC-50}$ BY DIFFERENT IONS.

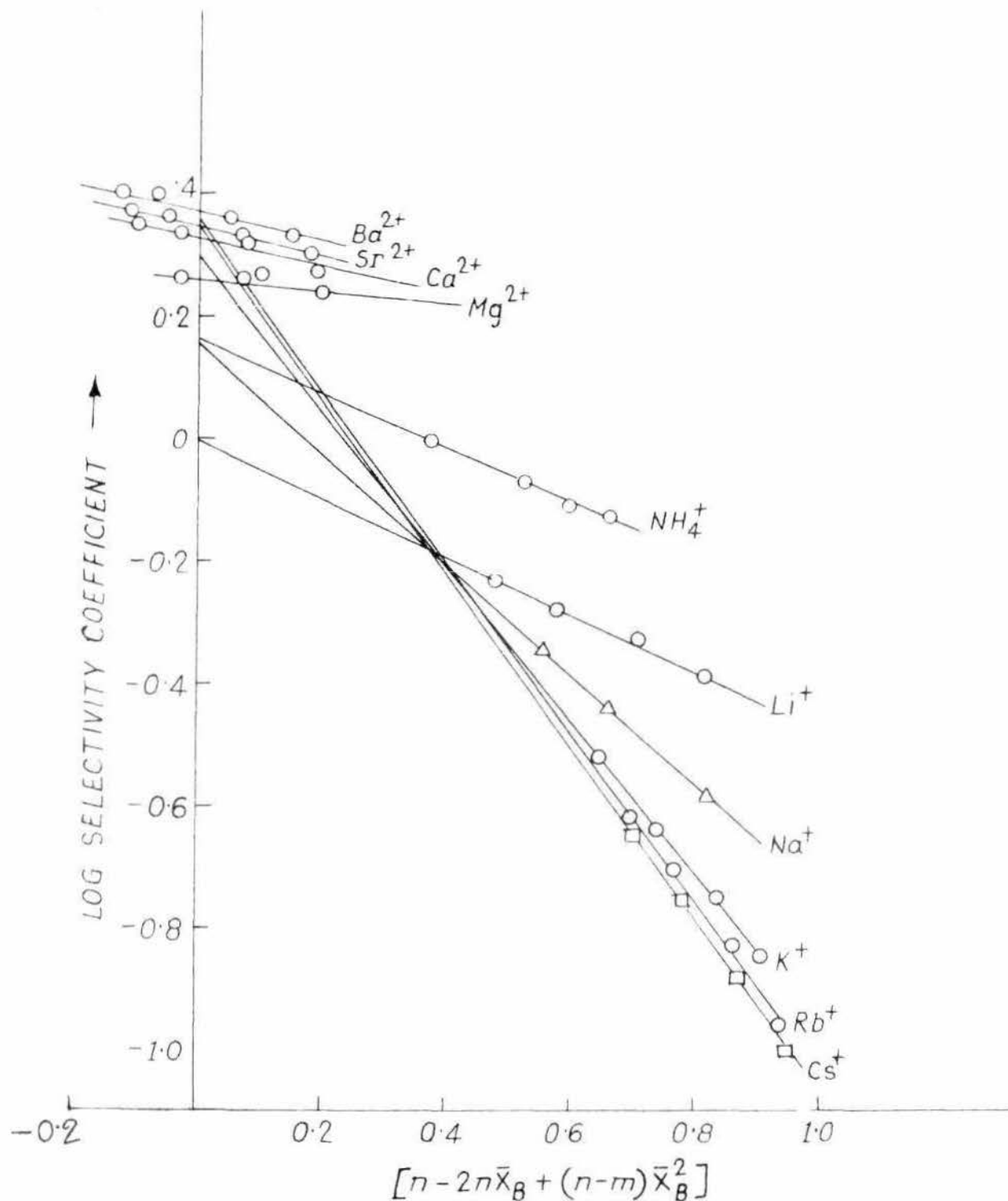


FIG. 107. PLOT OF LOG SELECTIVITY COEFFICIENT AGAINST $n - 2n\bar{x}_B + (n-m)\bar{x}_B^2$ IN THE EXCHANGE OF $Co(tn)_3^{3+}$ FROM Na-Cotn₃-IRC-50 BY DIFFERENT IONS.

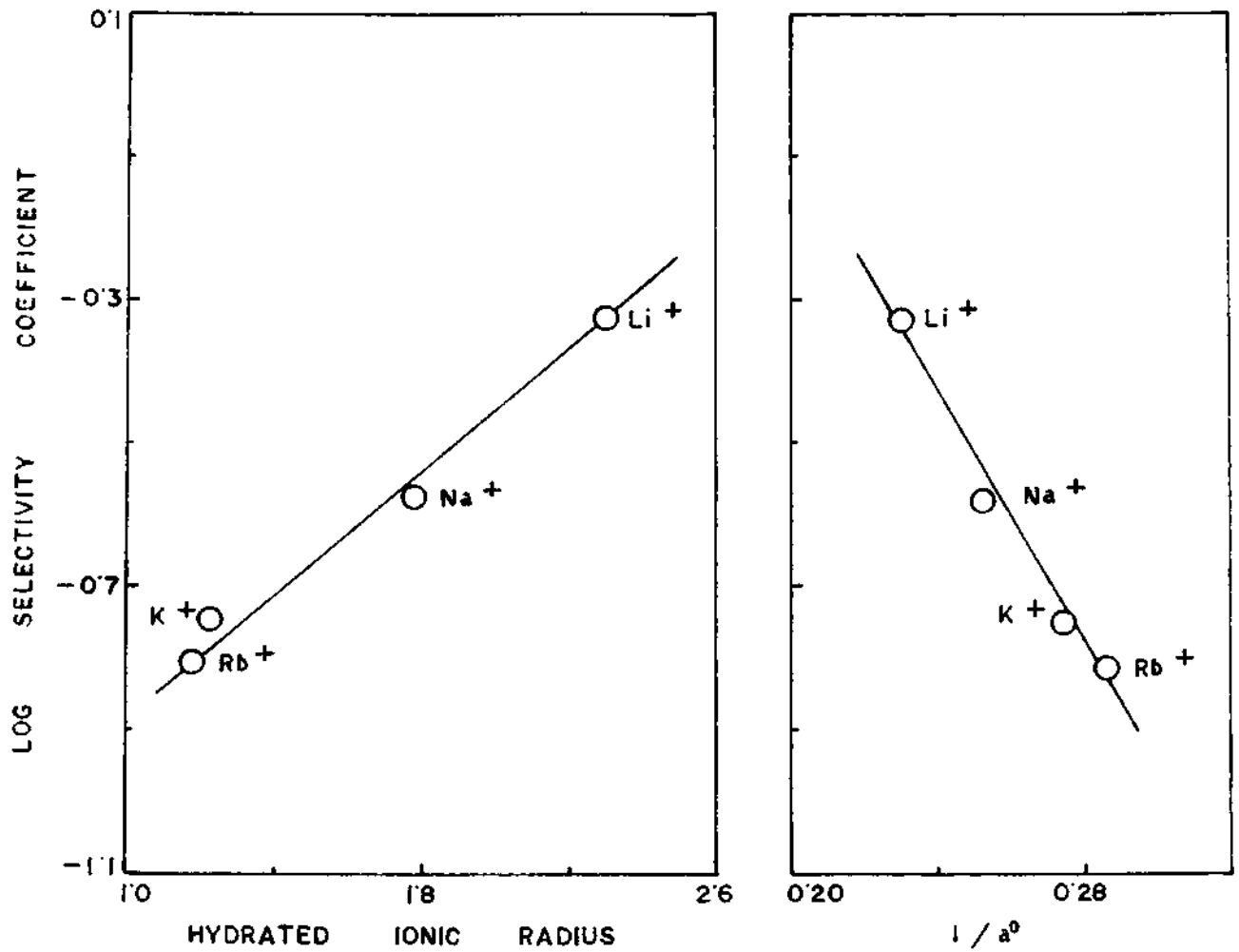
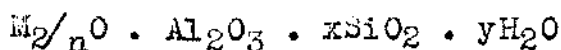


FIG. 10B. CORRELATION OF SELECTIVITY COEFFICIENT WITH HYDRATED IONIC RADIUS AND DEBYE HÜCKEL PARAMETER a^0 IN THE DESORPTION OF Na - Cohn₃ - RESIN.

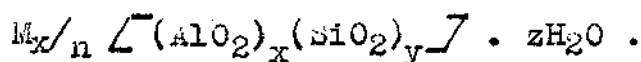
CHAPTER -VIII

Adsorption and Desorption of $[\text{Co}(\text{NH}_3)_6]^{3+}$, $[\text{Coen}_3]^{3+}$,
 $[\text{Copa}_3]^{3+}$ and $[\text{Cota}_3]^{3+}$ on Molecular Sieve 13 X.

The study of the use of molecular sieves in adsorption and catalysis has deservedly received a great deal of interest in recent years. Zeolites as synthesized or formed in nature are crystalline, hydrated aluminosilicates of Group I and II elements. Structurally, they comprise a framework based on an infinitely extending three-dimensional network of SiO_4 and AlO_4 tetrahedra linked together through common oxygen atoms. The isomorphic substitution of Si by Al gives rise to a net negative charge compensated by cations. Zeolites can be represented by the formula



where M is the compensating cation with valency n. Structurally, the formula of zeolites can be represented by its unit cell composition:



The framework structures of zeolites are composed of arrangements of tetrahedra in building units going from ring

structures to polyhedra. Usually zeolites are classified using common structural units. Zeolites A, X and Y consist of linked cubooctahedra (β cages or 24 - hedra). Such a polyhedron, also called a sodalite unit, has a central cage of diameter 0.65 nm, accessible through six membered rings of oxygen atoms with a free diameter of 0.22 nm. In the mineral faujasite and the synthetic faujasites (Zeolites X and Y), the cubo octahedra are linked with bridging oxygen atoms but in a tetrahedral symmetry. The sodalite units connected along two six-membered rings give rise to hexagonal prism. In this way, the polyhedra enclose a supercage with an internal diameter of 1.25 nm and accessible through four twelve-membered rings of oxygen atoms with a free aperture of 0.75 nm.

Owing to the isomorphous substitution of silicon by aluminium, the three-dimensional oxygen framework carries an excess negative charge, compensated by cations. These cations can be exchanged by other cations of different nature and valency. Not only single cations can be exchanged but also complexes of cations such as $\text{Cu}(\text{NH}_3)_4^{2+}$ and $\text{Pt}(\text{NH}_3)_4^{2+}$. The only limitation to the nature of the cations that can be introduced by ion exchange is the acid stability of the zeolite. Generally, the zeolite is more stable in acidic solutions when the Si : Al ratio is higher. Sieving of one type of molecule

out of a feed containing a mixture of molecules with different shapes and/or sizes is possible because the free apertures of the zeolites have molecular dimensions.

The ion exchange behaviour of some transition metal ions in Zeolite A was studied by Gal et al (218), and Zeolite X by Wolff et al (219,220). In contrast, relatively limited attention has been given to the sorption and desorption characteristics of the trivalent inorganic complex cations. In this section are presented the studies on sorption behaviour of four trivalent complex cations, namely, $\left[\text{Co}(\text{NH}_3)_6 \right]^{3+}$, $\left[\text{Coen}_3 \right]^{3+}$, $\left[\text{Copn}_3 \right]^{3+}$ and $\left[\text{Cotn}_3 \right]^{3+}$ with respect to the exchanger Linde Molecular Sieve 13X (powder form) supplied by B.D.H. Chemicals Ltd, England as gift and the desorption of Na-Copn₃-Sieve 13X (Na-Copn₃-X) and Na-Cotn₃ Sieve 13X (Na-Cotn₃-X) by the inorganic monovalent ions in line with similar studies reported earlier with bentonite systems.

Before use, the samples are saturated with 1 M NaCl and dialysed against distilled water until free of chloride (174). They are then dried at 50°C, ground and stored at room temperature over saturated NH₄Cl solution in a desiccator for at least a week. Then it was used for the exchange of Co(NH₃)₆Cl₃, Coen₃Cl₃, Copn₃Cl₃ and Cotn₃Cl₃. The Na-Copn₃-Sieve X and Na-Cotn₃-Sieve X were used for desorption studies.

The experimental procedures for studying the exchange of $\text{Co}(\text{NH}_3)_6^{3+}$, Coen_3^{3+} , $\text{Co}(\text{pn})_3^{3+}$ and $\text{Co}(\text{tn})_3^{3+}$ were almost similar to the clay minerals. About 0.1 gm of NaX was weighed into pyrex bottles to which increasing amounts of trivalent cobalt complex salt solutions were added. The total volume was kept constant (10 ml) in each case by adding the requisite amount of distilled water. They were then shaken for two to three hours and kept overnight to attain equilibrium. They were then centrifuged for 20 minutes and the amount exchanged was determined by means of absorbance measurements.

Similarly, for desorption study the Na-Copn₃-Sieve X or Na-Cotn₃-Sieve X was weighed accurately (~0.1 gm) in pyrex bottles to which varying amounts of desorbing electrolytes were added. The volume was kept constant (10 ml) in each case by adding distilled water. They were also shaken for about 3 hours, kept overnight and Copn₃Cl₃ or Cotn₃Cl₃ content of the solutions was measured colorimetrically.

SECTION -A

Sorption Studies

Sorption of $\text{Co}(\text{NH}_3)_6\text{Cl}_3$, Coen_3Cl_3 , Cotn_3Cl_3 and

$\text{Coptn}_3\text{Cl}_3$ on Molecular Sieve 13X.

In order to investigate the effect of cation size on the exchange behaviour of Molecular Sieve 13X, the above four trivalent Co(III) complex ions of varying ionic sizes have been chosen. The exchange isotherms of $\text{Co}(\text{NH}_3)_6^{3+}$, Coen_3^{3+} , Cotn_3^{3+} and Coptn_3^{3+} ions on Na-sieve X are shown in Fig. 109 (a,b,c,d), which are of the Langmuir type, indicating strong interaction between the adsorbate and the adsorbent. Accordingly, the plots of C/X against C [Fig. 109 (a',b',c',d')] are linear. From the slopes of the lines, the values of V_m are found to be 252 m.e./100 gm, 181 m.e./100 gm, 102 m.e./100 gm and 59.7 m.e./100 gm respectively.

It is interesting to note that the amount corresponding to the maximum exchange from the isotherms are 250 m.e./100 gm, 178 m.e./100 gm, 100 m.e./100 gm and 53 m.e./100 gm for $\text{Co}(\text{NH}_3)_6^{3+}$, Coen_3^{3+} , Cotn_3^{3+} and Coptn_3^{3+} respectively, which are much less than the total exchange capacity of the sieve 13X i.e. 632 m.e./100 gm (221). So the isotherms showed maximum

exchange of about 40%, 50%, 16% and 10% respectively for the above trivalent complex ions which appears to be inversely related to their ionic sizes. Steric factors based on cation size relative to the zeolite aperture diameters may explain the partial ion sieve effect and incomplete exchange observed with the $Co(III)$ complex ions in zeolite X.

SECTION -B

Studies on Desorption

Desorption of $\text{Co}(\text{pn})_3^{3+}$ from Na-Copnz-Sieve 13X.

The results of desorption of $\text{Co}(\text{pn})_3^{3+}$ from its Na-Copnz-Sieve 13X complex are shown in Fig. 110. According to the values of the selectivity coefficients (Table-25) the ions may be placed at low concentrations in the order: $\text{Rb}^+ > \text{K}^+ > \text{Na}^+ > \text{Cs}^+ > \text{Li}^+$ and at higher concentrations in the order: $\text{Na}^+ > \text{K}^+ > \text{Rb}^+ > \text{Cs}^+ > \text{Li}^+$. Barrer, et al (175) observed that for a low degree of cross linking of polystyrene sulphonate resin selectivity was in the order $\text{Na}^+ > \text{Cs}^+ > \text{K}^+ > \text{Li}^+ > \text{H}^+$, while with a high degree of crosslinking, with limited swelling, the selectivity sequence changed to $\text{Na}^+ > \text{Li}^+ > \text{H}^+ > \text{Cs}^+ > \text{K}^+$. Molecular Sieve X is to be regarded as an extremely highly cross-linked condensation polymer, virtually non-swelling, but neither of the above sequences correlates with that observed in the polystyrene sulphonate resin.

It appears that the experimental data for K^+ , Rb^+ and Cs^+ do not fit in Kielland's equation. The values corresponding to Li^+ and Na^+ may however be analysed and explained in the language of this equation (Fig. 111). The thermodynamic equilibrium constant and standard Gibbs free energy change

Table 25

Description characteristics of $\left[\text{Co}(\text{pn})_3 \right]^{3+}$ with respect to different ions from Na - Copn₃ - Sieve X.

Electrolyte used	Concentration of electrolyte	Distribution Coefficient	Selectivity Coefficient
<u>1:1 Electrolyte</u>			
LiCl	1.0 x 10 ⁻¹ (M)	0.25	0.0189
	2.0 "	0.225	0.021
	3.0 "	0.200	0.0209
	5.0 "	0.160	0.0188
NaCl	1.0 x 10 ⁻¹ (M)	0.902	0.11
	2.0 "	0.802	0.125
	3.0 "	0.65	0.1117
	5.0 "	0.47	0.0897
	6.0 "	0.417	0.0821
KCl	1.0 x 10 ⁻¹ (M)	1.2	0.165
	2.0 "	0.978	0.168
	3.0 "	0.769	0.145
	5.0 "	0.501	0.0986
	6.0 "	0.417	0.0821

(Contd..)

Table 25 (Contd..)

Electrolyte used	Concentration of electrolyte	Distribution Coefficient	Selectivity Coefficient
RbCl	1.0 x 10 ⁻¹ (M)	1.40	0.206
	2.0 "	0.752	0.114
	3.0 "	0.501	0.0765
CsCl	1.0 x 10 ⁻¹ (M)	0.505	0.0499
	2.0 "	0.425	0.0506
	3.0 "	0.334	0.0425
	5.0 "	0.210	0.0273

calculated on the basis of this equation are shown in Table 26.

The plot of log (selectivity coefficient) vs. hydrated ionic radius as well as reciprocal of Debye Huckel parameter a° is not linear.

Desorption of $\text{Co}(\text{tn})_3^{3+}$ from Na-Cotng-Sieve 13X.

The results of desorption of $\text{Co}(\text{tn})_3^{3+}$ from its Na-Cotng-Sieve 13X complex are shown in Fig. 112. It was observed that the shape of the isotherms is of Langmuir type. This type of curves are indicative of strong interaction between the adsorbate and the adsorbent. The selectivity sequence is $\text{Cs}^+ > \text{Rb}^+ > \text{K}^+ > \text{Na}^+ > \text{Li}^+$ (Table 27). So the desorption of $\text{Co}(\text{tn})_3^{3+}$ from its Na-Cotng-Sieve 13X complex follows the usual lyotropic series.

From a linear plot of $\log K_{\text{selectivity}}$'s equation (Fig. 113), the values of thermodynamic equilibrium constant and standard Gibbs free energy change have been evaluated and are presented in Table 28. It can be seen from Fig. 114 that the plot of log (selectivity coefficient) vs. hydrated ionic radius as well as reciprocal of Debye-Huckel parameter a° is, unlike that observed with clay minerals, linear. This suggests that both the parameters may be utilised to correlate the affinities

Table 26

Evaluation of thermodynamic quantities
from Kielland's equation at 25°C

Exchange system	Thermodynamic equilibrium constant	ΔG° Cal/mole
$\frac{\text{Li}}{\text{K}}_{\text{Copn}_3}$	0.0478	1800
$\frac{\text{Na}}{\text{K}}_{\text{Copn}_3}$	0.095	1390.9

Table 27

Description characteristics of $[\text{Co}(\text{tn})_3]^{3+}$ with respect to different ions from Na - Cotng - Sieve X.

Electrolyte used	Concentration of electrolyte	Distribution Coefficient	Selectivity Coefficient
<u>1:1 Electrolyte</u>			
LiCl	1.0 x 10 ⁻¹ (M)	0.40	0.031
	2.0 "	0.4006	0.0397
	3.0 "	0.367	0.0421
	4.0 "	0.35	0.0435
NaCl	1.0 x 10 ⁻¹ (M)	1.306	0.158
	2.0 "	1.206	0.1906
	3.0 "	1.105	0.201
	4.0 "	1.004	0.2008
	5.0 "	0.923	0.202
KCl	1.0 x 10 ⁻¹ (M)	4.58	0.999
	2.0 "	3.55	1.08
	3.0 "	2.79	1.096
	4.0 "	2.27	1.08
	5.0 "	1.91	1.19

(Contd..)

Table 27 (Contd..)

Electrolyte used	Concentration of electrolyte	Distribution Coefficient	Selectivity Coefficient
RbCl	1.0 x 10 ⁻¹ (M)	5.73	1.436
	2.0 "	4.22	1.658
	3.0 "	3.20	1.998
	4.0 "	2.449	1.804
CsCl	1.0 x 10 ⁻¹ (M)	6.35	1.719
	2.0 "	4.48	2.007
	3.0 "	3.27	2.389

of the ions for the molecular sieve.

It can be observed from Tables 25 and 27 that the values of the selectivity coefficient are higher with $\text{Co}(\text{tn})_3^{3+}$ and low with $\text{Co}(\text{pn})_3^{3+}$. The order of the affinity of the trivalent complex ions for the molecular sieve is : $\text{Co}(\text{pn})_3^{3+} > \text{Co}(\text{tn})_3^{3+}$.

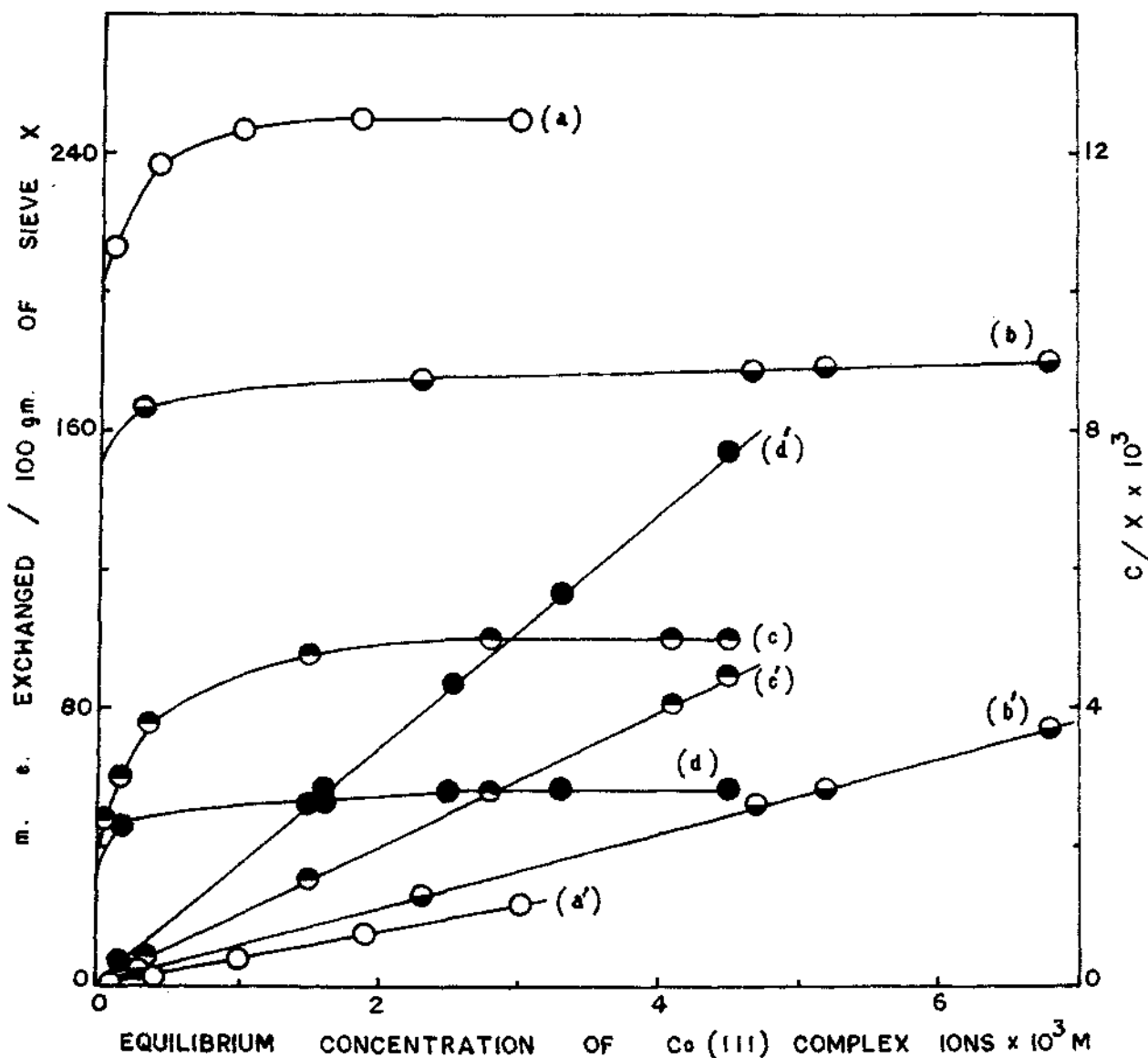


FIG. 109. EXCHANGE ISOTHERMS OF (a) $\text{Co}(\text{NH}_3)_6\text{Cl}_3$, (b) Coen_3Cl_3 , (c) Cotn_3Cl_3 AND (d) Copn_3Cl_3 ON MOLECULAR SIEVE 13 X.

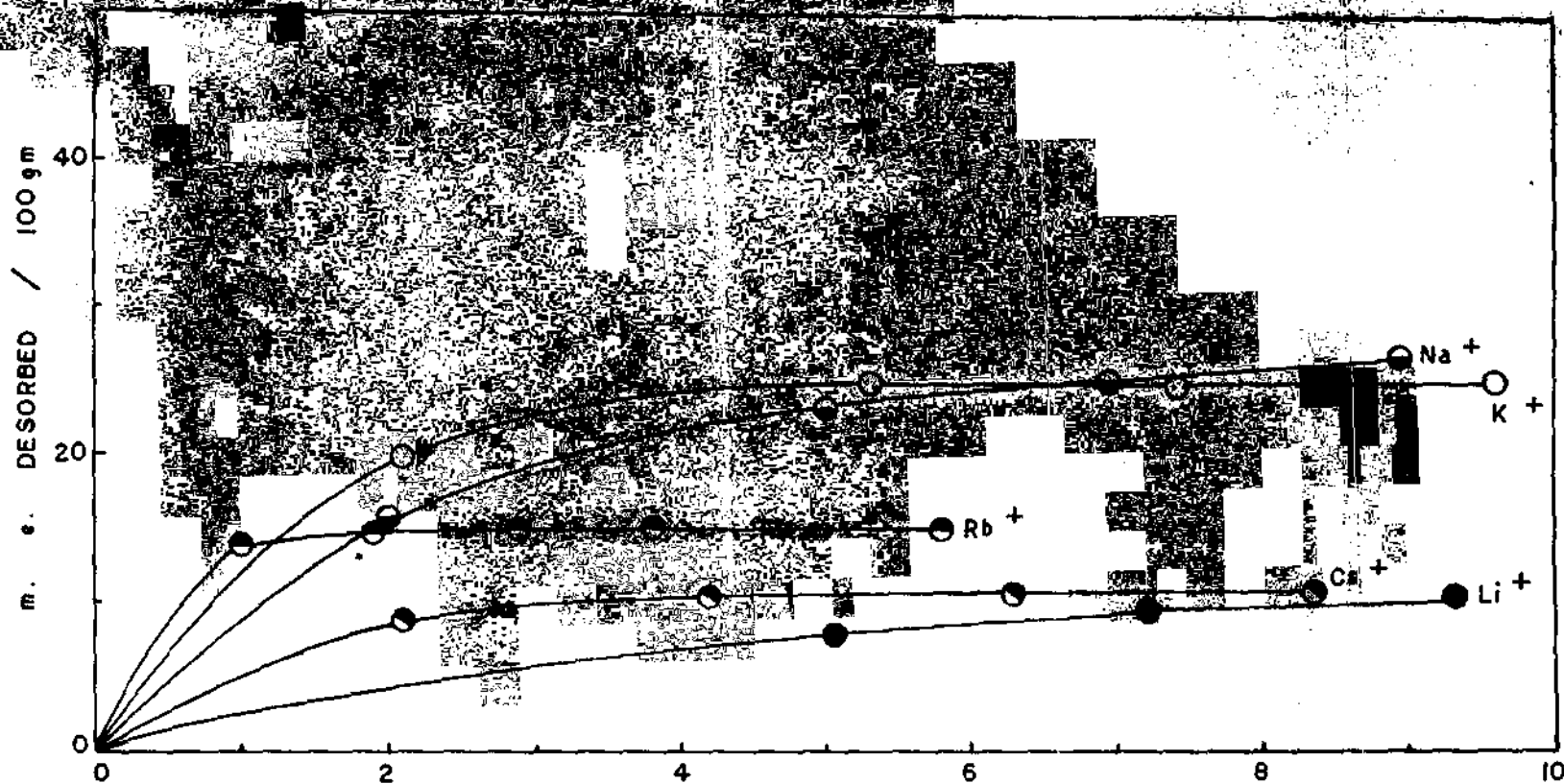


FIG. 110. DESORPTION OF $\text{Co}(\text{pn})_3^+$ FROM Na - $\text{Co}(\text{pn})_3$ - SIEVE, 13 X BY DIFFERENT IONS.

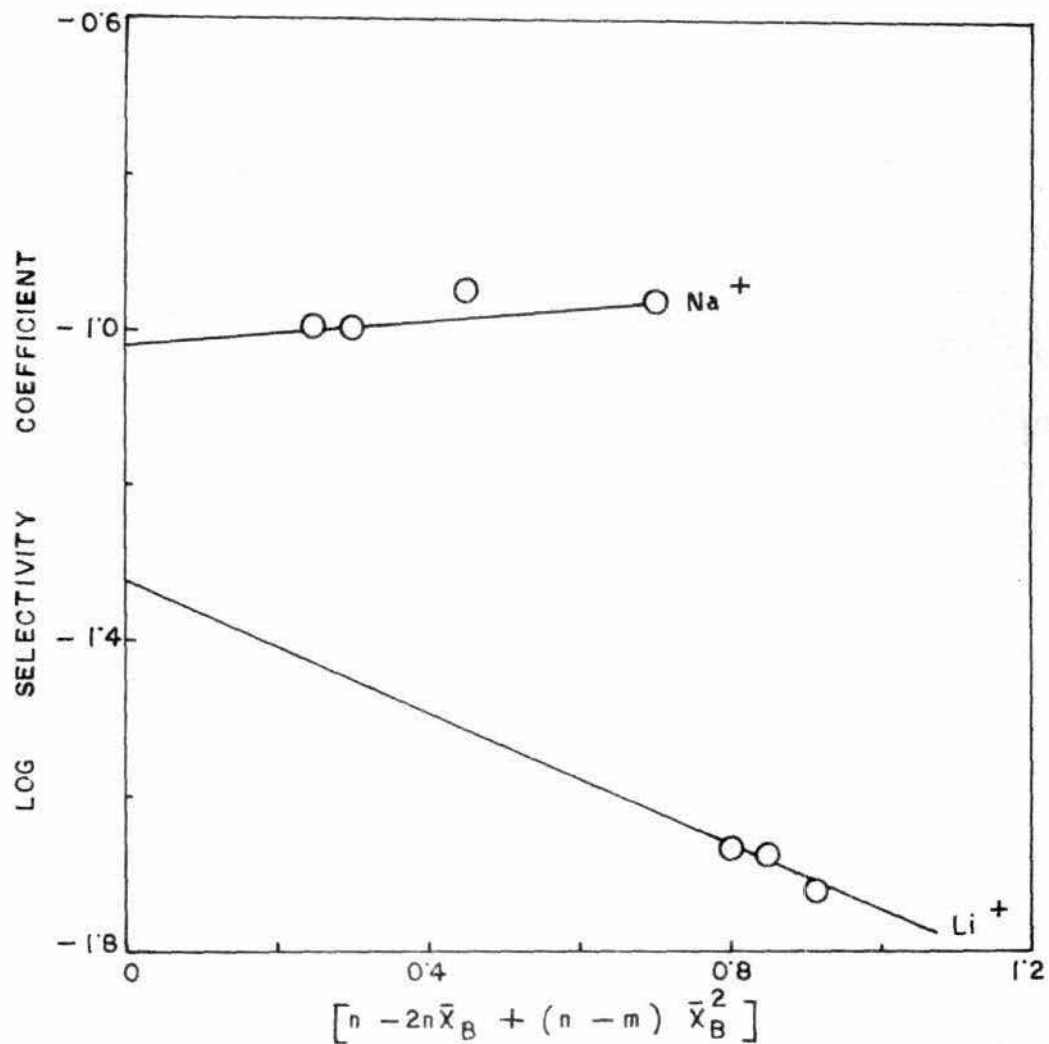
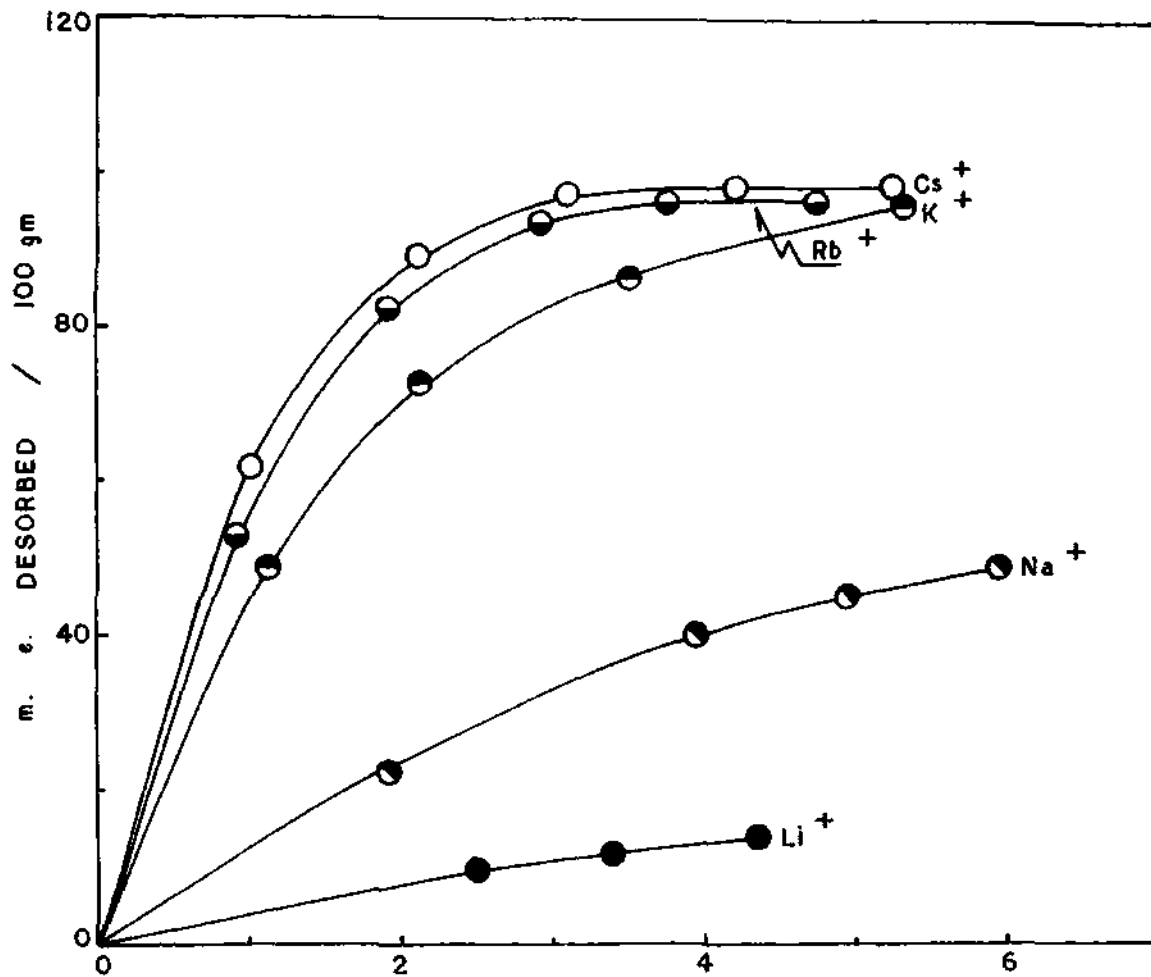


FIG. III. PLOT OF LOG SELECTIVITY COEFFICIENT AGAINST $n - 2n\bar{x}_B + (n - m)\bar{x}_B^2$ IN THE EXCHANGE OF $\text{Co}(\text{pn})_3^3+$ FROM $\text{Na} - \text{Co}(\text{pn})_3 - \text{SIEVE X}$ BY DIFFERENT IONS.



CONCENTRATION OF THE ELECTROLYTES ADDED $\times 10^3 \text{ M}$
 FIG. 112. DESORPTION OF $\text{Co}(\text{tn})_3^+$ FROM Na - $\text{Co}(\text{tn})_3$ -
 SIEVE 13 X BY DIFFERENT IONS.

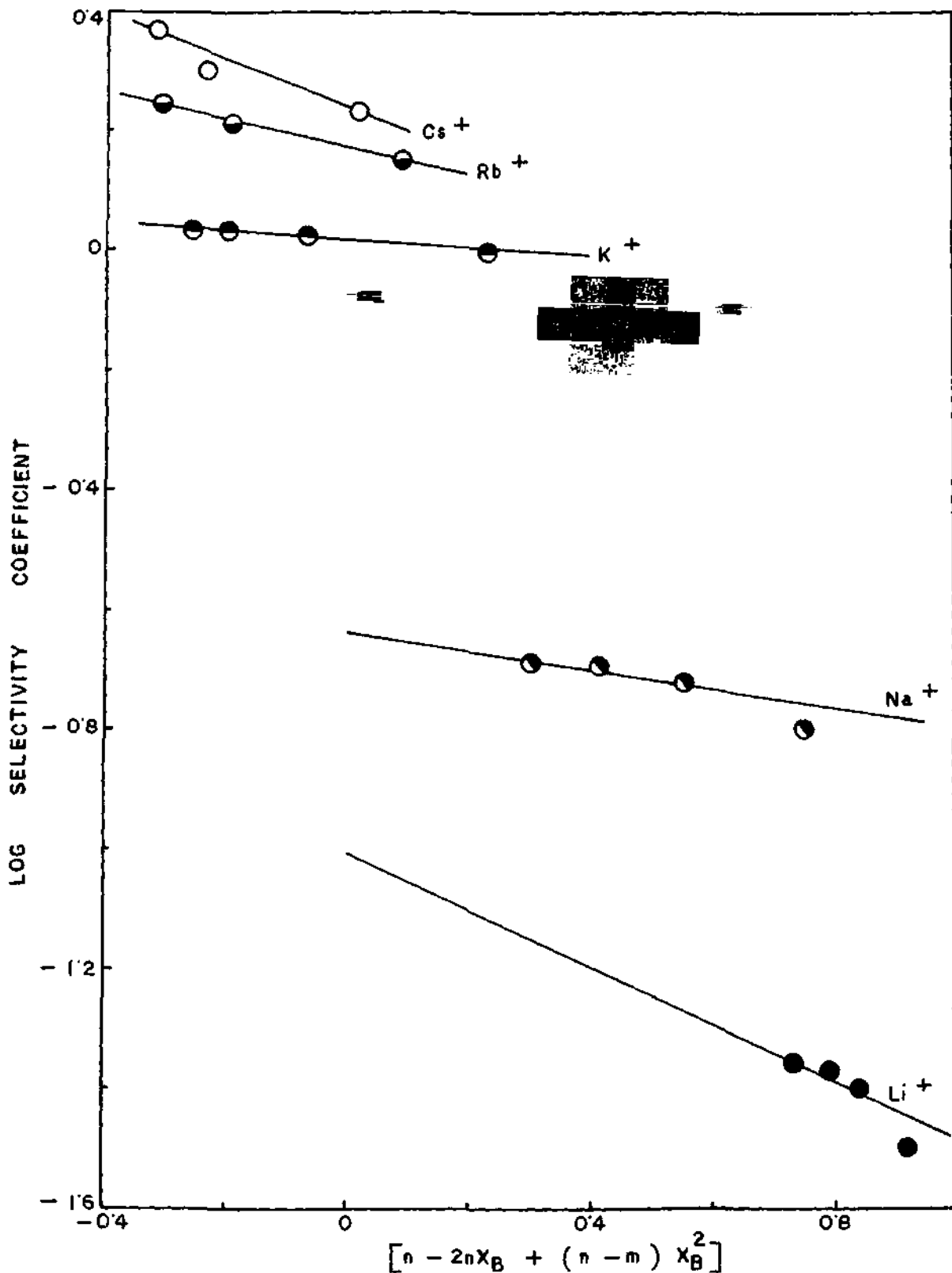


FIG. 113. PLOT OF LOG SELECTIVITY COEFFICIENT AGAINST $n - 2n\bar{X}_B + (n - m)\bar{X}_B^2$ IN THE EXCHANGE OF $\text{Co}(\text{tn})_3^{3+}$ FROM Na - $\text{Co}(\text{tn})_3$ - SIEVE X BY DIFFERENT IONS.

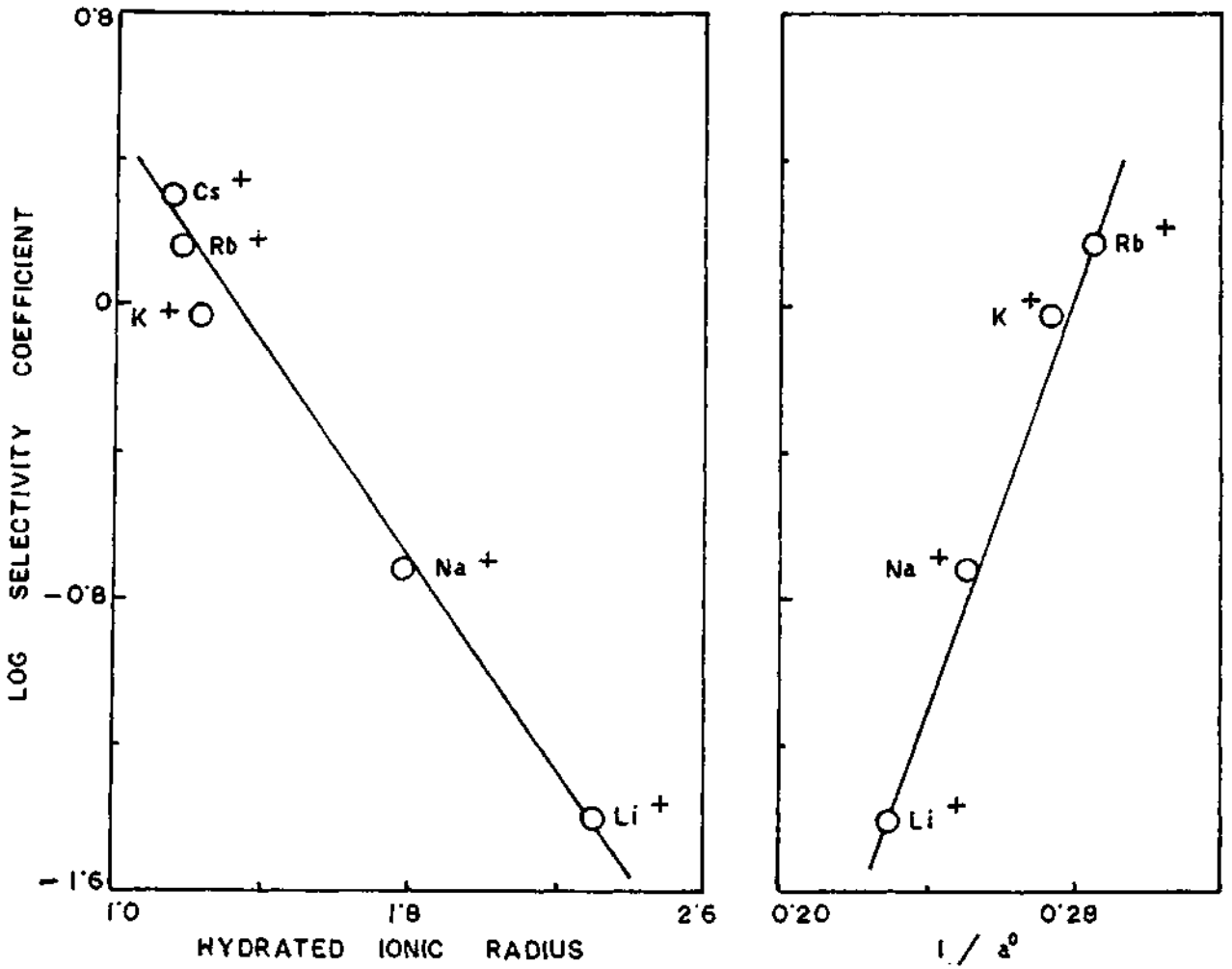


FIG. 114. CORRELATION OF SELECTIVITY COEFFICIENT WITH HYDRATED IONIC RADIUS AND DEBYE HÜCKEL PARAMETER a° IN THE DESORPTION OF Na - Cotn₃ - SIEVE 13 X.

CHAPTER - IX

Summary and Conclusion

The structures of the clay minerals, namely, kaolinite, montmorillonite, vermiculite and laponite are briefly described. A short review of the earlier work on adsorption and desorption of inorganic and organic ions on clay minerals and also on other substrates is presented in the introductory chapter (PP 1-29).

The methods of analyses and the preparation of materials, experimental details and the preparation of samples for X-ray diffraction, D.T.A. and B.E.T. surface area analysis are described in chapter III (PP 36-44).

The data of the adsorption experiments of $\text{Co}(\text{pn})_3\text{Cl}_3$ and $\text{Co}(\text{tn})_3\text{Cl}_3$ on H-bentonite and Na-bentonite are found to fit in with the Langmuir equation. The amount of $\text{Co}(\text{pn})_3^{3+}$ and $\text{Co}(\text{tn})_3^{3+}$ adsorbed on H-bentonite is less than the c.e.c. of the clay. This may be due to the low pH of the solution but as the pH is increased the adsorption of both the trivalent cations increases, indicating that two categories of H^+ are present in bentonite.

The adsorption at low pH probably corresponds to exchange due to isomorphous lattice replacement whereas the high adsorption value at higher pH corresponds to the sorption at the edges

primarily caused by Si-O and Al-O sites. Desorption studies with HCl also indicate two types of exchange sites. B.E.T. surface area, X-ray diffraction and D.T.A. studies of H-Co(pn)₃-bentonite and Na-Co(pn)₃-bentonite complexes throw considerable light on the mechanism of interaction. The exchange of Co(pn)₃³⁺ for Na⁺ is found to be extremely favourable, with a tendency toward segregation of the two kinds of cations in the mixed clays studied. Interestingly, it is observed that small amounts of Co(pn)₃³⁺ are found to lower the nitrogen sorption capacity of Na-bentonite or H-bentonite, while clays with high Co(pn)₃³⁺ content greatly enhance the sorption. The results has been explained by assuming two kinds of exchange sites on the clay that Co(pn)₃³⁺ can occupy and the exchange occurs on the clay edges first and then on the flat surfaces. The decrease in surface area could be caused due to the covering of the edge area ^{and/or face to face} by edge to edge binding of the clay platelets by the multivalent Co(pn)₃³⁺ and the resulting larger, denser aggregates would have a corresponding lower external surface area. Furthermore, in the D.T.A. curves little difference was seen between 60% and 100% Co(pn)₃³⁺ exchanged bentonites but the D.T.A. curve for the 20% exchanged sample was significantly different from the former curves. This observation may also relate to the change in the environment of a Co(pn)₃³⁺ cation as the occupancy of the clay exchange sites by the Co(pn)₃³⁺ increases. Similar X-ray diffraction

and D.T.A. studies of H-Co(tn)₃-bentonite and Na-Co(tn)₃-bentonite complexes are also done to interpret the mechanism of interaction. (PP 46-62)

The desorption of the two trivalent Co(III) complex ions from their respective bentonite complexes by the monovalent and bivalent inorganic ions follows the usual lyotropic series. The selectivity coefficients and the thermodynamic equilibrium constants indicate that the quaternary ammonium ions desorb more than the smaller inorganic ions. The extent of release of the above two complex ions from the bentonite surface follows the order: $(C_4H_9)_4N^+ > (C_3H_7)_4N^+ > (C_2H_5)_4N^+ > (CH_3)_4N^+$ at lower concentrations of the electrolytes but at higher concentrations the above sequence is just reversed. This interesting exchange behaviour of the quaternary salts has been explained by assuming contraction of the silicate layers in suspension once a critical level of surface coverage by the large alkyl ammonium ions has been reached. However, the desorbing efficiency of the long chain surface active ions are in the sequence : CP > CTA > DDTA > DTA, which is in the reverse order of their c.m.c. values. Further it is interesting to note that the smaller quaternary ions like $(CH_3)_4N^+$ or $(C_2H_5)_4N^+$ desorb more Co(pn)₃³⁺ or Co(tn)₃³⁺ from the bentonite surface than the long chain CP⁺ or CTA⁺ ions. This effect may be due to the covering-up of some of the exchange sites by the long chain organic ions. (PP 64 - 76)

It is observed that the swelling properties of the air dry (51% r.h.) mixed $\text{Co}(\text{pn})_3$ -tetra alkyl ammonium bentonites, determined by measuring d_{001} spacing by X-ray diffraction, depend strongly on the proportion of the ions. For instance, the $\text{Co}(\text{pn})_3$ - $(\text{CH}_3)_4\text{N}^+$ - bentonite system shows a gradual increase in d_{001} spacing as the % of $(\text{CH}_3)_4\text{N}^+$ in the clay phase is increased and reaches a constant value of 14.4 \AA at about 65% $(\text{CH}_3)_4\text{N}^+$ saturation and further exchange by $(\text{CH}_3)_4\text{N}^+$ does not alter this spacing. This indicates random interstratification of $\text{Co}(\text{pn})_3^{3+}$ and $(\text{CH}_3)_4\text{N}^+$ layers from 0 to 65% exchange while beyond 65% there is apparent ion-homogeneity. Similar conclusion has been drawn in the case of other $\text{Co}(\text{pn})_3$ -tetra alkyl ammonium bentonites on the basis of X-ray data. (PP 71-72).

The exchange of EDA and PrDA (alkane diammonium ions) present a smaller affinity for the bentonite as compared with the n-tetra alkyl ammonium ion

It is also observed from the d_{001} basal spacings of the bentonite - $\text{Co}(\text{III})$ -complexes at different humidities that the adsorption of $\text{Co}(\text{pn})_3$ or $\text{Co}(\text{tn})_3$ in bentonite suppresses the effect of swelling or expansion in moisture i.e. a water-proof character is developed. (PP 54-55).

It is observed that the values of the selectivity coefficients and the thermodynamic equilibrium constant are

greater in the desorption of $\text{Co}(\text{pn})_3^{3+}$ from Na-Copn₃-bentonite than those obtained from H-Copn₃-bentonite. Therefore, it may be said that $\text{Co}(\text{pn})_3^{3+}$ is attached to the Na-bentonite with a smaller affinity than H-bentonite. A similar behaviour is also noticed in the case of $\text{Co}(\text{tn})_3^{3+}$ for bentonite. The amounts of the ions desorbed from bentonite are in the order: $\text{Co}(\text{tn})_3^{3+} < \text{Co}(\text{pn})_3^{3+}$ (PP 63-77).

Almost all the desorption isotherms fit in with Nielland's equation from which the thermodynamic equilibrium constant and the standard Gibbs free energy change have been calculated. In all case, the plot of log (selectivity coefficient) vs. reciprocal of Debye Huckel parameter a^0 gives a better correlation than the hydrated ionic radius. Thus the parameter a^0 may be utilised to correlate the affinities of the ions for the mineral surface.

The adsorption isotherms of $\text{Co}(\text{pn})_3^{3+}$ and $\text{Co}(\text{tn})_3^{3+}$ on H-vermiculite and Na-vermiculite show that they fit in well with the Langmuir equation. As in the case of bentonite, here also adsorption with both the trivalent complex cations mentioned above increases with pH. This may be explained by assuming two types of H^+ present in vermiculite. X-ray diffraction data and D.T.A. studies have also helped to understand more completely the type of interaction that might be taking place between $\text{Co}(\text{pn})_3^{3+}$ ion and the vermiculite (PP 30-33).

The desorption isotherms with inorganic and organic ions are almost alike, as observed in bentonite, except with $(\text{CH}_3)_4\text{N}^+$, $(\text{C}_2\text{H}_5)_4\text{N}^+$, $(\text{C}_3\text{H}_7)_4\text{N}^+$ and $(\text{C}_4\text{H}_9)_4\text{N}^+$. With these organic ions, the amount desorbed is much smaller than in the case of bentonite and the relative order of desorbing power is also reversed. This behaviour has been explained on the basis of the known crystalline structure of vermiculite together with its limited c-axis expansion and the dimensions of these large tetra alkyl ions.

The thermodynamic equilibrium constants of some of the exchange reactions have been evaluated with the help of Kielland's equation. Gibbs free energy change at 25°C has been calculated from the relation $\Delta G^\circ = -RT \ln K$.

As observed with bentonite, the plot of \log (selectivity coefficient) against the reciprocal of Debye Huckel parameter a° is linear but when the former is plotted against the hydrated ionic radius, linearity is not observed. The behaviour of bivalent exchanging ions however is different from those of the monovalent ions in this respect. This deviation may result from the irregular hydration as well as the characteristic behaviour of Mg^{2+} towards the vermiculite surface. The results suggest that in such a process of desorption of $\text{Co}(\text{pn})_3^{3+}$ or $\text{Co}(\text{tn})_3^{3+}$ by smaller inorganic cations, the parameter a° rather than the hydrated ionic radius may be used to correlate the affinities of the monovalent ions for the vermiculite.

The desorption curves of $\text{Co}(\text{pn})_3^{3+}$ and $\text{Co}(\text{tn})_3^{3+}$ from vermiculite as well as the selectivity coefficients and thermodynamic equilibrium constants suggest that they are desorbed in the order : $\text{Co}(\text{pn})_3^{3+} < \text{Co}(\text{tn})_3^{3+}$, which is the reverse as observed in the case of bentonite. (PP 87-94)

The data of the adsorption experiments of $\text{Co}(\text{pn})_3\text{Cl}_3$ and $\text{Co}(\text{tn})_3\text{Cl}_3$ on Na-Laponite fit in with the Langmuir equation (P 97).

The desorption isotherms with inorganic and organic ions are almost alike, as observed in bentonite, except with tetra alkyl ammonium ions and surface active ions. It is noted that the amount of $\text{Co}(\text{pn})_3^{3+}$ or $\text{Co}(\text{tn})_3^{3+}$ desorbed from their respective laponite complexes by CP^+ or CTA^+ is greater than the smaller $(\text{CH}_3)_4\text{N}^+$ or $(\text{C}_2\text{H}_5)_4\text{N}^+$. This is unlike that observed in the case of similar studies in bentonite system.

Most of the desorption isotherms fit in with Kielland's equation from which the thermodynamic equilibrium constant and the standard Gibbs free energy change have been calculated. In all cases, the plot of \log (selectivity coefficient) vs. reciprocal of Debye-Huckel parameter a^0 gives a better correlation than the hydrated ionic radius.

The desorption curves of $\text{Co}(\text{pn})_3^{3+}$ and $\text{Co}(\text{tn})_3^{3+}$ from Laponite as well as the selectivity coefficients and thermodynamic equilibrium constants suggest that they are desorbed

in the order: $\text{Co}(\text{tn})_3^{3+} < \text{Co}(\text{pn})_3^{3+}$, which is the same as observed in the case of bentonite. (PP 98-101)

The exchange isotherms and the reciprocal plots of $\text{Co}(\text{pn})_3^{3+}$ and $\text{Co}(\text{tn})_3^{3+}$ exchange data on Ma-IRC-50 agree with the Langmuir equation. The maximum exchange is much less than the cation exchange capacity in both the cases. The lower value may be caused by the physical inaccessibility of the resin to the large sized trivalent complex cations.

It is noted that in the desorption of $\text{Co}(\text{pn})_3^{3+}$ and $\text{Co}(\text{tn})_3^{3+}$ by monovalent ions from this resin, the general lyotrope series is just reversed except in the position of NH_4^+ and H^+ , which is not observed with bentonite, vermiculite or laponite. It is also interesting to note that all the isotherms obtained with monovalent inorganic ions except H^+ are S-shaped. The results are explained on the basis of the hydrophobic character of $\text{Co}(\text{pn})_3$ -resin or $\text{Co}(\text{tn})_3$ -resin complex as well as solvation of the desorbing ions.

With quaternary ammonium ions, such as $(\text{CH}_3)_4\text{N}$, $(\text{C}_2\text{H}_5)_4\text{N}$, $(\text{C}_3\text{H}_7)_4\text{N}$, CTA, CP and DDTA the amount desorbed from the corresponding resin complex is much smaller than in the case of bentonite or laponite. This may be due to a very strong affinity of $\text{Co}(\text{pn})_3^{3+}$ or $\text{Co}(\text{tn})_3^{3+}$ for the resin and the comparatively large dimension of the quaternary ammonium ions.

The desorption data for the monovalent and bivalent ions fit in with Kielland's equation. The results of desorption of $\text{Co}(\text{tn})_3^{3+}$ from its resin complex show that the fraction of the $\text{Co}(\text{tn})_3^{3+}$ desorbed is higher than that observed in the case of $\text{Co}(\text{pn})_3^{3+}$.

In the case of desorption of $\text{Co}(\text{pn})_3^{3+}$ and $\text{Co}(\text{tn})_3^{3+}$ from their respective resin complexes, the plots of log (selectivity coefficient) vs. hydrated ionic radius as well as reciprocal of Debye-Huckel parameter a^0 give linear graphs. It may be noted that in the case of clay minerals studied, a similar plot of log (selectivity coefficient) vs. hydrated ionic radius is never linear.

In order to ascertain the role of ionic hydration, desorption studies have also been done in 50% aqueous ethanolic medium from Na- $\text{Co}(\text{pn})_3$ -IRC-50 and Na- $\text{Co}(\text{tn})_3$ -IRC-50 resin with Li^+ , Na^+ , K^+ , Rb^+ and Cs^+ . It is observed that in each case the amount desorbed is larger than in the pure aqueous medium.

The desorption isotherms of $\text{Co}(\text{pn})_3^{3+}$ and $\text{Co}(\text{tn})_3^{3+}$ from their respective resin complexes together with the selectivity coefficients and equilibrium constants indicate that they are desorbed from the resin in the order: $\text{Co}(\text{pn})_3^{3+} < \text{Co}(\text{tn})_3^{3+}$, the same as observed in the case of vermiculite studied in the present investigation (PP 104-111).

The exchange isotherms and the reciprocal plots of $\text{Co}(\text{NH}_3)_6\text{Cl}_3$, Coen_3Cl_3 , $\text{Coptn}_3\text{Cl}_3$ and Cotn_3Cl_3 exchange data on Linde Molecular Sieve 13X agree with the Langmuir equation. The maximal levels of exchange of $\sim 40\%$, $\sim 30\%$, $\sim 16\%$ and $\sim 10\%$ observed in Molecular sieve 13X with $\text{Co}(\text{NH}_3)_6^{3+}$, Coen_3^{3+} , $\text{Co}(\text{tn})_3^{3+}$ and $\text{Co}(\text{pn})_3^{3+}$ cations respectively. The incomplete exchange may be caused by the physical inaccessibility of the Sieve X to the large sized trivalent complex cations. (P 117).

It is also noted that in the desorption of $\text{Co}(\text{pn})_3^{3+}$ by monovalent ions from this Sieve X, the ions may be placed at low concentrations in the order: $\text{Rb}^+ > \text{K}^+ > \text{Na}^+ > \text{Cs}^+ > \text{Li}^+$ and at higher concentrations in the order: $\text{Na}^+ > \text{K}^+ > \text{Rb}^+ > \text{Cs}^+ > \text{Li}^+$. This selectivity sequence for the alkali ions does not correlate with the results for the resin. But the desorption of $\text{Co}(\text{tn})_3^{3+}$ by alkali ions from its molecular sieve complex follows the usual lyotrope series. (P. 119)

In the case of desorption of $\text{Co}(\text{tn})_3^{3+}$ from its Molecular Sieve complex, the plot of $\log(\text{selectivity coefficient})$ vs. hydrated ionic radius as well as reciprocal of Debye-Huckel parameter a^0 give linear graphs. It may be noted that in the case of desorption of $\text{Co}(\text{pn})_3^{3+}$ from its Molecular Sieve complex, a similar plot of $\log(\text{selectivity coefficient})$ vs. hydrated ionic radius as well as reciprocal of

Debye-Hückel parameter a° is not linear.

Almost all the desorption isotherms fit in with Mielland's equation from which the thermodynamic equilibrium constant and the standard free energy change have been calculated.

It is clear from the above that various attempts have been made to present a comprehensive picture on different aspects of exchange-equilibrium. In respect of sorption and desorption characteristics some uniformity has been observed while bentonite, laponite and vermiculite are the exchangers. With regard to the exchange characteristics, the carboxylated resin and the molecular sieve 13X exhibit a somewhat different picture. This is however understood while the peculiarity of the latter exchangers is recalled (PP 102, 103). The order of preference of ions for the clay minerals, the resin surface and the Molecular Sieve 13X against the two complex cations are summarised below: (Cf. Table 29).

Table 29

The order of preference of the ions for the silicate, resin and molecular sieve surface against the different trivalent complex cations.

Exchanger	H-Copn ₃ -Complex	Na-Copn ₃ -Complex	H-Co ₃ n ₃ -Complex	Na-Co ₃ n ₃ -Complex
Bentonite	Li < Na ≍ H < K < NH ₄ < Rb < Cs Mg < Ca < Sr < Ba (CH ₃) ₄ N ≍ (C ₂ H ₅) ₄ N ≍ (C ₃ H ₇) ₄ N ≍ (C ₄ H ₉) ₄ N < DTA < CTA < CP EDA < PrDA	Li < Na < H < K < NH ₄ < Rb < Cs Mg < Ca < Sr < Ba (CH ₃) ₄ N ≍ (C ₂ H ₅) ₄ N ≍ (C ₃ H ₇) ₄ N ≍ (C ₄ H ₉) ₄ N < DTA < DDTA < CTA < CP EDA < PrDA	Li < Na < H < K < NH ₄ < Rb < Cs Mg < Ca < Sr < Ba (CH ₃) ₄ N ≍ (C ₂ H ₅) ₄ N ≍ (C ₃ H ₇) ₄ N ≍ (C ₄ H ₉) ₄ N < DTA < DDTA < CTA < CP EDA < PrDA	Li < Na < K ≍ NH ₄ ≍ H < Rb < Cs Mg < Ca < Sr < Ba (CH ₃) ₄ N ≍ (C ₂ H ₅) ₄ N ≍ (C ₃ H ₇) ₄ N ≍ (C ₄ H ₉) ₄ N EDA < PrDA < DTA < DDTA < CTA < CP
Vermiculite		Li < Na < NH ₄ < K < H ≍ Rb < Cs Ca < Mg < Sr < Ba (C ₄ H ₉) ₄ N < (C ₃ H ₇) ₄ N < (C ₂ H ₅) ₄ N < (CH ₃) ₄ N < EDA < PrDA ≍ CTA < CP		Li < Na < NH ₄ ≍ K < Rb < H < Cs Mg ≍ Sr < Ca < Ba (C ₄ H ₉) ₄ N < (C ₃ H ₇) ₄ N < (C ₂ H ₅) ₄ N < (CH ₃) ₄ N < EDA < PrDA < DTA < DDTA < CTA < CP

Table 29 (Contd..)

Exchanger	H-Copn ₃ -Complex	Na-Copn ₃ -Complex	H-Cotn ₃ -Complex	Na-Cotn ₃ -Complex
Laponite		Li < Na < K < NH ₄ < Rb < Cs < H Mg < Ca < Sr < Ba (CH ₃) ₄ N < (C ₂ H ₅) ₄ N < (C ₃ H ₇) ₄ N < (C ₄ H ₉) ₄ N < DTA < DDTA < CTA < CP EDA < PrDA		Li < Na < K < NH ₄ < Rb < Cs < H Mg < Ca < Sr < Ba (CH ₃) ₄ N < (C ₂ H ₅) ₄ N < (C ₃ H ₇) ₄ N < (C ₄ H ₉) ₄ N < DTA < DDTA < CTA < CP EDA < PrDA
Resin		Cs < Rb < K < Na < Li < NH ₄ < Mg < Ca < Sr < Ba < H (C ₄ H ₉) ₄ N < (C ₃ H ₇) ₄ N < (C ₂ H ₅) ₄ N < (CH ₃) ₄ N < DDTA < CTA < CP < PrDA < EDA		H > NH ₄ > Li > Na > K > Rb > Cs Ba > Sr > Ca > Mg EDA > PrDA > CP > CTA > DDTA > (CH ₃) ₄ N > (C ₂ H ₅) ₄ N > (C ₃ H ₇) ₄ N

Table 29 (Contd..)

Exchanger	H-Copn ₃ -Complex	Na-Copn ₃ -Complex	H-Co ₃ n ₃ -Complex	Na-Co ₃ n ₃ -Complex
Molecular Sieve 13X		<p>Rb > K > Na > Cs > Li at low concentrations and Na > K > Rb > Cs > Li at higher concentrations</p>		<p>Cs > Rb > K > Na > Li</p>

B I B L I O G R A P H Y

1. Pauling, L. Proc. Natl. Acad. Sci. U.S., 16, 578, 1930.
2. Bragg, W.L. Atomic Structure of Minerals. Cornell Univ. Press, Ithaca, 1937.
3. Gruner, J.W. Z.Krist. 83, 75, 1932.
4. Brindley, G.W. and Robinson, K. Mineralogy Mag., 27, 242, 1946.
5. Hofmann, U., Edell, K. and Wilm, D. Z. Krist., 86, 340, 1933.
6. Marshall, C.E. ibid., 91, 433, 1935.
7. Hendricks, S.B. and Jefferson, M. Am. Mineral, 24, 729, 1939.
8. Mauguin, C.H. Bull. Soc. Franc. Mineral, 51, 285, 1928.
9. Jackson, W.W. and West, J. Z. Krist., 85, 160, 1933.
10. Mc Murchy, R.C. ibid., 88, 420, 1934.
11. Barshad, I. Am. Mineral, 34, 675, 1949
12. Walker, G.F. Nature, 163, 726, 1949.
13. Grim, R.E., Bradley, W.F. and Brown, G. The Mica clay Minerals. Chap. V, pp 138-172, Mineralogical Society of Great Britain Monograph, 1951.
14. Mac Ewan, D.M.C. J. Soil Sci., 1, 90, 1949.
15. Kelley, W.P. "Cation Exchange in Soils", Reinhold, New York, 1948.

Table 29 speaks for itself. Although in point of this exchange-behaviour, the alumino silicates are almost similar, occasional differences originate from their architectural dissimilarities as also from specificities of certain ions which are involved in the process. As pointed out earlier (PP 68-69) the geometric factor plays a significant role in such a fixation process. This is also in agreement with the expected values of selectivity coefficient, thermodynamic equilibrium constant and Gibbs free energy.

The sequence of the desorbing ions have also been justified from the above quantities. It should also be mentioned, in the conclusion, that throughout the present investigation attempts have been made to explain the data in quantitative language whenever possible. For this purpose, valuable theoretical models (PP 19-21) have been employed.

In addition to different quantitative methods, empirical approaches have also been given their due credit for a satisfactory interpretation of the experimental data.

(II)

16. Marshall, C.E. and Krinbill, C.A. J.Phys.Chem., 46, 1077, 1942.
17. Page, J.B. and Bayer, L.D. Proc. Soil Sci. Soc. Am., 4, 150, 1939.
18. Bar, A.L.S. and Tenderloo, H.J.E. Koll.Beih., 14, 97, 1936.
19. Hendricks, H.B. and Alexander, L.T. Proc. Soil Sci. Soc. Am., 5, 95, 1940.
20. Schachtschabel, P. Koll.Beih., 51, 199, 1940.
21. Mukherjee, S.K. Indian Soc. Soil Sci. Bull., 6, 67, 1951.
22. Marshall, C.E. 'The Colloid Chemistry of Silicate Minerals', Academic Press, Inc., N.Y., 1949.
23. Grim, R.E. Clay Mineralogy: MC Graw-Hill Book Co., Inc., New York. P 384, 1953.
24. Smith, C.R. J.Am.Chem.Soc., 56, 1561, 1934.
25. Gieseking, J.E. Advances in Agron., 1, 598, 1949.
26. Gieseking, J.E. and Easminger, L.E. Soil Sci., 51, 125, 1941.
27. Chakravarti, S.K. J.Indian Soc. Soil Sci., 5, 90, 1957.
28. Daskanungo, J.L. Clays and Clay Minerals, 23, 361, 1975.
29. Daskanungo, J.L. and Chakravarti, S.K. J.Colloid and Interface Sci., 35, 295, 1971.
30. Renold, A. Kolloid Beih., 43, 1, 1936.
31. Jenny, H and Engabaly, M.M. J.Phys.Chem., 47, 399, 1943.
32. Basu, A.N. and Mukherjee S.K. J.Indian Soc. Soil Sci., 14, 95, 1966.

(III)

33. Basu, A.N. and Mukherjee, S.K. *ibid*, 13, 251, 1965.
34. Martin, I and Glaeser, R. Bull. Groupe Franc. Argiles, 12, 88, 1960.
35. Mc Connel, Bobby L and Mastman, Russel W. Jour. Miss. Acad. Sci., 8, 169, 1962.
36. Matsuura, T. J.Inorg.Nucl.Chem., 27, 2269, 1965.
37. Kayas, G. and Sue, P. Bull. Soc. Chem. France, 17, 1145, 1950.
38. Ikeda, N, Yoshihara, K and Yamagishi, S. Bull. Chem.Soc. Japan, 34, 139, 1961.
39. Costea, T. J.Inorg.Nucl. Chem., 18, 27, 1961.
40. Saito, N, Tominaga, T and Sano, H. *ibid*, 24, 1539, 1962.
41. Chakravarti, S.K. and Laitinen, H.A. N.S.F. Report (U.S.A), 1962.
42. Daskanungo, J.L., Chakravarti S.K. and Mukherjee, S.K. J.Indian Chem. Soc., 44, 339, 1967.
43. Daskanungo, J.L., Chakravarti, S.K. and Mukherjee, S.K. *ibid*, 45, 685, 1968.
44. Daskanungo, J.L. and Chakravarti, S.K. Kolloid. Z.u.Z. Polymere 251, 154, 1973.
45. Thielmann, V.J. and McAtee, Jr. J.L. J.Chromatography, 105, 115, 1975.
46. Knudson, Jr. M.I. and McAtee, Jr. J.L. Clays and Clay Miner, 21, 19, 1973.
47. Barrer, R.M., Davies, J.A. and Rees, L.V.C. J.Inorg.Nucl. Chem., 31, 232, 1969.
48. Barrer, R.M. and Townsend, R.P. J.Chem.Soc., Faraday Trans. 1, 72, 2650, 1976.

(IV)

49. Smith, C.R. J.Am.Chem.Soc., 56, 1561, 1934.
50. Gieseking, J.E. Soil Sci., 47, 1, 1939.
51. Gieseking, J.E. and Ensminger, L.E. ibid, 48, 467, 1939.
52. Idem ibid, 53, 205, 1942.
53. German, W.L. and Harding, D.A. Clay Miner., 8, 213, 1969.
54. Hoffmann, R.W. and Brindley, G.W. Geochim. Cosmochim. Acta, 20, 15, 1960.
55. Mac Ewan, D.M.C. Trans. Faraday Soc., 44, 349, 1948.
56. Barshad, I. Soil Sci.Soc. Am.Proc., 16, 176, 1952.
57. Brindley, G.W. and Ray, S. Am. Mineralogist, 49, 106, 1964.
58. Glaeser, R. Clay Miner. Bull, 1, 88, 1948.
59. Kutilek, M. and Salingerova, J. Soil Sci, 101, 385, 1966.
60. Greene-Kelly, R. J.Colloid Sci, 11, 77, 1956.
61. Greenland, D.J., Quirk, J.P. and Theng, B.K.G. J.Colloid Sci, 19, 837, 1964.
62. Slabaugh, W.H. and Carter, L.S. J.Colloid Interface Sci, 27, 235, 1968.
63. Brooks, C.S. Soil Sci, 99, 182, 1965.
64. Lagaly, G., Stange, H., and Weiss, A. Kolloid Z.Z.Polym., 250, 675, 1972.
65. Greenland, D.J., Laby, R.H. and Quirk, J.P. Trans. Faraday Soc., 61, 2013, 1965.

(V)

66. Vansant, E.F. and
Uytterhoevan, J.B. Clays Clay Miner., 20,
47, 1972.
67. Schofield, R.K. J. Soil Sci, 1, 1, 1949.
68. Sen, B.C. D.Phil. Thesis, Calcutta
University, 1959.
69. Greenland, D.J.,
Laby, R.H. and
Quirk, J.P. Trans. Faraday Soc., 61,
2035, 1965.
70. De, D.K., Chakravarti,
S.K. and Mukherjee,
S.K. J. Indian Chem.Soc., 45,
570, 1963.
71. Mukherjee, S.K. Prof. J.N.Mukherjee's 60th
Birthday Commemoration Vol.,
p. 127, 1953.
72. Weigner, G. G.Zum Basenaustausch in der
Ackererde, J.Land. 60, 111,
197, 1922.
73. Marshall, C.E. and
Gupta, R.S. J.Soc.Chem. Ind., 52,
433T, 1933.
74. Vageler, P. Der Kationen und. Mineral
haushalt des Mineralbod ens,
Springer, Berlin, 1932.
75. Ganssen, R. Centr. Mineral Geol. Palaout.,
728, 1913.
76. Kerr, H.W. J.Am.Soc.Agron., 20, 309,
1928.
77. Bauman, W.C. J.Am.Chem.Soc., 69, 2830,
1947.
78. Gregor, H.P. ibid, 69, 1293, 1948.
79. Boyd, G.E., Schubert,
J. and Adamson, A.W. ibid, 69, 2818, 1947.
80. Vanselow, A.P. Soil. Sci., 33, 95, 1932.

(VI)

81. Wiegner, G. Trans. 3rd Intern. Cong. Soil Sci., 3, 5, 1935.
82. Jenny, H. J.Phys. Chem., 40, 501, 1936.
83. Davis, L.E. ibid, 49, 473, 1945.
84. Krishnamoorthy, C and Overstreet, R. Soil Sci., 48, 307, 1949.
85. Fowler, R.H. Statistical Mechanics, 1936.
86. Guggenheim, E.A. J.Phys. Chem., 33, 842, 1929.
87. Mukherjee, J.N. Trans. Farad. Soc., 16, 103, 1920-21.
88. Mukherjee, J.N. and Mitra, R.P. J.Coll. Sci., 1, 141, 1946.
89. Mitra, R.P. and Bagchi, S.N. J.Indian Soc. Soil Sci., 6, 1951.
90. Ganguly, A.K. and Mukherjee, S.K. J.Phys. Coll. Chem., 56, 1952.
91. Chakravarti, S.K. J.Indian Soc. Soil Sci., 2, 127, 1954.
92. Kielland, J. J.Soc. Chem. Ind., (London), 54, 232T, 1935.
93. Pauley, J.L. J.Am.Chem.Soc., 76, 1422, 1954.
94. Vanselow, A.P. ibid, 54, 1430T, 1932.
95. Shainberg, I and Kemper, W.D. Soil Sci., 103, 4, 1967.
96. Banin, A. Isr. J.Chem., 6, 27, 1968.
97. Carlson, R.M. and Overstreet, R. Soil Sci., 103, 213, 1967.
98. Clark, J.S. and Turner, R.C. Soil Sci.Soc. Amer. Proc., 29, 271, 1966.

(VII)

99. Foscolos, A.E. Soil Sci.Soc. Am. Proc., 32, 350, 1968.
100. Foscolos, A.E. and Barshad, I. ibid, 33, 242, 1969.
101. Gast, R.G., Van Bladel, R. and Deshpande, K.B. ibid, 33, 661, 1969.
102. Juo, A.S.R. and Barber, S.A. Soil Sci., 109, 143, 1970.
103. Kaddah, M.T. ibid, 106, 67, 1968.
104. Kunishi, M.M. and Heald, W.R. Soil Sci. Soc. Am. Proc., 32, 201, 1968.
105. Laudelout, H., Van Bladel, R. and Robeyns, J. Soil Sci., 111, 211, 1971.
106. Lin, C. and Coleman, N.T. Soil Sci. Soc. Am.Proc., 24, 44, 1960.
107. Sawhney, B.L. ibid, 28, 183, 1964.
108. idem. ibid, 29, 25, 1965.
109. Snyder, G.H., McLean, E.O., and Franklin, R.E. ibid, 33, 392, 1969.
110. Uehara, G. and Mortland, M.M. ibid, 24, 26, 1960.
111. Yaalon, D.H. and Koyumdjisky, H. Isr. J.Chem., 6, 189, 1968.
112. Cremers, A.E. and Thomas, H.C. ibid, 6, 949, 1968.
113. Franklin, R.E. and Snyder, G.H. Soil Sci. Soc. Am. Proc., 29, 508, 1965.
114. Gast, R.E. ibid, 33, 37, 1969.
115. idem ibid, 36, 14, 1972.

(VIII)

116. Daskanungo, J.L. and Chakravarti, S.K. Kolloid-Z & Z. Polym., 248, 953, 1971.
117. Uskova, E.T., Vasil'ev, N.G. and Uskov, I.A. Colloid J. USSR, 30, 118, 1968.
118. Tamers, M.A. and Thomas, H.C. J.Phys.Chem., 64, 29, 1960.
119. du Plessis M.C.F. and Kreontje, W. Soil Sci. Soc. Am.Proc., 31, 176, 1967.
120. Yaalon D.H. and Koyumdjisky, H. Soil Sci., 105, 403, 1968.
121. Gilbert, M. and Laudelout, H. ibid, 100, 157, 1965.
122. Deist, J. and Talibudeen, O. ibid, 104, 119, 1967.
123. Van Olphen, H. An Introduction to Clay Colloid Chemistry, Inter-Science Publishers, New York, N.Y, 241, 1963.
124. Mitra, R.P. and Kapoor, B.S. Soil Sci., 108, 11, 1969.
125. Bar-On, P. and Shainberg, I. Soil Sci., 109, 241, 1970.
126. Coleman, N.T. and Craig, D. ibid, 91, 14, 1961.
127. Eeckman, J.P. and Laudelout, H. Kolloid Z., 179, 99, 1961.
128. Kamil, J. and Shainberg, I. Soil Sci., 106, 193, 1968.
129. Pozer, W.L. and Hem, J.D. J.Geophys. Res., 70, 6233, 1965.
130. Barshad, I. Trans. Intern. Congr. Soil Sci., 7th, 2, 435, 1961.

(IX)

131. Riley, D. and Arnold, P.W. Soil Sci., 108, 414, 1969.
132. Banerjee, D.K., Bray, R.H. and Melsted, S.W. ibid, 75, 421, 1953.
133. Banin, A. Isr. J.Chem., 6, 27, 1968.
134. Hodgson, J.F. Soil Sci. Soc. Am. Proc., 24, 165, 1960.
135. Kown, B.T. and Ewing, B.B. Soil Sci., 108, 231, 1969.
136. Dolcater, D.L., Lotse, E.G., Syers, J.K. and Jackson, M.L. Soil Sci. Soc. Am. Proc., 32, 795, 1968.
137. Gilbert, M. Soil Sci., 109, 23, 1970.
138. Goldsmith W.A. and Middlebrooks, E.J. J.Am.Water Works Ass., 58, 1052, 1966.
139. Juo, A.S.R. and Barber, S.A. Soil Sci. Soc. Am. Proc., 33, 360, 1969.
140. McLean, E.O., Arscott, T.G. and Volk, V.V. ibid, 24, 453, 1960.
141. Rhoades, J.D. ibid, 31, 361, 1967.
142. Van Bladel, R. and Laudelout, H. Soil Sci., 104, 134, 1967.
143. McLean, G.W., Pratt, P.F. and Page, A.L. Soil Sci. Soc. Am. Proc., 30, 804, 1966.
144. Paliwal, K.V. and Maliwal, G.L. Proc. Indian Nat. Sci. Acad., Part A, 37, 114, 1971.
145. Peterson, F.F., Rhoades, J., Arca, M., and Coleman, H.T. Soil Sci. Soc. Am. Proc., 29, 327, 1965.
146. Wild, A. and Keay, J. J.Soil Sci., 15, 135, 1964.
147. Tiller, K.G. and Hodgson, J.F. Clay Clay Miner., 2, 393, 1962.

(X)

148. Gille, G.L. and
Graham, E.R. Soil Sci. Soc. Am. Proc.,
35, 414, 1971.
149. Bolt, G.H. Soil Sci., 79, 267, 1955.
150. Coulter, B.S. J. Soil Sci., 20, 72, 1969.
151. Levy, R. and Hillel,
D. Soil Sci., 106, 393, 1968.
152. Slabaugh, W.H. and
St. Clair, A.D. J. Colloid Interface Sci.,
29, 586, 1969.
153. Knibbe, W.G.J. and
Thomas, G.W. Soil Sci. Soc. Am. Proc.,
36, 568, 1972.
154. Vansant, E.F. and
Peeters, G. Clays and Clay Miner., 26,
279, 1978.
155. Vansant, E.F. and
Yariv, S. J. Chem. Soc. Farad. Trans.
1, 73, 1815, 1977.
156. Bonner, O.D. J. Phys. Chem., 58, 318,
1954.
157. Idem. ibid, 59, 719, 1955.
158. Bonner, O.D. and
Smith, L.L. ibid, 61, 326, 1957.
159. Salmon, J.E. and
Hale, D.K. "Ion Exchange. A Laboratory
Manual", Academic Press, Inc.,
New York, 1959.
160. Gregor, H.P., Hamilton,
M.J., Osa, R.J. and
Bernstein, F. J. Phys. Chem, 60, 263-267,
1956.
161. Sherry, H.S. J. Phys. Chem, 70, 1158, 1966.
162. Ames, L.L. J. Can. Miner., 8, 325, 1966.
163. Idem. Am. Miner., 49, 127, 1964.
164. Broussard, L. and
Shoemaker, D.P. J. Am. Chem. Soc., 82,
1041, 1960.

(XI)

165. Eulenberger, G.R.,
Shoemaker, D.P. and
Keil, J.G. J.Phys. Chem., 71, 1812,
1967.
166. Breck, D.W. J.Chem.Educ., 41, 678, 1964.
167. Barrer, R.M., Buser,
W. and Grutter, W.F. Helv. Chim.Acta., 39,
518, 1956.
168. Theng, B.K.G., Vansant,
E.F., and Uytterhoeven,
J.B. Trans. Far. Soc., 64,
3370, 1968.
169. Vansant, E.F. and
Peeters, G. J.Chem.Soc., Farad. Trans. I,
73, 1574, 1977.
170. Vansant, E.F. and
Wanhoof, L. J.Royal Netherlands Chem.
Soc., 97, 191, 1978.
171. Barrer, R.M., Davies,
J.A. and Rees, L.V.C. J.Inorg.Nucl. Chem., 30,
333, 1968.
172. Cremers, A. Am.Chem. Soc., 2, 179, 1977.
173. Barrer, R.M., Rees,
L.V.C. and Shamsuzzoha,
M. J.Inorg. Nucl. Chem., 28,
629, 1966.
174. Maes, A. and Cremers,
A. Advances in Chem. Series,
121, 19, 1973.
175. Clark, J.S. and
Turner, R.C. Soil Sci. Soc. Am. Proc.,
29, 3, 1965.
176. Barrer, R.M. and
McLeod, D.M. Trans. Faraday Soc. 51,
1290, 1955.
177. McAtee, J.L. Clays and Clay Miner., 9,
444, 1962.
178. Bernelius, W.C. "Inorganic Synthesis",
Vol. II, pp. 221-222. McGraw
Hill Book Co., N.Y., 1946.
179. Idem ibid, pp. 217-218.

(XII)

180. Jenkins^{I.L.} and Monk.C.B. J.Chem.Soc., 68, 1951.
181. Bailar, Jr., J.C. and Work, J.B. J.Am.Chem.Soc., 68, 232, 1946.
182. Van Olphen, H. "An introduction to Clay Colloid Chemistry", John Wiley, New York, p-94, 1977.
183. Ganguly, A.K. and Mukherjee, S.K. J.Phys. & Coll. Chem., 55, 1429, 1951.
184. Knudson, Jr, M.I. and McAtee, Jr, J.L. Clays and Clay Miner, 21, 19, 1973.
185. Idem. Ibid., 22, 59, 1974.
186. Mc Bride, M.B. and Mortland, M.M. Clay Miner, 10, 357, 1975.
187. Chakravarti, S.K. J.Indian Soc. Soil Sci., 7, 27, 1959.
188. Hendricks, S.B. J.Phys. Chem., 45, 65, 1944.
189. Landolt-Bornstein's Tabellen Erganzungsband, III C, 2059, 1936.
190. Stokes, R.H. and Robinson, R.A. J.Am.Chem. Soc., 70, 1870, 1948.
191. Kressman, T.R.E. and Kitchener, J.A. J.Chem.Soc., 1190, 1949 and J.Phys. Chem., 56, 118, 1952.
192. Pauley, J.L. J.Am.Chem. Soc., 76, 1422, 1954.
193. Barrer, R.M. and Reay, J.S.S. J.Chem.Soc., 3824, 1958.
194. Giles, C.H., Mac Ewan, T.H., Nakhwa, S.N. and Smith, D. J.Chem.Soc. (London), 3973, 1960.
195. Giles, C.H., Smith, D. and Huitson, A. J.Colloid and Interface Sci., 47, 755, 1974.

(XIII)

196. Walker, G.F. and Garrett, W.G. Nature, 191, 1389, 1961.
197. Wild, A. and Keay, J. Soil Sci., 92, 54, 1961.
198. Marshall, C.E. The Physical Chemistry and Mineralogy of Soils. Vol. I, John Willy and Sons Inc., 1964.
199. Peterson, F.F., Rhoades, J., Arca, M. and Coleman, N.T. Soil Sci. Soc. Am. Proc., 29, 327, 1965.
200. Daskanungo, J.L. Ph.D. thesis, 1969, University of North Bengal.
201. Fripiat, J.J. Summary review O.E.C.D. Project, 1969.
202. Neumann, B.S. and Sansom, K.G. Isr. J.Chem., 8, 315, 1970.
203. Idem. J.Soc. Cosmetic Chem., 21, 237, 1970.
204. Perkins, R., Brace, R. and Matijevic, E. J.Colloid and Interface Sci, 48, 417, 1974.
205. Gregor, H.P. and Bregman, J.I. J.Colloid Sci., 6, 323, 1951.
206. Harold, O, Phillips and Kurt, A. Karus J.Am.Chem. Soc., 84, 2267, 1962.
207. Kazokov, E.V. and Karpova, I.F. Vestn. Leningr. Univ. 21, (10), Ser. Fiz. I.Khim. No. 2, 139, 1966.
208. Helfferich, F. Ion Exchange, p. 186, McGraw Hill, New York, 1962.
209. Lindenbaum, S. and Boyd, G.E. J.Phys. Chem., 69, 2374, 1965.
210. Becker, K.E., Lindenbaum, S. and Boyd, G.E. J.Phys. Chem., 70, 3834, 1966.

(XIV)

211. Strauss, U.P. and
Leung, Y.P. J. Am. Chem. Soc., 87, 1476,
1965.
212. Gregor, H.P.,
Hamilton, M.J.,
Oza, R.J. and
Bernstein, F. J. Phys. Chem., 60, 263,
1956.
213. Bregman, J.I. Ann. N.Y. Acad. Sci., 57,
125, 1953.
214. Britz, D. and Nancollas,
G.H. J. Inorg. Nucl. Chem., 3,
3861, 1969.
215. Chatterjee, A. J. Indian. Soc. Soil Sci.,
2, 1954.
216. Chatterjee, A. J. Indian. Chem. Soc., 7,
37, 1960.
217. Chatterjee, A. and
Mukherjee, S.K. ibid., 43, No. II, 673,
1966.
218. Gal, I.J., Jankovic,
O., Malcic, S.,
Radovanov, P. and
Todorovic, M. Trans. Farad. Soc., 57,
999, 1971.
219. Wolff, F. and Hadicke,
U. Tonind. -Z., 91, 41, 1967.
220. Wolff, F., Ceacareanu,
D. and Pilchowski, K. Z. Phys. Chem. (Leipzig),
252, 50, 1973.
221. Marinsky, J.A. Ion Exchange, Vol. 2, p. 120,
Marcel Dekker, Inc., New
York, 1969.

(XV)

222. Barrer, R.M. and
Falconer, J.D. Proc. R.Soc. London,
A236, 227, 1956.
223. Barrer, R.M. and
Brummer, K. Trans. Faraday Soc.,
59, 959, 1963.
224. Barrer, R.M. and
McLeod, D.M. ibid., 50, 980, 1954.
225. Brooks, C.S. Soil Sci., 79,
331, 1955.
226. Aylmore, L.A.G.
and Quirk, J.P. J. Soil Sci., 18,
1, 1967.
227. van Olphen, H. An Introduction to
Clay Colloid Chemistry,
Interscience, New
York, p244, 1966.
228. Gruner, J.W. Am. Miner., 19,
557, 1934.
229. Ram Gopal and
Rastogi, A.K. J. Indian. Chem. Soc.,
43, 269, 1966.